EFFICIENT EXPRESSION OF VIRAL SURFACE PROTEINS BY TRANSIENT GENE EXPRESSION IN HI5 INSECT CELLS FOR FUNCTIONAL AND STRUCTURAL ANALYSIS

Von der Fakultät für Lebenswissenschaften

der Technischen Universität Carolo-Wilhelmina zu Braunschweig

zur Erlangung des Grades einer

Doktorin der Naturwissenschaften

(Dr. rer. nat.)

genehmigte

D i s s e r t a t i o n

von Margitta Schürig

aus Celle

1. Referent:	Professor Dr. Wulf Blankenfeldt
2. Referent:	Professor Dr. Stefan Dübel
Eingereicht am:	19.06.2018
mündliche Prüfung (Disputation) am:	14.09.2018
Druckjahr:	2019

VORVERÖFFENTLICHUNGEN DER DISSERTATION

Teilergebnisse dieser Arbeit wurden vorab, mit Genehmigung der Fakultät für Lebenswissenschaften, vertreten durch den Mentor der Arbeit in folgenden Beiträgen vorab veröffentlicht:

Tagungsbeiträge

Schürig M., Schinkowski C., Stricker R., Krauße J., Khera T., Schughart K., Pietschmann T. & van den Heuvel J.
"Expression of Viral Surface Proteins for Functional and Structural Analysis"
13th Protein Expression in Animal Cells conference (PEACe), Valencia, Spain (2017)

Schürig M., Schinkowski C., Stricker R., Krauße J., Khera T., Schughart K., Pietschmann T. & van den Heuvel J.
"Expression of Viral Surface Proteins Using the Multi-Host Expression System for Functional and Structural Analysis"
HZI Grad School, 8th Annual Retreat, Goslar-Hahnenklee, Germany (2017)

Schürig M., Witzgall F., Xiao Y. (all authors contributed equally to this presentation)
"Protein Expression, Purification and Crystallization - What can we learn from Protein Structures?"
HZI Grad School, 7th Annual Retreat, Goslar-Hahnenklee, Germany (2016)

Schürig M., Bock T., Schinkowski C. (all authors contributed equally to this presentation)
"From 'Gene' to Application"
HZI Grad School, 6th Annual Retreat, Braunschweig, Germany (2015)

Schürig M., Schinkowski C., Stricker R., Krauße J., Schughart J. & van den Heuvel J.
"Expression of Viral Surface Proteins Using the mHOST Expression System for Functional and Structural Analysis"
HZI, Progress Seminar, Braunschweig, Germany (2015)

Posterbeiträge

Schürig M., Schinkowski C., Stricker R., Krauße J., Khera T., Schughart K., Pietschmann T. & van den Heuvel J.
"Expression of Viral Surface Proteins Using the Multi-Host Expression System for Functional and Structural Analysis"
HZI Grad School, 9th International PhD Symposium, Braunschweig, Germany (2016)

Schürig M., Schinkowski C., Stricker R., Krauße J., Schughart J. & van den Heuvel J.
"Expression of Viral Surface Proteins Using the Multi-Host Expression System for Functional and Structural Analysis"
12th Protein Expression in Animal Cells conference (PEACe), San Diego, USA (2015)

Schürig M., Schinkowski C., Stricker R., Krauße J., Schughart K., & van den Heuvel J.
"Expression of Viral Surface Proteins Using the Multi-Host Expression System for Functional and Structural Analysis"
7th International PhD Symposium, Braunschweig, Germany (2014)

Schürig M.[*], Schinkowski C.[*], Stricker R., Krauße J., Schughart K., & van den Heuvel J. (*authors contributed equally to this work)
"Expression of Hemagglutinins and Tmprss2 for Novel Strategies Against Influenza Infection"
IGBMC Symposium New strategies for macromolecular complexes analysis, Strasbourg, France (2014)

Schürig M., Schinkowski C., Stricker R., Krauße J., Schughart K., & van den Heuvel J.
„Expression of Hemagglutinins and TMPRSS2 for Novel Strategies Against Influenza Infection"
5th Annual Retreat, Goslar-Hahnenklee, Germany (2014)

Diese Arbeit widme ich meinem Vater, der mir durch seine fortwährende Unterstützung all das überhaupt erst ermöglicht hat

Table of content

Abbreviations

AA	Amino acids
Amp	Ampicillin
AP	Alkaline phosphatase
BD	Becton Dickinson
BEVS	Baculovirus expression vector system
BIIC	Baculovirus infected insect cells
BRI	Biotechnology Research Institute
C	Core protein
CD	Circular dichroism
CHO	Chinese Hamster Ovary
CMV	Cytomegalovirus
CPL	Circularly polarized light
CPRO	Research group “cellular proteomics”
CV	Column volumes
DAAs	Direct-acting antivirals
DESY	Deutsches Elektronen-Synchrotron
D.I.T.	Digital integration time
DLS	Dynamic light scattering
DNA	Deoxyribonucleic acid
EBNA1	Epstein-Barr Nuclear antigen 1
E. coli	*Escherichia coli*
EMBL	European Molecular Biology Laboratory
Endo H	Endoglycosidase H
ER	Endoplasmic reticulum
ESI	Electrospray Ionization
E1/E2	Envelope protein 1/2
E2c	E2 core
FCS	Foetal calf serum
FDA	Food and Drug Administration
FRT	Flp recognition target
GlcNAc	N-Acetylglucosamin
Gm	Gentamicin
GNTI	N-Acetylglucosaminyltransferase I
HA (HA0/HA1/HA2)	Hemagglutinin (inactive precursor/ subunits 1 and 2)
HAT	Human airway trypsin-like protease
HCC	Hepatocellular carcinoma
HCV	Hepatitis C virus
HCVcc	Infectious cell culture-derived HCV particles
HCVpp	HCV pseudoparticle
HEK	Human Embryonic Kidney
HF	High fidelity
Hi5	Trichoplusia ni BTI 5B1-4 insect cell line
HMW	High molecular weight marker

hpi	Hours post infection
hpt	Hours post transfection
HPLC	High performance liquid chromatography
HVR1/2	Hypervariable region 1/2
HZI	Helmholtz-Zentrum für Infektionsforschung
H1 – H18	Hemagglutinin 1 – 18
IAV/IBV/ICV/IDV	Influenza A/B/C/D viruses
ICTV	International Committee for the Taxonomy of Viruses
IE	Immediate early
IFN	Interferon
Ig	Immunoglobulin
igVR	Intergenotypic variable region
IPTG	Isopropyl-β-D-thiogalactopyranoside
IRES	Internal ribosome entry site
K	Lysine
Kan	Kanacymin
LB	Lysogeny-Broth
LMW	Low molecular weight marker
mAb	primary monoclonal antibody
MALDI-TOF	Matrix Assisted Laser Desorption Ionization – Time-Of-Flight
MME	Monomethyl ether
MOI	Multiplicity of infection
MS	Mass spectrometry
MWCO	Molecular weight cut off
M1/M2	Matrix protein 1/2
N	Asparagine
NA	Neuraminidase
NEB	New England Biolabs
NEP	Nuclear export protein
nE1	N-terminal domain of E1
NPs	Nucleoproteins
NRCC	National Research Council Canada
NS1/NS2	Non-structural proteins 1/2
NTRs	Non-translated regions
N1 – N11	Neuraminidase 1 – 11
OD	Optical density
ORF	Open reading frame
PA	Polymerase acidic protein
pAb	Polyclonal antibody
PB1/PB2	Polymerase basic protein 1/2
PCR	Polymerase chain reaction
PDB	Protein data bank
PEG	Polyethylene glycol
PegIFN-α	Pegylated interferon alpha
PEI	Polyethylenimine
PES	Polyether sulfone

pFlpBtM	pFlp-Bac-to-Mam
PNGase F	Peptide -N-Glycosidase F
PTMs	Post translational modifications
PVDF	Polyviylidene difluoride
Q	Glutamine
R	Arginine
RBS	Receptor-binding site
RMCE	Recombinase-mediated cassette exchange
Rmsd	Root mean square deviation
RNA	Ribonucleic acid
RT	Room temperature
SA	Sialic acid
SAP	Shrimp Alkaline Phosphatase
scFv	Single chain variable fragment
SDS-PAGE	Sodium dodecyl sulphate- Polyacrylamide gel electrophoresis
SEC	Size exclusion chromatography
SFPR	Research group “structure and function of proteins”
S. frugiperda	*Spodoptera frugiperda*
Sf21	*S. frugiperda* cell line
SLIC	Sequence and ligation independent cloning
SLS	Swiss Light Source
SOC	Super optimal broth for catabolite repression
TCA	Trichloroacetic acid
Tet	Tetracyclin
TGE	Transient plasmid-based gene expression
TIPS	Titerless Infected-Cells Preservation and Scale-Up
TM	Transmembrane
T_m	Temperature at melting point
TMD	Transmembrane domain
TMPRSS2 /4/11D	Transmembrane serine protease 2/4/11D
T. ni	*Trichoplusia ni*
Tpa	Tissue Plasminogen Activator
TLPs	Trypsin-like proteases
TTSPs	Type II transmembrane serine proteases
VA	Virus amplification/ extracellular virus stock
VLPs	Virus-like particles
vRNP	Viral ribonucleoprotein complex
WHO	World Health Organization
Wt	Wildtype
YFP	Yellow fluorescence protein-coding gene

Zusammenfassung

Virale Oberflächenproteine spielen eine entscheidende Rolle in der Infektionsforschung, da sie an vielen wichtigen Funktionen in der Wechselwirkung zwischen dem Virus und dem Wirt beteiligt sind. Ihre rekombinante Expression für strukturelle und funktionelle Analysen ist daher sowohl in der Impfstoffentwicklung als auch in der strukturbasierten Wirkstoffforschung ein wichtiger Prozess. Für die rekombinante Expression solch anspruchsvoller Glykoproteine ist die Wahl eines geeigneten Expressionssystems besonders wichtig, da dieses in der Lage sein muss post-translationale Modifikationen und komplexe Faltungen vorzunehmen. Diese Doktorarbeit widmet sich daher der Expression von biologisch aktiven Oberflächenproteinen des Influenza A (IAV) und Hepatitis C Virus (HCV), da beide Viren Krankheiten auslösen, die ein globales Gesundheitsproblem darstellen. Ihre Oberflächenproteine Hämagglutinin (HA) und E2 sind wichtige Angriffspunkte für die Herstellung neuer Antigene in der Impfstoffentwicklung. Darüber hinaus ist die Untersuchung ihrer Struktur- und Funktionsbeziehungen wichtiger Bestandteil der strukturbasierten Wirkstoffforschung. Für diesen Zweck wurde im Rahmen dieser Doktorarbeit ein Verfahren für die effiziente rekombinante Expression und Reinigung der Oberflächenproteine HA und E2 entwickelt.

Der erste Teil der Arbeit befasst sich mit der sekretorischen Expression der Ektodomäne der humanpathogenen HA Subtypen H1 und H3 in ihrer ungespaltenen, inaktiven Form für strukturelle Analysen der HA Aktivierung. Hierbei hat sich herausgestellt, dass eine Expression in Hi5 Insektenzellen am besten für die Kristallisierungsanalysen geeignet ist. Außerdem wurde ein Protokoll für ein Scale-Up der HA Produktion entwickelt, das bis zur Produktion im Bioreaktormaßstab geeignet ist. Insgesamt wurde sowohl der HA Produktionsprozess als auch dessen Weiterverarbeitung („Downstream processing“) in der Art optimiert, dass sehr reines Protein von hoher Qualität gewonnen werden konnte.

Der zweite Teil dieser Arbeit beschäftigt sich mit der Entwicklung einer effizienten Strategie zur sekretorischen Expression von rekombinanten Varianten der E2 Ektododomäne. Die Methode der transienten Genexpression (TGE) in Hi5 Insektenzellen hat sich hierfür als besonders geeignet herausgestellt. Zudem wurde ein geeignetes Verfahren für das Downstream Processing etabliert. Anschließende Optimierungen des Produktionsprozesses konnten die Ausbeute der rekombinanten E2 Proteine auf 6 – 11 mg/L erhöhen. Des Weiteren wurden biochemische Analysen, in vitro Assays und Vakzinierungsversuche durchgeführt, die erste Hinweise auf ihre Funktionalität geben.

Alles in allem hat sich die TGE in Hi5 Insektenzellen über den gesamten Verlauf der Doktorarbeit als vorteilhaft für die rekombinante Expression der gewünschten Oberflächenproteine gezeigt, da diese Methode nicht nur eine schnelle Expressionsanalyse verschiedener Konstrukte ermöglicht, sondern auch sehr effizient im Rahmen eines Scale-Ups eingesetzt werden kann.

Synopsis

Viral surface proteins are the key players in virus – host interactions. Hence, their recombinant production for structural and functional analyses is an important step for vaccination and structure-based drug design. Recombinant expression of such sophisticated glycoproteins requires an expression system that is capable of posttranslational modifications and proper folding mechanisms. This PhD thesis addresses the expression and purification of Influenza A (IAV) and Hepatitis C virus (HCV) surface proteins, which both constitute a significant global health problem. Their surface proteins hemagglutinin (HA) and E2 are important targets for the generation of new antigens for vaccination. Besides, the investigation of their structure and function relations are a major task in structure-based drug design. Thus, a method was developed for the recombinant expression and purification of HA and E2 variants for their functional and structural analysis. For both parts of this project the viral surface proteins were successfully expressed and a purification strategy was developed that enables efficient purification of biological active recombinant proteins.

In the first part of this thesis, a method was developed for the secretory expression of the full-length ectodomain of the two IAV HA subtypes circulating in human, H1 and H3, in its uncleaved pre-fusion state for structural investigation of HA activation. Hi5 insect cells were discovered to be the most suitable expression host for the production of these HA precursors with an intact, non-modified cleavage loop for crystallization studies. Moreover, a protocol was established for HA expression up-scaling that was reliable, economic, easy to handle, comparatively fast and accessible for a scale-up in bioreactor dimensions. All in all, the production process and its optimized downstream processing resulted in very pure protein of high-quality.

In the second part of this thesis, a strategy for effective expression of recombinant secreted E2 ectodomain variants via transient gene expression (TGE) in Hi5 insect cells was established. First, the most suitable protein constructs and the most qualified expression host was evaluated. Subsequently, an efficient downstream processing was established and the whole production process was optimized resulting in marvelous protein titers of 6 – 11 mg/L. The different soluble E2 variants were subsequently applied to biochemical analysis, in vitro assays and vaccination studies for further analysis of their structure and function. The recombinant sE2 variants were found to inhibit HCV infection in an in vitro inhibition assay and to induce the production of E2-specific antibodies in mice, indicating proper folding and functionality.

Among the different expression systems evaluated in the course of this thesis the method of TGE in Hi5 insect cells pointed out to be advantageous for the expression of the desired viral surface proteins. This recently established method not only allows the fast expression analysis of different constructs, but is also very successful for process up-scaling.

1 Introduction

1.1 Infection research

Health research in general refers to research that is done to learn more about human health. It is mainly about new methods and better ways for efficient diagnosis, prevention and treatment of diseases. Its overall guiding principle is to translate research findings quickly and effectively into medical care. The main subjects are research in cancer, cardiovascular and metabolic diseases, infections, disorders of the nervous system and genetic and environmental influences on common diseases (Federal Ministry of Education and Research, 2018). Within this field of health research, infection research is a major topic contributing to about one-fifth of all deaths worldwide (Krämer, Kretzschmar and Krickeberg, 2010). It concentrates on the molecular mechanisms responsible for the development and course of bacterial and viral infectious diseases. For many of these diseases neither protective vaccination nor effective treatments exist. Precise knowledge of interactions between hosts and pathogens provides the foundation for the development of new strategies for the entire spectrum of diagnosis, prevention and treatment. Thus, one important aim in the field of infection research is to understand pathogen - host interactions.

1.2 Viral surface proteins

Viral surface proteins are the key players in virus – host interactions. They play important roles in their virus life cycle and are necessary for viral infectivity. It is therefore important to gain insights into their structure and to understand the mechanisms involved in order to fulfil their function. Viral surface proteins bind to host cell surface glycans that act as general attachment factors, co-receptors or primary receptors that mediate viral infection and entry (Raman *et al.*, 2016). Thus, it is important to understand the underlying mechanisms in order to interfere with viral entry or to inhibit fusion. However, they not only bind to host cell factors to initiate infection. Besides, they are the major targets for immune response and are thus important players in viral strategies for evading the host immune system. These strategies include several mechanisms that differ between viral species, but also some of them are species independent (Alcami and Koszinowski, 2000). The most widely reported viral strategy is mutational escape. In case of influenza the term “antigenic drift” was coined for these small genetic changes in order to distinguish it from the reassortment of genome segments from different host species that is called “antigenic shift” (Zambon, 1999). Those changes often occur in regions that are located next to conserved sequences as receptor- and neutralizing antibody-binding regions (Brown *et al.*, 2005, 2007). Besides, a common strategy for viral escape is the shielding of antigenic regions by glycosylation. These “evolving glycan shields” have been reported manifold to limit sensitivity of different viruses to antibody neutralization (Wei *et al.*, 2003;

Abe *et al.*, 2004; Drummer, 2014). Therefore, an important goal in vaccine development is to generate antigens that target antibody response towards more conserved regions in order to generate broadly neutralizing antibodies that are able to clear infection. Moreover, understanding the structural basis for neutralization can guide selection of vaccine targets.

Hence, this PhD thesis deals with the expression and purification of biological active surface proteins of influenza A virus and hepatitis C virus for both structural and functional aspects as well as for the generation of antigens for vaccination. More detailed information about these viruses and their surface proteins that are relevant in the scope of this project are given in the chapters 1.3 for influenza A and 1.4 for hepatitis C virus, respectively. Collectively, this information will pave the way to new strategic approaches for selecting vaccine antigens and demonstrates the potential for rational vaccine design.

1.3 Influenza A virus

Influenza viruses are human respiratory pathogens that cause both seasonal infections and pandemics, frequently called “flu”. Seasonal influenza epidemics turn up every year within the winter months in temperate climates, whereas pandemic outbreaks caused by a new influenza substrain occur at unpredictable intervals (Taubenberger and Morens, 2008; Taubenberger and Kash, 2010). Infections with seasonal human influenza display an illness range from mild to severe and even death. Based upon the frequency of hospitalization and death, certain high risk groups were defined. Among them are pregnant women, young children aged 6 - 59 months, elderly, individuals with specific chronic medical conditions such as HIV/AIDS, asthma, and chronic heart or lung diseases, as well as health-care employees. For all adult groups a yearly vaccination is recommended. Worldwide, these annual epidemics are estimated to result yearly in about 3 to 5 million cases of severe illness, and about 250000 to 500000 deaths (World Health Organization, 2016). These seasonal epidemics are caused by viruses with modifications within circulating strains. In addition to those epidemics, pandemic infections emerge as global outbreaks due to viruses with novel antigenic subtypes. Within these pandemics up to 50 % of the population can be infected in one single pandemic year. Moreover, those pandemics are associated with a dramatic increase in number of deaths. In the last 500 years, there have been at least thirteen influenza pandemics. Confirmed pandemics occurred in the past 120 years in 1889, 1918, 1957, 1968, 1977 and 2009 (Taubenberger and Morens, 2009). The worst pandemic in recorded history was the so-called “Spanish flu” in 1918 with up to 50 million deaths worldwide (Taubenberger and Morens, 2009).

Influenza viruses are RNA-viruses belonging to the *Orthomyxoviridae* family and were commonly known to consist of three genera: *Influenza A, B* and *C*. They differ in their pathogenicity and host tropism and are likely to have diverged evolutionarily at least several thousand years ago

(Taubenberger and Kash, 2010). Whereas influenza A viruses (IAV) have been isolated from many species, IBV and ICV have only been isolated from human and seals or pigs and dogs, respectively (Wright, Neumann and Kawaoka, 2007). Seasonal epidemics are caused by IAV and IBV with IAV evolving more rapidly than IBV and thus escapes more easily from the immune system (Nobusawa and Sato, 2006). Only recently, in September 2016, a new genus called influenza D (IDV) was determined by the International Committee of Taxonomy of Viruses (South Dakota State University, 2016). This virus was first discovered in 2011 in swine in Oklahoma, when it was provisionally designated as ICV, because of their genetic similarities (Hause *et al.*, 2013). Subsequently, it was found in cattle across North America, Europe and Asia arising the proposal of a new genus of influenza virus, IDV (Collin *et al.*, 2015; Foni *et al.*, 2017). To date they are not known to infect or cause illness in human.

Based on the two surface glycoproteins hemagglutinin (HA) and neuraminidase (NA) embedded in the viral envelope, IAVs are further classified into subtypes. So far, 18 different HA (H1 – H18) and 11 different NA subtypes (N1 – N11) have been discovered. The latest ones, H17 and H18 as well as N10 and N11, were found in 2013 in bats (Tong *et al.*, 2013). However, these bat IAV subtypes are remarkably different from other IAV subtypes leading to the suggestion that these bat viruses should rather be labeled as influenza-like viruses (Wu *et al.*, 2014). Further characterization of influenza virus strains includes information on the geographic origin, strain number, year of isolation and virus subtype (Hay *et al.*, 2001). For example, influenza virus A/Puerto Rico/8/34 (H1N1) is the 8th strain of H1N1 subtype, isolated in Puerto Rico in 1934.

1.3.1 IAV structure and replication cycle

Influenza virus particles, called virions, are roughly spherically or pleomorphically shaped with a diameter of about 80 – 120 nm. Figure 1.1 depicts an influenza virion that contains the surface glycoproteins HA and NA and the ion channel M2 within the envelope. The HA is a homotrimeric integral membrane protein responsible for virus attachment to sialic acids (SA) on the host cell surface, thereby initiating infection. Whereas the homotetrameric surface protein NA releases new virions from infected host cells due to cleaving SAs from glycolipids or glycoproteins. The matrix 2 (M2) protein forms a proton-specific transmembrane (TM) ion channel required for viral uncoating (Kelly *et al.*, 2003), while M1 builds the inner surface of the virion surrounding the viral ribonucleoprotein (vRNP) complex. This complex is constituted of viral RNA and the viral RNA-dependent polymerase consisting of the three subunits polymerase acidic protein (PA), polymerase basic protein 1 (PB1) and PB2. Each of its eight negative-sense, single-stranded genomic RNA segments is associated with these three proteins and encodes one to two of the viral proteins. Furthermore the vRNP complex is coated with multiple nucleoproteins (NPs) which mediate the

transport of RNPs to the nucleus and controls viral genome replication (Nayak, Hui and Barman, 2004; Nayak *et al.*, 2009). The last two proteins are designated as non-structural proteins (NS1 and NS2). NS1 was found to be responsible for virus replication in the host cell and NS2 is essential for vRNP export and thus is also referred to as nuclear export protein (NEP). Additionally, the NS1 protein represses the host cell antiviral response by multiple mechanisms (Geiss *et al.*, 2002).

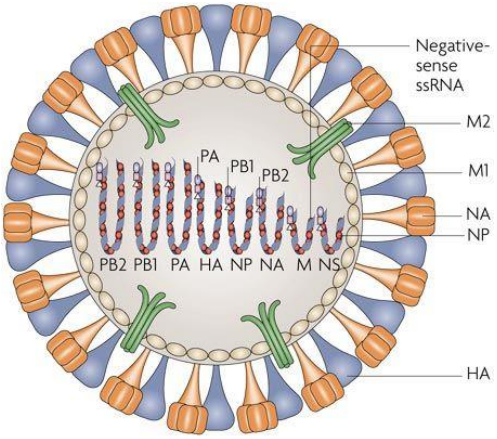

Figure 1.1: Schematic overview of IAV virions
The virus particle contains eight ribonucleoprotein complexes (vRNPs), which harbor negative sense single-stranded RNA segments, associated with the nucleoprotein (NP) and three polymerase proteins (PA, PB1, PB2). The vRNPs are connected via matrix protein (M1) with the viral envelope, which is spiked with the surface glycoproteins hemagglutinin (HA) and neuraminidase (NA). In addition, the M2-ion channel protein is inserted into the envelope (Nelson and Holmes, 2007).

The processes involved in the Influenza replication cycle are depicted as schematic diagram in Figure 1.2. The initial step is mediated by HA binding to SA-containing cell surface receptors followed by virus entry via endocytosis. In the next step acidification of endosomes triggers conformational changes in proteolytic activated HA resulting in fusion of the viral and endosomal membrane. Moreover, proton import via the M2 ion channel abrogates the interaction between vRNPs and the M1 matrix protein and thus results in the release of vRNPs into the host cell cytoplasm. After transport to the nucleus, the polymerase complex starts to synthesize viral mRNA segments that are subsequently exported followed by protein expression. The nascent polypeptides of the viral surface proteins HA and NA are imported and N-glycosylated in the endoplasmic reticulum together with the M2 matrix protein. In the Golgi apparatus the envelope proteins are post-translationally modified and subsequently directed to the cell surface for viral assembly via Golgi vesicles. The other viral proteins (PB1, PB2, PA, NP, NS1, NS2 and M1) are transported back into the nucleus where new vRNPs are produced. Subsequently, vRNPs are coated with M1 proteins and transported to the plasma membrane. At the cellular surface, vRNPS are incorporated into budding viruses via interactions between M1 and the cytoplasmic tails of viral surface proteins, while PB1-F2 induces

apoptosis by interaction with mitochondria. Finally, the NA protein abrogates the interaction of HA with SA receptors and the viral particle can be released from the host cell.

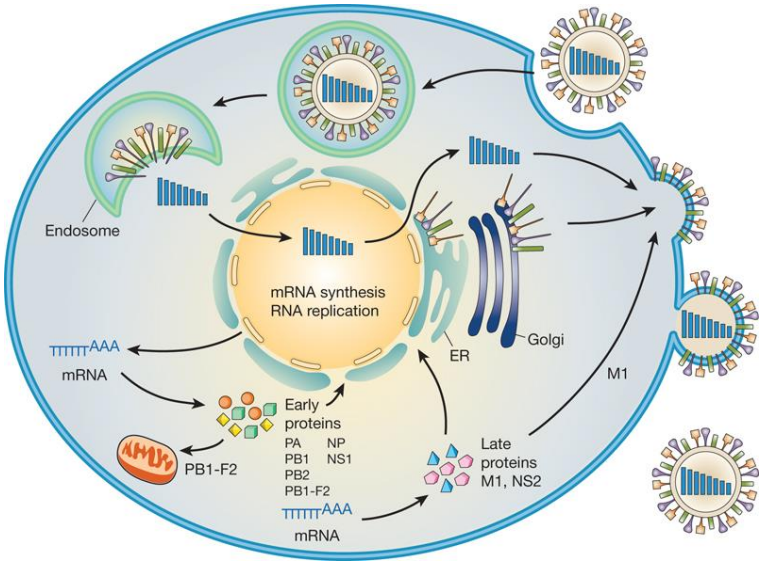

Figure 1.2: Replication cycle of IAV
Receptor-mediated endocytosis is followed by the release of viral ribonucleoprotein (vRNP) complexes into the cytoplasm that is subsequently transported to the nucleus, where replication and transcription take place. While messenger RNAs are exported to the cytoplasm for translation. Early viral proteins required for replication and transcription are transported back to the nucleus. Late in the infection cycle, the M1 and NS2 proteins facilitate the nuclear export of newly synthesized vRNPs while PB1-F2 associates with mitochondria. Finally the assembly and budding of progeny virions occurs at the plasma membrane (Neumann, Noda and Kawaoka, 2009).

1.3.1 Structure and function of IAV glycoprotein hemagglutinin

The major viral surface protein HA is a prime determinant of the pathogenicity of IAV. It initiates infection by binding to cell surface receptors resulting in membrane fusion. Besides, it is the primary target for the humoral immune response (Munk *et al.*, 1992; Tate *et al.*, 2014). HA is a homotrimeric type I transmembrane glycoprotein with a cylindrical shape (about 135 Å long and 35-70 Å wide) and forms spikes on the virion surface (Isin, Doruker and Bahar, 2002). It is synthesized as an inactive precursor (HA0) that depends on proteolytic processing by host cell proteases to become active (Bertram *et al.* 2010; Böttcher-Friebertshäuser *et al*. 2013). The cleavage of HA0 into its subunits HA1 and HA2, linked by a single disulfide bond, is necessary to become activated and gain its capacity to fuse to the membrane. It enables HA to undergo conformational changes at low pH thereby exposing the N-terminal hydrophobic fusion peptide of HA2 and trigger membrane fusion (Isin, Doruker and Bahar, 2002).

With the first HA crystal structure already obtained back in 1990 (Weis *et al.*, 1990), today many different HA isolates from diverse subtypes have been crystallized (Reid *et al.*, 1999; Ha *et al.*, 2002; Russell *et al.*, 2004, 2008, Stevens *et al.*, 2004, 2006; Lu *et al.*, 2012; Zhu *et al.*, 2013; Sun *et al.*, 2013;

Yang *et al.*, 2015; Ni, Kondrashkina and Wang, 2015; Song *et al.*, 2017). With this amount of distinct structures, comprising nearly 400 entries in the protein data bank (PDB) for HA (total amount of entries for "hemagglutinin", status February 2018), detailed structural information is available. This further indicates the vivid interest in structural knowledge about HA. Two major domains in the HA ectodomain have been identified: the globular head and a stalk-like stem domain (depictured in Figure 1.3).

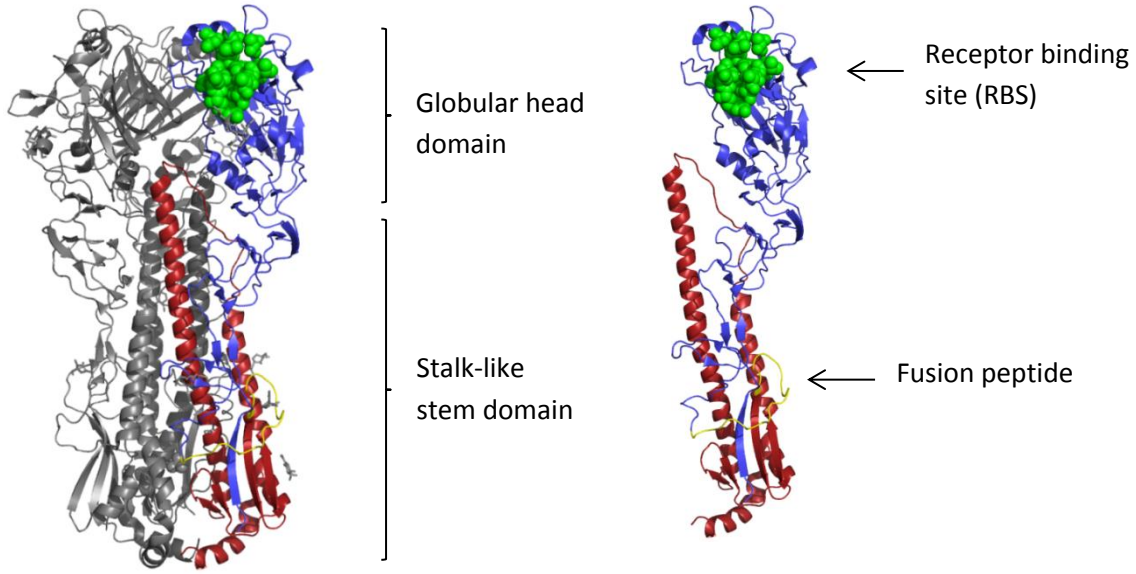

Figure 1.3: Structure of IAV hemagglutinin
A: The ectodomain of the IAV HA trimer is depicted in cartoon rendering. B: For clarity one monomer is depicted alone in different colors for its main structural features: HA1 regions are shown in blue and HA2 regions in red, the fusion peptide is colored in yellow and the receptor binding site is indicated as green spheres. The figure was derived from the X-ray structure of HA from the (H1N1) isolate A/California/04/2009 (PDB ID 3LZG) and was drawn with the program PyMOL.

The HA1 subunit of each HA monomer forms the membrane-distal globular head that contains the receptor-binding site (RBS) and highly variable immunodominant regions. The conserved stem on the contrary is formed by the N- and C-terminal regions of HA1 together with the HA2 subunit (Wiley and Skehel, 1987). The main part of HA1 builds the globular head domain, while the remaining part of HA1 contributes to the stem (Isin, Doruker and Bahar, 2002). The HA2 subunit is mostly folded into a helical coiled-coil structure that constitutes an 80 Å-long helix forming the stem backbone. Besides, HA2 contains both the hydrophobic peptide required for membrane fusion (fusion peptide) and the hydrophobic anchor (not depicted in Fig. 1.3) (Wiley and Skehel, 1987). The surface loop structure at the HA stem contains the proteolytic cleavage site for host cell proteases required for HA-driven fusion of viral and cellular membranes and thus for viral infectivity (Chen *et al.*, 1998). Cleavage site sequences determine which type of cellular host protease can cleave different types of HA (Horimoto and Kawaoka, 2005), as discussed later in detail (see 1.3.2). The major structural consequence of HA cleavage is the generation of a new C-terminus of the HA1 subunit and a new N-terminus of HA2,

schematically depicted in Figure 1.4, as well as the relocation of the N-terminal fusion peptide (Cross *et al.*, 2009). The newly-generated HA2 N-terminal fusion peptide positions itself into the trimer interior where it makes contacts with ionizable residues in order to generate a fusion competent neutral pH structure. Subsequent acidification of the endosomal environment can then induce the irreversible conformational changes that result in membrane fusion (Worch, 2014).

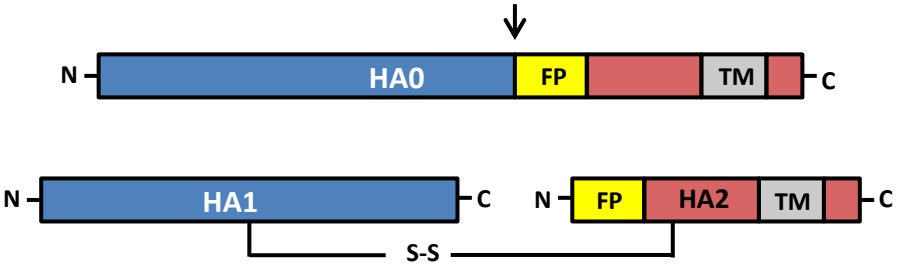

Figure 1.4: Schematic representation of proteolytic HA0 activation
Schematic illustration of the domain organization of HA0 precursor and the cleaved form consisting of the disulfide-linked subunits HA1 and HA2. The cleavage site is indicated by an arrow. FP = Fusion peptide. TM = transmembrane domain.

Both receptor-binding and fusion activation are partly modulated by HA glycosylation. Further, glycosylation is essential for correct folding of HA (Gallagher *et al.*, 1992; Roberts, Garten and Klenk, 1993). It was investigated that some of the HA glycosylation sites are involved in biological functions like receptor-binding, HA cleavage and membrane fusion (Klenk *et al.*, 2002; de Vries *et al.*, 2010). The presence of glycans in close proximity to the RBS was shown to modulate receptor binding affinity and specificity by masking the RBS (Ohuchi *et al.*, 1997; Cherry *et al.*, 2009). Additionally, the N-linked glycosylated elements can interact with cellular lectins and therefore affect the host innate immune system recognition and thus the ability of HA to induce adaptive immune response (Vigerust and Shepherd, 2007; Geijtenbeek and Gringhuis, 2009). Moreover, glycosylation of an antigenic epitope prevents antibody binding (Munk *et al.*, 1992; Tate *et al.*, 2014). It therefore contributes to immune escape and is an important mechanism underlying antigenic drift. The total number and the positions of glycosylation sites vary between HA subtypes and different strains (Cherry *et al.*, 2009). Generally the globular head possesses larger variations regarding glycosylation, while the stem is highly conserved (Ohuchi *et al.*, 1997; Chen, Sun and Li, 2012; Ni, Kondrashkina and Wang, 2015). Sequence analysis of human H1N1 virus isolates from 1918 to 2010 clearly indicated the contribution of HA glycosylation to viral antigenic drift. Thereby a gradual increase in glycosylation sites was observed, especially in the HA head domain, that ranges from one back in 1918 to four glycosylation sites in the seasonal H1N1 strain A/Puerto Rico/8/34 (Igarashi *et al.*, 2010).

1.3.2 IAV HA activation by proteolytic cleavage

HA cleavage represents an essential step for influenza infectivity (Klenk and Rott, 1973; Lazarowitz, Compans and Choppin, 1973; Klenk *et al.*, 1975; Chen *et al.*, 1998). Cleavage of HA0 of most avian

and mammalian IAVs occurs at a single arginine or lysine at its cleavage site. These monobasic cleavage sites are only cleaved by host trypsin-like proteases (TLPs) that are mainly expressed in the respiratory and gastrointestinal tract (Klenk and Garten, 1994; Garten and Klenk, 1999). Highly pathogenic avian IAVs instead contain a polybasic cleavage site with the consensus motif R-X-R/K-R (Bosch *et al.*, 1981; Webster and Rott, 1987; Perdue *et al.*, 1997). These polybasic motives can be recognized by ubiquitously expressed eukaryotic subtilisin-like proteases allowing systemic viral spread (Stieneke-Gröber *et al.*, 1992).

The necessity of cleavage by a host protease for fusion activity, infection, and pathogenicity has first been described in studies analyzing HA cleavage by trypsin (Klenk *et al.*, 1975). Subsequently, other TLPs were identified to activate monobasic HA (e.g. clotting factor Xa (Gotoh *et al.*, 1990) and the arginine-specific serine protease "tryptase Clara" (Kido *et al.*, 1992; Klenk and Garten, 1994; Steinhauer, 1999)). To date several TLPs were identified to cleave HA in vitro and also to activate IAV in cell culture (for overview see Laporte & Naesens 2017). Their role in the airways of influenza-infected individuals, however, remains to be proven for some of them. A study by Böttcher and colleagues discovered that influenza viruses of all subtypes pandemic in humans (H1N1, H2N2 and H3N2) can be activated by the type II transmembrane serine proteases (TTSPs), TMPRSS2 (trans-membrane serine protease 2) and HAT (human airway trypsin-like protease; also designated as TMPRSS11D) upon cell line derived expression (Böttcher *et al.*, 2006). Subsequent studies confirmed the activation of HA by TMPRSS2 and HAT and besides showed that another TTSP, TMPRSS4, can also activate HA (Chaipan *et al.*, 2009; Bertram *et al.*, 2010; Sawoo *et al.*, 2014).

Moreover, a series of studies identified that TMPRSS2 contributes to viral spread in the infected host. First, it was demonstrated that endogenous expression of TMPRSS2 is responsible for trypsin-independent spread of influenza A in the human cell lines Caco-2 (Bertram *et al.*, 2010) and Calu-3 (Böttcher-Friebertshäuser *et al.*, 2011). Furthermore, it was shown that TMPRSS2 is co-expressed with α-2,6-linked SA, the major HA receptor determinant, in human respiratory epithelia (Bertram *et al.*, 2012). Finally, Hatesuer and co-workers demonstrated for the first time that TMPRSS2 is essential for viral spread and pathogenesis of influenza virus H1N1 in mice. With TMPRSS2 knock-out mice they were able to show that these mice were protected from both viral spread and pathogenesis upon H1N1 infection, due to the lack of HA proteolytic processing (Hatesuer *et al.*, 2013). These results were confirmed by two subsequent studies (Sakai *et al.*, 2014; Tarnow *et al.*, 2014). Besides, TMPRSS2 deficient mice were found to survive not only infection with H1N1, but also with an H7N9 virus that was lethal in wt mice (Hatesuer *et al.*, 2013; Sakai *et al.*, 2014; Tarnow *et al.*, 2014). This human H7N9 isolate with avian-origin contains a monobasic cleavage site (Gao *et al.*, 2013) that is mainly cleaved by TMPRSS2 (Sakai *et al.*, 2016).

However, for another in human circulating Influenza A subtype, H3N2, the research groups obtained different results. Hatesuer and co-workers observed that the H3N2 virus was able to replicate in TMPRSS2 deficient mice, but also that those mice showed significantly reduced body weight loss and mortality (Hatesuer *et al.*, 2013). While Tarnow and co-workers detected only marginally effects in TMPRSS2 knock-out mice upon H3N2 infection (Tarnow *et al.*, 2014). Contrary to these findings Sakai and co-workers identified TMPRSS2 to be essential also for infection with H3N2 influenza virus (Sakai *et al.*, 2014). Thus, the proteolytic activation of H3 was thought to be dose and strain-dependent. This is further supported by the observation that the same H3N2 strain used by Sakai and colleagues that was first described to be avirulent in TMPRSS2 knock-out mice, became lethal after ten passages in mice (Sakai *et al.*, 2015). This passaged virus lost one N-glycosylation site at the bottom of the HA stalk region that is thought to alter the accessibility of the cleavage loop and thus provide access to alternative host proteases.

A study by Kühn and co-workers showed for the first time that H3 HA can recruit different host proteases for cleavage activation in vivo (Kühn *et al.*, 2016). In this study they used double-knockout mice with deletions for TMPRSS2 and TMPRSS4, which is another TTSP that was previously shown to cleave and therefore activate HA in vitro. This double knock-out significantly reduced morbidity after H3N2 virus infection, but the mice still showed limited body weight loss, indicating residual viral activity and viral spread. Consequently, besides TMPRSS2 and TMPRSS4, additional proteases are able to cleave and activate the HA of H3N2 viruses. This might also allow for more efficient replication of the H3N2 virus. Thus, it could be a reason why seasonal influenza viruses of the H3 subtype cause more severe symptoms in humans than H1 viruses, since increased accessibility could be associated with higher pathology (Kühn *et al.*, 2016). This hypothesis is further supported by a genome wide association study, which showed that increased TMPRSS2 expression levels lead to more severe infections caused by the 2009 pandemic H1N1 virus and increased susceptibility to influenza H7N9 (Cheng *et al.*, 2015).

A possible explanation for the differences in protease specificity lies in the structural differences that were observed in the available crystal structures of uncleaved HA0 variants of H1 and H3 (H1: PDB ID: 1RD8 (Stevens *et al.*, 2004), H3: PDB ID: 1HA0 (Chen *et al.*, 1998)). In the H3 HA0 crystal structure, the cleavage loop extends from the protein surface, whereas the cleavage site in H1 HA0 is less exposed, but instead extends toward the trimer interface. Thus, it is conceivable that this protrusion of the H3 cleavage loop provides an easier access for diverse proteolytic enzymes (Kühn *et al.*, 2016). The H3 protein used for structural analysis of the uncleaved H3 HA0, however, possesses a mutated cleavage site (R329Q) in which the arginine (R) 329 was replaced by a glutamine (Q) in order to prevent proteolytic cleavage upon crystallization. Yet, it is assumed that this amino acid exchange might have destroyed non-covalent interactions between the cleavage site and other HA domains

that might have led to the protrusion of the loop (Kühn, 2015). Crystallization of a non-modified H3 protein could therefore help to clarify the loop structure.

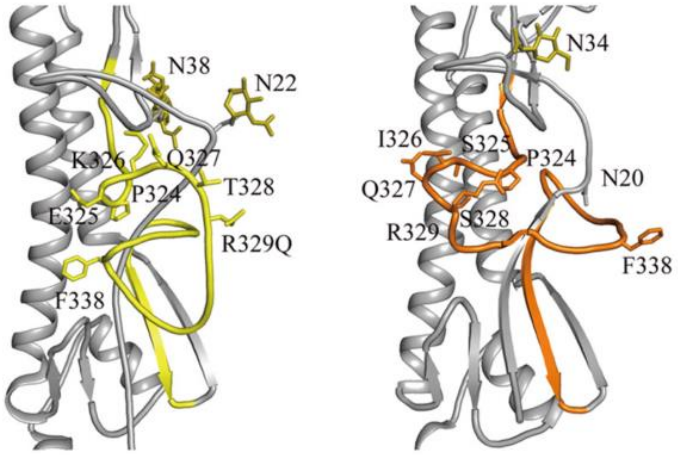

Figure 1.5: Illustration of different HA0 cleavage sites
Structures of noncleaved HA0 that have been solved for the subtypes H1 and H3. Structural analysis of the H3 precursor (R329Q cleavage site mutant) exhibits the HA cleavage site located in a prominent loop that protrudes from the surface (Chen *et al.*, 1998). The non-modified cleavage site loop of HA0 of the 1918 pandemic H1N1 virus ("Spanish flu") on the contrary is less exposed (Stevens *et al.*, 2004); (adapted from Lu et al. 2012).

Recent studies suggested that there are also other factors that could play a role in HA activation, because the amino acid sequence of the cleavage site is identical for most of the HAs (Hamilton, Gludish and Whittaker, 2012). Besides, protease accessibility can be enhanced by insertion of amino acids upstream of the cleavage site (Khatchikian, Orlich and Rott, 1989; Ohuchi *et al.*, 1991), while carbohydrate residues due to neighboring glycosylation sites may limit its access for proteases (Kawaoka and Webster, 1989; Ohuchi *et al.*, 1989).

1.3.3 Prevention and Treatment of Influenza Virus Infection

Vaccination provides the most effective protection against influenza viruses and is already available since the 1930s (Shope, 1936). Albeit, for ensuring an effective protection the vaccination has to be repeated annually with new vaccine strains due to continuous antigenic drift. Those annual vaccines contain antigens from IAV (subtypes H1 and H3) and IBV of the most widespread strains. Until 2007 all commercial available influenza vaccines were produced in chicken eggs, making it a restricted and time consuming process and in case of a pandemic this process might be too slow (Bommakanti *et al.*, 2010; Milián and Kamen, 2015). In 2013, however, the first recombinant influenza vaccine based on recombinant HA expressed in insect cells manufactured by Protein Science was licensed by the US Food and Drug Administration (FDA) (Cox, Patriarca and Treanor, 2008; Yang, 2013). This was one of

the most relevant milestones in the development of cell culture-based vaccines, because of its more efficient and scalable production system. However, the traditional egg-based vaccine production is still state-of-the-art and further development of cell culture-based vaccines is needed, especially in terms of effectiveness and speed in order to respond quickly to pandemic outbreaks (Milián and Kamen, 2015).

In case of a pandemic development of a vaccine might take too long and treatment of an influenza virus infection is necessary. At present anti-influenza therapy is limited and should be reserved for high-risk patients or individuals with a more severe outcome. Other patients should be given a symptomatic treatment and are advised to stay at home in order to minimize the risk of spreading the infection (World Health Organization, 2018). The therapies are built on only two classes of antiviral compounds. The first class of antivirals comprises M2 ion channel blockers like amantadine and rimantadine. By blocking the M2 ion channel they inhibit proton influx into the virus particle and thus uncoating of the virion (Hay *et al.*, 1985). Thereby, they prevent the release of genetic material of the virus into the cytoplasm and thus suppress viral replication (Król, Rychłowska and Szewczyk, 2014). However, they are only effective against IAV (Pinto and Lamb, 2007) and are often associated with severe side effects. Moreover, viruses may rapidly acquire resistance mutations against these antivirals. In fact, all currently circulating influenza viruses have developed resistance to adamantane antiviral drugs such as amantadine and rimantadine, and are thus not recommended for therapy by the WHO (World Health Organization, 2018). The second class of anti-influenza drugs comprises the NA inhibitors zanamivir, oseltamivir and peramivir that inhibit the release of progeny virions from infected cells. These compounds prevent IAV transmission by blocking the catalytic center of NA (Król, Rychłowska and Szewczyk, 2014). However, rapid emergence of resistant viral strains has also been reported for NA inhibitors, limiting their use (Hussain *et al.*, 2017). This demonstrates the need for new influenza therapeutics directed against new targets in order to combat the persistent threat of influenza viruses. New strategies that target highly conserved functional regions of influenza proteins, which are important for early stages of viral infection are thought to be highly effective, while reducing the probability of resistance mutations (Kadam and Wilson, 2017).

1.4 Hepatitis C virus

Hepatitis C virus (HCV) infections constitute a major global health problem with an estimated 130 – 170 million people infected with HCV worldwide. It is transmitted exclusively through direct blood-to-blood contacts between humans (Chevaliez and Pawlotsky, 2006). While acute HCV infection is usually asymptomatic, 60 – 80 % of infected individuals will develop chronic infection. Chronic infection is a major cause of cirrhosis, hepatocellular carcinoma (HCC), and liver-related death (World Health Organization, 2017). HCV is a highly variable, blood-born, positive-stranded RNA virus of the family *Flaviviridae* within the genus *Hepacivirus*. The HCV particle (virion) is spherical with a diameter of between 40 and 80 nm (Bradley *et al.*, 1985), composed of an envelope derived from host cell membranes in which the glycoproteins envelope 1 (E1) and E2 are embedded, encasing the viral genome. Due to the large degree of sequence variability, HCV is further categorized into different genotypes and subtypes. Now, up to seven genotypes further divided into 86 subtypes have been described (Smith *et al.*, 2017), regarding to the updated genotype and subtype assignments by the International Committee for the Taxonomy of Viruses (ICTV) in 2014 (Smith *et al.*, 2014). The variability of HCV permits immune evasion and thus facilitates viral persistence.

The HCV RNA genome, depicted in Figure 1.6 A, is 9.6 kb in length (Choo *et al.*, 1991), it is flanked by 5’ and 3’ non-translated regions (NTRs) and contains two open reading frames (ORF). The polyprotein of HCV is encoded by the large ORF while an alternative ORF produces a single so-called F protein (Xu *et al.*, 2001). Although the role of the F protein is not well understood, it is suggested that it could be implicated in immune evasion (Komurian-Pradel *et al.*, 2004). The polyprotein of about 3000 amino acids (AA) is cleaved by viral and cellular proteases into 10 distinct proteins (Suzuki *et al.*, 1999). These include the structural proteins: core and the two glycoproteins E1 and E2 that constitute the virus particle, the p7 ion channel protein and the nonstructural proteins NS2, NS3, NS4A, NS4B, NS5A and NS5B (Figure 1.1 A). Those non-structural proteins are involved in viral RNA replication and contribute to virion assembly but are not incorporated into virions (Moradpour et al. 2007). Before moving to their final destination, the proteins are integrated or anchored in the endoplasmic reticulum (ER) membrane, where posttranslational modifications take place in order to enhance their stability and to modify their activity and antigenicity (Dubuisson *et al.*, 2000). The membrane topology and major functions of each cleaved viral protein is illustrated in Figure 1.6 B.

The organization of the HCV envelope is subject to discussion as it incorporates or associates with host-derived lipoproteins, leading to a much lower buoyant density for HCV than of any other virus known so far (Thomssen *et al.*, 1992; Thomssen, Bonk and Thiele, 1993; Vieyres, Dubuisson and Pietschmann, 2014). Besides, it has been documented that HCV-associated lipoproteins may partially mask the virion from the action of neutralizing antibodies (Meunier *et al.*, 2005; Dreux *et al.*, 2006; Voisset *et al.*, 2006).

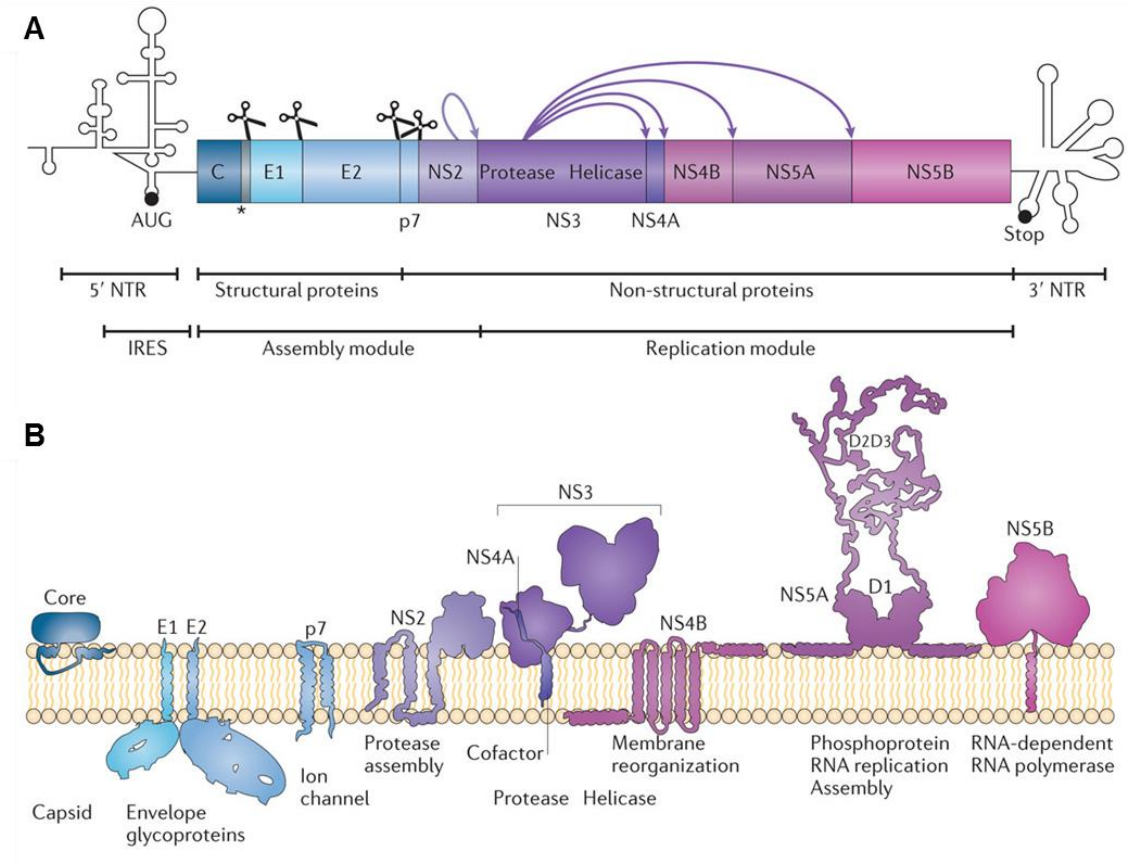

Figure 1.6: Hepatitis C virus genome organization and the membrane topology of cleaved viral proteins
A: The large HCV ORF encoding the polyprotein is flanked by 5′ and 3′ NTRs. Start and stop codons are indicated (AUG/Stop). The 5′ NTR contains an internal ribosome entry site (IRES), followed by the structural core (C) protein and the two envelope glycoproteins E1 and E2. Together with p7 and NS2 they build the so-called assembly module. The other non-structural proteins are required for RNA replication (replication module). Polyprotein cleavage by cellular signal peptidases is indicated by scissors at the corresponding ORF position, while arrows refer to cleavage by viral proteases. B: Membrane topologies and major functions of cleaved HCV proteins. Conveniently only NS5A is depicted as dimer, however, most, if not all, HCV proteins form homo- or heterodimers or oligomeric complexes (Bartenschlager, Lohmann and Penin, 2013).

1.4.1 HCV envelope glycoproteins E1 and E2

The E1 and E2 glycoproteins form a heterodimer that mediates fusion of the viral lipid envelope with the host cell endosomal membrane in a pH-dependent process (Lindenbach and Rice, 2013). However, the molecular details of this HCV fusion mechanism have not yet been elucidated (Freedman *et al.*, 2016). It is quite possible that the oligomeric status of the global HCV protein complex fluctuates during HCV replication cycle (Meertens, Bertaux and Dragic, 2006; Falson *et al.*, 2015). Indeed, a hierarchical organization of E1E2 was suggested, starting with E1E2 heterodimers, bound into E1-driven trimers, which are finally clustered with disulfides (Vieyres, Dubuisson and Pietschmann, 2014; Falson *et al.*, 2015). Nevertheless, the E1E2 heterodimer seems to be a stable basic entity, in particular at the envelopment and fusion stages (Dubuisson *et al.*, 1994; Duvet *et al.*, 1998; Meertens, Bertaux and Dragic, 2006; Rouillé *et al.*, 2006). Overall, the folding and maturation of E1 and E2 glycoproteins as well as the heterodimer formation are slow, interdependent and

complex processes that involve the ER chaperone machinery and disulfide bond formation as well as glycosylation (reviewed in Lavie, Goffard and Dubuisson, 2006; Vieyres, Dubuisson and Pietschmann, 2014).

A schematic representation of HCV glycoproteins with their individual features is depicted in Figure 1.7. Both E1 and E2 are type I transmembrane proteins with a large highly glycosylated ectodomain and a short C-terminal transmembrane domain (TMD). These TMDs have numerous functions, ranging from membrane anchoring, ER localization and heterodimer assembly (Cocquerel *et al*. 1998; De Beeck *et al*. 2000). The heterodimer formation is essential for interaction with receptors and neutralizing antibodies (Drummer and Poumbourios, 2004; Lavie, Goffard and Dubuisson, 2006). Both proteins are highly modified by intramolecular disulfide bonds (Dubuisson and Rice, 1996; Krey *et al.*, 2010; McCaffrey *et al.*, 2012) and N-linked glycans with their carbohydrate moieties making up approximately half of the mass of each protein (Goffard *et al.*, 2005; Falson *et al.*, 2015). Glycosylation depends on the viral genotype, is highly conserved between different strains and has an important role in protein folding and correct expression (Dubuisson *et al.*, 1999; Goffard *et al.*, 2005; Brown *et al.*, 2010). E1 contains up to five and E2 eleven N-glycosylation sites, depending on the viral genotype (Goffard and Dubuisson, 2003; Goffard *et al.*, 2005). Among them sequence analysis indicated four potential N-glycosylation sites to be strongly conserved for E1 among HCV genotypes, whereas nine of the eleven sites are strongly conserved in E2 (Goffard and Dubuisson, 2003; Zhang *et al.*, 2004). Relevant protein features like glycosylation sites, cysteines and domains of each protein are indicated in Figure 1.7.

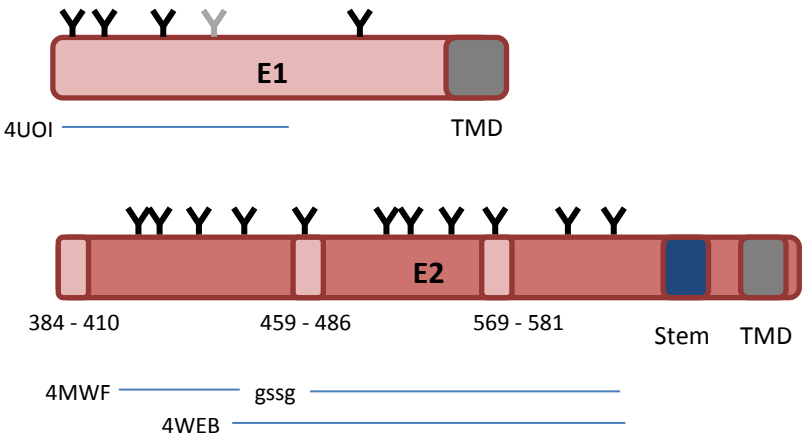

Figure 1.7: Schematic representation of HCV glycoprotein E1 and E2 features
Location of N-linked glycosylation sites (Y) are indicated for each protein at corresponding positions. The N-linked glycosylation site colored in grey is observed only in genotype 1b and 6, while the black ones can be found among different genotypes. The hypervariable regions of E2 are highlighted in light red, stem and transmembrane domain (TMD) are labeled accordingly. The PDB ID and the related construct design for the different crystal structures are given.

Despite these conservations, the E1 and E2 coding regions represent one of the most divergent parts of the HCV genome. Especially the E2 ectodomain (AA 384 – 661) has a high degree of genetic

diversity, mostly within its three hypervariable regions: hypervariable region 1 (HVR1, AA 384 – 411), hypervariable region 2 (HVR2, AA 460 – 485) and the so called intergenotypic variable region (igVR or HVR3, AA 570 – 580). Those HVRs differ up to 80 % between HCV genotypes and even between subtypes of the same genotype (Weiner *et al.*, 1991; Simmonds, 2004). Within these variable regions HVR1 displays the greatest genetic diversity between functional isolates and contain dominant neutralizing epitopes (Shimizu *et al.*, 1994; Zibert, Schreier and Roggendorf, 1995; Keck *et al.*, 2016). In part this diversity is driven by immune evasion (Brown *et al.*, 2007). Some functions of HVR1 have been proposed due to diverse studies. These include its involvement in binding to key HCV cell entry receptors and acting as an immune decoy to prevent effective antibody neutralization (von Hahn *et al.*, 2007; Bankwitz *et al.*, 2010, 2014).

1.4.1.1 Structural elucidation of E1 and E2 glycoproteins

An important step towards understanding the structure and function of HCV glycoproteins was achieved with the publication of the first crystal structures available for these proteins. In 2013 and 2014 two research groups independently determined the structure of the so called E2 ectodomain core. In the approach by Kong and co-workers a truncated version of the E2 protein from genotype 1a (strain H77) was expressed in mammalian HEK293F cells. This protein comprised the central core region (AA 384 – 645) in complex with the neutralizing antibody AR3C (Boivin, Kozak and Meijers, 2013). Since flexible regions and glycans can deter protein crystallization, various glycosylation sites and flexible parts like HVR1 were deleted within this construct. Besides, HVR2 was replaced by a flexible linker leading to crystals diffracting to 2.64 Å (PDB ID 4MWF; Kong *et al*. 2013). The second structure was solved by Khan and co-workers. They used enzymatically deglycosylated E2 from genotype 2a (strain J6) produced in HEK293T GnTI$^-$ cells by a lentiviral expression system. This shorter fragment, also named E2 core, lacking the first 72 AA from the N-terminus (AA 456-656) crystallized in complex with the non-neutralizing Fab 2A12 with diffractions to 2.4 Å (PDB ID 4WEB; Khan *et al*. 2014). Moreover, both groups truncated their E2 core (E2c) variants at the C-terminus thereby removing the stem and TMD. Since such hydrophobic, membrane-associated sequences can cause problems during crystallization, they have been removed in essentially all viral membrane envelope protein structural determinations (Sabahi *et al.*, 2014). Both E2c structures are depicted in Figure 1.8 as cartoon diagrams of the individual structures (B) and as topology diagrams (C). Besides, a superposition of both structures is shown in Figure 1.8 A.

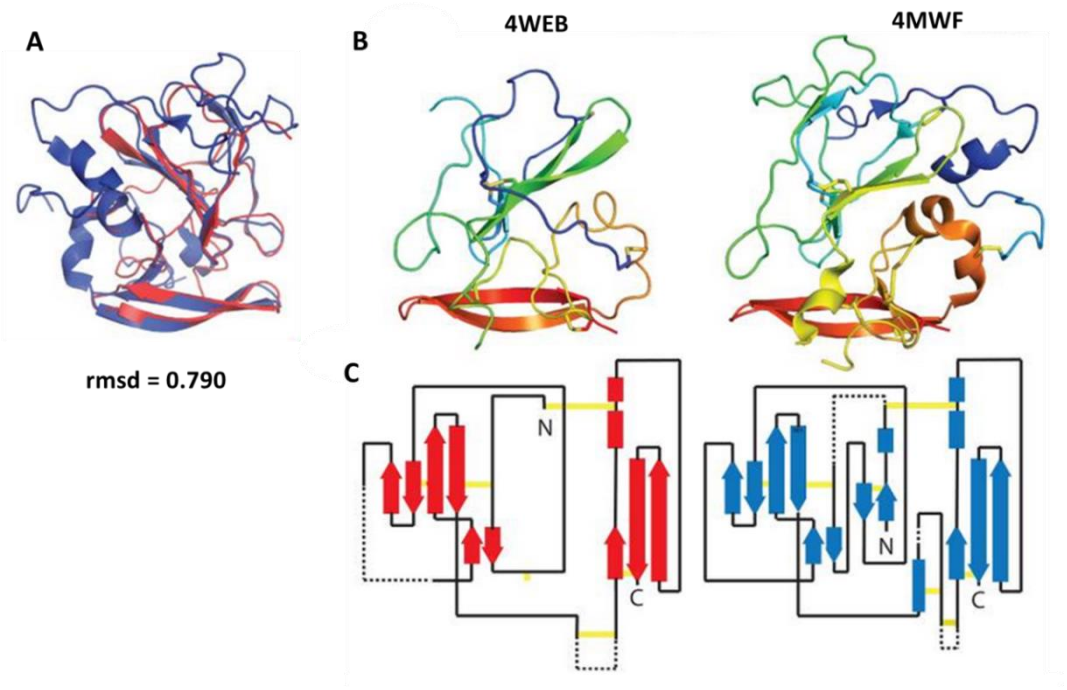

Figure 1.8: E2 core structures 4WEB and 4MWF
A: Superposition of E2 core from PDB ID 4WMF and 4WEB. B: Cartoon diagram of individual core structures. C: Topology diagram of the core domain, highlighting secondary structure and disulfide bonds (yellow) (Khan, Miller and Marcotrigiano, 2015).

The core domains of both structures are highly similar with a root mean square deviation (rmsd) of less than 0.8 Å for similar carbon α atoms (Khan *et al.*, 2014). They comprise a compact, globular architecture with a more basic front layer and a more hydrophobic back layer, but also many regions with no regular secondary structure. The front layer contains an immunoglobulin (Ig)-like β-sandwich stabilized by two disulfide cross-links. Such a motif consisting of a central β-sandwich is typically found in domains I, II and III of class II viral fusion proteins (Kielian 2006; Kielian and Rey 2006). While the back layer contains a second β-sheet with a novel fold roughly perpendicular to the plane of the central β-sandwich. The CD81 binding site is located at the interface of these two layers.

A rough outline of the positions of HVR1 and HVR2 and of the C-terminal region of the E2 ectodomain, that were missing in the crystal structures, were obtained by negative stain cryo-EM by Kong and co-workers (Kong *et al.*, 2013). Besides, it was used to further analyze CD81 binding. Combined with previous mutational studies it could be demonstrated that binding to CD81 is mediated by the loop connecting the inner and outer sheets of the β-sandwich. This exposed loop constitutes the composite CD81 binding site together with two segments that were distant to each other in the primary structure (Owsianka *et al.*, 2006; Rothwangl *et al.*, 2008; Kong *et al.*, 2013). The CD81 binding loop is stabilized by the co-crystallized Fab fragment in 4MWF, but disordered and solvent exposed in 4WEB. Combined with the observation that the disulfide connectivity in the two

reported structures is the same except for one disulfide bond, this highlights the conformational flexibility of HCV E2.

Further insights into the structural organization of neutralizing epitopes within E2 have been derived from co-crystallization experiments of Fab fragments originating from neutralizing antibodies in complex with peptides of their respective epitopes (Pantua *et al*. 2013; Kong *et al*. 2012; Potter *et al*. 2012; Krey *et al*. 2013; Deng *et al*. 2013). Furthermore, more recent studies with different antibodies in complex with similar epitope peptides indicate that these epitopes are either conformational flexible or at least adopt two distinct conformations (Kong *et al*. 2016; Deng *et al*. 2014; Keck *et al*. 2016; Li *et al*. 2015; Meola *et al*. 2015). Just recently those distinct conformations were also revealed at the surface of HCV pseudoparticles (HCVpp) and infectious cell culture-derived HCV particles (HCVcc) with antibodies that share contact residues but recognize distinct conformations of the Ig-like domain (Vasiliauskaite *et al.*, 2017). With this it was demonstrated that the structural flexibility within E2 extends beyond the composite CD81 binding site and that also the Ig-like domain undergoes conformational rearrangement.

The N-terminal domain of the HCV E1 ectodomain (nE1; AA 192 – 270) lacking the flexible region from 245 - 259 was determined with 3.5 Å resolution by El Omari and co-workers (PDB ID 4UOI; El Omari *et al*., 2014). The crystal structure reveals a complex network of covalently linked intertwined homodimers that do not harbor the expected truncated class II fusion protein fold, depicted in Figure 1.9 A. The N-terminus of nE1 instead consists of a β-hairpin followed by a long α-helix flanking a three-strand antiparallel β-sheet. The two N-terminal β-hairpins from two monomers are arranged into a non-covalently linked antiparallel β-sheet in what is most likely a domain-swapped formation (Liu and Eisenberg, 2002; Khan, Miller and Marcotrigiano, 2015). It was suggested that the two types of interfaces formed in the dimer may be replaced by an inter domain interface in the monomer, in which the β-hairpin folds back. As a result, E1 may be more compact as observed in the crystal structure (Freedman *et al.*, 2016).

It was discovered that the closest structural homologue to nE1 is a phosphatidylcholine transfer protein (PDB code 1LN2), which binds to hydrophobic ligands such as sterol and lipid like molecules. The superposition of HCV nE1 covalent dimer on its structural homologue by El Omari is depicted in Figure 1.9 B. It reveals that the extended β-sheet matches in part the steroidogenic acute regulatory protein-related transfer domain responsible for binding hydrophobic ligands. This finding is quite interesting as the N-terminal domain of E1 is hypothesized to be responsible for its binding to apolipoproteins (Khan, Miller and Marcotrigiano, 2015; Wang *et al.*, 2017). However, there are some doubts that the nE1 structure determines the native fold of the E1 protein. In fact, it is suggested that the current structure may represent a post-fusion form, as nE1 crystals were obtained at low pH (Khan, Miller and Marcotrigiano, 2015). Besides, the construct used for crystallization was not

validated functionally or immunologically. Aside from that it was shown that E1 on virions is in a homotrimeric state leading to the suggestion that E1E2 heterodimers form trimers with a hetero-hexamer core constituted by E1 (Falson *et al.*, 2015). Moreover, it is thought to be more likely that the native E1 monomer adopts a structure similar to that of the structural homologue. In fact, using Rosetta "ab initio" modeling for extending the structure in presence of E2, Freedman and co-workers observed structural similarity between both proteins that prolongs even further than observed with the crystal structure. Furthermore the structural homology persists even beyond the sequence homology between those two (Freedman *et al.*, 2017).

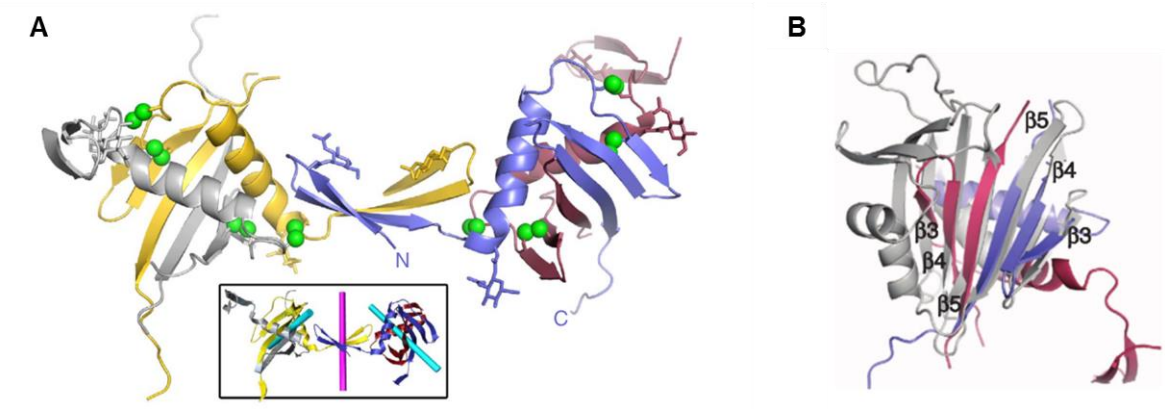

Figure 1.9: Structure of nE1 4UOI
A: Cartoon diagram of nE1 as a dimer of dimers with each monomer colored differently. Sulphur atoms forming disulfide bridges are shown as green spheres and sugar moieties as sticks. The box underneath shows the twofold axis at covalent and non-covalent dimer interfaces in cyan and magenta, respectively. B: Superposition of nE1 covalent dimer (red and blue) on human phosphatidylcholine transfer protein (grey). Structures are presented in cartoon rendering (El Omari *et al.*, 2014).

Based on these partial crystal structures for both envelope glycoproteins, combined with additional experimental data, two independent in silico models of the E1E2 heterodimer structure were recently proposed. Castelli and co-workers made predictions for the fully glycosylated ectodomain of the E1E2 heterodimer (Castelli *et al.*, 2017), whereas the model of Freedman and co-workers comprise the full-length E1E2 heterodimer and its higher-order structure (Freedman *et al.*, 2017), depictured in Figure 1.10. These models combine diverse available data in a valuable way and can therefore further increase our understanding of the nature of the HCV glycoproteins. However, they cannot surrogate structural investigations of the heterodimer for instance by x-ray crystallography. Hence, a complete picture of the E1E2 protein complex is still missing.

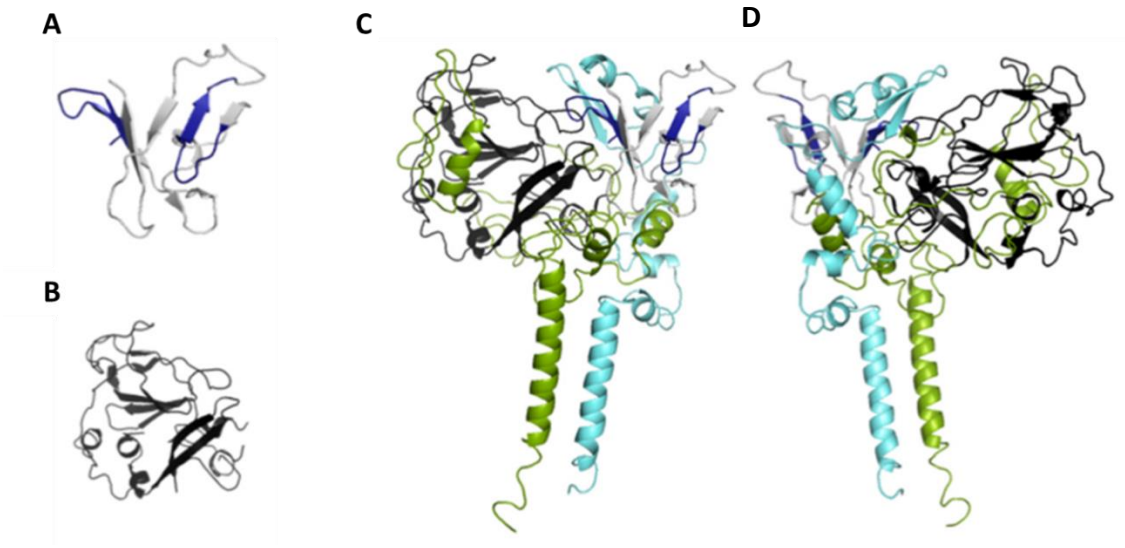

Figure 1.10: Full-length E1E2 heterodimer model with E1 and E2 structures used for model building
A: nE1 model with residues modeled after the structure reported under PDB ID 4UOI shown in dark blue and those based on homology to the structure reported under PDB ID 1LN2 in gray. B: The part of the nE2 model taken from the crystal structure reported under PDB ID 4MWF. C - D: Full-length model of the E1E2 heterodimer in back (C) and front view (D) with the same color scheme used for the regions in A and B; additional parts of E1 are colored in cyan and in green for E2 (Freedman *et al.*, 2017).

1.4.2 HCV Treatment and vaccine development

Until 2011 the available treatment options for HCV infection were limited to interferon (IFN)-based therapies in combination with ribavirin, which are associated with side effects and suboptimal response rates (Haid *et al.*, 2012). Through a combination of compound screening and rational drug design, small molecules with potent activity against various HCV enzymes were discovered that paved the way for a cascade of new direct-acting antivirals (DAAs). The first generation DAAs licensed for use in HCV genotype 1 infection, telaprevir and boceprevir, target the viral protease NS3-4A and thereby prevent polyprotein cleavage and virus replication (Ghany *et al.*, 2011; Pawlotsky *et al.*, 2015). However, they must be administered combined with pegylated interferon alpha (PegIFN-α) and ribavirin. This combination was associated with severe side effects that often led to early termination of therapy (European Association for Study of Liver, 2014; Gogela *et al.*, 2015). Hence the development of additional HCV DAAs that address one of the three viral targets, the NS3-4A protease, the viral phosphoprotein NS5A, and the RNA-dependent RNA polymerase NS5B, has occurred rapidly. These second generation DAAs can eliminate the virus and cure infection, because HCV does not stably integrate into the host cell genome. By this development there are currently highly efficacious and well-tolerated treatments for the entire spectrum of HCV genotypes available (Gogela *et al.*, 2015; Pietschmann, 2017).

Despite these enormous achievements some challenges remain. First of all, these drugs are quite expensive, especially for most countries with moderate to high HCV prevalence. Besides, they do not

protect against reinfection after successful therapy. This is especially of relevance for high risk groups. Last but not least the majority of infected patients are not diagnosed. As a result, less than 5 % of the world's HCV-infected population is aware that they are infected (Gravitz, 2011; Holmberg *et al.*, 2013). Those people will not receive any treatment and the risk for transmitting the infection to others remains. These challenges highlight the need for a prophylactic vaccine against HCV. However, this approach remains elusive despite extensive research in this area. The major challenges for vaccine development are the genetic diversity of the virus and its numerous mechanisms for evading immune response, facilitating viral persistence (Houghton and Abrignani, 2005). Furthermore, the narrow host tropism of HCV for humans hampers vaccine development with chimpanzees being the only fully immunocompetent animal model experimentally susceptible to HCV infection (Pfaender *et al.*, 2017).

1.5 Recombinant expression of glycoproteins

The beginning of heterologous protein expression started in the early 1970s with the development of recombinant DNA technology (Cohen *et al.*, 1973). Since then, many improvements led to rapid progress in this field. Today proteins can be modified in various ways via recombinant expression making it a very powerful tool in the field of biotechnology. It is not only possible to create mutated and truncated proteins, but also to fuse them with markers for identification, purification or improved solubility (Arnau *et al.*, 2006; Malhotra, 2009). Moreover, it enables expression of novel engineered protein species like single chain variable fragment (scFv) antibody variants or chimeric proteins (Carter, 2006; Kontermann, 2010). Next to those diverse genetic modifications, recombinant protein expression also enables overexpression of the target proteins. Combined, this allows the production of high-quality protein with high yields compared to its isolation out of natural sources.

Bacteria are the simplest and most often used expression hosts. Among them *Escherichia coli* (*E. coli)* has evolved to be the first choice in many cases, because of its wide-ranging advantages (Rosano and Ceccarelli, 2014). Firstly, it is very well genetically characterized and easy to manipulate. Secondly, *E. coli* grows in high cell density in low cost media and often leads to high protein yields (Baneyx, 1999). However, as being a gram-negative bacterium *E. coli* lacks an ER and thus the machinery necessary for posttranslational modifications (PTMs) like N-glycosylation. This often results in incorrectly folded non-functional proteins that accumulate in inclusion bodies (Gray and Subramanian, 2001). Therefore, *E. coli* is often not capable to produce higher eukaryotic proteins, especially glycoproteins, leading to the requirement of eukaryotic expression hosts. Heterologous expression in yeasts as *Saccharomyces cerevisiae* and *Pichia pastoris* represents a compromise between prokaryotic and eukaryotic expression. However, one of its major drawbacks for their use for glycoproteins as therapeutics is their lack of human-like glycosylation. Instead yeasts tend to

hyper glycosylate heterologous proteins even at positions that are not glycosylated in the native host (Frenzel, Hust and Schirrmann, 2013). This heterologous glycosylation can influence the activity of recombinant proteins. Besides it can hinder crystallization of glycoproteins thereby limiting the use of X-ray crystallography for protein structure solution (Nettleship, 2012). Human-like glycosylation is often required for full functionality and plays an important role for therapeutic glycoproteins and vaccines. Whereas heterologous glycosylation is a potential source of immunogenicity and thus can cause allergic reactions (Frenzel, Hust and Schirrmann, 2013). Furthermore, many protein interactions like receptor-binding are mediated by their glycans (Cohen, 2015). In fact, 50 % of all human proteins are thought to be glycosylated (Apweiler, Hermjakob and Sharon, 1999), indicating the importance of glycosylation for recombinant protein expression. Human or human-like glycosylation can be achieved in mammalian expression hosts, which will be considered in more detail in the next section.

1.6 Mammalian expression systems

Two of the most common mammalian cell lines used for recombinant expression are Human Embryonic Kidney (HEK) and Chinese Hamster Ovary (CHO) cells. Both cell lines are used for different strategies for the production of recombinant proteins in mammalian cells. While transient expression is frequently used for construct screening in small scale formats in HEK cells, CHO cells are generally used for generation of stable producer cell lines (Almo and Love, 2014). Stable expression enables rapid scale-up in bioreactors and reproducible protein production that is especially needed when it comes to protein production at industrial scale (Bandaranayake and Almo, 2014). However, generation of stable CHO producer cell lines is a significantly more time-consuming task in comparison to plasmid based transient expression (Edros, McDonnell and Al-Rubeai, 2013).

The CHO cell line was first isolated by Theodore Puck in the late 1950`s (Puck, Cieciura and Robinson, 1958) and soon became the predominant mammalian host cell line for stable expression, because of its ability to integrate exogenous DNA with high efficiency (Hoeijmakers, Odijk and Westerveld, 1987). After approval of the first recombinant biopharmaceutical produced in CHO in 1985 (Kaufman *et al.*, 1985), stable CHO cells are nowadays the workhorse for the production of therapeutic antibodies (Kunert and Reinhart, 2016; Voronina *et al.*, 2016). Numerous cellular processes in CHO cells were genetically engineered over the years in order to achieve various desired properties. These include improved glycosylation patterns, proper gene amplification and adaptation to suspension culture, to name just a few.

The cell line HEK293 originates from a primary HEK epithelia cell culture that were transformed with sheared adenovirus type 5 DNA (Russell *et al.*, 1977). Since its development, it has become one of the most commonly used human cell lines for protein production (Bandaranayake and Almo, 2014).

To further improve recombinant protein expression, genetically engineered variants of this cell line have been developed. One of these strains is HEK293-6E that enables episomal replication of expression plasmids by genomic integration of the Epstein-Barr virus EBNA1 protein (Van Craenenbroeck *et al*. 2000; Durocher *et al*. 2002). Accordingly, the expression vector is retained in the nucleus of the host cells leading to semi-stable expression and consequently higher expression yields. Thus, this qualifies this cell line particularly for transient protein production. HEK293-6E cells were used in this work for the transient expression and screening of protein targets by using an optimized protocol published by Jäger and co-workers (Jäger *et al.*, 2013) that is based on the established method by Durocher and co-workers (Durocher, Perret and Kamen, 2002).

Whereas human- or human-like glycosylation is favored for therapeutic proteins, the heterogeneity introduced by glycosylation can hinder crystallization. Therefore, glycosylation deficient mammalian cell lines such as CHO Lec3.2.8.1 or HEK293-GNTI$^-$ cells that only express truncated glycan patterns are employed (Stanley, 1989; Reeves *et al.*, 2002). The glycosylation deficient cell lines SMT_dneo(2)_24 and TE3-B4-H1 (Baser *et al.*, 2015) based on CHO Lec3.2.8.1 cells were used in this thesis to generate cell lines for stable expression of protein targets. An alternative option to mutant cell lines is to inhibit N-glycosylation by glycosylation inhibitors like kifunensine (Elbein *et al.*, 1990), swainsonine (Elbein *et al.*, 1981) or N-butyl-deoxynojirimycin (NB-DNJ). Otherwise expression hosts that exhibit simpler glycosylation patterns like insect cells can be applied for the expression of recombinant proteins.

The Multi-Host expression system was developed for protein expression screening and production in the diverse expression systems routinely used in our facility (Meyer, 2012; Meyer *et al.*, 2013). An overview of the underlying vector and its applications is depicted in Figure 1.11. Next to the already mentioned transient expression in HEK293-6E cells and stable expression in CHO cells, it also incorporates baculoviral-driven expression in insect cells that will be covered in the next section. It is based on the multi-host vector pFlp-Bac-to-Mam (pFlpBtM) that offers all the elements needed for the three mentioned expression systems.

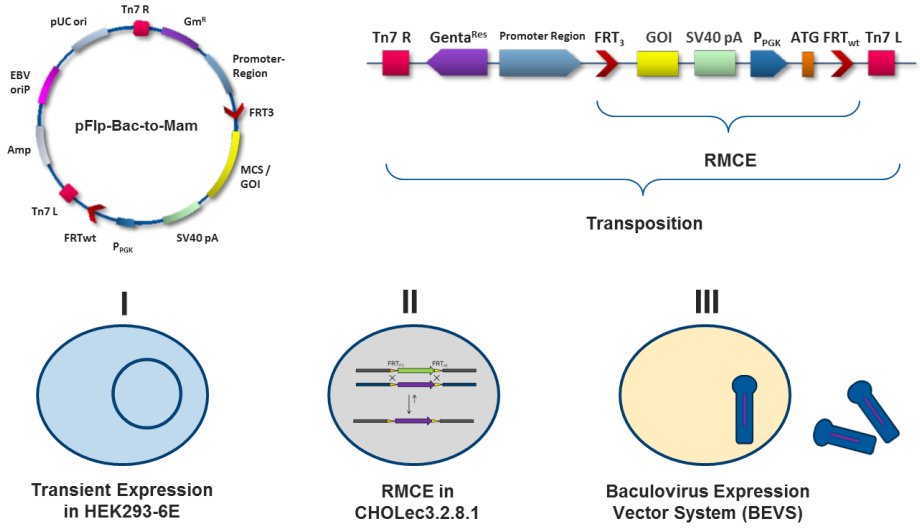

Figure 1.11: Multi-host expression system
The multi-host expression system can be used for construct screening in several expression systems. It is based on pFlp-Bac-to-Mam vectors that contain all necessary elements needed for fast transient expression on HEK293-6E cells (I), fast generation of stable CHO cells via RMCE (II) and is applicable to Tn7 based Baculovirus Expression Vector Systems (III) (Meyer *et al.*, 2013).

1.7 Insect cell expression systems

The first insect cell lines have already been isolated and established more than five decades ago by Grace in 1962 (Grace, 1962). Since then, over hundreds of different insect cell lines have been developed from over hundred different insect species (van Oers *et al.*, 1999; Kumar *et al.*, 2009). The most frequently applied cell lines for recombinant protein expression are the Lepidoptera moths *Spodoptera frugiperda* (*S. frugiperda*) and *Trichoplusia ni* (*T. ni*). The Sf21 cell line (IPLB-Sf21-AE) was isolated from pupal ovarian tissue of the fall armyworm *S. frugiperda* in 1977 (Vaughn *et al*. 1977) and was later adapted to serum-free suspension cultivation. Five years later the Sf9 cell line was described as a subclone thereof at Texas A&M University (Summers, Station and Smith, 1987). In addition to the *S. frugiperda* cell lines, the cell line Hi5 was developed from embryonic tissue of *T. ni*. It was first described in 1984 by Granados and co-workers at the Boyce Thomson institute and was named BTI-Tn5B1-4 (Granados, Derksen and Dwyer, 1986). Since Lepidoptera are the natural hosts for baculoviridae (Blissard and Rohrmann, 1990) the described insect cell lines Sf21, Sf9 and Hi5 are widely used in the Baculovirus Expression Vector System (BEVS) (Summers, 2006). Within BEVS *T. ni* based cell lines are often favored for protein production, because they have a low capacity to produce infective baculovirus particles, whereas *S. frugiperda* cell lines are mostly preferred for amplification of baculovirus (Wilde *et al.*, 2014). Glycoproteins produced in insect cells typically contain paucimannosidic N-glycans that are advantageous for crystallization, since this type of glycosylation is more homogenous, quite simple and thus less flexible (Tomiya *et al.*, 2004; Nettleship, 2012).

1.7.1 Baculovirus expression vector system

BEVS has a broad range of applications. Predominantly it is used for heterologous protein expression in basic and applied research (Jarvis, 2009; Trowitzsch *et al.*, 2010; Scholz and Suppmann, 2017). Lepidoptera cell lines, for instance, are favorable for the production of proteins for crystallization due to their simple glycosylation pattern (Tomiya *et al.*, 2004) and the scalability of virus-dependent expression in suspension culture. Hence, BEVS is predominantly used for protein expression for structural analyses with a share of almost 50 % among all eukaryotic systems based on total number of protein chains deposited in the PDB in 2012 (Meyer *et al.*, 2013). Besides, it is well-suited for producing antigens and virus-like particles (VLPs) for the development of vaccines (Metz and Pijlman, 2011; Vicente *et al.*, 2011) such as the influenza vaccine Flublok™ (Treanor *et al.*, 2011) and vaccines against hepatitis E (Shrestha *et al.*, 2007; Zhang *et al.*, 2015).

The power of BEVS for heterologous protein expression particularly lies in its ability of extreme overexpression driven by very strong late viral promoters (polH, p10) (Sriram, Palhan and Gopinathan, 1997). Those promoters are designated as late promoters because of their onset of transcription in the late phase of infection. Since the corresponding genes are not essential for viral replication they can be replaced by the genes of target proteins (Kuzio *et al.*, 1984; Williams *et al.*, 1989; Summers, 2006). Today there are two different strategies for the generation of recombinant baculovirus that have been developed and commercialized. The Bac-to-Bac (DH10Bac Invitrogen, Multibac and EMBacY (Trowitzsch *et al.*, 2010)) uses Tn7 transposition of the target gene from a donor vector into the baculovirus genome within *E. coli* cells that already carry the virus genome, the so-called bacmid. Recombinant baculovirus is subsequently selected by blue-white screening and the bacmid DNA can easily be isolated and further analyzed for correct gene integration. The BagMagic™ (Novagen) and flashBAC™ (Oxford Expression Technologies) systems generate recombinant baculovirus directly in insect cells by homologous recombination after co-transfection of transfer vector and bacmid DNA (Possee *et al.*, 2008; Hitchman, Possee and King, 2012). With this the flashBAC system is faster compared to Bac-to-Bac and also leads to higher viral stability due to the absence of a putative instable transposon element (Pijlman, 2003). However, the costs of these systems limit their use (Stolt-Bergner *et al.*, 2018), so that baculoviruses produced in the scope of this work were generated by the use of Tn7 transposition.

The major disadvantage is that baculovirus generation is rather time- and work-intensive compared to plasmid-based transient systems. Furthermore, recombinant baculovirus might not remain stable over several rounds of viral amplification. Thus, it can cause problems during scale-up when a large amount of amplified virus is needed that could result in instable virus (Kool *et al.*, 1991; van Lier *et al.*, 1992; Krell, 1996; Pijlman, van Schinjndel and Vlak, 2003). Hence there are recently published approaches that address these problems by using transient plasmid-based gene expression (TGE)

(Shen *et al.*, 2014, 2015; Bleckmann *et al.*, 2015) or the combination of TGE with baculoviral coinfection, the so-called transactivation method (Radner *et al.*, 2012; Bleckmann *et al.*, 2016) that are both predominantly used in terms of construct screening.

1.7.2 Transient plasmid-based gene expression in insect cells

Aside from BEVS, TGE is a promising method for recombinant protein expression in insect cells. It is based on recombinant expression of a suitable transient transfected expression vector. The vector is transported into the cells by the help of the cationic polymer, polyethylenimine (PEI) that is capable of delivering DNA molecules into mammalian and insect cells as charged complexes (Boussif *et al.*, 1995; Meunier-Durmort *et al.*, 1997; Ringenbach *et al.*, 1998; Ogay *et al.*, 2006; Shen *et al.*, 2014). In contrast to BEVS, where the expression is based on strong very late promoters, these promoters cannot be applied in TGE, because they require the viral transcription machinery. In this case baculoviral promoters, which are not dependent on the viral transcription machinery, can be used. Among them, the immediate early and early promoters can be used in insect cells in the absence of baculovirus. The most common used early viral promoter is the *Autographa californica* (Ac) immediate early 1 (IE1) promoter, with or without its enhancer homologous region 5 (hr5) (Guarino and Summers, 1987). While the use of the *Orgyia pseudotsugata* (Op) OpIE1 (Theilmann and Stewart, 1991) and OpIE2 promoters (Theilmann and Stewart, 1992) is more rare. Plasmid-based expression driven by the immediate early OpIE2 promoter in Hi5 cells was recently discovered as a valuable alternative to BEVS (Bleckmann, 2016). An important step in TGE development was the establishing of PEI usage for transfection of insect cells by Ogay and co-workers (Ogay *et al.*, 2006). This protocol was further optimized for Sf9 cells by Shen and co-workers (Shen *et al.*, 2014) and later also for transfection of Hi5 cells (Shen *et al.*, 2015) leading to transfection efficiencies of about 70 % to over 90 %, respectively. With this strategy yields for recombinant protein expression were achieved that lie in the range of expression via BEVS, while expression was much faster, thus representing a valid alternative to BEVS. Based on these strategies a protocol was established in our laboratory that was recently described in Methods in Molecular Biology (Karste, Bleckmann and van den Heuvel, 2017). This method was used for the expression of different viral surface proteins described in this thesis.

1.8 Crystallization of proteins for structure elucidation

The molecular function of a protein is closely linked to its structure. Thus, the determination of protein structures can help to reveal and understand their biological functions. In order for an object to diffract light and hence become visible under magnification, it must be in the size range of the wavelength of the used light. Since visible light has a wavelength of 400 – 700 nm, light microscopy is not sufficient to resolve atomic details of a protein structure in which the typical bond-lengths

between atoms are about 0.15 nm (1.5 Å). The electromagnetic radiation corresponding to the required wavelength falls into the range of X-rays (Egli, 2016). Single molecules in a protein, however, interact only weakly with an X-ray beam. To overcome this problem, a protein crystal with molecules arranged in a repetitive pattern in a defined crystal lattice is needed. The scattering of the X-rays by the electrons of every single molecule in this ordered crystal causes interference effects having two major beneficial consequences: In the case of destructive interference, the diffracted waves cancel each other out and only in the case of constructive interference signals are recorded, leading to discrete spots ("reflections") on the X-ray film or detector. The constructive interference also causes amplification of the diffracted waves by many times and thus makes the reflections technically detectable.

To put it in a nutshell, for structure elucidation by X-ray crystallography, high-quality crystals of the purified protein are needed that can be used to measure the directions and intensities of X-ray beams diffracted by those crystals. This data set is then used to compute the three-dimensional distribution of electrons within the crystal. In the final step this electron density map is interpreted by the crystallographer, which comprises the building of a molecular model explaining the experimentally determined electron density distribution (Rhodes, 2006a).

1.8.1 Protein crystallization

Protein crystallization is in general an unpredictable process that depends on many variables in addition to quality and concentration of the protein sample. External parameters like temperature, pH and composition of the precipitant solution are crucial factors for crystallization so that it often requires extensive screening and optimization to obtain crystals of sufficient X-ray diffraction quality (D'Arcy *et al.*, 2014; Gorrec, 2016). The basic principle of crystallization is the stepwise reduction of protein solubility in a closed system. For this purpose, a protein solution is mixed with precipitants to lower the solubility limit of the protein leading to formation of a supersaturated, metastable solution. Considering a phase diagram, like the one depicted in Figure 1.12, crystallization of proteins in solution follows a two-step process.

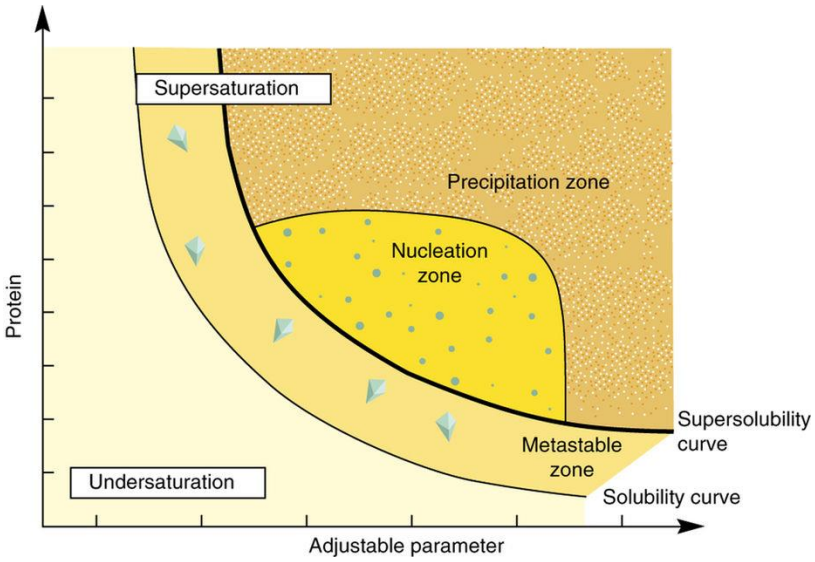

Figure 1.12: Scheme of a protein crystallization phase diagram
In the phase diagram, the different zones for precipitation, nucleation and crystal growth (metastable zone) are shown, assuming the adjustable parameter is precipitant concentration. The solubility is defined as the concentration of protein in the solute in equilibrium with crystals. The supersolubility curve is defined as the line separating conditions where spontaneous nucleation occurs from conditions where the crystallization solution remains clear if left undisturbed (adapted from Chayen 2004).

The first step, called nucleation, is the initial formation of molecular clusters from which crystals start to grow. This involves a transition at which the protein molecules are present in a concentration higher than their solubility level. This supersaturated state comprises the precipitation zone and conditions that support both nucleation and growth (nucleation zone) as well as conditions that only support crystal growth (metastable zone). Due to the attachment of molecules in all dimensions to the very first para-crystalline nuclei, three-dimensional nucleation takes place (McPherson, Malkin and Kuznetsov, 1995, 2000). This results in a reduced local protein concentration so that it drops back into the metastable phase where further crystal growth takes place.

In theory the supersaturated state can be reached by changing various parameters like temperature, salt concentration and addition of polymers or precipitant concentration. In practice, however, usually these conditions are predefined by the use of initial crystallization conditions of commercial screens. Instead, the protein concentration is elevated towards supersaturation via vapor diffusion by using either the hanging drop or the sitting drop experimental set-up, depicted in Figure 1.13.

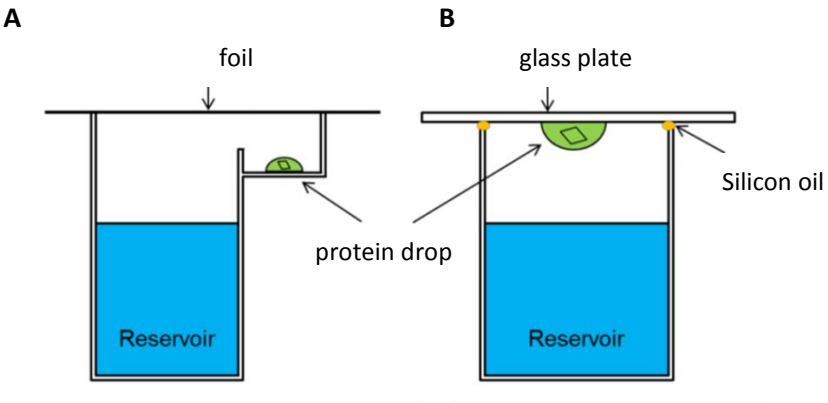

Figure 1.13: Vapor diffusion by hanging and sitting drop methods
The schematic representation of the hanging drop (A) and sitting drop (B) vapor diffusion methods used for crystallization is illustrated.

In both cases the protein drop contains less concentration of the precipitant compared to the reservoir solution. This results in a net transfer of water by vapor diffusion from the protein drop to the reservoir. Thus, the protein concentration in the drop steadily increases until the equilibrium is established. Added polymers further induce molecular crowding by the volume-exclusion effect that leads to the separation of protein molecules and solution (McPherson, 1976; Ingham, 1990). After identifying initial crystallization conditions, a systematic optimization of the conditions that resulted in those hits is usually carried out until high diffraction quality crystals are obtained.

1.8.2 Structure determination by X-ray crystallography

The underlying principle of X-ray diffraction is the interaction of an electromagnetic wave with a crystalline substance. The diffraction is thus dependent on the internal order of the crystal: the more uniform the molecules are arranged within the crystal lattice the higher is the resolution of its diffraction. Lawrence Bragg and his father William Henry Bragg proposed a simple model in which X-rays can be treated as reflections by planes of molecules or atoms instead of considering diffraction by each molecule (Bragg, 1913). This theory provides the basis for Bragg's law:

$$n\lambda = 2d \sin\theta \qquad \text{eq 1.1}$$

With n = integer, λ = wavelength of the incident wave, d = spacing between the planes and θ = diffraction angle between the incident beam and the plane.

The Figure 1.14 depicts the constructive diffraction when the equation of Bragg's law is fulfilled. This rule constitutes that interference can only be constructive when the path difference is equal to integer number of the wavelength ($n\lambda$). When this constructive interference occurs, a diffracted beam of X-rays will leave the crystal at an angle equivalent to that of the incident photon beam that

will be visible as a reflection. From the X-ray diffraction pattern that is generated by these planes crystal parameters can be calculated.

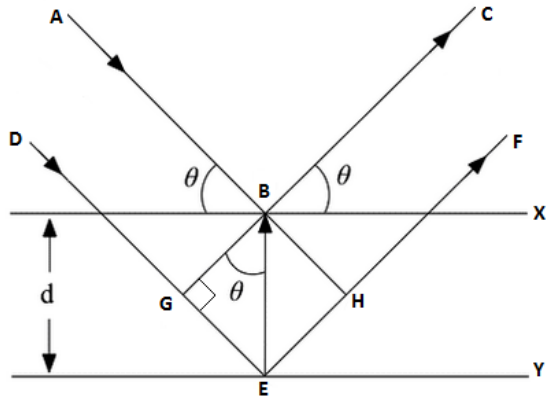

Figure 1.14: Schematic representation of Bragg's law
Two X-ray beams A and D that are in phase strike the planes with an angle θ. The diffracted X-rays can only be constructive when the distance between the paths ABC and DEF is an integer number of the wavelength (figure adapted from www.sciencetopia.net).

The goal of every diffraction experiment is to determine the electron density for all atoms within the crystal. In order to calculate this electron density distribution, information on the intensity and the phases of the reflections are required. The intensities are directly measured by the detector, but there is no technical way to also measure the phase angle, resulting in the so-called phase problem, considered later. The first step of data processing aims at determining the unit cell parameters and the space group of the crystal. The space group defines the internal symmetry of the crystals lattice and thereby describes the reconstruction of the unit cell from its smallest element, the asymmetric unit, by symmetry operations as translation, rotation and reflection. The relative positions of the reflections are used to obtain the unit cell parameters, the orientation of the crystal and to propose the possible space group (Rhodes, 2006b). This allows the attribution of the Miller indices *hkl* for each reflection and furthermore to predict the position of every reflection in the dataset. With this knowledge the data processing software will integrate the data and finally reduce it to obtain one intensity value for each reflection.

The reflections can be described by a structure-factor equation $\mathbf{F_{hkl}}$ that contains the amplitude and phase of the beam diffracted by the different planes in the crystal. The amplitude is proportional to the measured intensities and can be calculated from the obtained data. $\mathbf{F_{hkl}}$ is the sum of contributions from each volume element of electron density in the unit cell. Its Fourier transformation is the representation of the crystal content that precisely describes the mathematical relationship between the object and its diffraction pattern (Rhodes, 2006c). It allows the conversion of a Fourier-sum description of the reflections to a Fourier-sum description of the electron density resulting in equation 2:

$$\rho(xyz) = \frac{1}{V}\sum_h \sum_k \sum_l F_{hkl} * e^{i\alpha_{hkl}} * e^{-2\pi i(hx+ky+lz)} \quad \text{eq 1.2}$$

With ρ(xyz) = electron density at grid point xyz, V = volume of the unit cell, F_{hkl} = amplitude term of complex structure factor $\mathbf{F_{hkl}}$, α_{hkl} = phase angle term of complex structure factor $\mathbf{F_{hkl}}$.

1.8.3 Molecular replacement

The phase information that is lost during data collection can be obtained from an existing similar structure, if available, in a procedure called molecular replacement. It is based on the assumption that the phases of a homologous protein model will provide the estimation of the real phases. For this purpose, it uses the phase from an existing model and combines this with the experimentally obtained structure factor amplitudes of the target protein structure. This method is very efficient, but it can only be employed if the target protein reveals sufficient similarity to an already existing model. After determination of the phases by molecular replacement the initial electron density map is calculated that will be used for model building.

1.8.4 Model building and refinement

After the determination of the phases by molecular replacement, the calculated electron density map is interpreted and a first model is build. The obtained phases are likely to be partially incorrect, which is reflected by errors in the electron density that can be corrected by structure refinement using manual adjustments in real space and by computer software in reciprocal space.

First, the initial model is refined against the experimental data by algorithms implemented in typical refinement programs like phenix.refine. This model is then used as starting point for iterative rounds of manual adjustments and refinement software runs for further phase improvement. The refinement process is monitored among other things through the development of so-called R-factors: R_{work} and R_{free}. These factors represent the correlation between the current model and the experimental data. In order to avoid overfitting of the data 10 % of the reflections are excluded from the refinement and are used in the calculation of the R_{free} value that hence is an unbiased indicator for refinement (Brünger, 1992).

After solving the three dimensional structure of a protein, this structural information can be linked with biological data in order to understand and explain the functioning of the protein.

1.9 Aim of this work

Viral surface proteins are the key players in virus – host interactions. Hence, their recombinant production for structural and functional analyses is an important step for vaccination and structure-based drug design. This PhD thesis deals with the expression and purification of biological active

surface proteins of IAV and HCV for the investigation of their structure and function relations as well as for the generation of new antigens for vaccination.

As described in section 1.3 millions of people suffer IAV infections of the respiratory tract every year in seasonal epidemics since its high genetic variability hinders efficient vaccination strategies. This is why a major emphasis of recent research is focusing on the identification of host cell factors essential for the viral life cycle and on targeting conserved regions of the HA antigen. This thesis therefore aims at the production and purification of different variants of the influenza A surface protein HA in its inactivated pre-fusion state. This paves the way for precise structural investigation of HA activation and provides a first step for novel approaches against IAV by interfering with HA activation.

In order to get deeper insights into HA activation by proteolytic cleavage, structural analysis of the uncleaved, non-modified cleavage loop of HA subtypes with substantial differences in their protease specificity was intended. For this purpose, the most suitable expression host for recombinant expression of three HA subtypes H1, H3 and H7 in their unprocessed non-cleaved form has been evaluated. In the next step the downstream processing for recombinant HA production has been optimized, followed by HA0 crystallization. Besides, a protocol for large scale expression and purification of HA subtype H1 has been developed for application in transfollicular vaccination strategies. For this approach it is not only desired to produce very pure material in large quantities, but the process should also be economic, easy to handle and accessible for a scale-up in bioreactor dimensions.

As described in section 1.4 HCV infections constitute a major global health problem and the need for a prophylactic vaccine against HCV remains. One of the major challenges for vaccine development is the genetic diversity of the virus and its numerous mechanisms for evading host immune response, facilitating viral persistence. Its surface proteins E1 and E2 mediate virus receptor interactions and virus uptake into human liver cells. Besides, they are the targets of neutralizing antibodies that inactivate circulating viruses in vivo. Still, so far no effective vaccine against HCV is available due to the limited broadly-neutralizing activities of these antigens. Therefore, the second part of the project deals with the recombinant expression and efficient purification of new HCV protein variants. First, the most suitable protein constructs and the most qualified expression host was evaluated. Subsequently, the downstream processing was established and the whole production process was optimized resulting in protein yields suitable for biochemical analysis and vaccination studies. Subsequent to secondary structure and glycosylation analysis, the purified E2 variants are applied to further investigation by functional in vitro assays and in vivo vaccination studies by collaboration partners.

2 Materials and methods

2.1 Chemicals, kits and reagents

If not stated otherwise, all chemicals were obtained from the companies Amersham Biosciences, Bayer, Becton Dickinson (BD), GE Healthcare, Gibco, Invitrogen, Life Technologies, Lonza, Macherey-Nagel, Merck, Millipore, New England Biolabs (NEB), Qiagen, Riedel de Haen, Roche, Roth, Sigma-Aldrich, Stratagene and Thermo Fisher Scientific.

2.1.1 Enzymes and molecular weight standards

Enzymes and molecular weight standards used in this work are listed in Table 2-1, Table 2-2 and Table 2-3.

Table 2-1: Restriction Endonucleases

Restriction Endonucleases	Supplier
AvrII (5.000 U/mL)	NEB
BamHI-HF (20.000 U/mL)	NEB
BbsI (5.000 U/mL)	NEB
EcoRI-HF (20.000 U/mL)	NEB
DpnI (20.000 U/mL)	NEB
HindIII-HF (20.000 U/mL)	NEB
KpnI-HF (20.000 U/mL)	NEB
NcoI (10.000 U/mL)	NEB
NcoI-HF (20.000 U/mL)	NEB
Not-I-HF(20.000 U/mL)	NEB
MfeI (10.000 U/mL)	NEB
PacI (10.000 U/mL)	NEB
XhoI (20.000 U/mL)	NEB

Table 2-2: Enzymes

Name	Supplier
Antarctic Phosphatase	NEB
DNAse	SFPR, HZI
EndoH	NEB
Fusion enzyme	Biotool
KOD Hot Start DNA Polymerase	Merck
Phusion® Hot Start II DNA Polymerase	Finnzymes
PNGaseF	NEB
RNase A	Qiagen
SAP (Shrimp Alkaline Phosphatase)	Roche
Taq DNA Polymerase	NEB
Thrombin	SERVA/ GE Healthcare
T4 DNA Ligase	Roche

Table 2-3: Molecular weight standards

Name	Usage	Supplier
Smart Ladder	agarose gel electrophoresis	Eurogentech
PageRuler Plus prestained	SDS-PAGE	Fermentas
PageRuler prestained	SDS-PAGE	Fermentas
Precision Plus AllBlue	SDS-PAGE	BioRad

2.1.2 Antibodies

Antibodies that were used in western blot analysis in this work are listed below in Table 2-4.

Table 2-4: Antibodies used in this work

Antibody	Supplier/source
Mouse IgG1 α-His-Tag	Merck
Mouse α-E2 AP33	prepared by Tanvi Khera at Twincore
Goat α-mouse IgG (H+L)-AP	Promega

2.1.3 Culture media & supplements

Bacterial cultures were grown in Lysogeny-Broth (LB) media (Table 2-5) supplemented with the respective antibiotics or reagents required for selective growth and screening (Table 2-6). For LB agar plates, the LB medium was supplemented with 16 g/L of Bacto-Agar (BD) prior to sterilization. Subsequent to transformation super optimal broth for catabolite repression (SOC) media was used (Table 2-7). All media were heat-sterilized at 121 °C for 20 min. Heat unstable components were sterilized by filtration through a 0.2 µm filter and added after cooling down the autoclaved media.

Table 2-5: LB medium

Composition	Final concentration
Bacto-Tryptone	10 g/L
Yeast extract	5 g/L
NaCl	5 g/L
In H_2O	

Table 2-6: Antibiotics and supplements for bacterial cultures

Name	Final concentration
Ampicillin (Amp)	100 µg/mL
Gentamicin (Gm)	7 µg/mL
Kanamycin (Kan)	50 µg/mL
Tetracyclin (Tet)	10 µg/mL
Bluo-Gal	100 µg/mL
IPTG	40 µg/mL

Table 2-7: SOC medium

Composition	Final concentration
Bacto-Tryptone	20 g/L
Yeast extract	5 g/L
KCl	0,186 g/L
MgCl2	10 mM
NaCl	50 mg/L
Glucose	10 mM
In H_2O	

Cell culture media for insect and mammalian cell lines (Table 2-8) were purchased as ready-to-use solutions. Supplements were added according to Table 2-9 after filtration (0.2 µm).

Table 2-8: Cell culture media

Cell culture medium	Cell lines	Supplier
EX-CELL™ 405	Hi5	SAFC
EX-CELL™ 420	Sf21	SAFC
F17	HEK293-6E	Invitrogen
ProCHO5	CHO Lec3.2.8.1	Lonza
CD Hybridoma	CHO Lec3.2.8.1	Invitrogen

Table 2-9: Supplements

Supplements	Supplier
Fetal Calf Serum (FCS)	Gibco
Fungizon (250 µg/mL)	Gibco
Gentamicin (10 mg/mL)	Gibco
Geneticin G418 (50 µg/mL)	Gibco
Pluronic F68 (100 g/L)	Invitrogen
L-Glutamine (200 mM)	Invitrogen
Phenol red	Sigma
Tryptone N1	Organotechnie S.A.S.
Valproic acid (80 mM)	Sigma-Aldrich

2.1.4 Transfection reagents

The delivery of recombinant DNA to mammalian and insect cells was performed by cationic lipofection techniques. Reagents used for transfection of each cell line are listed below in Table 2-10.

Table 2-10: Transfection reagents

Reagent	Usage	Supplier
Superfect	Bacmid Transfection	QIAGEN
Polyethylenimine (linear, MW ~25 kDa)	Transfection of HEK293-6E and Hi5	Polysciences
Nucleofection solution I	Transfection of CHO	Lonza

2.1.5 Kits

All applied kits were used according to the manufacturer's instructions and are listed in Table 2-11.

Table 2-11: Commercial kits used in this work

Kit	Usage	Supplier
NucleoSpin® Plasmid	Plasmid preparation small scale	Machery-Nagel
PureYield™ Plasmid Midiprep System	Plasmid preparation mid-scale	Promega
QIAGEN Plasmid Giga Kit	Plasmid preparation preparative scale	QIAGEN
NucleoSpin® Gel and PCR Clean-up	Purification of PCR products and extraction of DNA from agarose gels	Machery-Nagel

2.1.6 Columns and Resins for purification

The following columns and resins were used for purification via affinity chromatography (Table 2-12) or size exclusion chromatography (Table 2-13) according to the protocols described in section 2.6.

Table 2-12: Resins used for affinity chromatography

Resin	Usage	Supplier
HisTALON™ Superflow	Purification of His-tagged proteins	Clontech
HisTrap™ excel	Purification of His-tagged proteins	GE Healthcare
Bio-Scale Mini Profinity IMAC Cartridge	Purification of His-tagged proteins	Bio-Rad
His Mag Sepharose™ excel	Small scale purification of His-tagged proteins	GE Healthcare
MagStrep "type3" XT beads	Small scale purification of Twin-Strep-tagged proteins	iba
Strep-Tactin Superflow	Purification of Twin-Strep-tagged proteins	iba

Table 2-13: Columns used for Size exclusion chromatography

Column	Supplier
Superdex 200 16/60	GE Healthcare
Superdex 200 10/300 HR	GE Healthcare
Superdex 200 increase 10/300	GE Healthcare
Superdex 75 10/300 GL	GE Healthcare

2.1.7 Crystallization Screens

For crystallization setups commercial screens and self-prepared screens were used. A list all used screens is summarized in Table 2-14.

Table 2-14: List of crystallization screens used

Screen	Supplier
JCSG+	QIAGEN
PEGs Suite I	QIAGEN
RI	self-prepared
RII	self-prepared
RIII	self-prepared
H1_Grid	self-prepared

2.2 Oligonucleotides and plasmids

All oligonucleotides were synthesized at MWG Eurofins Operon in HPLC purified quality and are listed in Table 2-15.

Table 2-15: Oligonucleotides

Name	Sequence 5'-3'	Use
PCR FAST R (M13)	AGCGGATAACAATTTCACACAGG	Bacmid-PCR (KOD)
PCR FAST F (M13)	CCCAGTCACGACGTTGTAAAACG	Bacmid-PCR (KOD)
NcoI-CoreE1E2_f	GGATCCATGGACCTCATGGGGTAC	PCR - Insert
CoreE1E2-XhoI_r	AGGAGCTCGAGTGCTTCGGCCTGGCCCAAC	PCR - Insert
IgSSCoreE1E2_f	GGATGAATTCATGGACCTCATGGGGTAC	PCR - Insert
IgSSCoreE1E2_r	GGATAAGCTTTGCTTCGGCCTGGCCCAAC	PCR - Insert
EcoRI-sE2_f	GGATGAATTCCGCACCCATACTGTTGGGGG	PCR - Insert
sE2-HindIII_r	GGATAAGCTTGGCGGGCAGGTCCGAGTAAG	PCR - Insert
EcoRI-sE2_dHVR1_f	GGATGAATTCATCCAGCTCGTTAACACCAATGG	PCR - Insert
sE2661_f	GGATGAATTCACGCACCCATACTGTTGGGGG	PCR - Insert
sE2.698_r	GGATAAGCTTGAGGCGGGCAGGTCCGAGTAAGAGC	PCR - Insert
sE2661_r	GGATAAGCTTTCTGTCCTCCAAGTTGCAAC	PCR - Insert
sE2dH661_f	GGATGAATTCGATCCAGCTCGTTAACACCAATGG	PCR - Insert
sE2_661_r	GGATAAGCTTGATCTGTCCTCCAAGTTGCAAC	PCR - Insert
sE2.689_r	GGATAAGCTTGAGGCGGGCAGGTCCGAGTAAGAGC	PCR - Insert
SL-OpIE2-IgGSS_f	CTGTTCGAGGATCCATGGGCTGGAGCTGCATC	
SL-OpIE2-tstrepHis_r	CCTGAGGCCTAGGTTAATGGTGATGGTGATGGTGC	
H1-R326Q-f_CSC	CATTCCGTCCATTCAATCCCAAGGTCTATTTGGAGCC ATTGC	mutagenesis
H1-R326Q-r_CSC	CAATGGCTCCAAATAGACCTTGGGATTGAATGGACGG AATGTTC	mutagenesis
CoreE1E2_seq_for	ACCAATGGCAGCTGGCACATCAA	sequencing
CoreE1E2_seq_rev	GAGGATAATGTCACCAATCC	sequencing
pFlpBtM_seq_for	CGGATCGGGAGATCAGCTTGAAG	sequencing
pFlpBtM_Seq_rev	CAGCCATACCACATTTGTAGAGG	sequencing
CoreE1E2_seq_r	GGATTGGTGACATTATCCTC	sequencing
CoreE1_seq_f	GTTGTCATCCTTCTGTTGGCCGC	sequencing
pTT5_Seq_for	GGCCATACACTTGAGTGACAATGAC	sequencing
pFlpBtM13_seq (for)	GGATCCGAAGTTCCTATTCCG	sequencing

All plasmids generated in this work, used for cloning and for recombinant protein expression are listed in Table 2-16.

Table 2-16: Plasmids

Vectors used for generation of bacmids
pFlpBtM-II-H1, pFlpBtM-II-H3, pFlpBtM-II-H7 (R. Lambertz, HZI) These variants of pFlpBtM-II were used for the generation of recombinant HA(H1/H3/H7)-expressing bacmids via Tn7 transposition. The HA constructs are fused to an IgG secretion signal for secretory expression and they are fused C-terminally to T4 foldon sequence allowing trimerization (see Figure 3.1), followed by pFlpBtM-II derived tags for purification and cleavage sites for removing these parts.
Vectors used for TGE in Hi5 cells
pOpIE2-eGFP-HA (S. Meyer, HZI) This vector was used to monitor transfection efficiencies via TGE in Hi5 insect cells due to eGFP expression upon OpIE2 derived transient expression. **pOpIE2-H1 and pOpIE2-H3** These vectors were used for TGE of HA (H1 and H3) in Hi5 insect cells upon OpIE2 derived transient expression. **pOpIE2-tpa-sE2(1a)wt, pOpIE2-sE2(2a)wt, pOpIE2-sE2(2a)ΔHVR1, pOpIE2-sE2(2a)ΔHVR1-N534A (M. Sommer, HZI)** These vectors were used for TGE of the E2 variants sE2(1a)wt, sE2(2a)wt, sE2(2a)ΔHVR1 and sE2(2a)ΔHVR1-N534A, ending at AA position 661 of the E2 protein (numbering refers to HCV polyprotein) in Hi5 insect cells upon OpIE2 derived transient expression. The constructs are fused N-terminally to an IgG secretion signal for secretory expression and C-terminally to pFlpBtM-III derived tags for purification and cleavage sites for removing these parts.
Vectors used for TGE in HEK293-6E cells
pTTo/GFPq (NRC, BRI, Montreal, Canada) This vector was used to monitor transfection efficiencies via TGE in HEK293-6E cells due to eGFP expression upon CMV derived transient expression. **pcDNA3.1_tpa_E2661-6xHIS (W. Li, HZI)** This vector was provided by Wei Li for recombinant expression of sE2(1a)wt. It contains a CMV promoter for transient expression in HEK cells and comprises the sE2(1a)wt variant, ending at AA position 661 of the E2 protein (numbering refers to HCV polyprotein) with an N-terminal tpa fusion peptide. **pFlpBtM-III-sE2_661, pFlpBtM-III-sE2ΔHVR1_661 and pFlpBtM-III-sE2ΔHVR1-N534A_661** These vectors were used for TGE of the E2 variants sE2(2a)wt, sE2(2a)ΔHVR1 and sE2(2a)ΔHVR1-N534A, ending at AA position 661 of the E2 protein (numbering refers to HCV polyprotein) in HEK293-6E cells upon CMV derived transient expression. The constructs are fused N-terminally to an IgG secretion signal for secretory expression and C-terminally to pFlpBtM-III derived tags for purification and cleavage sites for removing these parts. **pFlpBtM-III-sE2_688, pFlpBtM-III-sE2ΔHVR1_688 and pFlpBtM-III-sE2ΔHVR1-N534A_688** These vectors were used for TGE of the E2 variants sE2(2a)wt, sE2(2a)ΔHVR1 and sE2(2a)ΔHVR1-N534A, ending at AA position 688 of the E2 protein (numbering refers to HCV polyprotein) in HEK293-6E cells upon CMV derived transient expression. The constructs are fused N-terminally to an IgG secretion signal for secretory expression and C-terminally to pFlpBtM-III derived tags for

purification and cleavage sites for removing these parts.

pFlpBtM-III-cE1E2-J6, pFlpBtM-III-cE1E2ΔHVR1-J6 and pFlpBtM-III-cE1E2ΔHVR1-N534A-J6

These vectors were used for TGE of the E1E2 variants cE1E2(2a)wt, cE1E2(2a)ΔHVR1 and cE1E2(2a)ΔHVR1-N534A in HEK293-6E cells upon CMV derived transient expression. The constructs. comprise the last 60 AA of the core protein followed by full-length E1 and E2, fused N-terminally to an IgG secretion signal for secretory expression and C-terminally to pFlpBtM-III derived tags for purification and cleavage sites for removing these parts.

Vectors used for generation of stable CHO cell lines

pFlpBtM-II-H1 and pFlpBtM-II-H3 (R. Lambertz, HZI)

These variants of pFlpBtM-II were used for the generation of recombinant HA(H1/H3)-expressing CHO Lec3.2.8.1 master cell lines employing FRT F_3 and F_{wt} sites (SMT_dNeo(2)_24) via RMCE.

pFlpBtM-II-H1 F13 14 and pFlpBtM-II-H3 F13 14

These variants of pFlpBtM-II were used for the generation of recombinant HA(H1/H3)-expressing binary CHO Lec3.2.8.1 master cell lines employing FRT F_{13} and F_{14} sites (TE3-B4-H1) via RMCE.

Parental vectors

pFlpBtM-II (S. Meyer, HZI)

Second version of multi-host expression and donor vector for transient expression in mammalian cell lines, Tn7 transposition based generation of recombinant bacmids and it also contains FRT sites for RMCE in CHO Lec3.2.8.1 master cell lines employing FRT F3 and Fwt sites. For secretory expression, pFlpBtM-II offers an IgG secretion signal and 8xHis- and Twin-Strep-tags for purification.

pFlpBtM-II F13 14 (B. Baser, HZI)

Variation of the second version of multi-host expression and donor vector for recombinant protein integration into the binary CHO cell line TE3-B4-H1. It contains FRT sites for RMCE in CHO Lec3.2.8.1 master cell lines employing FRT F_{13} and F_{14} sites.

pFlpBtM-III (S. Meyer, HZI)

Third version of multi-host expression and donor vector for transient expression in mammalian cell lines, Tn7 transposition-based generation of recombinant bacmids and it also contains FRT sites for RMCE in CHO Lec3.2.8.1 master cell lines employing FRT F_3 and F_{wt} sites. Besides it can be used in the Acembl system (Trowitzsch *et al.*, 2010) for co-expression through cre/LoxP assembly. For secretory expression, pFlpBtM-III offers an IgG secretion signal and a 8xHis-tag for purification and a BirA ligase for in vitro biotinylation.

pOpIE2-eGFP-HA (S. Meyer, HZI)

This vector was used for recombinant HA and E2 expression via TGE in Hi5 insect cells by replacing the eGFP-HA with the respective constructs.

pcDNA3_DcE1E2-J6 GKp, pcDNA3_DcE1E2/dHVR1 and pcDNA3_DcE1E2delHVR1534 (T. Khera, Twincore, Hannover)

These vectors were provided by the group of Thomas Pietschmann and contain the last 60 AA of the core protein, followed by full-length E1 and E2. They were used for generation of sE2 variants and for cloning of cE1E2 variants into the pFlpBtM-III expression vector.

2.3 Bacterial strains and cell lines

The electro competent *E. coli* strain Top10 was used for plasmid amplification and cloning via electroporation. Chemical competent One Shot® OmniMAX™ 2 T1^R cells were used for sequence and ligation–independent cloning (SLIC) with the Quickfusion Cloning Kit (Bimake). For generation of recombinant bacmids *E. coli* DH10 strains were used, that contain the EmBacY bacmid and a transposase expressing helper plasmid (DH10EmBacY). The genotype of each strain is listed together with its source in Table 2-17.

2.3.1 Bacterial strains

Bacterial strains used in this work are listed below in Table 2-17.

Table 2-17: Bacterial strains

***E. coli* strain**	**Genotype**	**Source**
Top10	F-, *mcr*A Δ(*mrr-hsd*RMS-*mcr*BC) Φ80(*lacZ*) ΔM15Δ*lac*X74 *rec*A1 *ara*D139 Δ(*ara, leu*) 7697 *gal*U *gal*K *rps*L (StrR) *end*A1 *nup*G	Invitrogen
One Shot® OmniMAX™ 2 T1^R	F´ {*pro*AB *lac*I^q *lac*ZΔM15 *Tn*10(Tet^R) Δ(*ccd*AB)} *mcr*A Δ(*mrr hsd*RMS-*mcr*BC) Φ80(*lac*Z)ΔM15 Δ(*lac*ZYA-*arg*F)U169 *end*A1 *rec*A1 *sup*E44 *thi*-1 *gyr*A96 *rel*A1 *ton*A *pan*D	Invitrogen/Thermo Fisher Scientific
DH10EMBacY	F- *mcr*A Δ(*mrr-hsd*RMS-*mcr*BC) Φ80(*lacZ*) Δ(ara, leu)7697 *gal*U *gal*K l- *rps*L *nup*G /BacloxP/ pBADZ-His6Cre/pMON7124	EMBL (Berger)

2.3.2 Cell lines

The following mammalian and lepidopteran cell lines have been used as host cell lines for virus amplification or protein expression in this work.

CHO Lec3.2.8.1 cell lines SMT_dNeo(2)_24 and TE3-B4-H1

Derived from the parental Chinese hamster ovary (CHO) clone Por-5 (ATCC no. CRL 1781) the CHO Lec3.2.8.1 glycosylation mutant cell line was developed (Stanley, 1989) and adapted to grow in suspension. The CHO Lec3.2.8.1 cell lines SMT_dNeo(2)_24 and TE3-B4-H1 were used in the scope of this thesis for the generation of stable cell lines expressing recombinant hemagglutinin. The RMCE master cell line was generated by stable transfection of CHO Lec3.2.8.1 cells with tagging vector pEF-FS-eGFP-FRTwt-Δneo (Sarah Tokarski, HZI). The binary cell line TE3-B4-H1 was generated by tagging of SMT_dNEo(2)_24 with the linearized pEF-F13F14-tdTomato-dpuro vector in order to create a second locus for the integration of recombinant proteins.

HEK293-6E

The parental human embryonic kidney (HEK) epithelial cell line HEK293 was established in 1977 by transformation of a primary cell culture with an adenovirus (Russell *et al.*, 1977). The subclone

HEK93-6E derived from this cell line is adapted to suspension and has a truncated Epstein-Barr nuclear antigen 1 (EBNA1) integrated (Durocher, Perret and Kamen, 2002). It was used within this project for transient gene expression (TGE) of diverse target proteins.

IPLB-SF-21AE (Sf21)

The used insect cell line IPLB-SF-21AE (DSMZ no. ACC 119), short Sf21, was originally isolated form ovary cells of the fall armyworm *Spodoptera frugiperda* (Vaughn *et al.*, 1977). This cell line is adapted to suspension and was used in BEVS for transfection with bacmids, virus amplification and protein production.

BTI-Tn-5B1-4 (Hi5)

The cell line BTI-Tn-5B1-4 is an ovary cell line originating from the cabbage looper *Trichoplusia ni* (Wickham and Nemerow, 1993). It is the subclone of the BTI-Tn-5B-28 cell line commercialised by Invitrogen under the brand name High Five™. According to its high expression rates for many target proteins it is often used as an alternative host for recombinant protein expression with BEVS. Besides, it was used in this thesis for recombinant protein expression via TGE.

2.4 Molecular biological methods

Protocols for molecular biological methods have been adapted from standard collections such as Sambrook 2001. All DNA plasmids were subjected to validation by restriction digestion (2.4.3) and sequencing. Sequencing was performed at the Genome Analytics platform GMAK at the HZI Braunschweig.

2.4.1 Polymerase Chain Reaction (PCR)

PCR was applied for DNA amplification for both cloning and analysis. For standard cloning reactions Phusion® Hot Start II DNA Polymerase (NEB) was used. For analysis of bacmid DNA KOD Hot Start DNA Polymerase was preferred. The standard reactions and standard programs are listed in Table 2-18 to Table 2-19 and Table 2-20 to Table 2-21, respectively.

Table 2-18: Standard PCR reaction with Phusion Hot Start DNA Polymerase

Component	Volume /50 µl reaction	Final conc.
H_2O	33 µL	
5x Phusion HF Buffer	10 µL	1x
10 mM dNTPs	1 µL	200 µM each
Forward-Pr (10 µM)	2,5 µL	0.5 µM
Reverse-Pr (10 µM)	2,5 µL	0.5 µM
template DNA (10 ng/µL)	0,5 µL	
Phusion Hot Start DNA Polymerase (2 U/µl)	0,5 µL	0.02 /µl

Table 2-19: Standard PCR program for Phusion HotStart DNA Polymerase

Program Steps	Temperature	Time	Cycles
Initial denaturation	95 °C	1 min	
Denaturation	95 °C	30 sec	25x
Annealing (adjusted in a range suitable for the primers Tm)	50 °C – 72°C	30 sec	
Extension	72 °C	15-30 s **/1 kb	
Final extension	72 °C	5 min	
Pause	12 °C	Pause	

Table 2-20: Standard PCR reaction with KOD Hot Start DNA Polymerase

Component	Volume /50 µl reaction	Final conc.
H_2O	30 µL	
10x PCR Buffer for KOD Hot Start DNA Polymerase	5 µL	1x
10 mM dNTPs	1 µL	200 µM each
$MgSO_4$	2 µl	1 mM
Forward-Pr (10 µM)	3 µL	0.3 µM
Reverse-Pr (10 µM)	3 µL	0.3 µM
template DNA	1 µL	
KOD Hot Start DNA Polymerase (1 U/µl)	1 µL	

Table 2-21: Standard PCR program for KOD Hot Start DNA Polymerase

Program Steps	Temperature	Time	Cycles
Initial denaturation	94 °C	2 min	
Denaturation	94 °C	15 sec	30–40
Annealing	60 °C	30 sec	
Extension	72 °C	20 sec/kbp	
Final extension	72 °C	5 min	
Pause	12 °C		

2.4.2 Agarose gel electrophoresis

DNA agarose gel electrophoresis was performed with gels comprising 0.8 - 1 % (w/v) agarose in 1x TAE buffer. Prior to use, the agarose was completely dissolved by heating and was supplemented with ethidium bromide (10 mg/ml stock solution) or Roti®-GelStain (Carl Roth; 1.5 µL staining substance per 100 mL gel) after cooling and cast on prepared gel trays. DNA samples were mixed with 6x DNA loading buffer before loading into the sample pockets. After solidifying the gels were run in 1x TAE buffer at 100 V for 30 - 40 min and were subsequently documented under UV illumination at 254 nm using Kodak Gel logic 212 Imaging system.

2.4.3 Restriction digestion of DNA

Amplified gene fragments and cloning vectors were digested with appropriate restriction enzymes from NEB following standard protocols. Briefly, 1 µg of either purified PCR product or plasmid DNA was mixed with 1 µl of both 3' and 5' restriction enzymes in 1x reaction buffer and incubated at 37 °C for 1 h. For plasmid dephosphorylation 1 µl phosphatase was added to digested vector and the reaction was further incubated at 37 °C for 1 h in order to remove the free 5´-phosphate group to minimize relegation of the linearized plasmid. Digested products were loaded on agarose gels and genetic material was extracted from the gel with Gel Extraction Kit (2.1.5) according to the manufacturer's instructions. The concentration of purified DNA was determined by NanoDrop spectrometer.

2.4.4 Ligation of DNA fragments

Ligation of target gene inserts into linearized vectors was carried out using the T4 DNA Ligase and 1x ligation buffer (Roche). The ligation reaction was prepared with 4-fold molar excess of the insert DNA compared to linearized vector together with 1 µl (5 U) T4 DNA ligase. The mixture was incubated at room temperature (RT) for 1 – 2 h or overnight at 4 °C followed by heat-inactivation of the ligase at 65 °C for 10 min prior to transformation.

2.4.5 Preparation of competent E. coli cells

Electro competent cells were used in this thesis for plasmid transformation. For preparation of those competent cells first glycerol stocks of *E. coli* Top10 or XL1 blue were stroke out on non-selective LB-agar plates and incubated overnight at 37 °C. An isolated colony was used to inoculate 40 ml pre-culture and was incubated overnight at 37 °C and 130 rpm. With this pre-culture the main culture of 500 mL – 1 L was inoculated in a 1:100 or 1:50 dilution and grown at 37 °C and 130 rpm until an optical density $(OD)_{600}$ between 0.5 – 1.0 was reached. Then, sterile centrifuge tubes were used to chill the cell suspension on ice for 30 min with occasionally mixing. Centrifugation of the chilled bacterial solution for 10 min at 4 °C and 3000 rpm was followed by a washing step with 500 mL of sterile ice-cold HEPES-glycerol washing buffer (1 mM HEPES, 10% (v/v) glycerol, pH 7.0) per pellet. The washing step was repeated twice. The supernatant of the final wash was removed and the pellet was washed with 20 mL ice-cold sterile 15 % glycerol once, pelleted and then carefully resuspended in 10 mL ice-cold sterile 15 % glycerol. It was aliquoted in sterile Eppendorf tubes, shock frozen in liquid nitrogen and stored at -80 °C.

2.4.6 Transformation of E. coli

Transformation of E. coli was carried out either via electroporation or by heat shock transformation. Electroporation was performed in a 1 mm cuvette using the Gene Pulse™ Controller (BioRad) applying an electric pulse at 25 µF, 200 Ω and 1.8 kV for 5 ms. For this purpose, 50 µL electro competent cells are thawed on ice and transferred to a chilled cuvette containing 2 µL ligation reaction or < 4 ng of purified plasmid DNA. After addition of 1 mL of SOC-medium the cells were incubated for 1 h at 37 °C and 300 rpm. Transformed clones were selected on LB-agar plates with appropriate antibiotic selection.

Chemical transformation was accomplished by heat shock treatment of chemically competent cells. 5 - 10 ng of plasmid DNA was added to thawed cells and incubated for 30 min on ice. A heat shock of 45 s at 42 °C was applied and the mixture was subsequently cooled down on ice for 2 min. 1 mL SOC-medium was added and the cells were incubated for 1 h at 37 °C and 300 rpm. Transformed clones were selected as described above.

2.4.7 DNA preparation and purification

2.4.7.1 DNA gel extraction and purification from reaction mixes

To extract DNA fragments from agarose gels, the NucleoSpin® Gel and PCR Clean-up Kit (Macherey-Nagel) was used according to the manufacturer's protocol. Besides, the kit was used for direct purification of DNA from PCR and restriction digestion samples.

2.4.7.2 DNA plasmid mini and midi preparations

For plasmid isolation in small scale the NucleoSpin R plasmid kit (Table 2-11) was applied. For plasmid in larger scale PureYield Plasmid Midiprep kit (Promega) or Plasmid Giga Kit (Qiagen) was used. Prior to plasmid preparation LB-medium with appropriate selection pressure (antibiotic, Amp) was inoculated with transformed *E. coli* Top 10 cells. These cultures were incubated overnight at 37 °C and 130 rpm. Purifications were performed according to the manufacturers' protocol. Finally, yields and purity of plasmid DNA were measured by spectrophotometry using NanoDrop (section 2.4.9).

2.4.8 Generation and preparation of recombinant bacmids

Isolation of recombinant bacmid DNA was performed according to the MultiBac manual (Bieniossek, Richmond and Berger, 2008) based on the Tn7 transposition method by using the EMBacY bacmid (Trowitzsch *et al.*, 2010). The EmBacY bacmid is a derivative of the Multibac bacmid with an integrated enhanced yellow fluorescence protein-coding gene (YFP) that enables monitoring of virus performance using either fluorescence microscopy or spectrophotometry. The donor vectors used in

this study for Tn7 transposition are pFlpBtM-II based vectors carrying the constructs for HA-expression. The vectors were transformed into E. coli DH10 (EmBacY) cells that already carry the baculovirus genome. Recombinant baculovirus is subsequently selected by blue-white screening and the bacmid DNA can further be analyzed for correct gene integration by PCR. For selection the cells were plated on LB agar plates supplemented with tetracycline, gentamicin and kanamycin, bluo gal and IPTG. After growth, white colonies were picked and streaked out on fresh agar plates to avoid false positives.

After this selection step recombinant bacmids were prepared by inoculation of 3 - 5 mL LB medium supplemented with kanamycin, gentamicin and tetracycline with a single white colony. The culture was incubated at 37 °C and 130 rpm for up to 24 h. 1.5 mL of the culture was then transferred to reaction tubes and centrifuged for 2 min at 13,000 x g and 4 °C. The supernatant was completely removed and the cells were resuspended in 300 µL of the solution P1 (Qiagen), followed by addition of 300 µL lysis solution P2 and gently mixing. After about 5 min incubation at RT the mixture becomes translucent and 300 µL of the neutralization solution P3 was added. The sample was incubated on ice for 5 - 10 min followed by for 10 min at 13,000 x g and 4 °C. The clear supernatant was transferred to a fresh reaction tube containing 800 µL of isopropanol to precipitate the bacmid DNA. The sample was mixed by inverting the tube a few times and was incubated on ice for 5 - 10 min and the centrifuged for 15 min at 13,000 x g and 4 °C. The supernatant was removed, the DNA pellet was washed with 500 µL of 70 % ethanol and it was again centrifuged for 15 min at 13,000 x g and 4 °C. The ethanol was completely removed and the pellet was air dried at RT. Finally, the bacmid DNA was resuspended in 40 µL of TE buffer (5 mM TrisHCl, pH 8.5). The buffers P1-P3 are listed in Table 2-22.

Table 2-22: Buffers for bacmid preparation

Buffer	Composition
Solution P1 (Resuspension, Qiagen)	50 mM TrisHCl (pH 8.0), 10 mM EDTA, 100 µg/mL RNAse A
Solution P2 (Lysis, Qiagen)	0.2 M NaOH, 1 % (w/v) SDS
Solution P3 (Neutralization, Qiagen)	3 M Potassium Acetate (pH 5.5)

2.4.9 Quantification of DNA and protein concentrations

The concentration of DNA and proteins was determined by spectrophotometry with a NanoDrop ND-2000c (Thermo Fisher Scientific) as described in the manufacturers' manual. Nucleic acid concentrations were quantified at 260 nm. Besides, the quality of prepared DNA can be determined by additional measurement of absorption of 280 nm (A280). A280 is the absorption maximum of proteins caused by their aromatic amino acids tyrosine and tryptophane. Hence, the relation between A260 and A280 can be used to assess the amount of protein impurities within each sample. A highly pure sample has a A260/A280 ratio of 1.8 in case of DNA and 2.0 for RNA. Protein

quantifications were carried out with the absorbance of 280 nm accordingly. To relate the absorbance to the actual protein concentration, it had been divided by the molar extinction coefficient of the measured protein according to the Beer-Lambert law. The molar extinction coefficient of each target protein was calculated by Vector NTI.

2.5 Cell culture techniques

2.5.1 Maintaining cells in culture

If not stated otherwise cell lines were maintained as suspension cultures in either TPP Bioreactor tubes at 155 rpm and 25 mm orbit for small scale cultivation or shake flasks ranging from 125 mL (culture volume of 20 – 50 mL) up to 3 L fernbach shake flasks (with culture volume of 1 L) at 110 - 130 rpm on 50 mm orbital shakers. Media and supplements for each cell line were used according to Table 2-8 and Table 2-9. Sf21 and Hi5 insect cells were cultivated at 27 °C in ExCell420 media (Sf21) or ExCell405 (Hi5) media, respectively. Cells were maintained in exponential growth and diluted by passaging to a cell density of 3 - 5 x 10^5 cells/mL every 2 to 3 days. Adherent cultures were grown in 6-well plates in a humidified incubator to prevent evaporation.

HEK293-6E and CHO Lec3.2.8.1 derived cell lines were cultivated in suspension at 37 °C and 100 rpm in humidified atmosphere (95 %) with 5% CO_2. To maintain them in the exponential growth phase, they were diluted by passaging to a cell density of 3 - 5 x 10^5 cells/mL every 2 to 3 days or of 1.5 – 3 x 10^5 cells/mL every 3 to 4 days. Adherent cultures were incubated at 8 % CO_2 and were expanded to larger vessels or transferred to suspension culture when reaching confluency.

2.5.2 Determination of cell count and viability

Cell count and viability was assessed either by trypan blue exclusion method in a Neubauer hemocytometer or by flow cytometry after staining with propidium iodide. In both methods the dye is only able to permeate dead cells so that only dead cells are stained, thus allowing to distinguish between dead and alive cells. While trypan blue binds to intracellular proteins, propidium iodide intercalates with nucleic acids. For manual determination of the cell count and viability the trypan blue exclusion method was applied with 25 µL cell suspension diluted in 75 µL of 0.5 % trypan blue staining solution. Both stained and unstained cells were counted within all four large squares of the hemocytometer and cell density and viability were subsequently calculated with equation 2.1 and 2.2.

$$cell\ density\ [\frac{c}{mL}] = \frac{counted\ cells * 10^4 * dilution\ factor}{number\ of\ large\ squares\ counted} \qquad \text{eq. 2.1}$$

$$viability\ [\%] = \frac{viable\ cell\ density * 100}{total\ cell\ density} \qquad \text{eq. 2.2}$$

The determination of cell count and viability by flow cytometry was performed using a Guava EasyCyte™ Mini System (Millipore). Cell suspensions were diluted 10-fold in PBS and stained with a final concentration of 50 µg/mL propidium iodide for the identification of dead cells.

2.5.3 Cell size determination

The size of cells in suspension is a parameter frequently used in BEVS for identification of successful infection with recombinant baculovirus and was monitored with the CASY Cell Counter (Innovatis). The CASY Cell Counter enables simultaneous readouts for the cell number, the viability and the size of measured cells. The devise uses the principle of electric current exclusion of particles diluted in an electrolyte. While the particles flow through a capillary, they pass an electrical field, which induces a resistance that is proportional to the size of each particle. Since the intact membrane of living cells exhibits a significantly higher resistance compared to dead cells, it can also be used for viability determination. The device was used according to the manufacturer's guidelines after the samples were diluted in an isotonic, particle pure buffer.

2.5.4 Analytic flow cytometry

The flow cytometry is, in comparison to the electrically-based CASY technology, a laser-based high-throughput real time measurement technology that allows cell counting, cell sorting and fluorescence detection. Within this method cell suspension samples are aspirated into a capillary in a liquid stream and the optical response is recognized. The cell size is measured by a detector in line of the beam (forward scatter), whereas granularity (side scatter) and fluorescence is simultaneously determined by perpendicular detectors. The data is directly analyzed by associated software and presented either as histograms or two-dimensional scatter plots. Besides, clusters of cells with similar properties can be defined through a gate which enables to mark certain subpopulations for evaluation purposes. Thereby, for instance determination of transfection efficiencies or viability is possible on the basis of the number of eGFP-positive cells or cells stained by propidium iodide, respectively.

In this work the Guava EasyCyte Mini System (Millipore) was used for flow cytometric analysis. Its incorporated 488 nm diode laser allows the excitation of samples and 3 band pass filters can be selected for the detection of fluorescence emission signals (525/30 nm (green), 583/26 nm (yellow) and 680/30 nm (red)). Flow cytometry was mainly used for the determination of cell count, viability (see section 2.5.2) and efficiencies of both transfection and infection with recombinant baculoviruses (section 2.5.5 - 2.5.6 and 2.5.7 - 2.5.8).

2.5.5 Transient transfection of HEK 293-6E cells with PEI

Transfection of serum-free cultivated HEK293-6E cells was performed using the optimized protocol by Jäger and co-workers (Jäger *et al.*, 2015) based on the protocol of the National Research Council of Canada (NRCC). The cells were transfected in their exponential growth phase at a cell density of 1.5 – 2.0 x 10^6 cells/mL using linear 25 kDa polyethylenimine (PEI) (Polysciences) with a 1 : 2.5 DNA : PEI ratio. The transfected DNA comprised a mix of 95 % expression vector and 5 % of pTTo/GFPq allowing monitoring of transfection efficiency. The transfection mix was prepared with 1 µg DNA mix and 2.5 µg PEI per mL culture, each diluted in 1.5 mL supplemented F17 medium. The DNA : PEI mixture was incubated for 15 min at RT to allow complex formation before it was added to the HEK293-6E cells.

2.5.6 Transient transfection of Hi5 insect cells with PEI

For transient transfection of Hi5 insect cells with linear 25 kDa PEI a protocol was established in our laboratory adapted from the protocol recently described by Shen and co-workers (Shen *et al.*, 2015). The cells were kept in exponential growth phase and were adjusted to a cell density of 5 x 10^6 cells/mL by centrifugation and media exchange prior to transfection. Transfection was performed with a DNA : PEI ratio of 1 : 4 with 1 - 2 µg DNA per 1 x 10^6 cells. In order to monitor transfection efficiency, the used DNA comprised a mix of 95 % expression vector and 5 % of pOpIE2-eGFP. The DNA mix was directly added to the suspension culture followed by the addition of PEI. Suspension cultures were then incubated for 3 – 4 h at 100 rpm and 27 °C. Afterwards suspension cultures were diluted to a cell density of 1 x 10^6 cells/mL with pre-warmed (27 °C) ExCell 405 medium at 110 – 130 rpm.

2.5.7 Transfection of adherent insect cells for baculovirus generation

To generate recombinant viruses adherent Sf21 cells were transfected with recombinant EMBacY-bacmids (2.4.8). For transfection Sf21 cells from a culture supplemented with 5 %FCS were seeded on 6-well plates with a density of 0.75 - 1 × 10^6 per well. After adhesion the cells were transfected with 5 µg bacmid DNA in a solution of 100 µL ExCell420 without FCS and 10 µL SuperFect. The solution was incubated for 10 min at room temperature and then diluted with 600 µL ExCell420 containing 5 % FCS before addition onto the cells. After 2 h incubation the transfection mixture was replaced by fresh medium containing FCS. The successful transfection was evaluated with a fluorescence microscope (Evos, PeqLab). The supernatant containing the first-generation virus was harvested 5 – 7 days post transfection.

2.5.8 Virus amplification

To amplify first generation virus harvested from transfection supernatants, Sf21 cells were seeded with a density of 0.5 × 10^6 cells/mL in 50 -200 mL serum free ExCell420 and infected with 10 - 20 % (v/v) transfection supernatant. The infected suspension culture was incubated at 100 rpm and 27 °C up to five days. Cell number, viability and diameter were determined every 24 h. Besides, the number of fluorescent cells was measured at the Guava flow cytometer in order to further monitor the infection process. The supernatant was harvested at a viability of approximately 80 % and after showing a significant increase in diameter through centrifugation for 15 min at 5000 rpm. The cleared supernatant was subsequently sterilized by filtration using a Stericup vacuum system (Millipore) with a 0.45 µm filter and stored at 4 °C until further use.

2.5.9 Cryoconservation of baculovirus-infected insect Cells

To prevent a loss of infectivity during long-term storage, the virus was preserved using the method of baculovirus infected insect cells (BIIC) (Wasilko and Lee, 2006). For BIIC preparation 200 – 300 mL of a Sf21 suspension culture with a density of 1 x 10^6 cells/mL with an estimated multiplicity of infection (MOI) of 3 and cultivated at 27 °C and 100 rpm. When a significant increase in cell diameter was observed at 24 hpi, the cells were harvested by centrifugation for 4 min at 180 × g. The infected cells were subsequently resuspended in ExCell420 supplemented with 10 % DMSO and 45 % conditioned medium in a concentration of 1 × 10^7 cells/mL followed by aliquotation in cryo vials (Nunc). The aliquots were cooled down to -80 °C with a constant rate of -1 °C per minute in a special freezing container (Nalgene). After 24h the cryo vials were transferred into the gas phase of a liquid nitrogen tank for long-term storage.

2.6 Protein Production and Purification

2.6.1 Plasmid based transient protein expression in HEK 293-6E cells

Transfection of HEK293-6E cells was carried out according to Section 2.5.5. Transfection efficiency was monitored daily using flow cytometry (2.5.4). Besides, cell number and viability were observed every 24 h (2.5.2). 48 h post transfection (hpt) the culture volume was doubled by adding fresh F17 medium. Additionally, the culture was supplemented with tryptone (TN1) to a final concentration of 0.5 %. At 72 hpt supplementation of glucose (final concentration of 4.5 g/L) was carried out in order to avoid nutrient depletion. Finally, if stated, 96 hpt 3.75 mmol/L valproic acid was added at 96 hpt to boost expression rates in the stationary phase of the culture (Backliwal *et al.*, 2008). Cultures were harvested 72 – 168 hpt at 4.000 rpm in a bench top centrifuge. The culture supernatants were

pooled and supplemented with 0.1 % sodium acid for storage at 4 °C. If the cell pellets were needed those were washed with 1x PBS pooled in one Falcon tube and stored at -20 °C.

2.6.2 Plasmid based transient protein expression in Hi5 insect cells

Transfection of Hi5 insect cells was carried out according to Section 2.5.6. Transfection efficiency, cell number and viability were monitored daily using flow cytometry and microscopy (2.5.4, 2.5.2). 48 hpt the culture volume was increased according to the cell number to maintain the culture in logarithmic growth phase. The supernatants were harvested 72 – 96 hpt by a first centrifugation step at 200 x g for 5 min followed by a second centrifugation step at 5000 x g for 10 min. The culture supernatants were pooled and supplemented with 0.1 % sodium acid for storage at 4 °C. If the cell pellets were needed those were washed with 1x PBS, pooled in one Falcon tube and stored at -20 °C.

2.6.3 Protein expression in insect cells using BEVS

The virus amplification prior to protein expression was carried out as described in 2.5.8. For protein expression Sf21 or Hi5 insect cells were seeded in suspension cultures with an initial cell density of 1x 10^6 cells/mL and were subsequently infected with 10 - 20 % (v/v) of virus stock. Infection kinetics were monitored every 24 h by determining cell count, cell diameter and percentage of fluorescent cells. Samples of the culture supernatant were taken for analysis and stored at -20 °C until further use. The supernatant was harvested 72 – 96 hpi by centrifugation once at 5000 x g or in two steps (5 min at 200 x g, followed by 10 min at 5000 x g) depending on further purification strategy. The supernatants were pooled and supplemented with 0.1 % sodium acid for storage at 4 °C. If the cell pellets were needed those were washed with 1x PBS pooled and stored at -20 °C.

2.6.4 Protein production in stable CHO cell lines

For test expressions in CHO producer cell lines cultures were expanded and cultivated for 3 - 5 days in shaker flasks. Culture supernatants or cell pellets were typically harvested at 2000 x g for 10 – 20 min or at 4.000 rpm in a bench top centrifuge using 50 mL Falcon tubes. Cell pellets were further washed with 1x PBS transferred to a 50 mL Falcon tube and centrifuged again at 4000 rpm. Culture supernatants were supplemented with 0.1 % sodium acid and stored at 4 °C. Cell Pellets were stored at -20 °C.

2.6.5 Cell lysis of HEK 293-6E, Sf21 and Hi5 cells

Pellets of 1x 10^6 cells/mL were resuspended by vortexing with ice cold lysis buffer, incubated on ice for 15 min. Afterwards the mixture was centrifuged at 16,000 x g for 15 min to separate the soluble and insoluble fractions. The samples were stored at -20 °C or directly used for analysis.

2.6.6 Trichloroacetic acid (TCA) precipitation of proteins

To preliminary test protein expression in stable CHO producer cells TCA precipitation was used to concentrate the protein for Western blot analysis. 1 mL of culture supernatant or total cell lysate was mixed with 100 µL of 100 % TCA, incubated on ice for 30 min and centrifuged at 13000 x g and 4 °C for 15 min to pellet the precipitated protein. The protein pellet was washed in 1 mL of ice-cold 70 % ethanol followed by 5 min centrifugation at 13000 x g and 4 °C. The protein pellet was dissolved in 50 µL water and 50 µL 2x Laemmli buffer, heated for 5 min at 95 °C for denaturation and then the sample was analyzed by SDS-PAGE (2.7.1).

2.6.7 Dialysis and diafiltration

Dialysis was performed for buffer exchange of small volumes (< 50 mL per sample) by using dry Spectra/Por® dialysis tubes (Spectrum Laboratories Inc., Rancho Dominguez, California, USA) with a MWCO depending on protein size. Prior to use, the tubes were soaked in the desired exchange buffer. Dialysis was conducted at 4 °C with slow stirring of the buffer with up to 10-fold volumes of exchange buffer compared to the volume of the original sample. Larger samples were buffer exchanged by diafiltration with the KrosFlow® research IIi TFF system. Prior to use the 10 % storage ethanol was removed from the MidiKros column and the system was cleaned with at least 500 mL MilliQ water to remove residual ethanol. Afterwards the complete system was filled with buffer and approximately 200 mL of the cell culture supernatant was placed into the concentrate reservoir. The remaining cell culture supernatant was connected as feed reservoir. The sample was concentrated down to approximately 50 mL - 100 mL by re-circulation through the system. After concentration of the sample the exchange buffer was connected to the feed reservoir and the concentrated sample was diafiltrated through re-circulation through the system with at least 500 mL exchange buffer. The concentrated and diafiltrated sample was recovered, the system cleaned according to the manufacturers guidelines and stored in 10 % ethanol.

2.6.8 Small scale protein purification with magnetic anti-His beads

His Mag Sepharose™ excel beads (GE Healtchare) were used for small scale protein purification for analytics according to the manufacturers' protocol. 200 µL slurry magnetic beads was equilibrated with equilibration buffer and then used for incubation with 10 ml culture supernatant for at least 4 h with slow end-over-end mixing. Beads were 3x washed with washing buffer and protein was eluted with 200 µL elution buffer after 1 minute of incubation. The eluted protein was then analyzed by SDS-PAGE and western blot.

2.6.9 Small scale Strep-Tactin purification with magnetic beads

MagStrep “type3” XT beads (iba) were used for a first test of reverse Strep-Tactin purification after cleavage with thrombin in order to remove all tagged contaminants in small scale. Purification was performed according to the manufacturers’ protocol. 100 µL slurry (5 % (v/v) beads) magnetic beads was washed and equilibrated with buffer W and then used for incubation with samples from thrombin-cleavage (1 mg protein in 1 mL) overnight with slow end-over-end mixing. The supernatant containing the purified samples was removed and the beads were 3x washed with washing buffer W. For elution sample buffer was added to the beads and the mixture was heated for up to 10 min at 95 °C. The samples were then analyzed by SDS-PAGE (2.7.1).

2.6.10 Affinity chromatography

Purifications of cell extracts or cell culture supernatants were performed with self-packed Mobicol columns (MoBiTec) or an ÄKTA-FLPC unit (GE Healthcare) using commercially available or self-packed columns with the materials and methods listed below. Fractions were collected and analyzed by SDS-PAGE and Western blot (sections 2.7.1 and 2.7.2).

IMAC Profinia

For the purification of His-tagged proteins with the Profinia protein purification system Bio-Scale™ Mini Profinity™ IMAC Cartridges with 1mL bed volume were used. The purification step was followed by desalting of the eluate with Bio-Scale™ Mini Bio-Gel® P-6 Desalting Cartridge with 10 mL bed volume. Pre-programmed methods and the respective buffers were used for the purification and desalting of target proteins.

HisTALON™ Superflow

For the purification of diafiltered cell culture supernatant or Ni-NTA pre-purified proteins 1 – 5 mL HisTALON™ Superflow columns (prepacked or self-prepared) were used. Prior to purification the protein sample was dialyzed against 50mM TrisHCl, 150mM NaCl, pH7.4 and imidazole was added to a final concentration of 10 mM before the sample was loaded with a flow rate of 1 mL/min. The washing step was performed with 10 mM imidazole for 15 CV (ÄKTA-FLPC usage) or until the UV monitor (280 nm) signal decreased to zero (Mobicol usage). The target protein was eluted in a series of 500 µL to 1 mL fractions with elution buffer containing 150 mM imidazole for up to 10 – 20 CV by ÄKTA-FLPC usage or until the UV signal significantly decreased (Mobicol usage).

HisTrap™ excel

HisTrap™ excel material was used for the purification of his-tagged proteins directly from the supernatant with 1 or 5 mL columns. Prior to use the columns were equilibrated with buffer

containing 20 mM sodium phosphate, 0.5 M NaCl, pH 7.4 before the sample was loaded with a flow rate of 1 – 5 mL. This was followed by a washing step of 20 CV with wash buffer containing 30 – 75 mM imidazole. Elution was performed with 500 mM imidazole for up to 10 – 20 CV.

Strep-Tactin Superflow

Strep-Tactin superflow purification was performed in order to remove tagged contaminants after thrombin cleavage. The protein sample is loaded to self-packed columns washed with washing buffer (100 mM TrisHCl, 150 mM NaCl, 1 mM EDTA, pH 8.0), and eluted with 4 mL elution buffer (100 mM TrisHCl, 150 mM NaCl, 1 mM EDTA, 2.5 mM desthiobiotin, pH 8.0) or by boiling the material with loading buffer.

2.6.11 Thrombin cleavage

In order to remove the heterologous trimerization domain, elution fractions were pooled and dialyzed (2.6.7) before thrombin was added in a concentration of 2.5 U/mg protein. Incubation was carried out for 4 - 16 h (overnight). The fusion tag, TEV protease and uncleaved protein were removed by SEC (2.6.13) or reverse Strep-Tactin purification (2.6.9/2.6.10).

2.6.12 Concentration of protein samples with Vivaspin concentrators

Vivaspin concentrators (Sartorius AG) with polyether sulfone (PES) membranes were used to concentrate protein samples and to change buffer in small volumes. For this, protein solutions were centrifuged at 15,000 x g (Vivaspin 500), < 5,000 x g (Vivaspin 20) or < 4,000 x g (Vivaspin 2 and Vivaspin 6) until the desired volume or concentration was reached. Buffer exchange could be performed by refilling the columns with the exchange buffer after concentration. This was done with at least 10 volumes (related to the original sample).

2.6.13 Size exclusion chromatography

Size exclusion chromatography (SEC) is performed for further polishing the affinity-purified proteins and for isolation of distinct oligomeric states with an ÄKTA-FLPC unit. This technique separates molecules on the basis of their differences in size that leads to different retention volumes in the column packed with SEC medium. The SEC media consists of particles with pores of different sizes that allow small molecules to enter the pores thereby retarding them compared to larger molecules. Concentrated protein samples are loaded on Superdex 75 or Superdex 200 columns (list of used columns can be found in Table 2-13) depending on the size of the purified protein. The separation of the protein sample was performed with a flow rate of 0.3 mL/min. Fractions of 0.5 mL were collected and analyzed by SDS-PAGE (section 2.7.1).

2.7 Protein analytical methods

2.7.1 SDS-PAGE

SDS-PAGE (sodium dodecyl sulphate polyacrylamide gel electrophoresis) was used to analyze protein quality and yields under denaturing conditions (Laemmli, 1970). Self-prepared gels were used consisting of a lower resolving gel (10 % or 12 % acrylamide) and an upper stacking gel (5 % acrylamide) (Table 2-23 and Table 2-24). Usually about 12 µL of protein sample was mixed with an appropriate amount of 4 x SDS loading buffer (Table 2-25) and heated for 5 min at 95 °C for denaturation. In case of non-reducing SDS gels samples were prepared with loading buffer without beta-mercaptoethanol and were not heated. For a better resolution, the samples were collected in the stacking gel by an initial run at 120 V for 5 min. Thereafter, the gels were run at 160 V for about 1 h. The SDS gel was subsequently washed 3 x 5 min in H_2O to remove SDS and was then stained with InstantBlue (Expedeon). Additionally, Mini-PROTEAN® TGX™ gels and Criterion™ precast gels (Bio-Rad) were used according to the supplier's protocols. With these gels the electrophoresis was performed at 150 V. The used molecular weight standards are listed in Table 2-3.

Table 2-23: Compositions of SDS-PAGE gels (for eight gels)

Component	12 % Resolving Gel	10 % Resolving Gel	5 % Stacking Gel
Acrylamide/bisacrylamide 30 % (v/v)	12 mL	10 mL	1.5 mL
4× Upper buffer	-	-	2.5 mL
4× Lower buffer	7.5 mL	7.5 mL	-
10 % SDS in H_2O	0.3 mL	0.3 mL	-
H_2O	10.1 mL	12.4 mL	5.9 mL
TEMED	40 µL	40 µL	30 µL
40 % APS	60 µL	60 µL	30 µL

Table 2-24: Buffers for SDS-PAGE

Buffer	Composition
4× Upper buffer	0.5 M Tris/HCl pH 6.8, 0.4 % SDS (v/v)
4× Lower buffer	1.08 M Tris-base, 0.42 M Tris-HCl, pH 8.8
SDS Running Buffer	3 g/L Tris-base, 14.4 g/L Glycine, 1 g/L SDS, pH 8.3

Table 2-25: 4x SDS loading buffer

Component	Final concentration
SDS	7 % (v/v)
Glycerol p.a.	0.22 % (v/v)
Tris/HCl pH 6.8	9.6 mM
Beta-mercaptoethanol	2.4 mM
Bromphenol blue	0.22 mg/mL
In H_20	

2.7.2 Native PAGE

Native PAGE allows the separation of protein samples without denaturation of its secondary structures. The migration is therefore not only influenced by its mass but also by the net charge of the protein surface and its hydrodynamic radius. A slightly negative charge is applied through Coomassie G-250 usage in order to ensure migration to the cathode in the absence of SDS. The NativePAGE™ Novex Bis-Tris Gel System (Thermo Fisher Scientific) was used according to the manufacturer's instructions. The gels had a gradient of 4 to 16 % and the used molecular weight markers were HMW Native (66 - 669 kDa) and LMW Native (14.4 - 97 kDa) standards from GE Healthcare.

2.7.3 Western blot

Western blot analysis was used for the detection of specific proteins or tags with high sensitivity. The blotting was performed with a Trans-Blot-SD device or a Trans-Blot Turbo Transfer System (Bio-Rad) in a semi dry blotting procedure. The SDS gel was washed with water and was then incubated together with two pieces of western blot filter paper in transfer buffer for 10 min. The polyvinylidene difluoride (PVDF) membrane (Immobilon-P, Merck) was briefly hydrated with 100 % methanol and subsequently equilibrated in transfer buffer for 10 min. The transfer was performed for 30 – 40 min at 12 V (Trans-Blot-SD) or for 7 min with the mixed MW program (Trans-Blot Turbo). To prevent unspecific binding, the membrane was blocked by incubation at RT for 1 - 2 h in 10 mL blocking solution consisting of TBS-T-2.5% SMP (TBS-T supplemented with 2.5% (w/v) skim milk powder). The saturated membrane was then washed 3 x for 5 min in TBS-T (20 mM Tris-base, pH 8.0, 150 mM NaCl, 0.05 % (v/v) Tween) and incubated at RT for at least 1.5 h over at 4 °C overnight with 10 mL of TBS-T supplemented with an appropriate amount of the primary antibody. Again, the membrane was washed 3 x with TBS-T before the membrane was incubated with the secondary antibody conjugated to AP (alkaline phosphatase) for 2 h. Prior to detection it was again 3 x for 5 min washed with TBS-T in order to remove unbound secondary antibodies. For AP staining, the membrane was equilibrated for 5 min shaking in AP buffer (100 mM Tris-base pH 9.5, 100 mM NaCl, 5 mM $MgCl_2$). Staining was performed by the BCIP/NBT Color Development Substrate (Promega) with 33 µL BCIP (50 mg/mL)

and 66 µL NBT (50 mg/mL) in 10 mL AP buffer. Antibodies used in western blot analysis are listed in Table 2-4.

2.7.4 Mass spectrometry

MALDI-TOF (Matrix Assisted Laser Desorption Ionization – Time-Of-Flight) mass spectrometry (MS) was used to identify protein fragments of SDS-PAGE samples by tryptic digestion. The corresponding protein bands were cut out of a stained SDS gel and were then transferred into 1 mL H_2O. After tryptic digestion, proteins were co-crystallized with organic acids and desorption of protein fragments was triggered by a UV laser beam. The TOF measurements exposed mass-to-charge ratios of the ions. The results were compared with the MASCOT database to identify the analyzed proteins. For intact mass analyses by ESI (Electrospray Ionization), the buffer of purified protein samples was changed with Vivaspin concentrators (2.6.7) to H_2O in order to remove any salts within the sample. All MS analyses were conducted by the MS platform of the research group Cellular Proteomics (CPRO) at the HZI (Braunschweig, Germany).

2.7.5 Deglycosylation analysis

In order to remove N-glycans of glycosylated proteins, deglycosylation experiments were performed with two different endoglycosidases. Endoglycosidase H (Endo H) is a glycosidase that cleaves within the chitobiose core of high mannose and some hybrid oligosaccharides from N-linked glycoproteins. Whereas the glycoamidase Peptide-N-Glycosidase F (PNGase F) cleaves between the innermost GlcNAc and asparagine residues of high mannose, hybrid, and complex oligosaccharides from N-linked glycoproteins. Deglycosylation analysis was performed according to the manufacturers' protocol both with native and denatured protein samples. Deglycosylation of the different approaches were analyzed after distinct time points by SDS-PAGE (2.7.1).

2.7.6 Thermofluor Buffer Screen

A Thermofluor Buffer Screen was conducted in order to find the optimal buffer conditions for protein samples. The buffer of the protein sample influences protein stability by pH, ion strength and several additives (Newman, 2004). Thermofluor buffer screen, also called thermal shift assay, allows determining the optimal buffer conditions for each protein sample by assessing its melting point (T_m). The principle of this assay is the binding of a fluorescence dye as a function of protein unfolding and temperature, depicted in Figure 2.1. The added dye shows only weak fluoresce in buffer solutions, but its fluorescence increases in a nonpolar environment. A gradual increase of temperature leads to protein unfolding resulting in binding of the fluorescent dye to the hydrophobic protein core. The more the protein unfolds the more dye binds to the protein thereby increasing the fluorescence

(Ericsson *et al.*, 2006; Niesen, Berglund and Vedadi, 2007). Due to this increase in fluorescence by rising temperature the melting-curve can be calculated. If certain buffer conditions increase protein stability, T_m that corresponds to 50 % unfolded protein and is calculated by the apex of the melting curve and the minimum of its first derivative, is elevated.

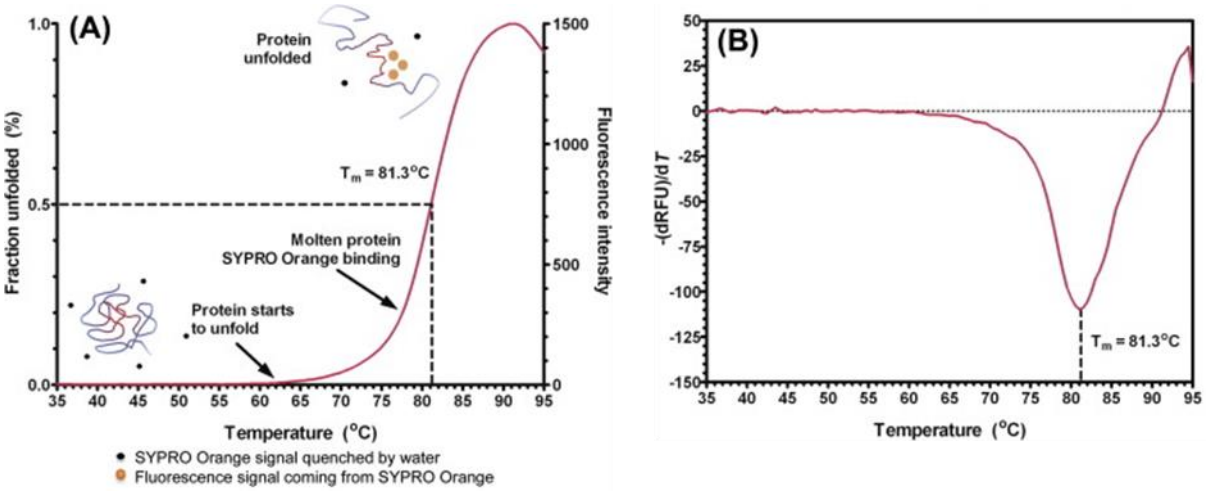

Figure 2.1: Thermofluor thermal denaturation assay
A: Exemplary melting curve with a protein solution heated in the presence of the hydrophobic dye SYPRO Orange. The dye binds to the internal hydrophobic protein core upon denaturation thereby increasing the fluorescence signal. The maximal fluorescence intensity is obtained when the protein is completely unfolded. Subsequently, the SYPRO Orange signal decreases because of dissociation of protein and dye. B: Alternative representation of the melting curve using the first derivative – (dRFU)/d*T* of the raw data. The apex of the melting curve and the minimum of its first derivative represent the T_m that corresponds to 50 % unfolded protein (adapetd by Boivin et al. 2013b).

At first a concentration test is performed to analyze the optimal amount of protein and dye. For this purpose the dye 10x SYBRO Orange (Invitrogen) was diluted from 5000x to 100x, 50x and 10x and the protein sample was diluted to 0.5 mg/ml, 1 mg/ml and 2 mg/ml. A screen was set up on an appropriate 96-well PCR plate with the different protein and dye concentrations. Afterwards the actual measurement with the buffer screen (tested conditions listed in APPENDIX V) was performed. The assay was performed in a real time PCR-system (BIO RAD CFX96 Real-Time System C1000 Thermal Cycler) and results were evaluated with CFX Manager (BIO-RAD).

2.7.7 Dynamic light scattering

Dynamic light scattering (DLS) was used to measure the hydrodynamic radius of the protein sample and its size distribution in solution by scattered laser light. This technique is often used to investigate the homogeneity of a protein sample and judge its potential to crystallize (Zulauf and D'Arcy, 1992). In this thesis it was additionally used as another approach to determine the size and thereby the oligomeric state of protein samples. Prior to the measurements protein samples were centrifuged at 60000x g for 30 min. Then 60 µL of the sample was transferred in a cuvette (UVette® 220-1600 nm;

Eppendorf) that is subsequently inserted in the DynaPro Titan DLS (Wyatt technology). Data points were accumulated over ten seconds, averaged and analyzed by the DYNAMICS software (version 6.10.1.2; Wyatt technology). Up to 20 measurements were carried out to obtain redundant data. The resulting graph and table indicate the percentage of polydispersity (peak broadening) and the average particle size in nm for each determined peak.

2.7.8 Circular dichroism spectroscopy

Circular dichroism (CD) spectroscopy was employed in order to analyze the secondary structure composition of protein samples with a Jasco J-815 CD spectrometer (Jasco, Inc). This technique is widely used for rapid determination of secondary structure and folding properties of recombinant proteins (Greenfield, 2006). The basic principle is the difference in absorption of left-handed and right-handed circularly polarized light (CPL) by chiral molecules. The electrons within a chiral molecule absorb energy and undergo transition to an excited state when it is hit by a circularly polarized wave (Garab and van Amerongen, 2009). The resulting excitation depends on the polarization (left or right-handed), on the wavelength and also on the geometry of the chiral molecule. In proteins the geometry is determined by specific angles of the peptide backbone which allows to analyze the CD spectra between 260 and 180 nm for the different secondary structure components (Johnson, 1990). Each sample was measured at 20 °C in a 0.1 cm path-length cuvette. Spectra were recorded in the range of 190 – 260 nm and 1 nm bandwidth and 4 s digital integration time (D.I.T.). Signal-to-noise correction of each measurement was achieved by recording ten spectra per sample. For buffer-signal correction, a spectrum was recorded with buffer only using the same experimental setup and the identical quartz cuvette. The buffer spectrum was subtracted from the other spectra prior to secondary structure analysis.

2.8 Protein crystallographic methods

2.8.1 Initial screening and crystal optimization

Initial crystal screening was performed by the sitting drop vapor diffusion method using commercially available JCSG+ and PEGs Suite I Screens (Qiagen). The purified protein was used at a concentration of 10 mg/mL. Drops of 200 nl protein and 200 nl buffer were prepared with HoneyBee pipet robot (Digilab Genomic Solutions) on an 96 well Intelli Plate (Art Robinson) with sitting drop method. Crystallization plates were sealed with Quick-Combi Sealer plus (HJ-BIOANALYTIK GmbH) and then transferred into the Rock Imager 1000 (Formulatrix), which enables automatic documentation during storage. All crystallization setups were incubated at 20 °C in the temperature controlled imaging system and screened on a regular basis.

Initial crystals hits were further optimized during several rounds of random screening optimization with the self-prepared screens RI, RII, RIII and H1_Grid. The screens RI, RII and RIII were randomly generated with the software Rock Maker (Formulatrix) on the basis of conditions that yielded first hits by using the Formulator liquid handling system (Formulatrix). In case of H1_Grid only the parameters pH (range of 7.2 – 7.8) and the concentration of the precipitant PEG 550 MME (20 – 30 %) were varied along X-axis and Y-Axis of the 96 well plate. In order to avoid crystal damage after harvesting, the crystals were transferred into a drop containing mother liquor supplied with (2-R, 3-R)-2,3-Butandiol that functions as cryo-protecting agent prior to freezing in liquid nitrogen.

2.8.2 Data collection

X-ray diffraction data of H1 crystal used for structure determination was collected at beamline 14.2 of BESSY II (Helmholtz center Berlin, Germany). The diffraction data of H3 crystal used for structure determination was collected at DESY (Deutsches Elektronen-Synchrotron, Hamburg) beamline P11 at PETRA III.

2.8.3 Model building and refinement

Molecular replacement of H1 and H3 was performed with HA0 crystal structure PDB ID: 1HA0 (Chen *et al.*, 1998). The model building and refinement of H1 was performed by Jörn Krausze (HZI, Braunschweig). In case of H3 the initial model was received by the AutoBuild wizard (Terwilliger *et al.*, 2008) implemented in phenix software. It was further improved by iterative steps of manual building in Coot (Emsley *et al.*, 2010) and refinement in Phenix.refine (Afonine *et al.*, 2012) by help of Peer Lukat (HZI, Braunschweig).

3 Influenza surface protein Hemagglutinin

3.1 Recombinant HA expression in the multi host expression system

Influenza A is a viral infection of the respiratory tract affecting millions of people every year. The infection process is initiated through binding and fusion of the viral envelope to the host cell membrane via the surface glycoprotein HA. Therefore, the HAs, which are produced as inactive homotrimeric precursor proteins, are cleaved by host cell proteases and transferred into their active form. Since this cleavage represents an essential process for viral infectivity, the idea is to interfere with HA cleavage as a novel approach against IAV. For this purpose three HA subtypes (H1, H3 and H7) should be recombinantly expressed in their unprocessed non-cleaved form for structural and functional analysis. Besides, a protocol for large scale expression and purification of H1 HA should be developed for application in transfollicular vaccination strategies.

Expression constructs were designed and cloned by Joop van den Heuvel and Ruth Lambertz (HZI). They comprise the whole HA ectodomain followed by the T4 foldon sequence allowing recombinant trimer expression since it functions as an artificial trimerization domain (Stevens *et al.*, 2004). An N-terminal IgG secretion signal is implemented to secrete the proteins into the supernatant, while His- and Strep-tags can be used for purification and Thrombin and TEV cleavage sites are necessary to eliminate heterologous parts after purification.

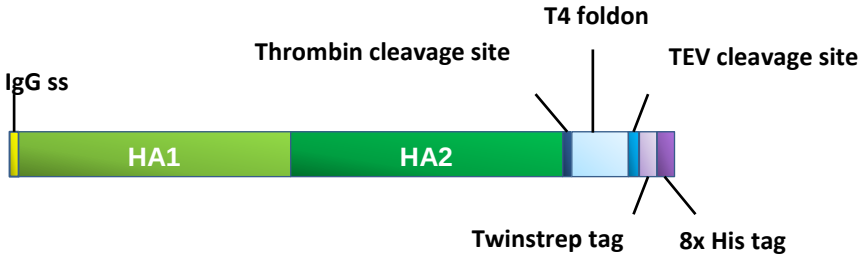

Figure 3.1: Construct design for recombinant hemagglutinin expression

The IgG secretion signal (IgG ss) is fused N-terminally to HA ectodomain comprising the subunits HA1 and HA2 to direct it to the supernatant. A trimerizing sequence (T4 foldon) was incorporated with a thrombin cleavage site introduced between the C-terminus of HA ectodomain and foldon. At the extreme C-terminus of the construct a TEV cleavage site followed by Twinstrep and an 8xHis tag are fused to the protein to enable purification and detection.

Expression was initially tested for the different subtypes in the multi host expression system developed in our department for evaluation of the optimal expression host (Meyer *et al.*, 2013). For this approach the constructs were cloned into the pFlpBtM-II vector and first expression tests were performed.

3.1.1 Insect cell expression

Insect cells are very promising as expression host for recombinant HA expression since successful expression of HA proteins in insect cells has already been reported (Stevens *et al.*, 2004; Wang *et al.*, 2006; X. Li *et al.*, 2015). Furthermore, lepidoptera cell lines are widely used to express heterologous proteins for crystallization as they offer various advantages due to their safety, ease of use and simple glycosylation pattern (Tomiya *et al.*, 2004; Nettleship *et al.*, 2010; Nettleship, 2012).

First of all, recombinant baculoviruses were produced for protein expression via BEVS that express HA of the subtypes H1, H3 or H7, respectively. As described in 2.4.8 the HAs were integrated via Tn7 transposition into the baculovirus genome maintained as a bacmid in DH10B *E. coli* cells. Recombinant bacmids could be screened by blue-white selection in consequence of lacZ gene disruption. Afterwards they were further analyzed by PCR (2.4.1) and subsequently used for transfection 2.5.7. The integration of an YFP expression cassette within the backbone of the baculovirus EmBacY enables efficient monitoring of virus performance. Upon transfection of adherent *S. frugiperda* (Sf21) cells recombinant YFP expression could be used as indication for effective infection confirmed by fluorescence microscopy (shown in Appendix I, Figure 8.1).

Transfection supernatants were subsequently used for virus amplification to generate viral stocks for recombinant protein expression. Throughout virus amplification growth kinetics, fluorescence and changes in cell diameter of cells infected with recombinant baculovirus were observed to identify successful infection. Growth kinetics, fluorescence and variations in cell diameter during virus amplification are presented in Appendix I, Figure 8.2.

After successful generation of recombinant baculoviruses their ability to produce HA variants was determined in Sf21 and Hi5 cell lines in 40 mL scale. Suspension cultures with an initial cell density of $1 * 10^6$ cells/ml (Sf21) and $0.7 * 10^6$ cells/ml (Hi5) were infected with either 5 vol% or 10 vol% of external virus stock and cultivated for 96 h. Infection was monitored during cultivation by fluorescence measurements with FACS and additionally by determining the mean cell diameter with CASY Cell Counter. Supernatants were analyzed every 24 h for recombinant protein expression via western blot incubated with His-tag primary monoclonal antibody (mAb) and secondary goat-anti-mouse AP-conjugated polyclonal antibody (pAb) (2.7.3, Table 2-4). Detection of recombinantly expressed HA was successful in Hi5 cells, whereas the expression was too low in Sf21 cells within 96 h of cultivation to detect the recombinant proteins (Figure 3.2 A).

In order to further verify HA-expression additional SDS-PAGE was performed with Hi5 derived supernatants (Figure 3.2 B) for mass analysis. The corresponding bands (indicated by an arrow in Figure 3.2 B) were cut out of the gel and were subsequently subjected to tryptic digestion for protein analysis via MALDI-TOF. MALDI-TOF analyses were conducted by the MS platform of the research group Cellular Proteomics (CPRO) at the HZI, Braunschweig (2.7.4). With that up to 95 % of the amino

acid sequence was verified for each subtype. The observed variation in size of different HA subtypes are thought to depend on differences in their glycosylation.

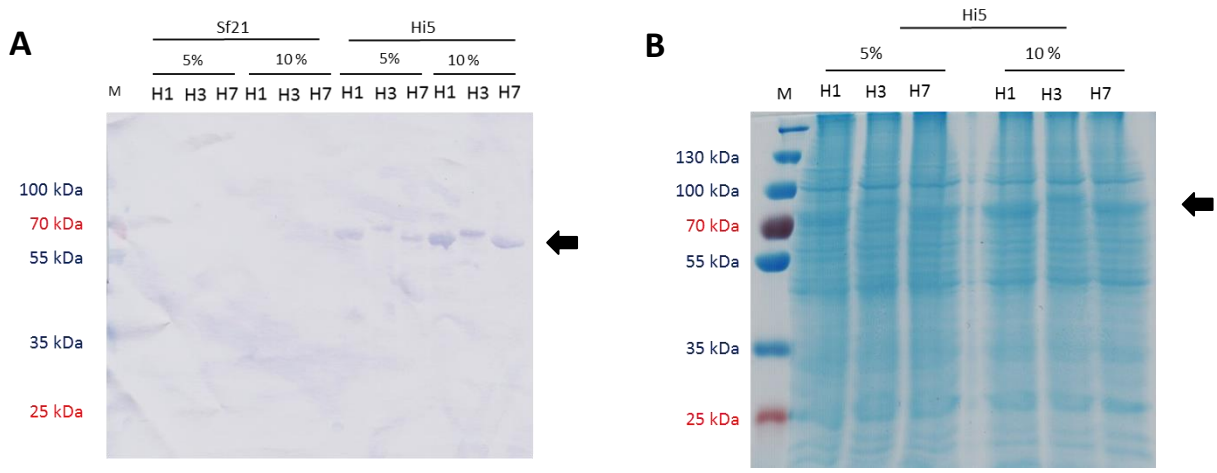

Figure 3.2: Small scale HA Expression test in Sf21 and Hi5 cells with BEVS
Expression of the three HAs (H1, H3 and H7) via BEVS could be detected in crude culture supernatants by SDS-PAGE and western blot analyses using a primary mouse α-His mAb and a secondary goat AP-conjugated α-mouse pAb. Infection was performed with 5 vol% or 10 vol% virus stock in Sf21 and Hi5 cells as idicated above the gel/blot. A: Western blot of Sf21 and Hi5 samples. B: SDS gel with Hi5 samples. Colorimetric AP staining of the western blot was done with NBT and BCIP. The SDS gel was stained with InstantBlue. M: PageRuler Prestained, all samples were taken at 96 hpi.

After the success of small scale expression in Hi5 cells, expression was performed in larger scale (500 mL) for subsequent purification. Here, suspension cultures with an initial cell density of 0.5 * 10^6 cells/ml were infected with 15 vol% (H1) or 10 vol% (H3 and H7) virus stock according to their infection performance in small scale. Infection and growth kinetics were monitored during cultivation (Figure 3.3). The infection of Hi5 suspension cultures by the recombinant baculoviruses was verified via measurements of YFP fluorescence by flow cytometry and through a distinct increase of the mean cell diameter of about 3 µm during the first 24 h. While the respective YFP fluorescence indicates infection efficiencies of at least ~ 50 %. The culture supernatants were harvested at a viability of about 80 % at 75 hpi, except for H1. Due to the higher virus dose that was applied cells infected with EMBacY-H1 already had a decrease in viability below 70 % after 48 hpi so that they were harvested at 48 hpi.

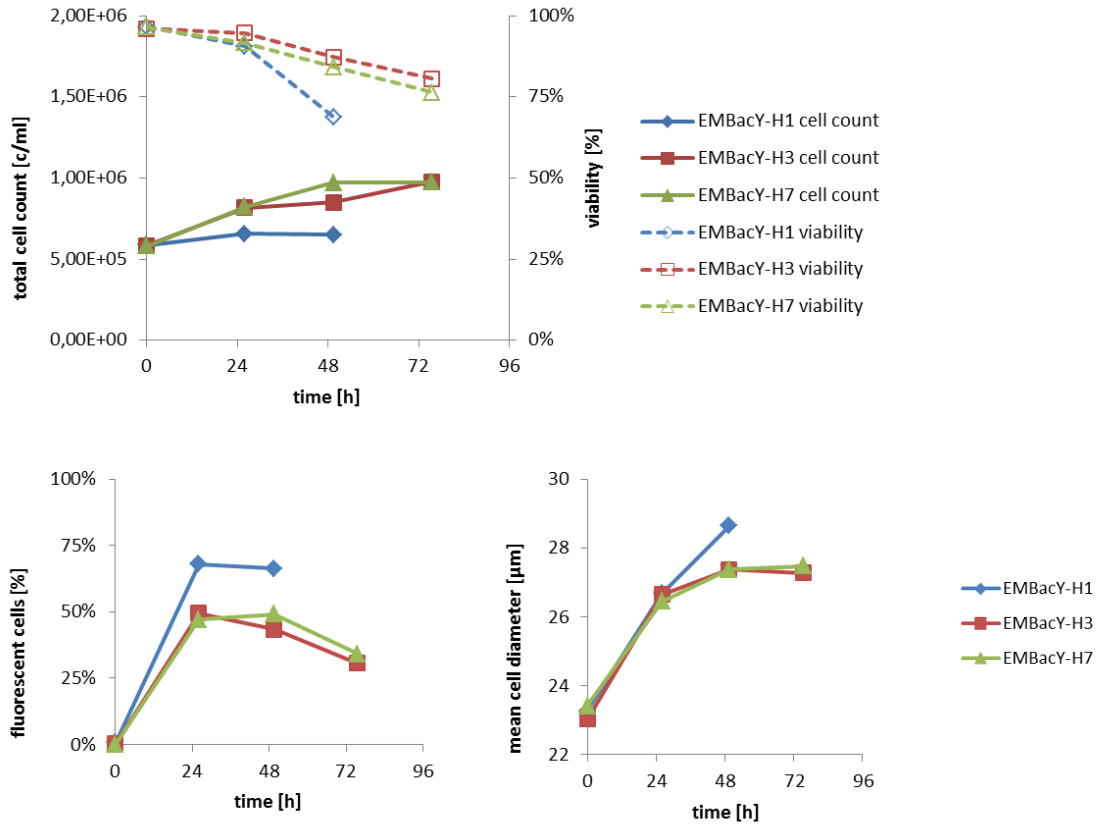

Figure 3.3: Growth kinetics, fluorescence and cell diameter of Hi5 cells infected with indicated baculoviruses

The graphical data depicts the daily assessed growth and infection parameters. Hi5 suspension cultures with a cell density of 0.5 × 10^5 cells/mL were infected with recombinant baculovirus (EMBacY-HA variants). The cells were counted manually with a Neubauer hemocytometer. The vitality was assessed by trypan blue staining. The YFP expression of EmBacY was monitored by flow cytometry in the GFP channel (488 nm excitation). The mean cell diameter was analyzed with CASY counter. Significant increase in cell diameter and YFP fluorescence indicate successful infection.

The crude culture supernatants were subsequently diafiltrated and the buffer was exchanged to 50 mM NaH_2PO_4, 300 mM NaCl, pH 8.0 with the KrosFlo Research IIi TFF System (2.6.7). Purification was performed via Ni-NTA IMAC using the Profinia Protein Purification System (IMAC-catridge 1 mL, Desalting catridge 10 mL, according to the protocol described in 2.6.10). IMAC fractions and supernatants were further analyzed via SDS-PAGE and western blot, shown in Figure 3.4.

Recombinant HA accumulated in the supernatants and a first rough purification was achieved. Each eluate fraction contained up to 3 mg protein. However, contamination by non-specifically bound protein and degradation was observed. The high amount of degraded H1 is probably due to the low viability of its expression culture 48 hpi (<70 %) caused by the lytic nature of BEVS. In comparison to H1 and H3 that were predominantly purified in its uncleaved form, high amounts of H7 were already cleaved by host proteases during insect cell cultivation and purification.

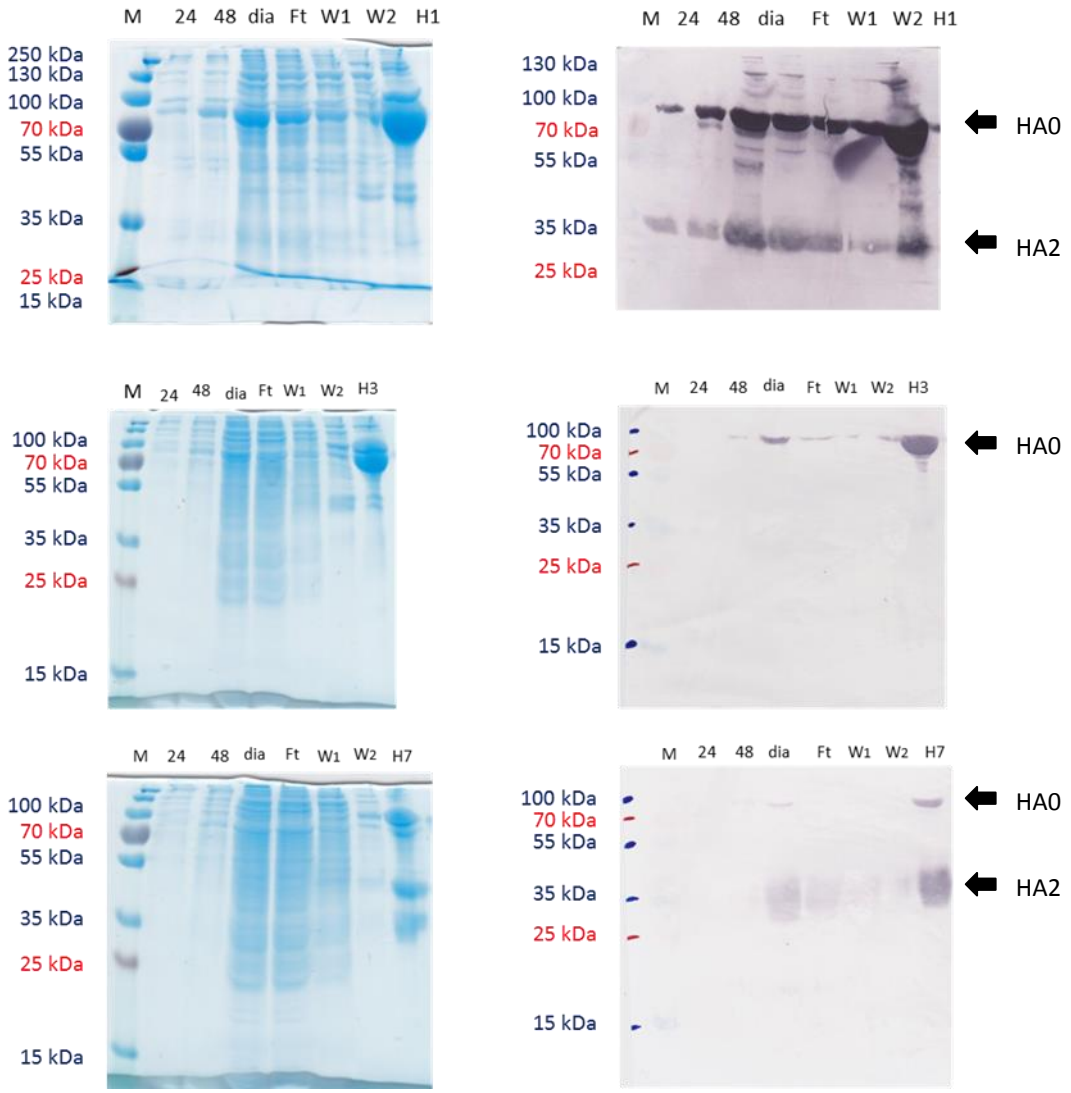

Figure 3.4: SDS-PAGE and Western Blot analysis of IMAC purification of HA

The HA (H1, H3, H7) protein was expressed upon BEVS in Hi5 cells. Diafiltrated cell culture supernatants were applied to a BioRad Profinia system equipped with a Profinity IMAC Cartridge (1 mL) and a Bio-Gel P6 Desalting Cartridge (10 mL). Daily samples of supernatants and fractions from IMAC purification are presented in each gel and western blot. The SDS gel was stained with InstantBlue. The Western blot was performed with primary anti-His mAb together with a secondary goat-anti-mouse AP-conjugated pAb. Colorimetric AP staining was done with NBT and BCIP. M = PageRuler™ Protein Ladder, 24: sample at 24 hpi, 48: sample at 48 hpi, dia: diafiltrated supernatant, Ft = flow through, W1 = wash fraction 1, W2 = wash fraction 2, H1/H3/H7: purified HA of indicated subtype.

Overall, the generation of HA-expressing bacmids resulted in recombinant baculovirus suitable for infection of Sf21 and Hi5 insect cells. While the expression via BEVS was too low for a successful detection in Sf21 cells, recombinant HA of the subtypes H1, H3 and H7 was successfully expressed and purified in Hi5 cells. In comparison to H1 and H3 that were predominantly purified in its uncleaved form, high amounts of the subtype H7 were already cleaved by host proteases during insect cell cultivation and purification.

3.1.2 Mammalian expression

In order to find the optimal expression host, both transient gene expression in HEK293-6E cells as well as stable expression in engineered CHO cell lines, implemented in the multi-host system for expression in mammalian cells, were performed. The transient expression in HEK293-6E was analyzed in 25 mL scale as described in 2.6.1. pTTo-GFPq was co-transfected to determine efficiency of transfection. Growth kinetics and fluorescence signals are presented in Figure 3.5. Transfection rates of about 70 % could be observed for all three HA constructs ensuring efficient transfection.

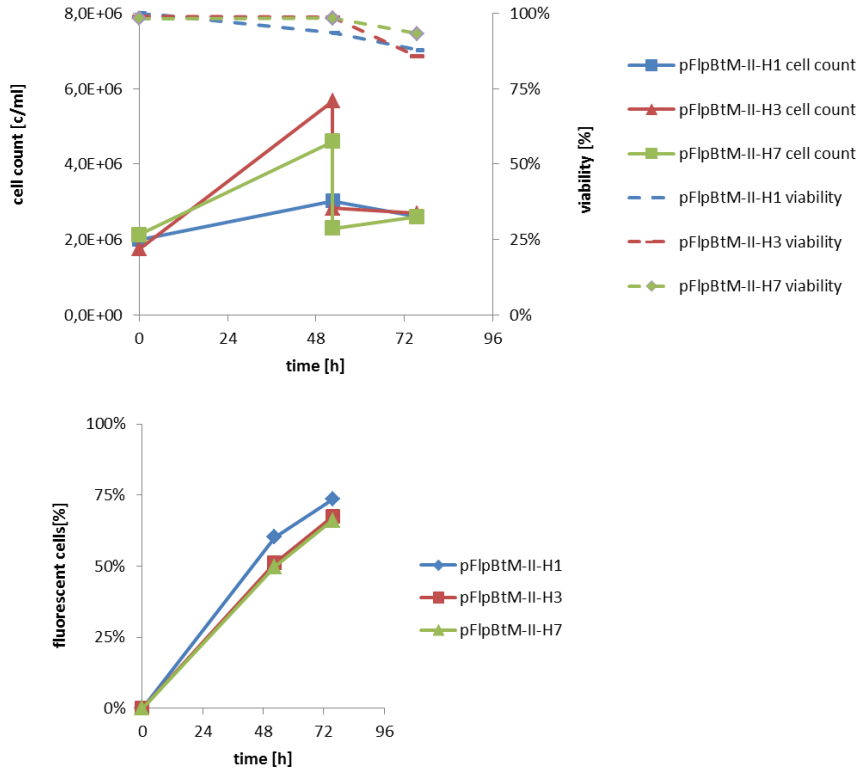

Figure 3.5: Growth kinetics and fluorescence of HEK 293-6E cells transfected with HA H1, H3 or H7

HEK293-6E suspension cultures with a cell density of 2 × 10^6 cells/mL were transfected with pFlpBtM-II-HA variants and the cultures were expanded to 50 mL and supplemented with 0.5 % tryptone 48 hpt. The cells were counted manually with a Neubauer hemocytometer. The viability was assessed by trypan blue staining. The GFPq expression of co-transfected pTTo-GFPq was determined at a Guava EasyCyte flow cytometer using a 488 nm laser for extinction and allowed to monitor transfection efficiencies.

Since recombinant HA expression was detected for the three subtypes H1, H3 and H7 by Western blot (data not shown), the next step was a large scale expression with subsequent purification for subtype H1. For this large scale expression a slightly different approach was used than for small scale expression. In this case herring sperm DNA was used as filler DNA to test its effect on enhancing transfection as already described for other proteins (Kiseljak *et al.*, 2011). 1 L suspension culture was transfected with 25 µg DNA (12.5 µg pFlpBtM-II-H1 + 11.25 µg Herring sperm DNA + 1.25 µg pTTo-

GFP) and 62.5 µg PEI (DNA PEI ratio 1:2.5). For even further improving recombinant expression valproic acid was added 96 hpt to a final concentration of 3.75 mmol/L in order to possibly increase recombinant mRNA and protein levels (Wulhfard *et al.*, 2010). With this changed protocol a rather scant transfection rate below 20 % was observed (Appendix I, Figure 8.3). The supernatant was harvested 168 hpt followed by purification via Ni-NTA IMAC with the Profinia Protein Purification System as described above for insect cell derived HA, resulting in ca. 22 mg rather pure protein (Appendix I, Figure 8.4). Unfortunately, the protein was not very stable and tended to precipitate after purification.

Besides, stable glycosylation deficient CHO cell lines expressing HA (derived from different CHO Lec 3.2.8.1 master cell lines) were generated by the Protein Sample Production Facility (PSPF) at the HZI. However, the HA expression was so low that it could only be detected in concentrated samples of TCA precipitation via western blot so this approach was not pursued further.

3.1.3 Analysis of quality of the HA expressed in insect and mammalian cells

Since glycosylation can hinder crystallization of proteins because of the chemical and conformational heterogeneity of their carbohydrate moieties (Wulhfard *et al.*, 2010), deglycosylation experiments were performed with both HEK and insect cell derived H1 (2.7.5). For this approach the two different endoglycosidases Endo H and PNGase F were applied. Herewith PNGase F is the most effective enzyme for removing almost all N-linked oligosaccharides from glycoproteins (Freeze and Kranz, 2010). Yet, most glycoforms produced by insect cells can also be trimmed by treatment with Endo H (Nettleship, 2012). Both endoglycosidases, however, are sensitive to some kind of core fucosylation frequently occurring in insect cells (Altmann *et al.*, 1999; Walski *et al.*, 2017).

H1 expressed in Hi5 cells was not susceptible to deglycosylation at all, neither with Endo H nor PNGase F, even after prolonged incubation or with denatured protein. While H1 expressed in HEK293-6E cells was affected by severe degradation and increased precipitation after treatment with PNGaseF (data not shown). For more details on particular glycosylation both glycosylated proteins were subjected to mass spectrometry performed by the MS platform of the research group CPRO at the HZI. The determination of each protein mass by MALDI-TOF is depicted in Figure 3.6.

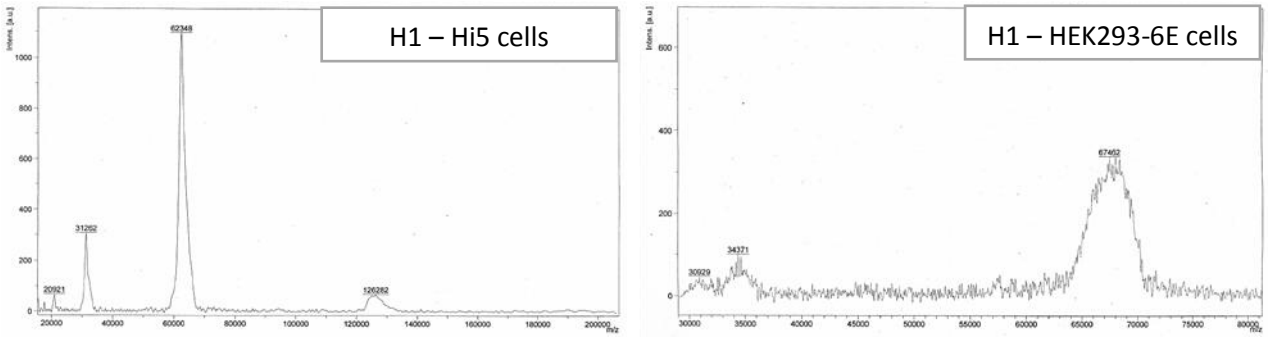

Figure 3.6: Mass analysis of H1 derived from Hi5 and HEK293-6E cells
The MALDI analysis of H1 expressed in Hi5 cells showed a major peak at the size of ~62 kDa (left hand site), whereas the dominant peak at the size of ~67 kDa was observed for H1 expressed in HEK293-6E cells (right hand site). Peaks with smaller molecular weight correspond to multiply charged monomers. Besides, the spectra demonstrate a homogenous glycosylation for H1 expressed in Hi5 cells and a heterogenous glycosylation pattern for H1 expressed in HEK293-6E cells.

Both proteins differ in their total mass with 62.3 kDa for the H1 monomer expressed in Hi5 cells (H1-Hi5) and 67.5 kDa for the HEK293-6E derived monomer (H1-HEK). Besides, the observed masses are higher than the theoretical mass of 57.4 kDa of the thrombin-cleaved monomer. Increased masses of ca. 5 kDa for H1-Hi5 and ca. 10 kDa for H1-HEK can be most likely explained by their different glycosylation with almost 1 kDa for each glycosylation site for H1-Hi5 and 2 kDa for H1-HEK, respectively. Besides, the spectra clearly demonstrate a very homogenous glycosylation of H1-Hi5 compared to the heterogeneous pattern of H1-HEK indicated by the broad irregular mass peak. Additionally, dynamic light scattering (DLS) analysis was performed with both protein batches in order to confirm trimeric HA-expression and to further examine the molecular weight of the non-cleaved samples. The data derived from DLS measurements clearly indicate higher molecular weights for H1-HEK compared to H1-Hi5, confirming the previous results derived from mass analysis by MALDI-TOF (Appendix I, Figure 8.5).

Taken together these results indicate a quite homogenous H1 protein derived from Hi5 insect cell expression. Its uniform glycosylation pattern should not hinder crystallization. As opposed to this, H1 transiently expressed in HEK293-6E cells has a more diverse glycosylation that probably would hinder crystallization and could not be removed without protein degradation. All results indicate that the HA produced in HEK293-6E cells is not of such a good homogeneity as HA produced in Hi5 cells, even though it had a much higher product titer. Further efforts would need to be done in order to try to overcome those obstacles, whereas recombinant HA expression in Hi5 already was very promising. Hence, Hi5 cells represent a better expression host for recombinant HA. Consequently, expression was performed in Hi5 cells thereafter.

3.2 Optimization of downstream processing for recombinant HA production

3.2.1 Improving protein purity by affinity chromatography

In order to further improve the HA purity Ni-NTA purified samples were subsequently subjected to HisTALON purification. The Co^{2+}–CMA matrix of Talon resin (Clontech) has a lower affinity for the polyhistidine affinity tag than the Ni^{2+}–NTA resin, resulting in elution of the tagged proteins under milder conditions. Besides, the Co^{2+}–CMA has been reported to exhibit less nonspecific protein binding than the Ni^{2+}–NTA resin, resulting in higher elution product purity (Bornhorst and Falke, 2000). Hence, Talon purification was performed subsequent to previous Ni-NTA purification.

Ni-NTA purified HA was dialyzed against 50mM Tris/HCl 300 mM NaCl pH 7.4 for ensuing HisTALON™ Superflow purification. Following dialysis, purification was performed for each HA, H1, H3 and H7 according to the manufacturers' protocol (2.6.10). Eluted fractions were analyzed by SDS-PAGE and Western Blot as shown in Figure 3.7. Nice single bands of about 70 kDa corresponding to monomeric HA protein could be observed in SDS-PAGE for the subtypes H1 and H3 after this second affinity purification. The pooled eluate fractions of H1 and H3 contained 0.6 mg and 1.4 mg of purified protein, respectively. For H7, however, the major part of the purified protein was already cleaved into its subunits HA1 and HA2 due to host proteases during purification steps. Proteolytic H7 cleavage even increased after the second purification step, resulting in nearly completely processed H7. Hence, further purification steps and crystallization setups were only performed with H1 and H3.

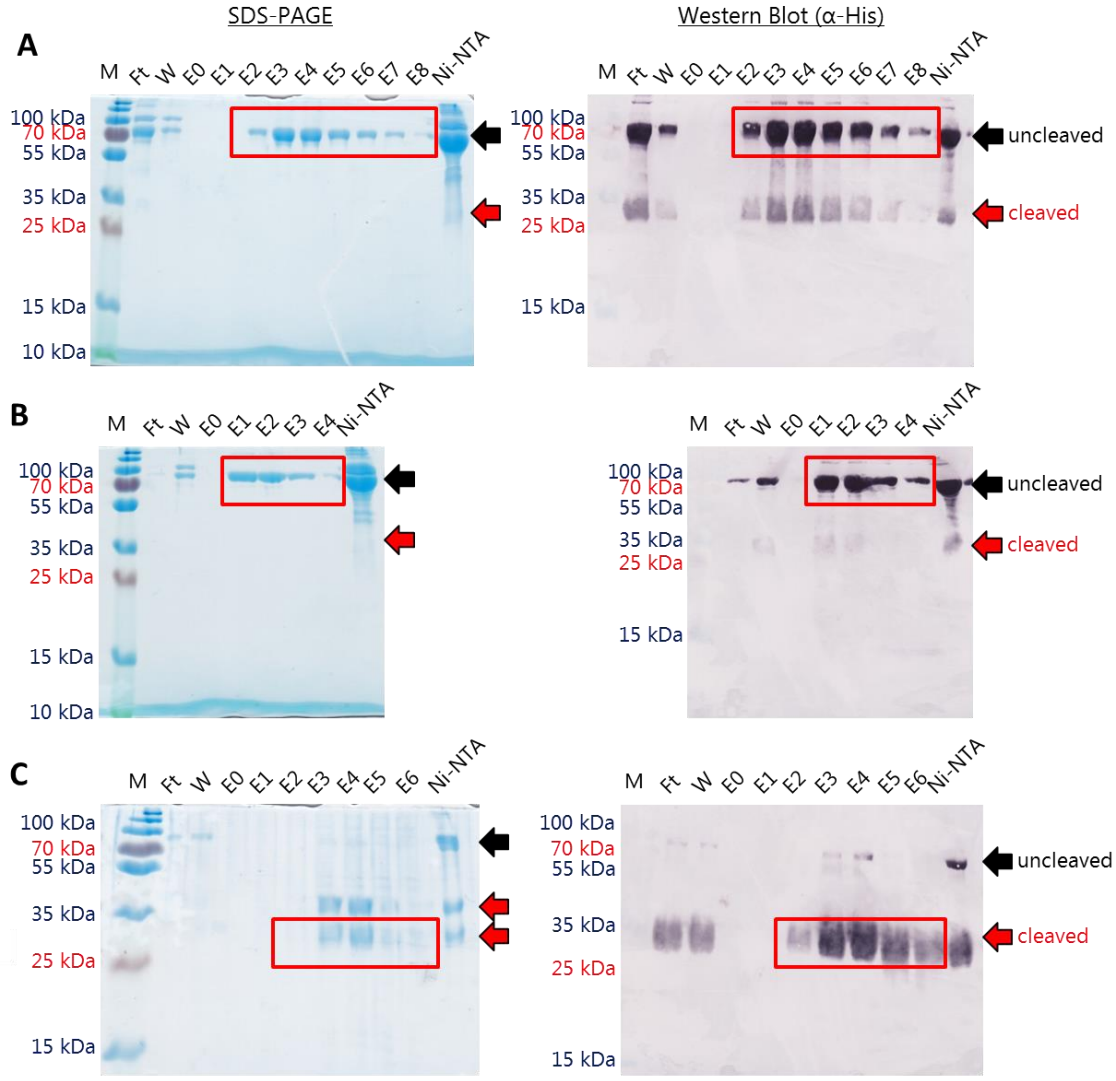

Figure 3.7: SDS-PAGE and Western Blot analysis of HisTALON purified HA subtypes H1, H3 and H7
The Ni-NTA purified HA proteins (A: H1, B: H3, C: H7) were subjected to HisTALON purification. The samples of different fractions are presented in each gel and western blot. The SDS gel was stained with InstantBlue. The Western blot was performed with primary anti-His mAb together with a secondary goat-anti-mouse AP-conjugated pAb. Colorimetric AP staining was done with NBT and BCIP. M = PageRuler™ Protein Ladder, Ft = Flow through of the HisTALON column, W = Wash fraction, E0 – E8 = Elution fractions, Ni-NTA = Ni-NTA purified sample used for HisTALON purification.

In the next step HisTALON purification of the dialyzed supernatants was examined without prior Ni-NTA purification. In this way the yield should be improved from only 1.2 (H1) and 2.8 mg/L (H3) after two rounds of affinity purification and dialysis. For this approach 1 L suspension culture of Hi5 cells with an initial cell density of 0.9 * 10^6 cells/ml was infected with 10 vol% of virus stock and was harvested 48 h after infection. Purification of the HA protein was performed according to the manufacturers' protocol with HisTALON™ Superflow (5 mL HisTALON™ Catridge) and the purification achievement was analyzed by SDS-PAGE (Appendix II, Figure 8.6).

With this adapted purification strategy with HisTALON™ Catridge a total amount of 5.9 mg/L pure protein was successfully purified. This represents a five-fold increase to the previous strategy

regarding to the protein yield per liter suspension culture. The H1 protein already reached a high grade of purity and could be used for further processing by thrombin cleavage (3.2.3) and size exclusion chromatography (3.2.4) as well as first crystallization trials (3.4).

3.2.2 Direct HA capture from the supernatant

In the previous purification strategies recombinant HA was purified from the culture supernatant in two steps: First, the supernatant was concentrated and buffer exchanged during diafiltration and afterwards it was purified by affinity chromatography. Especially for HA production in large scale, up to 6 L expression cultures, this procedure was cumbersome, time-consuming and lead to varying loss of the target proteins. Furthermore, the required time for this two-step purification set up could have a severe influence on protein quality. Proteolytic processing and degradation by proteases was already observed for the HA subtypes H1 and H7 (Figure 3.4 and Figure 3.7) and was thought of as a critical factor for the purification protocol.

For direct HA capture, the supernatant of infected Hi5 cells was harvested 72 hpi in two steps: First suspension cultures were centrifuged for 5 min. at 200 x g in order to carefully remove the cells. Afterwards the supernatant was supplementary centrifuged for 10 min. at 5000 x g to thoroughly remove remaining particles to avoid clogging of the cartridge. Thereafter the supernatant was directly loaded onto a HisTrap excel column (1 mL HisTrap excel IMAC column, GE Healthcare) and purification was performed according to the manufacturers' protocol (2.6.10). Elution fractions of 1 mL were analyzed by SDS-PAGE and western blot as shown in Appendix II, Figure 3.8. HA capture was effective; however, some minor impurities remained within the elution samples. Nevertheless, further purification with HisTALON did not increase the level of purity (data not shown). Therefore, the imidazole concentration was increased up to 75 mM in the next purification set-ups due to stronger binding of the target protein according to the trimeric His tag (see section 3.3.2).

All in all, the optimization of affinity purification of recombinant HA was very effective. The purity and the yield were successfully increased by both HisTALON™ and HisTrap excel purification strategies. Furthermore, the implementation of the fast and more gentle HisTrap excel purification was able to replace the more cumbersome and time-consuming previous procedure of diafiltration prior to affinity purification. With this changed protocol the overall purification process was some days up to more than a week faster, depending on the applied expression volume. Moreover, the saved time and the gentle process also improved the product quality by minimizing protein degradation.

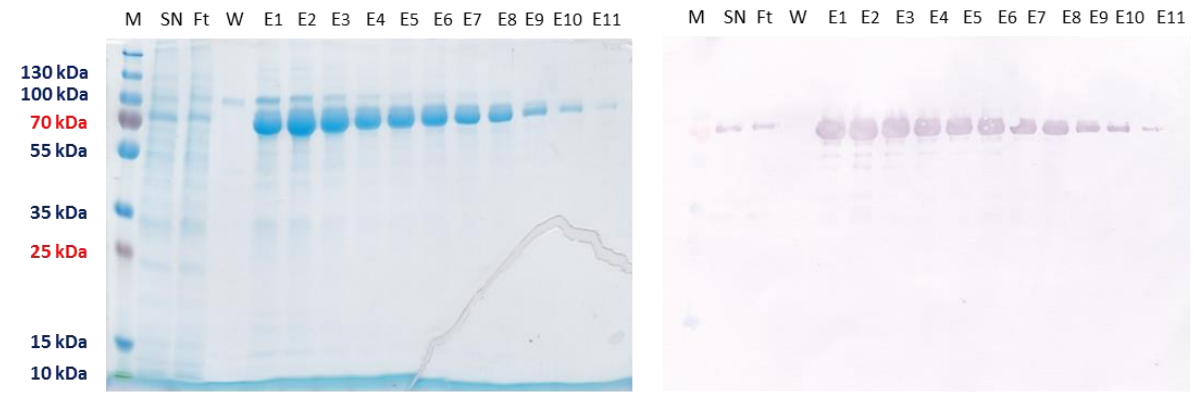

Figure 3.8: SDS-PAGE and western blot analysis of HA expression and subsequent purification with HisTrap excel
The H1 protein was expressed in BEVS using an EMBacY-pFlpBtM-II-H1 virus and was subsequently subjected to HisTrap excel purification. The SDS gel was stained with InstantBlue. The Western blot was performed with primary anti-His mAb together with a secondary goat-anti-mouse AP-conjugated pAb. Colorimetric AP staining was done with NBT and BCIP. The samples of different fractions are presented in each gel and western blot. M = P PageRuler™ Plus Protein Ladder, SN = crude supernatant after harvesting, Ft = flow through, W = wash fraction, E1 – E11 = elution fractions 1 – 11.

3.2.3 Thrombin cleavage

For both immunization and crystallization further processing of the purified recombinant HA is necessary. First, the heterologous part of the protein, consisting of the trimerization domain foldon and tags for purification, should be removed by cleavage with thrombin (2.6.11). Therefore cleavage analysis of the H1 and H3 trimer was performed using Thrombin from bovine plasma (SERVA). Samples were taken at different time points and analyzed by SDS-PAGE and western blot for validation of cleavage efficiency (Appendix II, Figure 8.7).

After initial tests cleavage was routinely performed with Thrombin (SERVA) in a concentration of 2.5 U/mg for at least 5 h. However, cleavage was not of constant quality. Therefore an additional optimization of H3 cleavage using Thrombin of different suppliers was conducted. Analysis was performed with Thrombin from SERVA and GE Healthcare. Evaluation was done by SDS-PAGE as depicted in Figure 3.9. Successful cleavage was observed due to the reduction in size according to the separation of a roughly 10 kDa large fragment from the remaining part of about 60 kDa. For further purification, thrombin-cleaved proteins were subsequently applied to either size exclusion chromatography (3.2.4) or reverse Strep-Tactin purification (3.2.5).

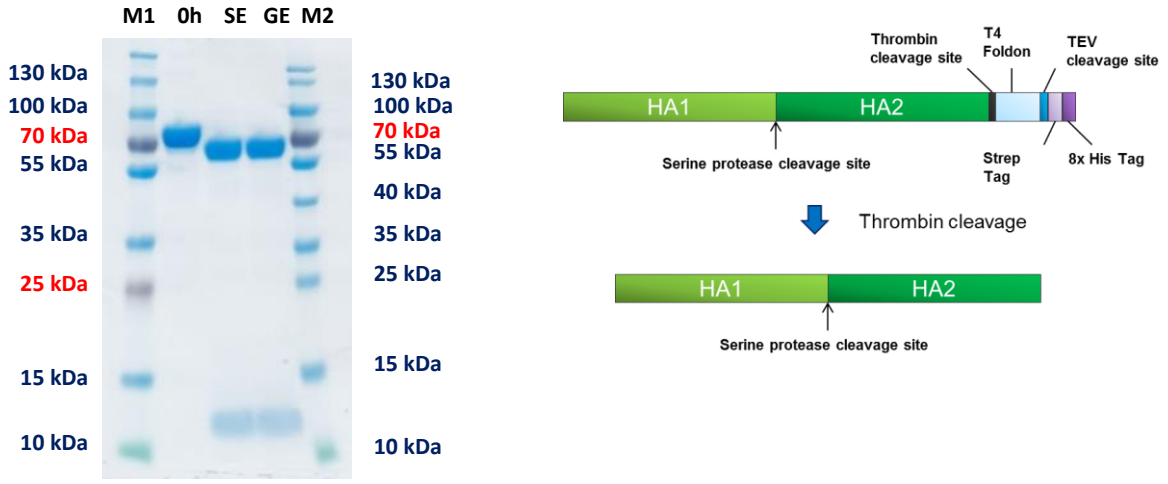

Figure 3.9: SDS-PAGE analysis of H3 cleavage with Thrombin
H3 cleavage with Thrombin was performed in order to remove the heterologous trimerization domain including tags for purification. Cleavage was performed according to the manufacturers' protocol with 2.5 U (SERVA) or 10 U (GE Healthcare) / mg protein for 16 h at RT. Successful cleavage can be observed due to reduction in size because of the separation of ~ 10 kDa fragment, as illustrated in the right hand site. The SDS gel was stained with InstantBlue. M1 = PageRuler™ Plus Protein Ladder, 0h = sample prior to cleavage, SE = Thrombin from SERVA, GE = Thrombin from GE Healthcare, M2 = PageRuler™ Protein Ladder.

3.2.4 Size Exclusion Chromatography

After thrombin cleavage size exclusion chromatography (SEC) was performed using a Superdex 200 16/60 column. In a first experiment thrombin-cleaved protein samples as well as uncleaved HA samples were used to determine their individual retention volumes (Figure 3.10).

Selected elution fractions were analyzed by SDS-PAGE. Their retention volumes were compared among each other and the molecular weight was calculated using the calibration curve provided by the manufacturer. Additionally, the isolated peak of monomeric H1 was further analyzed by DLS (Lorber *et al.*, 2012) for determining its molecular weight and size distribution (Appendix II, Figure 8.8).

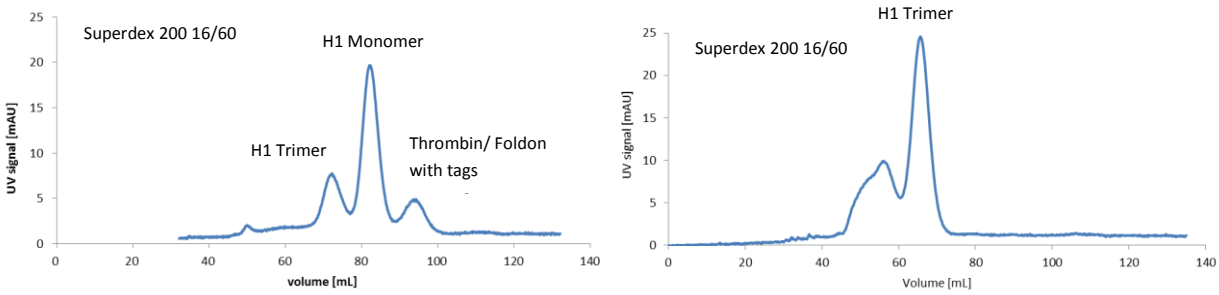

Figure 3.10: Elution profile of thrombin cleaved H1 (A) and uncleaved H1 (B) during size exclusion chromatography
A: Superdex 200 16/60 gel filtration was used to separate cleaved H1 from both foldon with tags and thrombin as well as uncleaved H1. B: Superdex 200 16/60 gel filtration was used to analyze the molecular weight of uncleaved H1 compared to thrombin cleaved H1 shown in A.

Table 3-1 summarizes the calculated masses compared to the theoretical ones and those obtained with DLS measurements. Notably, the calculated mass of every protein sample, based on its retention volume, is below its theoretical mass, based on its amino acid composition. Probably this is caused by the fact that the stokes radius of globular proteins is the underlying principle of those calculations. Hence, the cylindrical shape of the trimeric HA protein leads to underestimation of its size. Nevertheless, the size range of each type of protein observed during SEC provides valuable information about its oligomeric state. With this approach it was observed that the major part of the thrombin-cleaved protein has been dissociated into HA monomers after the separation of the trimerization domain.

Table 3-1: Summarized data of molecular mass of monomeric and trimeric H1 obtained by different approaches

	Ve	Kav	Mw_calculated	Mw_theoretical	Mw_DLS
Monomeric cleaved H1	81,0	0,48	43	59	44
Trimeric uncleaved H1	65,7	0,28	155	205	191
Trimeric cleaved H1	72,0	0,36	91	178	-

Since high ionic strength can influence the oligomer dissociation into monomers, the ionic strength was decreased by reducing the salt concentration to 50 mM NaCl prior to and during SEC. Indeed, this led to an increased isolation of trimeric H1 with only little dissociation into monomers as depicted in Figure 3.11. The isolated trimeric protein was subsequently pooled, concentrated and used for first crystallization trials (3.4).

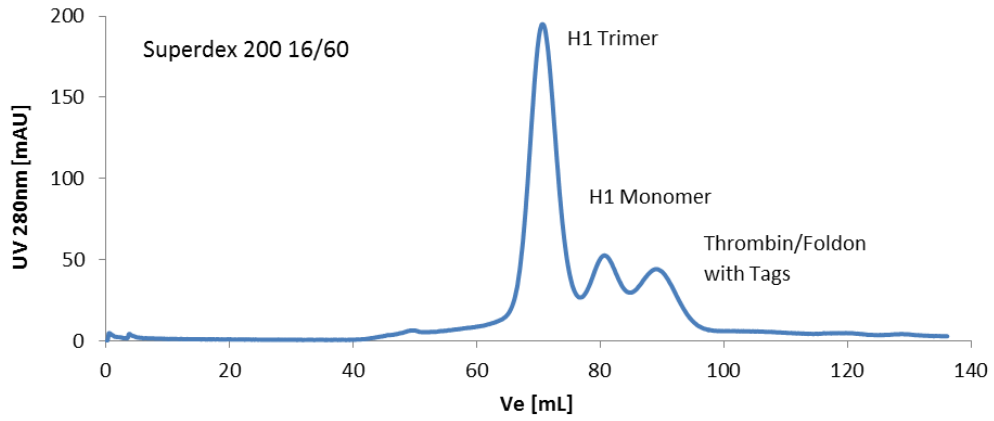

Figure 3.11: Elution profile of thrombin cleaved H1 during SEC using low salt concentrations
Superdex 200 16/60 gel filtration was used to separate the trimeric thrombin cleaved H1 from monomeric protein and foldon with tags and thrombin as well.

3.2.5 Reverse Strep-Tactin purification

In order to ensure the complete removal of uncleaved HA and potentially remaining parts of the trimerization domain, another affinity purification step with Strep-Tactin resins was included to remove all tagged contaminants. In a first test experiment small scale purification of H3 with magnetic beads (MagStrep "type3" XT beads, iba) was performed (2.6.8) prior to SEC and purification was analyzed by SDS-PAGE, depicted in Appendix II, Figure 8.9. With this additional purification step all tagged contaminants could be removed successfully. Hence, additional large scale Strep-Tactin purification was performed by using Strep-Tactin Superflow residue (iba) (2.6.10). The complete removing of tagged protein was evaluated by SDS-PAGE, presented in Figure 3.12 A for H3, and purified material was then applied to SEC. In case of H1 that was used for reverse Strep-Tactin purification after SEC (Figure 3.12 B), the purified protein was afterwards utilized for crystallization set-ups.

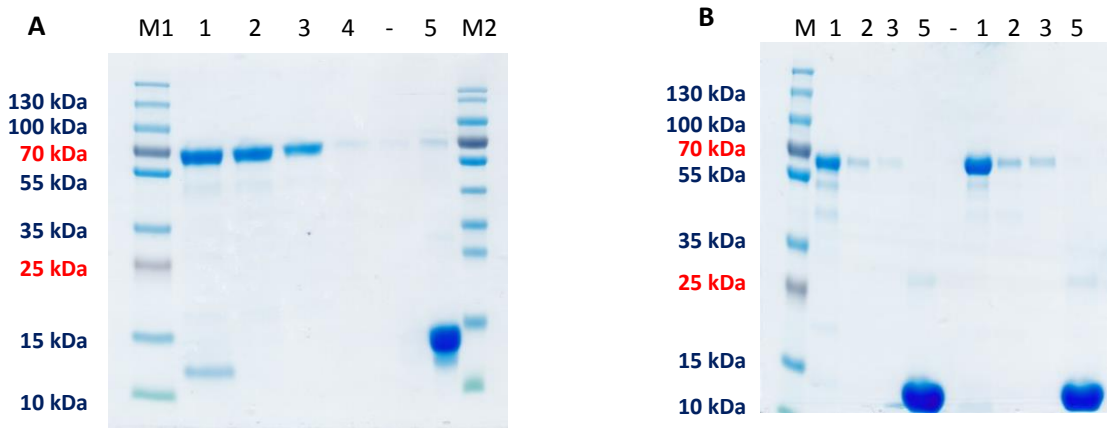

Figure 3.12: HA batch purification with Strep-tactin superflow
For removing tagged contaminants Strep-Tactin purification of H3 (A) and H1 (B) was performed according to the manufacturers' protocol. M1 = PageRuler™ Plus Protein Ladder, 1 = Thrombin-cleaved HA, 2 = flow-through containing purified protein, 3 = wash fraction, 4 = elution fraction under native conditions, 5 = elution fraction under denaturing conditions, M2 = PageRuler™ Protein Ladder.

3.3 Scale-up of H1 expression for transfollicular vaccination strategies

One aim of this project was to produce the HA isolate H1 (A/Puerto Rico/8/34) in high amounts and with high quality for transfollicular vaccination strategies by our collaboration partners Guzman and co-workers. For this approach it was not only necessary to produce lots of very pure material, the process was also desired to be both affordable and easy to handle. For this purpose three different methods were evaluated to optimize the production process that should lead to high yields while being accessible for a scale-up in bioreactor dimensions with a production scale of up to 1 g.

3.3.1 Baculoviral Expression using BIICs

In a first approach for up-scaling of the HA production process it was investigated to use the TIPS (Titerless Infected-Cells Preservation and Scale-Up) method described by Wasilko and Lee. This method depends on application of cryopreserved Baculovirus Infected Insect Cell (BIIC) stocks for infection and recombinant protein expression (Wasilko and Lee, 2006). Those BIICs are harvested and frozen after infection with recombinant baculovirus, but prior to cell lysis, when virus would be released into the culture supernatant. With this method cell stocks densely packed with recombinant baculovirus can be generated. This virus stocks can subsequently be used to infect insect cells for large-scale productions since as little as 1 mL of BIICs is needed for a 100 L expression scale (Wasilko *et al.*, 2009). Besides, the TIPS method eliminates repeated virus amplification steps and at the same time provides a long-term stable storage form of recombinant virus. Thus, it not only enables a stable virus stock suitable for scale-up, but also leads to higher reproducibility. By applying BIICs there are no differences in infection efficiency depending on the individual virus stocks and no loss of infection over time. Furthermore, in large scale expression set-ups the handling is much easier compared to external virus stocks generated by virus amplification (Wasilko and Lee, 2006; Wasilko *et al.*, 2009).

Unfortunately, this method was not very convenient in our hands as we could not achieve infections that were comparable to that with the extracellularly virus stock used before (3.1.1). Therefore different BIIC-culture ratios were tested for infection efficiency in Sf21 cells in order to test their ability to infect the cells. However, only very high amounts of applied BIICs (1:20, 1:50 and 1:100) led to successful infection of at least 50 % Sf21 cells within 48 h, whereas lower BIIC volumes of 1:500 and 1:1000 showed only very little potential for effective infection (depicted in Appendix III, Figure 8.10). Hence, different approaches for increasing the infectivity of BIICs were tested. For instance, the effect of time for harvest of the BIIC was analyzed for different time points between 5 and 16 hpi, but none of these approaches led to remarkably increased infection.

Due to the low infectivity arising from BIICs in our hands another approach for BIIC use was implemented, where the protein should be expressed and recombinant virus should be amplified at the same time. BIICs are much more infective in Sf21 than in Hi5 cells, because Sf21 are better suited for baculovirus amplification (Wilde *et al.*, 2014). In contrast to Hi5 cells, Sf21 cells can produce intact virus particles from BIICs that should be capable to infect cells for protein production. Thus, a combination of Sf21 and Hi5 cells was investigated for its ability for enhanced protein production due to better infectivity. The cells were infected with conditioned medium containing the virus (extracellular virus stock) or with BIICs (1:400) in order to test the hypothesized increase in infectivity. For this purpose expression was tested for one extracellular virus stock and two BIIC stocks in parallel, so that we were able to compare the infectivity and protein expression between those different virus stocks

and the used cell setup. Infection was monitored by determining growth kinetics of suspension cultures as well as their mean cell diameter shown in Figure 3.13.

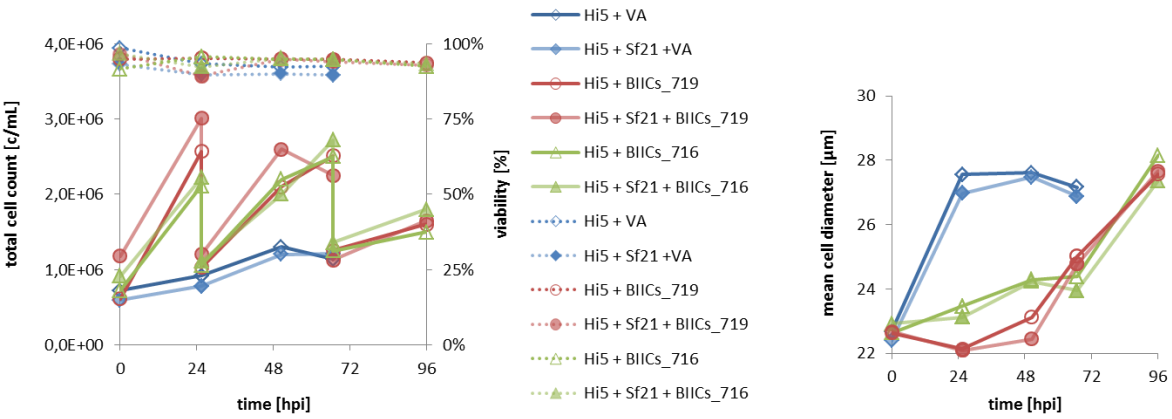

Figure 3.13: Infection test of Hi5 cells and a combination of Hi5 and Sf21 cells infected with BIICs or virus stock
Hi5 suspension cultures with a cell density of ~ 0.75 × 10^6 cells/mL and suspension cultures with 90 % Hi5 and 10 % Sf21 cells with an initial cell density of ~ 0.5 × 10^6 cells/mL were infected with extracellular virus stock (VA) or two different BIIC stocks (BIICs_716 and BIICs_719). The cultures were expanded 24 hpi when the number of cells reached 2 × 10^6 cells/mL or more. Cell count and viability were assessed with the Guava EasyCyte flow cytometer. The mean cell diameter was analyzed with CASY counter. Significant increase in cell diameter and stagnation of cell proliferation indicate successful infection.

Both, Hi5 cells as well as the combination of Hi5 and Sf21 cells infected with BIICs do not show any signs of infection within the first 48 hpi. No significant increase in diameter was observed nor reduced proliferation. Infection slightly starts within these cultures between 48 hpi and 72 hpi, while as late as 96 hpi a significant decrease in cell growth and increase in cell diameter was observed. In contrast to that, both setups infected with extracellular virus stock (VA) were successfully infected within 24 hpi, as shown in Figure 3.13. Infection is indicated by an increase of the mean cell diameter of about 5 µm and decreased cell growth. However, no obvious differences concerning infection efficiency were obtained between the homogenous Hi5 expression cultures and the mixture of Hi5 and Sf21 cells. The supernatants were harvested (at 72 hpi or 96 hpi) and subsequently analyzed for recombinant protein expression via western blot (Appendix III, Figure 8.11). Besides, some of the cultures were used for purification using the Profinia protein purification system (Appendix III, Figure 8.12). However, no increase in protein expression was detectable for any of the tested setups and the yield for recombinant HA was only between 2 and 3 mg/L.

3.3.2 Transient gene expression in Hi5 cells

The previous attempts showed that recombinant H1 expression in Hi5 insect cells was qualified. However, efforts for up-scaling the process by using BIICs were not very promising. Meanwhile our research group established a protocol for transient gene expression (TGE) in Hi5 insect cells, because high expression levels were recently observed in Hi5 cells with the viral OpIE2 promoter (Bleckmann

et al., 2015). With this protocol yields for recombinant protein expression in Hi5 cells were achieved in our department that lie in the range of expression via BEVS, while expression was much faster. Besides, no problems concerning viral infectivity or stability occur, making it a well suited alternative to BEVS. Thus, the protocol should be used in order to test its ability for recombinant HA expression and for its capability for process scale-up.

In order to analyze the potential of TGE in Hi5 cells for recombinant H1 expression four suspension cultures of 350 mL were used in parallel for transient transfection (2.5.6 and 2.6.2). Transfection efficiency was determined by fluorescence measurements due to the co-transfected pOpIE2-eGFP plasmid. Besides, cell count and viability were observed every 24 h during cultivation. The obtained data of growth kinetics and transfection efficiency is depicted in Figure 3.14. The cells stayed in the exponential growth phase and at a viability of about 80 % without addition of fresh media within 72 h of cultivation. Besides, quite uniform transfection efficiencies of 64 – 70 % were observed in the individual cultures, indicating a good reproducibility and reliable results.

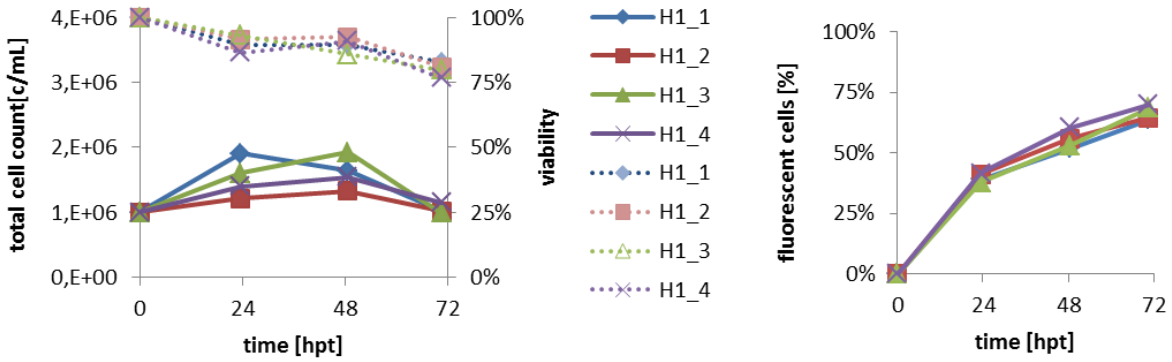

Figure 3.14: Growth kinetics and transfection efficiency of Hi5 insect cells expressing H1 upon TGE
Hi5 suspension cultures with a cell density of 1 × 10^6 cells/mL were transfected with 95 % pOpIE2-H1 and 5 % pOpIE2-eGFP. Expression of eGFP can thus be used to measure transfection efficiency. Cell count, viability and fluorescence were assessed with the Guava EasyCyte flow cytometer.

Supernatants were analyzed for recombinant protein expression at 24, 48 and 72 hpt (hours post transfection) via western blot incubated with His-tag primary mAb and secondary goat-anti-mouse AP-conjugated pAb in order to analyze the amount and quality of recombinant H1 at different time points, depicted in Appendix III, Figure 8.13. Due to this successful H1 detection, purification with an ÄKTA purification system using HisTrap excel columns was conducted as established for BEVS derived H1 in 3.2.2. As already indicated there the imidazole concentration in the washing buffer was increased for the reduction of impurities due to stronger binding of the target protein according to the trimeric His tag (3.2.2). Elution fractions of 1 mL were analyzed by SDS-PAGE. Purification of H1 via TGE in Hi5 insect cells was very efficient as depicted in Figure 3.15. The elution fractions (11-17) were collected, dialyzed, concentrated and used for thrombin cleavage (3.2.3), SEC (3.2.4) and

reverse Strep-Tactin purification (3.2.5) before they were used for crystallization set-ups (3.4.1). With this method of TGE in Hi5 cells a total amount of 8.2 mg pure H1 was successfully purified corresponding to ca. 6 mg recombinant H1 per liter.

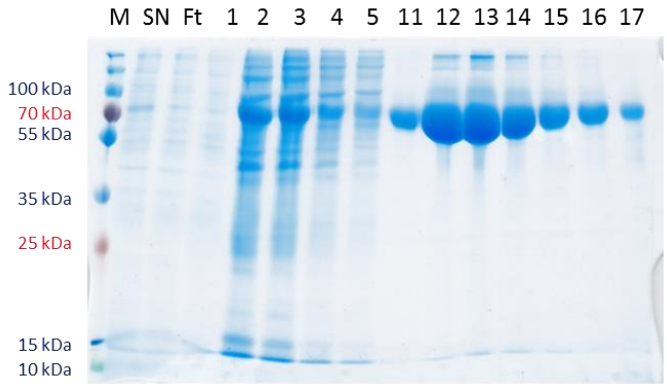

Figure 3.15: Purification of TGE derived H1 with HisTrap excel
H1 was expressed upon TGE in Hi5 cells and was subsequently subjected to HisTrap excel purification. The SDS gel was stained with InstantBlue. The samples of different fractions are presented. M = P PageRuler™ Plus Protein Ladder, SN = crude supernatant after harvesting, Ft = flow through, 1 - 5 = wash fractions, 11 – 17 = elution fractions.

The obtained product titer of 6 mg/L pure H1 corresponds to about 70 % of the average titer of H1 purifications after expression via BEVS. Yet, the expression of the H3 protein even increased with an average titer of 13.4 mg/L up to four-fold compared to BEVS. Besides, only very low variations in purified protein titer between the individual experiments were observed via TGE.

Moreover, in contrast to BEVS, in case of TGE no expression experiment failed, but all were subjected to purification, while the expression via BEVS was aborted occasionally due to low or even no infection. This clearly indicates an advantage over the expression via BEVS, because it prevents phases without recombinant protein production within the process. Taking the protein quality into consideration another advantage of TGE in relation to BEVS was observed. During protein expression via BEVS a fairly quick decrease in viability can happen, as it was observed in Figure 3.3 in section 3.1.1 for H1. This decrease in viability results in cell lysis, which causes the release of proteases into the cell culture supernatant. The target protein thus is susceptible to degradation by those proteases resulting in reduced unprocessed protein of good quality that will be co-purified with those degraded contaminants (depicted in Figure 3.4). The non-lytic nature of virus-free expression systems like TGE on the other hand prevents degradation and thus ensures an overall increased product quality (Bleckmann, 2016).

3.4 Crystallization of recombinant HA of the subtypes H1 and H3

Large scale expression, further purification experiments and crystallization setups were performed with HA subtypes H1 and H3 only, because H7 was already cleaved by host proteases during purification. Since only the unprocessed/uncleaved HA0 can be used to determine the structure of the HA cleavage site, cleaved H7 was not appropriate for this approach.

The purified trimeric H1 protein derived from baculoviral expression in Hi5 insect cells was used for initial crystallization screening using commercially available screens. Jörn Krausze (HZI Braunschweig) carried out the very first setups with the sitting drop vapor diffusion method with protein concentrations in the range of 3 – 5 mg/mL. However, no crystals could be observed until the concentration was increased up to 10 mg/mL. Hence, 10 mg/mL was used as a standard for further crystallization experiments. Protein and reservoir volume ratio was set to 1 : 1 (0.2 µL : 0.2 µL) with Honey bee robot and crystallization was carried out at 19 °C. With this setup the first crystals started to grow in various sizes and shapes after two – 13 days, depicted in Figure 3.16. Their buffer conditions are listed in Appendix IV, Table 8-1.

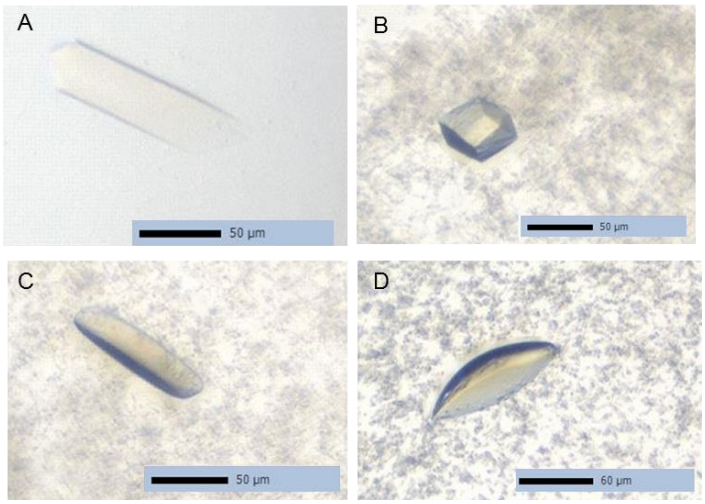

Figure 3.16: Initial hits of H1 crystallization
Initial hits of H1 crystals obtained from expression via BEVS. The harvested supernatant was diafiltered with the KrosFlow® research IIi TFF system, subjected to HisTALON™ purification and thrombin digestion. The trimeric protein was then isolated by SEC with a S200 16/60 column and concentrated to 10 mg/mL with VivaSpin concentrators. Crystallization was carried out by Jörn Krausze (HZI) at 19 °C with 1:1 protein to reservoir volume by using commercial available screens. Observed crystals grew after two – 13 days in the conditions listed in Appendix IV, Table 8-1.

Additionally, crystallization setups were performed with 10 mg/mL trimeric H3 derived from baculoviral expression in Hi5 insect cells. The H3 was purified by diafiltration, HisTALON™ affinity chromatography, thrombin digestion and SEC with usage of a Superdex 200 Increase 10/300 GL column. For initial screening the commercial screen JCSG+ was used, because it yielded in several hits for the first H1 crystallization trials. Crystallization again was performed with the sitting drop vapor diffusion method as described in 2.8.1. The first crystals within this setup started to grow after five

days and had a highly branched shape (Figure 3.17 A and B). The next crystals with a much more uniform triangle shape were first observed at day 8 (Figure 3.17 C). While the last very nice shaped crystal occurred after 13 days and continued to grow further until it was harvested, flash frozen and tested in-house on day 21. The buffer conditions of each crystal are listed in Appendix IV, Table 8-2.

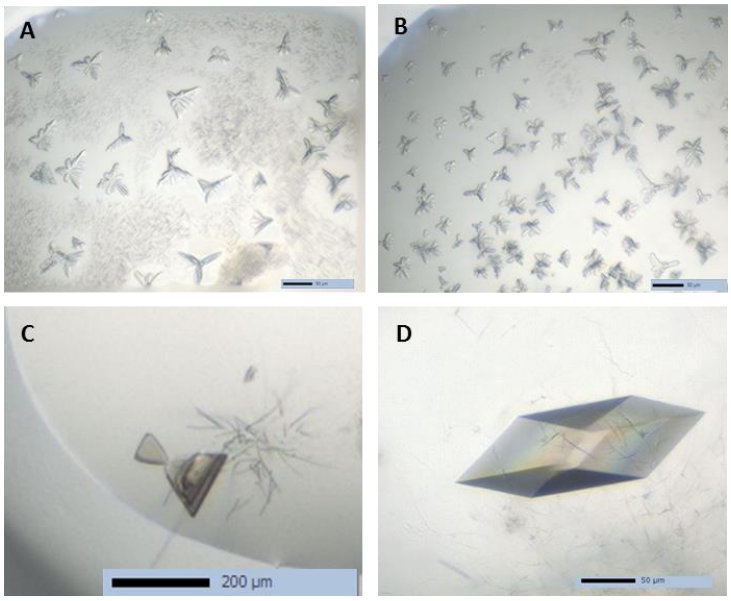

Figure 3.17: Initial hits of H3 crystallization
Initial hits of H3 crystals obtained from expression via BEVS. The harvested supernatant was diafiltered with the KrosFlow® research IIi TFF system, subjected to HisTALON™ purification and thrombin digestion. The trimeric protein was then isolated by SEC with a S200 Increase 10/300 GL column and concentrated to 10 mg/mL with VivaSpin concentrators. Crystallization was carried out at 19 °C with 1:1 protein to reservoir volume by using commercial available screens. Observed crystals grew after five – 13 days in the conditions listed in Appendix IV, Table 8-2.

Promising H1 and H3 crystals were used in-house or at synchrotrons for first diffraction experiments in order to test their ability for structure determination upon X-ray crystallography. The best results were obtained with H1 crystal depicted in Figure 3.16 D which had a resolution of up to 2.7 Å and H3 crystal depicted in Figure 3.17 D with a resolution of up to 1.6 Å. The H3 crystal already obtained quite high resolution; however, ice rings that occurred due to crystal freezing interfered with the diffraction pattern of the crystal. Furthermore, data analysis demonstrated low electron density at the location of the cleavage site, thus indicating an open loop structure due to protease cleavage. In case of H1 the resolution was desired to be higher in order to get more detailed information of the H1 cleavage loop. Besides, the crystal is twinned and a twinned crystal is not very well suited for structure determination. The twinning prevents simple diffraction patterns and thus hampers structure determination, because it complicates data analysis. Hence, after those initial hits, it was tried to further optimize the crystallization conditions in order to obtain crystals of better quality for X-ray data collection as described in 3.4.1.

3.4.1 Crystal optimization

For crystal optimization random screens were generated based on the buffer conditions of initial hits by using the Formulator liquid handling system (Formulatrix). The first optimization trial was set up with H1 protein derived from TGE in Hi5 insect cells, purified with the optimized HisTrap excel strategy, subjected to thrombin cleavage and finally SEC was performed using a Superdex 200 Increase 10/300 GL column for trimer isolation. Due to the first hits in the JCSG+ screen for both H1 and H3, this screen was used in parallel to the first self-prepared screen, called Random Screen RI. This screen was created based on the conditions of the H3 crystal shown in Figure 3.17 D, since this crystal already obtained a pretty good diffraction pattern.

The very first crystals in this setup grown in JCSG+ screen were already observed within one week, depicted in Appendix IV, Figure 8.14. However, they did not have a nice shape that would result in a good in reflection pattern, since they are kind of intergrown crystals (Appendix IV, Figure 8.14 D). In contrast to the JCSG+ screen no crystals obtained within the first week in RI. First crystals were observed only after 33 days, because the imager system was out of order in between, but then a diverse variability of crystals ranging from plates and needles to 3-D crystals was noticed in crystallization screen RI, depicted in Appendix IV, Figure 8.14 A - C. The crystals were tested for their diffraction pattern at our in-house device or were analyzed at Swiss Light Source (SLS) at X06DA/PXIII beamline. However, none of those crystals resulted in a better diffraction pattern than previous ones and thus were not utilized for data collection and structure determination. The crystallization conditions of these first auspicious hits were used for the next random screen optimization (RII) with the objective of directing crystal growth in a more uniform way.

The second optimization trial was conducted with H1 protein derived from baculoviral expression in Hi5 insect cells, purified with optimized HisTrap excel strategy, subjected to thrombin cleavage and trimer isolation by SEC using a Superdex 200 Increase 10/300 GL column. Here random screen RII, which was created upon the first optimization trial, was used in parallel to the commercial screens JCSG+ and PEG Suite I. However, this time no crystals grew within the first three weeks in those two commercial screens. The plates were imaged again at day 82 to analyze whether new crystals occurred. Indeed, first crystals were eventually observed in PEG Suite I, depicted in Appendix IV, Figure 8.15. The crystals were quite big, but mostly intergrown crystals or plates. The first crystals in random screen RII occurred already after three days, followed by smaller ones with a smoother surface on day 18 (Appendix IV, Figure 8.16 A). The only other crystals within this screen were also observed as late as day 82 (Appendix IV, Figure 8.16 B). In the JCSG+ screen no crystals were observed at all. Several of those crystals were used for diffraction analysis. Nevertheless, none of them exhibited a diffraction pattern suitable for data collection.

The last optimization trial was conducted with H1 derived from both baculoviral expression and TGE in Hi5 insect cells, purified with optimized HisTrap excel strategy, subjected to thrombin cleavage and trimer isolation by SEC using a Superdex 200 Increase 10/300 GL column. Afterwards the protein was additionally purified with magnetic Strep-Tactin beads in order to remove potential contamination with protein that was not successfully cleaved with thrombin, which would still harbor the heterologous trimerization domain or other tagged contaminants (3.2.5). This step was implemented to ensure a homogenous protein sample that should result in uniform crystallization and improved reproducibility.

For the last H1 crystal optimization a new screen was generated that is based on the conditions of the H1 crystal depicted in Figure 3.16 D (25% (v/v) PEG MME 550 + 0.1 M HEPES pH 7.5). This screen, called H1-Grid, covers a pH range of 7.2 - 7.8 and besides different PEG MME 550 concentrations in the range of 20 – 30 % (v/v) and was thus supposed to generate crystals similar to the so far best crystal of H1. Next to this new screen the commercial screen PEG Suite I and random screen RI were used with both protein preparations. However, the only crystals within this setup were observed in PEG Suite I on day 12 (Appendix IV, Figure 8.17 A) and 21 (Appendix IV, Figure 8.17 B) with H1 derived from baculoviral expression. Whereas no grow of crystals was observed in the other tested screens.

For H3 crystal optimization the commercial screens JSCG+ and PEG Suite I as well as self-prepared random screens RI, RII and RIII were utilized. The random screen RIII was created upon the observation that both H1 and H3 crystals tend to grow in various conditions containing PEG and di-sodium malonate (second H1 crystal optimization trial, H3 crystal in Figure 3.17 D). The H3 protein used for crystal optimization was expressed via TGE in Hi5 insect cells, purified with optimized HisTrap excel strategy, subjected to thrombin cleavage, reverse Strep-Tactin purification and trimer isolation by SEC using a Superdex 200 Increase 10/300 GL column.

After two – five days the first H3 crystals started to grow in random screen RI (Figure 3.18 A and B) and JCSG+ (Figure 3.18 C and D). The next crystals started to grow on day 17 (Figure 3.18 E - G). One of these continued growing until it was harvested at day 32. Figure 3.18 H depicts the crystal with its final size at day 32. The crystals depicted in Figure 3.18 A, E and H were harvested at day 32 and were tested for their diffraction potential at “Deutsches Elektronen Synchrotron” (DESY) PETRA III beamline, but only the crystal in Figure 3.18 H, exhibited a diffraction pattern suitable for data collection.

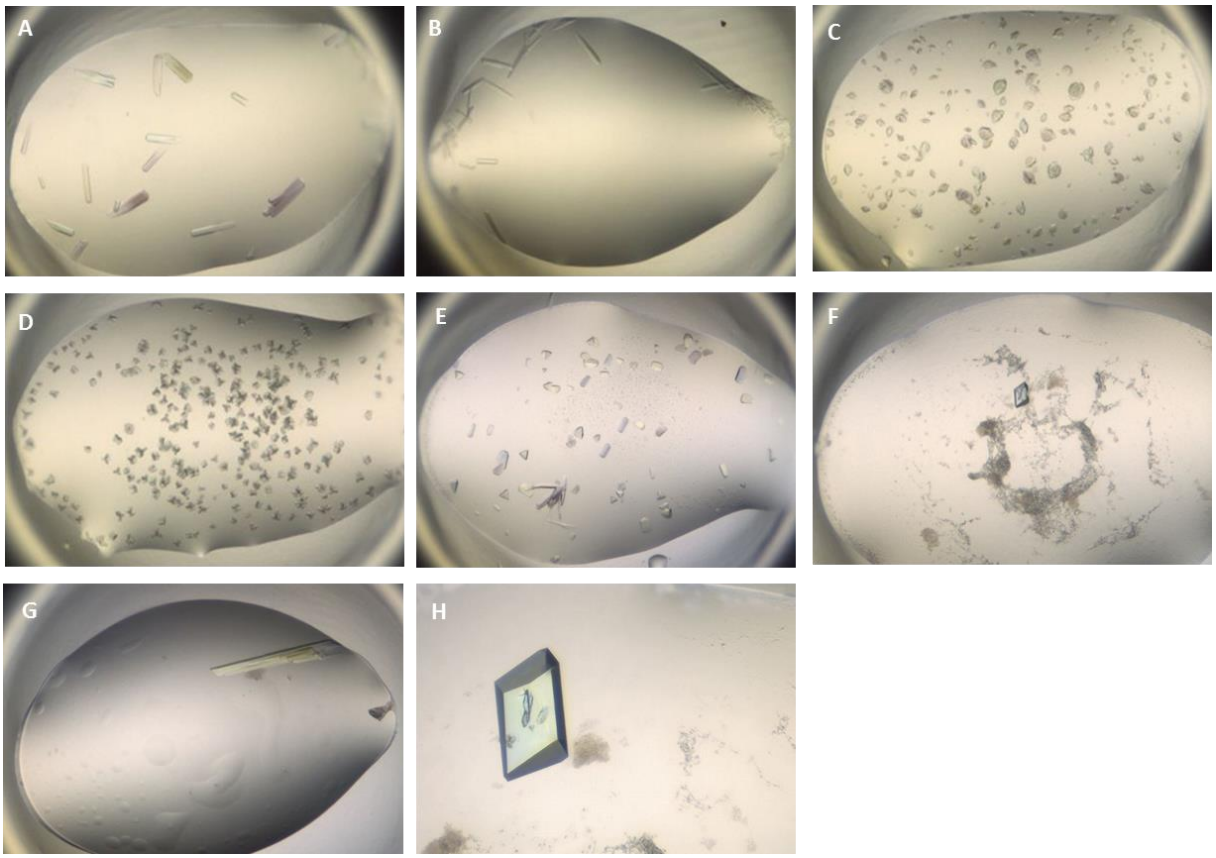

Figure 3.18: H3 crystals of crystal optimization
H3 crystals obtained in the optimization trial with H3 derived from TGE in Hi5 insect cells. The cell culture supernatant was directly subjected to HisTrap excel purification, followed by thrombin cleavage, reverse Strep-Tactin purification and SEC with a S200 Increase 10/300 GL column for trimer isolation. Samples were concentrated to 10 mg/mL and crystallization was carried out at 19 °C with 1:1 protein to reservoir volume. The first hits of H3 obtained in the commercial screen JCSG+ and random screen RI after two – five days (A – D). At day 17 more crystals of different size and shape were observed (E - G). The crystal depicted in F further grew to day 32, when it was harvested (H).The buffer conditions of each depicted crystal are listed in Appendix IV, Table 8-7.

3.4.2 Data collection and structure determination

The best diffracting H1 and H3 crystals resulting from the preceding optimization trials were used for data collection and their datasets were then applied to molecular replacement by using the structure of another HA (PDB ID: 1HA0) to determine its distinct structure.

In case of H1 the best diffracting crystal, depicted in Figure 3.19 A, was a twinned crystal with a relative poor diffraction up to 2.7 Å. The twinning of the crystal tremendous hampers structure determination which was performed by Jörn Krausze (HZI). The diffracting pattern was sufficient enough for a first rough structural elucidation, but no detailed information could be acquired from this dataset. Furthermore, it was not possible to define the structure over the complete ectodomain sequence. In some parts of the protein the electron density is so poorly defined that it was not possible to incorporate the particular AA, which leads to some gaps in the H1 model. This also includes the proteolytic cleavage site, so that unfortunately no structural information of the cleavage

loop could be obtained. Either, it was already processed by proteolytic cleavage or it was just not defined in the available electron density.

The H3 structure elucidation was performed with the help of Peer Lukat (HZI). In contrast to H1 the best diffracting H3 crystal, depicted in Figure 3.19 B, exhibits a very high resolution of 1.45 Å. The statistics of data collection and data refinement are listed in Appendix IV, Table 8-8 and Table 8-9. The dataset resulting from this crystal reveals a very good defined electron density map that enabled detailed insights into the H3 structure. However, it was unambiguous that the obtained structure belongs to a proteolytic cleaved protein as it was already observed for the first H3 crystal of good diffraction quality (Figure 3.17 D). Thus, a well-defined H3 structure was gained, but still we were not able to get structural information of its cleavage loop.

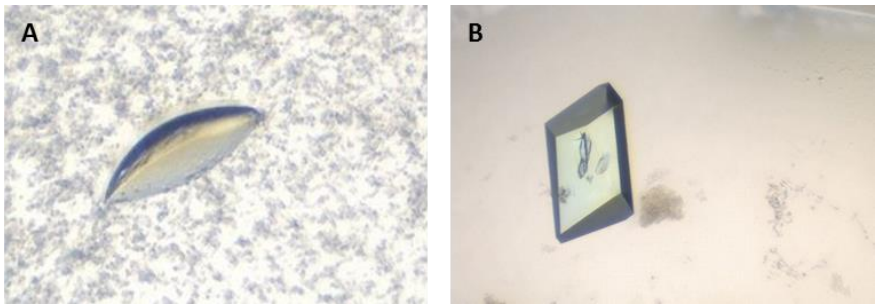

Figure 3.19: H1 and H3 crystals used for data collection and structure determination
A: The best diffracting H1 crystal was obtained from the first crystallization setup with BEVS derived H1 in a crystallization buffer composition of 25% (v/v) PEG monomethyl ether (MME) 550 + 0.1 M HEPES pH 7.5. It started to grow after 3 days and continued growing until it was harvested at day 25. B: The best diffracting H3 crystal was obtained from the very last optimization trial with H3 derived from TGE in Hi5 cells. The crystal started to grow at day 17 in a crystallization buffer of 0.1 M di-Sodium malonate + 23.3 % w/v PEG 3350 + 0.1 M HEPES pH 7.889. The crystal further grew until it reached its final size at day 32, when it was harvested.

The structure of recombinant H1 and H3, depicted in Figure 3.20 as a cartoon diagram of α-helices and β-sheets, represent their overall trimeric architecture. Each HA monomer is presented in different colors. Most of their HA1 subunits folds into the globular head domain, while HA2 forms a stalk that projects it outward from the surface of the virus. The N-terminus of HA2 that comprises the fusion peptide, marked in yellow, points to the inside of the threefold axis as it is common for the HA pre-fusion state. Additionally, both proteins carry N-linked oligosaccharides at their glycosylation sites that are not depicted in Figure 3.20. A figure of one H3 monomer with the visible N-linked oligo-saccharides at its glycosylation sites is depicted in Figure 3.21.

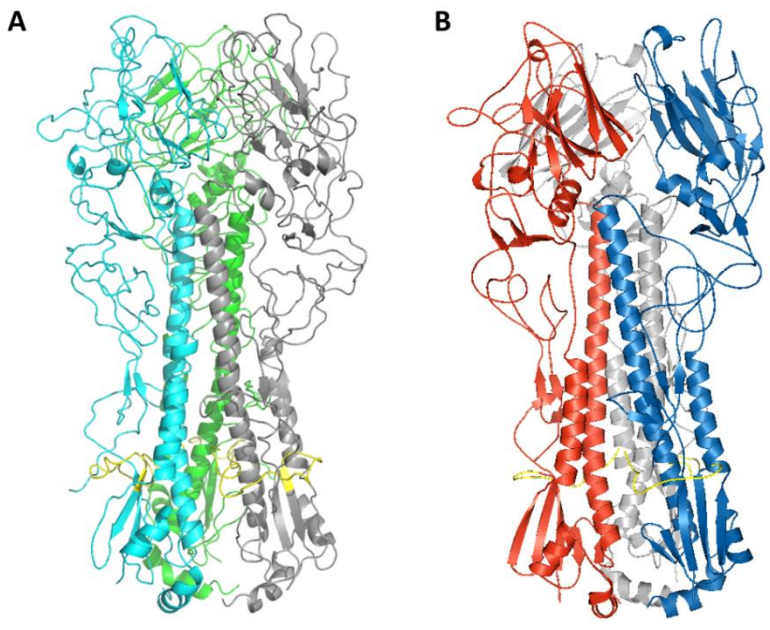

Figure 3.20: Structure of recombinant H1 and H3
Cartoon diagram of recombinant H1 (A) and H3 (B) structure. Each monomer is presented in different colors (H1: cyan, grey and green, H3: Red, blue and grey). The sequence of each fusion peptide is shown in yellow. The figures were drawn with the program PyMOL.

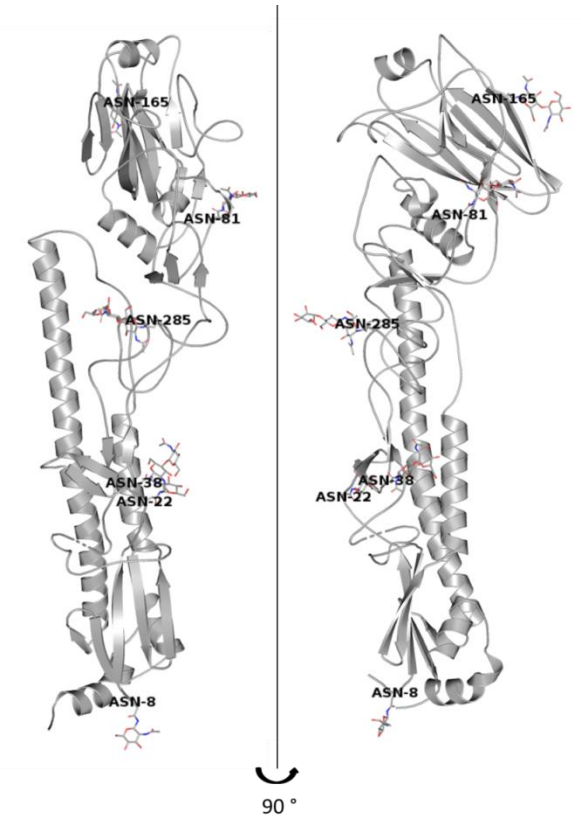

Figure 3.21: H3 monomeric structure with N-glycosylation sites
One Monomer of trimeric H3 is depicted in two different views with 90 ° rotation with its occupied N-glycosylation sites. Each glycosylation site is indicated with the corresponding asparagine and its AA position (e.g. ASN-8). N-linked glycans were incorporated in the structure as far as they were clearly visible in the electron density (the figure was drawn with the program PyMOL by Peer Lukat, HZI).

All in all, recombinant HA of the subtypes H1 and H3 was successfully expressed in Hi5 insect cells via BEVS and TGE in its uncleaved, non-modified HA0 pre-fusion state for crystallization studies. Additionally, an efficient purification strategy was developed and the production process was analyzed for its potential for process up-scaling. Eventually, a protocol was established for large scale HA expression that was reliable, economic, easy to handle, comparatively fast and accessible for HA production in bioreactor dimensions. Among the different expression systems evaluated for recombinant HA expression the method of TGE in Hi5 insect cells pointed out to be advantageous as it not only allows fast and easy expression of homogenous HA, but is also very successful for process up-scaling. Overall, the production process and its optimized downstream processing resulted in very pure protein of high-quality. Crystallization setups with recombinant H1 and H3 led to a diverse range of crystals. Nevertheless, the structures that were derived from these crystals did not obtain an intact cleavage loop, so that unfortunately no structural information of the different cleavage loops was acquired. Further attempts need to be conducted to overcome this obstacle.

4 Hepatitis surface proteins

4.1 Recombinant E2 expression

HCV infections constitute a major global health problem being one of the main causes of chronic liver disease with approximately 130 – 170 million people infected worldwide (World Health Organization, 2017). Still, there is no effective vaccine against HCV available. The envelope glycoproteins E1 and E2 of HCV are critical to mediate virus receptor interactions and to permit virus uptake into human liver cells. Besides they are the target of neutralizing antibodies, which inactivate circulating viruses in vivo. However, HCV has evolved various strategies that ensure virus persistence in the presence of large amounts of glycoprotein-specific antibodies (von Hahn *et al.*, 2007). Therefore this part of the project deals with the expression and purification of HCV protein variants that ought to re-direct antibody responses towards hidden and more conserved viral epitopes.

The first strategy to express such glycoprotein variants encompasses both envelope proteins co-expressed together with the last 60 residues (AA 175 - 191) of the core protein. This last core domain corresponds to the signal sequence for E1 (Polyak *et al.*, 2006) and is followed by the full-length envelope glycoproteins E1 (AA 192 – 383) and E2 (AA 384 – 750) from the HCV genotype 2a (isolate HC-J6, Taxonomy ID: 11113). The different variants of this cE1E2 construct include the *wildtype* (*wt*) of E1 and E2 as well as variations of E2 in combination with *wt* E1. In order to re-direct antibody responses a few primary approaches were tested. The first variant (cE1E2ΔHVR1) comprises the deletion of HVR1, which is the most variable domain of the E2 protein that is known to act as an immune decoy to prevent effective antibody neutralization (von Hahn *et al.*, 2007; Haid *et al.*, 2012). The second variant (cE1E2ΔHVR1-N534A) combines this deletion with the inactivation of a glycosylation site within E2 through an AA exchange of Asparagine to Alanine at position 534 (numbering corresponds to AA position in HCV polyprotein). This glycosylation site (N6; N532/N534 depending on HCV genotype) was found to be highly conserved between various genotypes (98 %) and it was identified through various mutational studies to mask epitopes with its glycan residues (Helle *et al.*, 2007, 2010). This modification should thus induce the neutralizing activity of anti-HCV antibodies compared to the *wt* protein. For detection and purification, a C-terminal fusion with to different tags was generated to each construct. Upstream of the tags there was a TEV protease cleavage site inserted for removing the tags after purification. A schematic overview of the constructs used for E1E2 co-expression can be found in Figure 4.1.

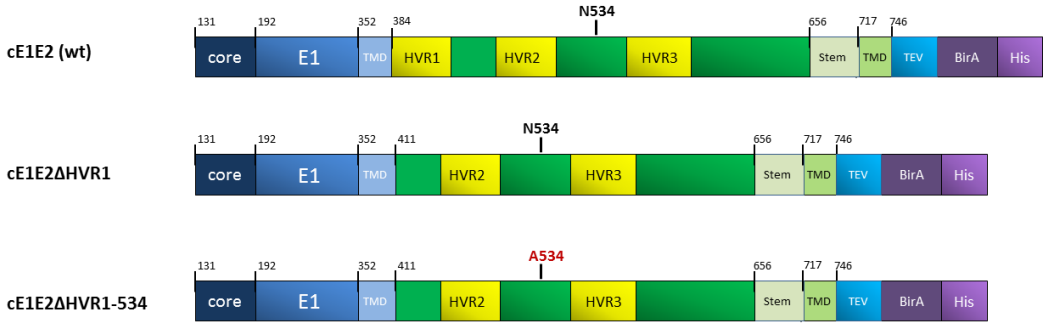

Figure 4.1: Schematic overview of cE1E2 constructs for recombinant E1E2 co-expression
The cE1E2 constructs are N-terminally fused to the last 60 AA of core protein (core 131-191), followed by full-length E1 and E2. C-terminally, an Avi-tag (BirA) and an 8xHis tag are fused to the proteins for purification and detection. Upstream of the tags, a TEV protease site is located to cleave the tags off. Transmembrane domains (TMD), hypervariable regions within the E2 ectodomain (HVR), and the mutated glycosylation site in cE1E2ΔHVR1-N534 are indicated. The amino acid numbering corresponds to the HCV polyprotein.

Additionally, another strategy was pursued dealing with the expression of secreted E2 variants (sE2). For this approach the same E2 variations were constructed with an N-terminal IgG secretion signal (IgG ss) fused to E2, which ends either at AA position 661 or 688, thus comprising the whole ecto-domain or even extend to part of the E2 stem region. Expression was already described by various groups to be successful for E2 truncations ending at AA 661 (Michalak *et al.*, 1997; Dubuisson *et al.*, 2000; Rodríguez-Rodríguez *et al.*, 2009; Tello *et al.*, 2010; McCaffrey *et al.*, 2012) and to be independent of E1 co-expression (Michalak *et al.*, 1997; McCaffrey *et al.*, 2012). Next to that an additional *wt* sE2 variant (sE2(1a)wt, AA 384-661, (Li, 2014)) ending at AA 661 of genotype 1a (isolate H77, Taxonomy ID: 11108) was used. This variant is N-terminally fused to tissue plasminogen activator (tpa) secretion signal and comprises a C-terminal His-tag. A schematic overview of these sE2 constructs is depicted in Figure 4.2.

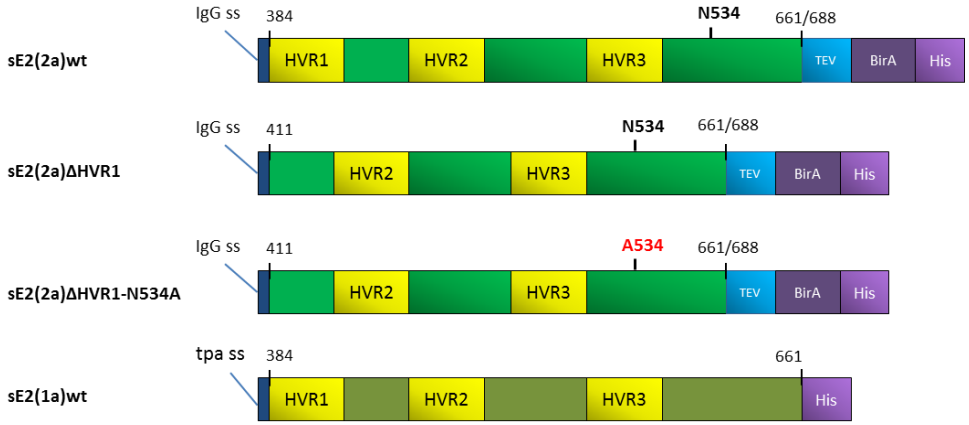

Figure 4.2: Schematic overview of sE2 variants used for recombinant E2 expression
The sE2(2a) constructs are N-terminally fused to the IgG secretion signal (IgG ss) to allow secretion in the supernatant, followed by E2 ectodomain ending either at AA 661 or 688. C-terminally, an Avi-tag (BirA) and an 8xHis tag are fused to the proteins for purification and detection. Upstream of the tags, a TEV protease site is located to cleave the tags off. Whereas, the sE2(1a)wt variant is N-terminally fused to tpa secretion signal (tpa ss) and C-terminally to an 6xHis tag. The numbering of AA corresponds to the HCV polyprotein.

4.1.1 Co-expression of E1E2 in HEK293-6E cells

For co-expression of the HCV E1 and E2 glycoproteins the different coreE1E2 variants of genotype 2a were cloned into the pFlpBtM-III vector (Steffen Meyer, HZI; unpublished work based on Meyer et al., 2013) and were transiently transfected in HEK293-6E cells. The expression of the secreted E2 construct of genotype 1a (sE2(1a)wt, AA 384-661) in a pcDNA 3.1-tpa eukaryotic expression vector was performed in parallel and served as control for recombinant E2 expression. Transfection was conducted according to the protocol by Jäger et al. 2015, described in detail in 2.5.5. Co-transfection of pTTo/GFPq was used to control the transfection rates via fluorescence measurements by flow cytometry of daily samples. Valproic acid was added 96 hpt to a final concentration of 3.75 mmol/l in order to possibly increase the recombinant protein levels and each culture was harvested 168 hpt. With this setup about 60 – 75 % of the cells expressed GFPq after 48 hpt, indicating successful transfection. Samples of cell culture supernatants were taken every 24 h and were analyzed for recombinant protein expression by SDS-PAGE and Western blot. However, upon detection with anti-His mAb mainly higher molecular weight bands that seem not to enter the gels were observed, which could correspond to aggregates (data not shown). Such aggregates have been commonly observed upon heterologous E2 expression by various research groups (Michalak *et al.*, 1997; Whidby *et al.*, 2009; Tello *et al.*, 2010; Neyshabouri *et al.*, 2012; Khan *et al.*, 2014; Li, 2014). In fact, it is so common that a non-productive folding pathway has been proposed to be a physiologically relevant part of the HCV life cycle (Whidby *et al.*, 2009).

In another set-up transfection was carried out as described before, but culture supernatants were already harvested 96 hpt due to low viability after valproic acid addition in the previous experiment. Transfection efficiencies were quantified via fluorescence measurements as depicted in Figure 4.3. They vary widely between these cultures, ranging from 74 % for the cE1E2ΔHVR1-N534A variant to as low as 17 % for cE1E2ΔHVR1.

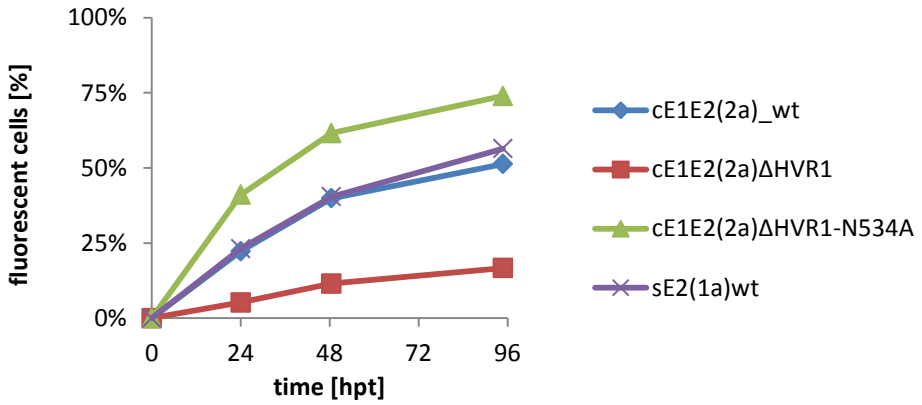

Figure 4.3: Graphical overview of transfection efficiencies of HEK 293-6E cells transfected with cE1E2 constructs
The GFPq expression was monitored as a control for transfection efficiency by flow cytometry. Fluorescence was determined at a Guava EasyCyte flow cytometer using a 488 nm laser for extinction.

This time both, supernatants and cell lysates (2.6.5), were analyzed for the presence of the glycoproteins in order to verify successful secretion. Detection with anti-His mAb, however, resulted in a pattern of only unspecific protein bands. Therefore the mouse mAb, AP33 (Potter *et al*. 2012; prepared by Tanvi Khera at Twincore) that recognizes a conserved, linear epitope on E2, was used for detection. The cE1E2 constructs have a theoretical size of about 70 kDa and 31 kDa for sE2(1a)wt, respectively. However, N-linked glycans constitute nearly 50 % of the molecular weight in the E2 ectodomain (Goffard *et al.*, 2005; Falson *et al.*, 2015), thus increasing its size. In case of sE2(1a)wt the protein was reported to migrate on SDS-PAGE at a size about 55 kDa due to its glycosylation upon expression in HEK 293-6E cells (Li, 2014). Indeed, a protein band of about that size was detected upon western blot analysis in the supernatant and cell lysate (depicted in Figure 4.4), which accumulates in the supernatant during the experiment. This band appears quite smeary, because of heterogeneous glycosylation of the protein. In case of cE1E2(2a) variants, however, only very slight expression was observed. While transfection with cE1E2ΔHVR1-N534A was quite efficient with 74 %, the expression was barely detectable. While expression of cE1E2(2a)wt and cE1E2ΔHVR1 variants was slightly better despite their obvious lower transfection efficiencies of 51 % and 17 %, respectively. All in all, expression of the cE1E2(2a) variants was quite low. Furthermore, the different protein variants did not accumulate during the experiment, neither in the supernatant nor in the cell lysate.

Since satisfying expression was only detected for the $E2_{661}$ variant, sE2(1a)wt, further co-expression experiments were adjourned for a start, while more emphasis was put on the recombinant sE2 expression, that will be covered in the next chapters.

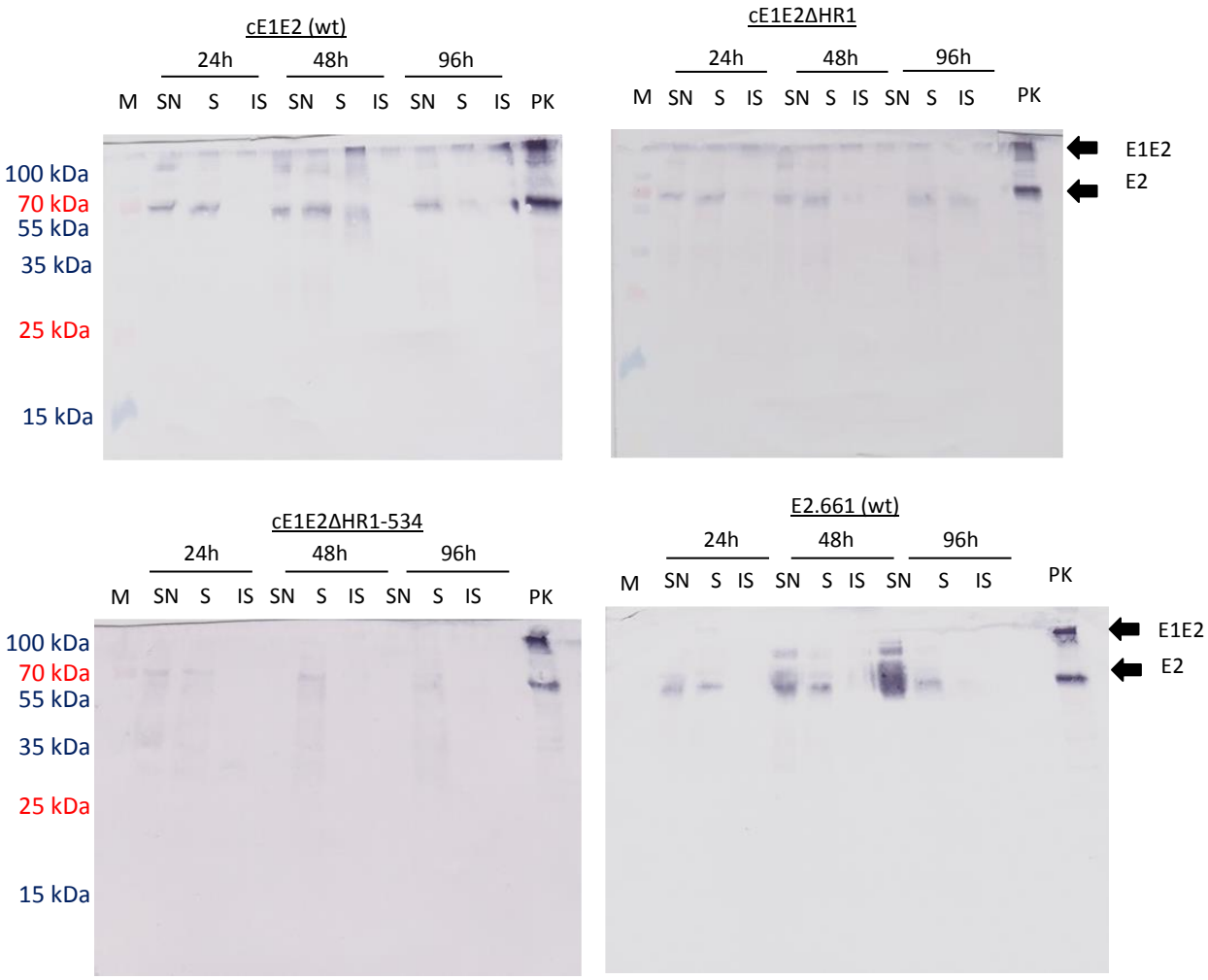

Figure 4.4: Western blot analysis of HCV glycoprotein expression in HEK293-6E cells
Supernatants (SN) and cell lysates (S: soluble, IS: insoluble) of HEK293-6E cells transiently transfected with cE1E2 variants or sE2(1a)wt, as indicated above, were taken 24, 48 and 96 hpt and were analyzed by Western blots using E2 specific mouse monoclonal antibody, AP33, and a secondary goat-anti-mouse AP-conjugated pAb. Colorimetric staining was done with NBT and BCIP. M: PageRuler Plus Prestained, PK: positive control (cell lysate sample containing E2 from Tanvi Khera).

4.1.2 sE2 expression in HEK 293-6E cells

For the approach of recombinant expression of secreted E2, the three variants of genotype 2a as well as sE2(1a)wt were used for transient expression in HEK293-6E cells, as already described in 4.1.1 for E1E2 co-expression. The new genotype 2a constructs contain either the full-length ectodomain including the first residues of E2 stem (688) or the E2 ectodomain up to residue 661 that already led to successful expression and secretion for sE2(1a)wt in the transient HEK293-6E system (see section 4.1.1). Besides, expression and secretion of soluble E2 constructs ending at AA position 661 was already described to be successful and independent of E1 (see section 4.1). The truncated sE2 variants were generated via PCR (2.4.1) and subsequently cloned into pFlpBtM-III vectors thereby obtaining the IgG secretion signal and tags for purification. Upon transient expression in HEK 293-6E

cells growth kinetics and transfection efficiencies were monitored. Transfection efficiencies of about 30 % up to 60 % were observed for the different variants and are displayed in Figure 4.5.

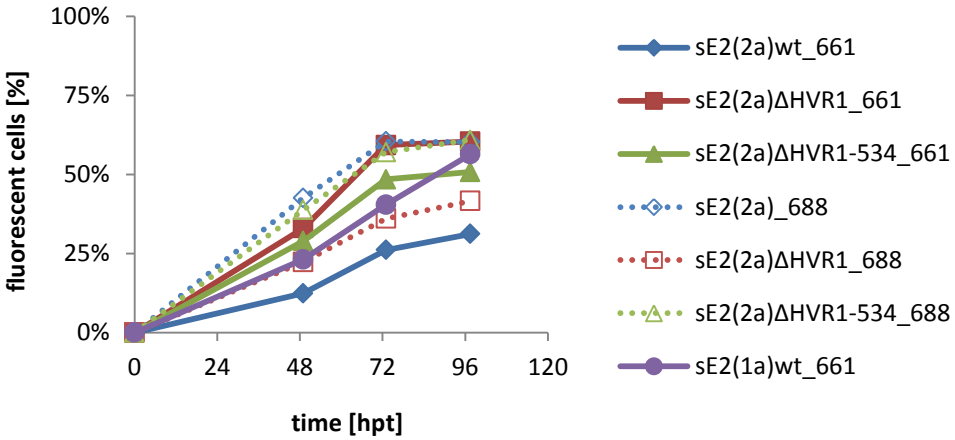

Figure 4.5: Graphical overview of transfection efficiency of HEK 293-6E cells transfected with sE2 constructs
The GFPq expression was monitored as a control for transfection efficiency by flow cytometry. Fluorescence was determined at a Guava EasyCyte flow cytometer using a 488 nm laser for extinction.

Cultures were harvested 96 hpt and expression was analyzed via western blot using both an anti-His (Figure 4.6 A) and anti-E2 mAb (Figure 4.6 B) combined with a secondary goat-anti-mouse AP-conjugated pAb. Additional samples of HEK derived sE2(1a)wt (4.1.1) were used as positive controls for E2 expression. In order to determine unspecific signals supernatants of untransfected HEK cells as well as cells transfected with an empty pFlpBtM-III vector served as negative control.

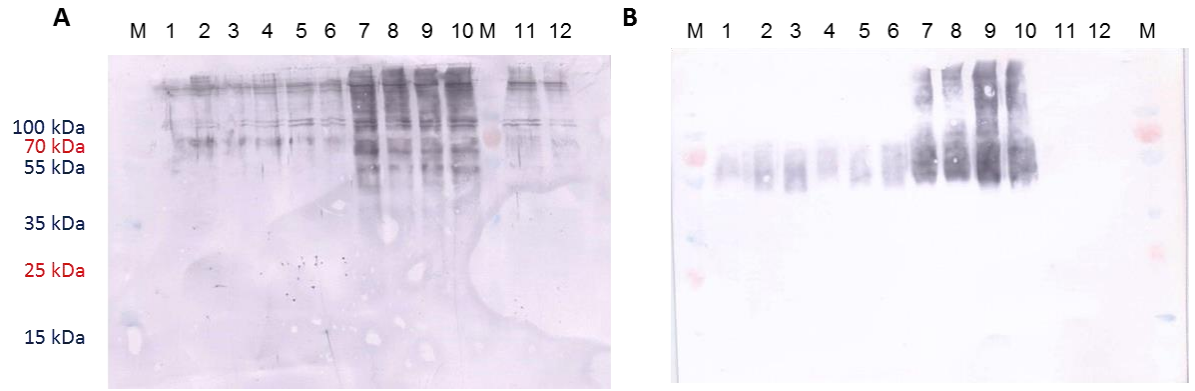

Figure 4.6: Western blot analysis of sE2 expression in HEK293-6E cells
Samples of culture supernatants of transiently transfected HEK293-6E cells were analyzed for the presence of sE2 variants by Western blot. Detection was performed with primary anti-His mAb (A) and anti-E2 mAb AP33 (B) together with a secondary goat-anti-mouse AP-conjugated pAb. Colorimetric staining was done with NBT and BCIP. M: PageRuler Plus Prestained, 1-3: sE2-661 variants, 1: sE2(2a)wt 2: sE2(2a)ΔHVR1, 3: sE2(2a)N534A, 4-6: sE2-688 variants, 4: sE2(2a) wt, 5: sE2(2a) ΔHVR1, 6: sE2(2a) N534A, 7-10: sE2(1a)wt, 11: untransfected HEK 293-6E cells, 12: cells transfected with pFlpBtM-III (empty vector), all samples of crude supernatants were taken at 96 hpt, except for 9 - 10, taken at 168 hpt.

Detection with anti-His mAb resulted in a pattern of only unspecific protein bands (Figure 4.6 A), since the negative controls exhibit the same pattern as the other samples. Only for sE2(1a)wt a

stronger signal due to E2 expression was observed next to those unspecific bands. The E2-specific antibody AP33, however, allowed E2 detection within all expression cultures (Figure 4.6 B), whereas no signals were observed within the negative controls. Expression was detectable, but still quite low for the diverse sE2(2a) variants, yet a strong signal resulted from sE2(1a)wt within both 96 hpt and 168 hpt samples. These samples also seem to contain higher oligomeric states and maybe even aggregates of the E2 protein. Moreover, it is conspicuous that the recombinant sE2 proteins are highly glycosylated since they appear as very smeary protein bands due to their heterogeneous glycan moieties.

4.1.3 sE2 Expression in Hi5 cells

Due to quite poor expression in HEK 293-6E cells and their large amount of heterogeneous glycosylation, sE2 expression was also performed via transient gene expression in Hi5 cells (2.5.6). For this approach each construct was cloned with an IgG secretion signal and tags into the pOpIE2 vector that contains the strongest immediate early baculoviral promoter OpIE2 suitable for transient expression in absence of viral factors (Bleckmann *et al.*, 2015). Cloning and first expression tests were conducted by Mirjam Sommer and are reported in her bachelor thesis (Sommer, 2016). Here, the variants containing the E2 ectodomain to AA 661 showed slightly better expression. Based on these results only those variants were used for establishing purification and expression strategies.

First expression experiments were performed in small scale (20 mL) with the three sE2(2a) variants and sE2(1a)wt. The suspension cultures were cultivated for 96 h and growth kinetics and transfection efficiencies were monitored via FACS due to eGFP co-expression. Fluorescence characteristics are presented in Figure 4.7, indicating transfection efficiencies of 60 – 70 % among sE2 variants. The decrease of fluorescent cells after 72 hpt corresponds to a significant decrease in viability.

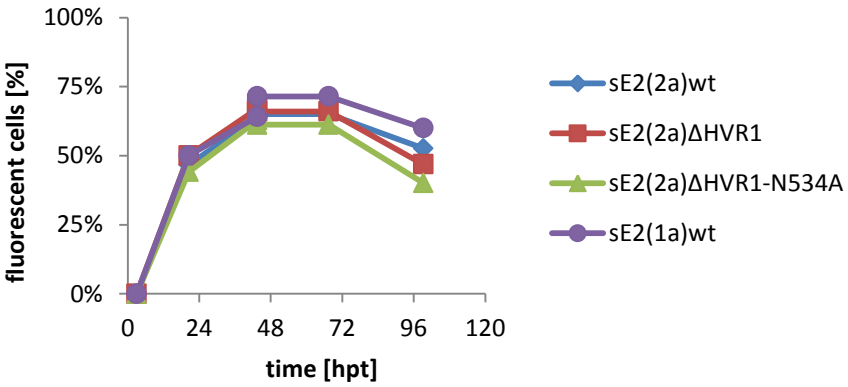

Figure 4.7: Transfection efficiencies of Hi5 insect cells transfected with sE2 constructs
The GFPq expression was monitored as a control for transfection efficiency by flow cytometry. Fluorescence was determined at a Guava EasyCyte flow cytometer using a 488 nm laser for extinction.

After 96 hpt cultures were harvested and subsequently analyzed for recombinant E2 expression by small scale purification with magnetic His beads (His Mag Sepharose excel, GE Healthcare). Those beads are advantageous for analysis of secreted proteins derived from insect cells as they can directly purify his-tagged proteins from the crude cell culture supernatant. Recombinant E2 expression was analyzed using SDS-PAGE and western blot (Figure 4.8).

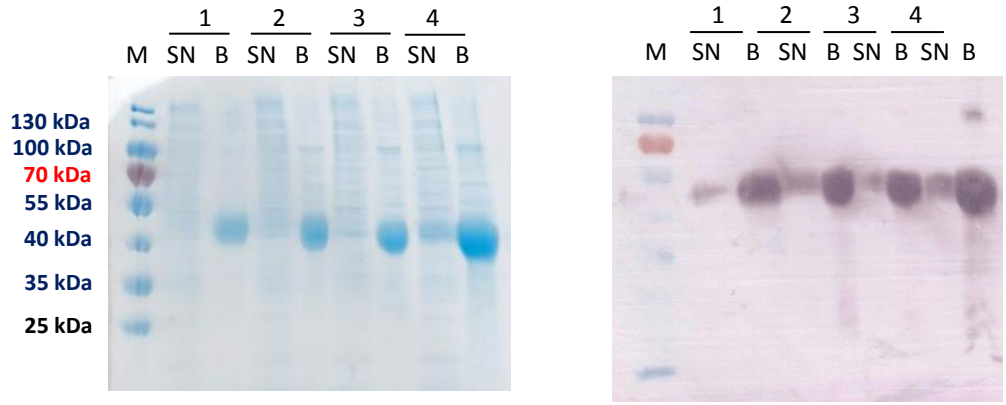

Figure 4.8: small scale purification of sE2 variants derived from transient expression in Hi5 cells
Samples of culture supernatants (SN) and magnetic His beads elution samples (B) of transiently transfected Hi5 cells were analyzed for the presence of sE2. The SDS gel was stained with InstantBlue. The Western blot was performed with primary anti-His mAb together with a secondary goat-anti-mouse AP-conjugated pAb. Colorimetric AP staining was done with NBT and BCIP. M: PageRuler Prestained, 1: sE2(2a)wt 2: sE2(2a)ΔHVR1, 3: sE2(2a)N534A, 4: sE2(1a)wt, all samples of crude supernatants were taken at 96 hpt, elution samples correspond to a 50-fold concentration.

Expression and secretion of sE2 variants was verified via western blot analysis. All four variants were detected not only in the purified and thus concentrated samples but also to a lesser extent in each cell culture supernatant. Judging from the minor smear of the protein bands the proteins are likely glycosylated but not as much as HEK derived proteins. Besides, in contrast to HEK cell supernatants, no unspecific signals were obtained using anti-His mAb. The protein bands of roughly purified E2 were subjected to mass spectrometry for further identification by the MS platform of the research group Cellular Proteomics at the HZI (2.7.4).

Based on these initial achievements in small scale, large scale expression was performed. Here, supernatants were already harvested 72 hpt, because of the low viability observed in the initial experiments after 72 hpt. The establishment of the purification strategy for sE2 variants is explained in detail in section 4.2.

4.2 Establishing purification strategy of recombinant sE2

After successful detection of sE2 expression the secreted recombinant protein variants should be further purified. For affinity purification the supernatants were harvested in two steps as described in 2.6.10. Thereafter the supernatants were directly loaded onto HisTrap excel columns (GE Healthcare) with the use of ÄKTA chromatography system and purification was performed according to the manufacturers protocol. Compared to HA purification (3.2.2) the amount of imidazole in the washing buffer was as low as the recommended 30 mM (6 % buffer B), because of the monomeric nature of the sE2 proteins compared to the trimeric HA. Elution fractions of 1 mL were analyzed by SDS-PAGE as shown in Figure 4.9 A for samples derived from purification of the glycosylation mutant sE2(2a)ΔHVR1-N534A. E2 capture was effective, but still some undesirable impurities remained. Accordingly, further polishing of sE2(2a)ΔHVR1-N534A was performed with Talon metal affinity resin as it was already successful in increasing the purity of insect cell derived HA proteins after Ni-NTA purifications (see 3.2 for comparison).

After dialysis HisTalon purification was performed according to the manufacturers' protocol using an ÄKTA chromatography system, however, the purity of the sample did not increase upon this additional purification (Figure 4.9 B). So the buffer again was exchanged by dialysis and purification was repeated with HisTrap excel columns with more stringent washing conditions (50 mM imidazole, 10 % buffer B). With this improved protocol the amount of impurities could be markedly reduced (Figure 4.9 B), but only as low as 1.2 mg of the E2 protein remained after this three-step purification procedure, representing a loss of 2/3 of the amount after the first purification step and thus does not correspond to the removed impurities.

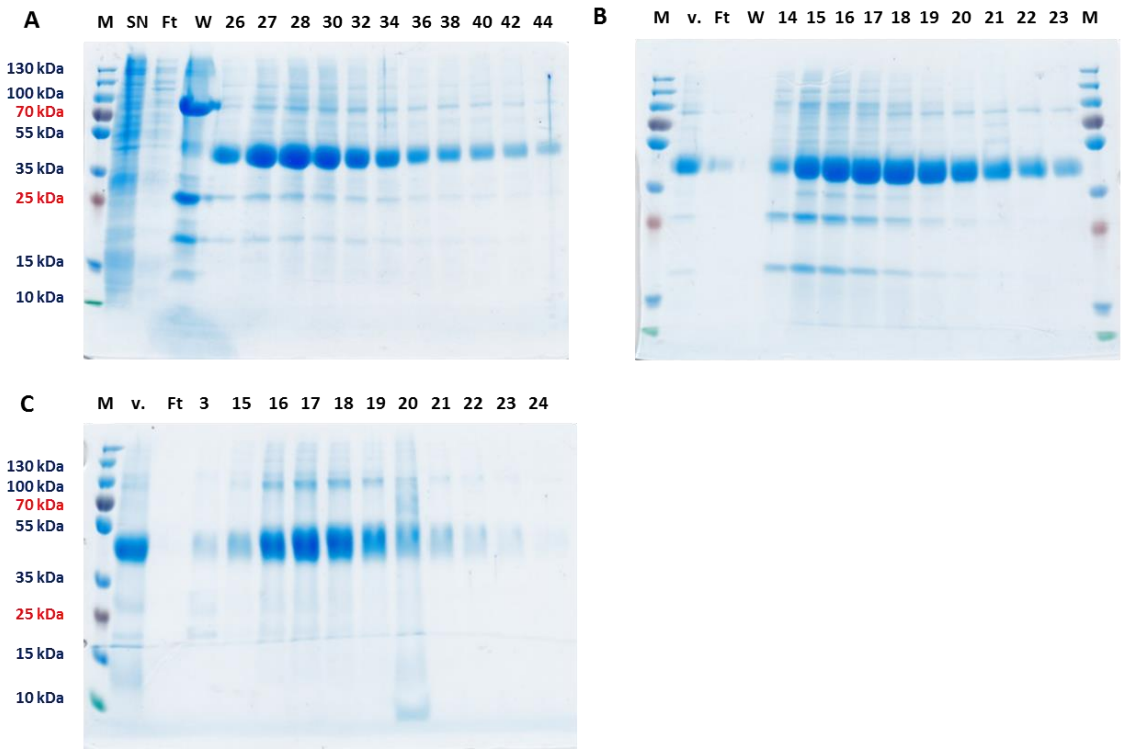

Figure 4.9: SDS-PAGE analysis of affinity purification strategies for sE2(2a)ΔHVR1-N534A
Purification of sE2(2a)ΔHVR1-N534A was analyzed with an ÄKTAFPLC and the samples of different fractions were loaded onto the gel. A: HisTrap excel purification according to manufacturers` protocol. B: HisTalon purification according to manufacturers` protocol. C: HisTrap excel purification with more stringent washing conditions. Staining of the SDS gel was performed with InstantBlue. M: PageRuler Prestained Plus, SN: cell culture supernatant, Ft: Flow through of purification column, W: Wash fraction, v.: sample prior following purification, numbers correspond to numbering of elution fractions.

For the next purifications the stringent washing protocol was applied right after harvesting of the supernatant. With this new protocol quite pure protein could be acquired with just one purification step resulting in significantly less protein loss and thus higher protein yields. The SDS-PAGE showing purification analysis of sE2(2a)ΔHVR1 with a total yield of 6.5 mg/l expression culture is shown in an exemplary way in Figure 4.10.

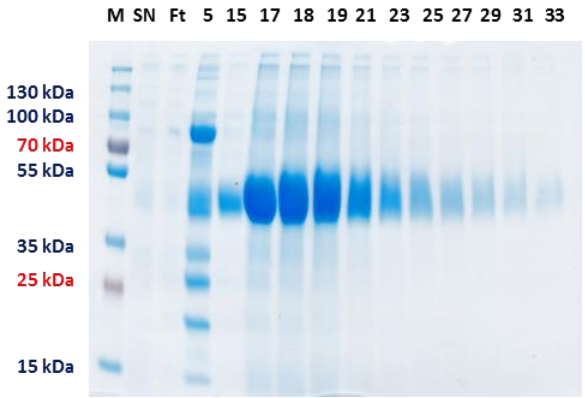

Figure 4.10: SDS-PAGE analysis of HisTrap excel sE2(2a)ΔHVR1 purification with adjusted protocol
Purification of sE2(2a)ΔHVR1 with adjusted stringent washing protocol was analyzed with an ÄKTAFPLC and the samples of different fractions were loaded onto the gel. Staining of the SDS gel was performed with InstantBlue. M: PageRuler Prestained Plus, SN: cell culture supernatant, Ft: Flow through of purification, 5: Wash fraction 5, 15 - 33: elution fractions.

The affinity purified proteins were then applied to size exclusion chromatography (SEC) for further purification. SEC was first performed using a S75 10/300 GL column with 1.5mg sE2(2a)wt in 20 mM TrisHCl 50 mM NaCl buffer at pH 7.4. Unfortunately, upon this approach the protein eluted in the void volume of the column (Figure 4.11 A) indicating protein aggregation. Fractionated samples were analyzed via SDS-PAGE, but only a very faint band of the E2 protein was visible (data not shown). Consequently, another SEC was performed using a S200 10/300 HR column in order to distinguish between higher oligomers of E2 and protein aggregates (Figure 4.11 B). Besides, 10 % glycerol was added to buffer and sample to avoid aggregation by minimizing hydrophobic interactions. Nevertheless, the major part of the E2 protein again eluted in the void volume and close behind. However, the peak now was much broader and had a little shoulder at about 14 mL V_e. Roughly there, monomeric HA eluted during SEC using that kind of column at V_e = 15 mL (see Figure 3.10 and Figure 3.11 in section 3.2.4. for comparison). This indicates a protein size of about 70 kDa, which could pretty much correspond to sE2 dimers. Calculation of the protein size corresponding to that shoulder also results in 70 kDa, confirming the data. The maximum of this peak correlates to a protein size of about 450 kDa according to the calibration curve of the column, thereby indicating a great amount of higher oligomers and aggregates within the sample.

Due to the observation that the E2 protein still tends to aggregate and form higher oligomers via SEC a second buffer adjustment was implemented by adding 2 mM TCEP to hinder non-native disulfide bridges and by further increasing the salt concentration up to 500 mM NaCl thereby increasing the ionic strength. With this buffer adjustments SEC was performed for sE2(2a)ΔHVR1-N534A (Figure 4.11 C) and sE2(1a)wt (Figure 4.11 D) using a S200 10/300 HR column. These modifications led to a shift towards lower molecular weights, but in case of sE2(2a)ΔHVR1-N534A the major part of the protein still eluted as higher oligomers and aggregates with the maximum at a protein size of about 480 kDa. The second peak lies in the range between 14 mL and 17 mL indicating sizes from 70 kDa to 18 kDa with a maximum at about 15 mL that corresponds to a calculated size of 43 kDa. It reaches two-thirds of the major peak indicating a remarkably increase compared to the little shoulder observed with the very first buffer adjustment in Figure 4.11 B. For the variant sE2(1a)wt the elution profile looked similar, but the major peak starts a little bit later thus shifting its maximum to a size of about 250 kDa and the smaller peak corresponding to lower molecular weights reaches its maximum at a size of about 40 kDa.

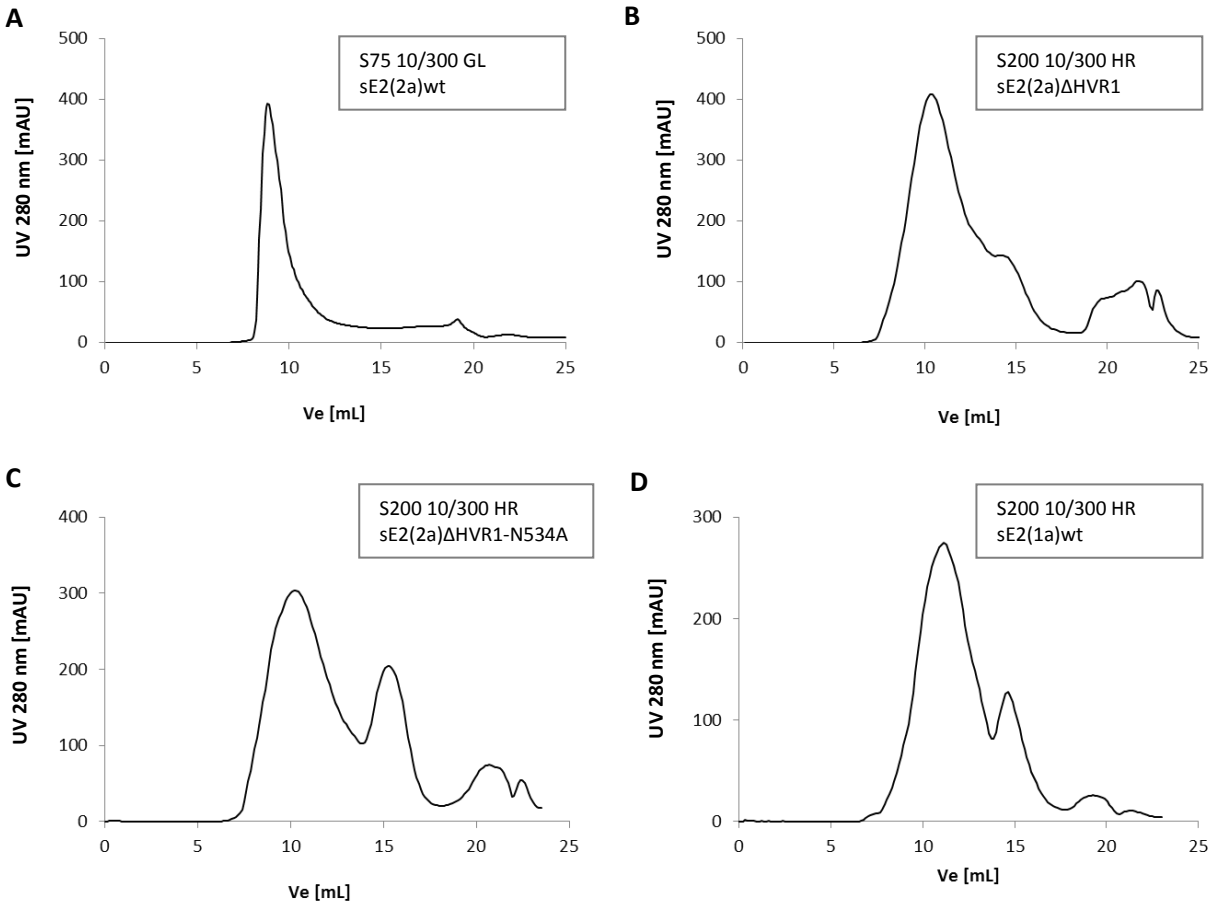

Figure 4.11: Size exclusion chromatography of sE2 variants
A: Size exclusion chromatography (SEC) with Superdex 75 10/300 GL column of sE2(2a)wt in 20mM TrisHCl pH 7.4, 50mM NaCl, B: SEC with Superdex 200 10/300 HR of sE2(2a)ΔHVR1 in 20mM TrisHCl pH 7.4, 50mM NaCl, 10% glycerol, C: SEC with Superdex 200 10/300 HR of sE2(2a)ΔHVR1-N534A in 20mM TrisHCl pH 7.4, 500mM NaCl, 2mM TCEP, 10% glycerol, D: SEC with Superdex 200 10/300 HR of sE2(1a)wt in 20mM TrisHCl pH 7.4, 500mM NaCl, 2mM TCEP, 10% glycerol.

Thereupon thermal stability assays were performed in order to further improve the buffer composition. However, this method was unrewarding due to binding of the reporter dye SYPRO Orange prior to protein unfolding. Possibly this is due to large hydrophobic parts of the E2 surface that were described for epitopes involved in protein-protein interactions (Kong *et al.*, 2012; Kong *et al.*, 2015; Freedman *et al.*, 2016). Since buffer optimization would need more time than left for finishing this thesis, the affinity purified proteins were used for further analysis.

4.3 Characterization of recombinant sE2 variants

In order to further analyze the oligomeric state of the sE2 variants, several protocols for native gels were performed, but none of them displayed distinct protein bands, but instead resulted in an overall smear. Hence, non-reducing SDS-PAGE was performed, according to the strategy that was published by Li (Li, 2014). With this approach for the first time protein bands of different size were detected for all sE2 variants that probably correspond to monomeric, dimeric, trimeric and higher oligomers according to their size, depicted in Figure 4.12.

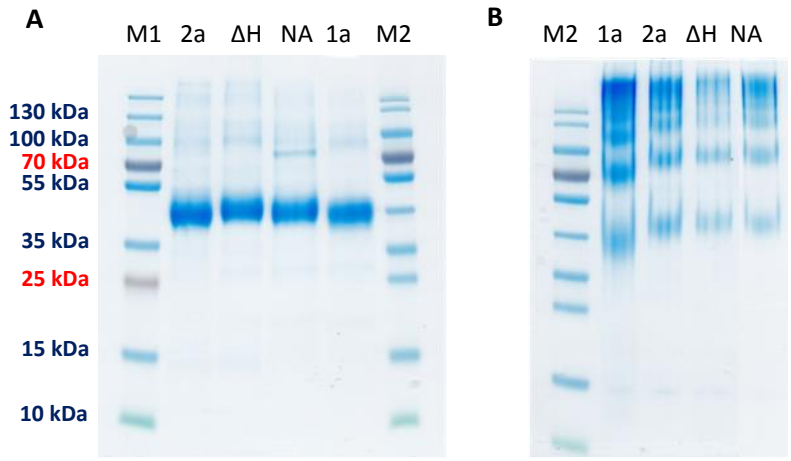

Figure 4.12: Oligomeric state of sE2 variants in reducing and non-reducing SDS-PAGE
A: Reducing SDS-PAGE was performed with 5 µg of each sE2 variant as a quality check prior to further analysis. B: Non-reducing SDS-PAGE was performed to analyze the oligomeric state. Loading buffer without BME was added to samples of 10 µg of each variant without boiling the sample. M1: PageRuler Prestained Plus, 2a: sE2(2a)wt, ΔH: sE2(2a)wtΔHVR1, NA: sE2(2a)wtΔHVR1-N534A, 1a: sE2(1a)wt, M2: PageRuler Prestained.

4.3.1 Secondary structure analysis

As it was not possible to determine the 3-dimensional structures of the sE2 variants within the scope of this project, Circular dichroism (CD) spectroscopy was employed for analyzing their secondary structure composition. This technique is widely used for rapid determination of secondary structure and folding properties of recombinant proteins (Greenfield, 2006). Signal-to-noise correction of each measurement was achieved by recording ten spectra per sample. For buffer signal correction, a spectrum was recorded with buffer only using the same experimental setup and the identical quartz cuvette. The buffer spectrum was subtracted from the other spectra prior to data analysis. The obtained spectra of the analyzed sE2 variants are indicated in Figure 4.13.

The typical CD spectrum of α-helical proteins has two minima at 208 nm and 220 nm with the same intensity and a maximum at 192 nm (Holzwarth and Doty, 1965). In contrast to that proteins with well-defined antiparallel β-sheets possess a single minima at 217/218 nm and a maximum at around 195 nm (Greenfield and Fasman, 1969), while the random-coil element displays a minimum around 200 nm (von Bergen *et al.*, 2005). The sE2 variants showed similar overall spectra that are related to CD spectra published for different E2 and E1E2 constructs (Whidby *et al.*, 2009; Rodríguez-Rodríguez *et al.*, 2009; Krey *et al.*, 2010; Tello *et al.*, 2015; Castelli *et al.*, 2017). All of the displayed variants exhibit minima at around 207 – 209 nm and all but sE2(2a)ΔHVR1 have a little shoulder at 211 – 216 nm.

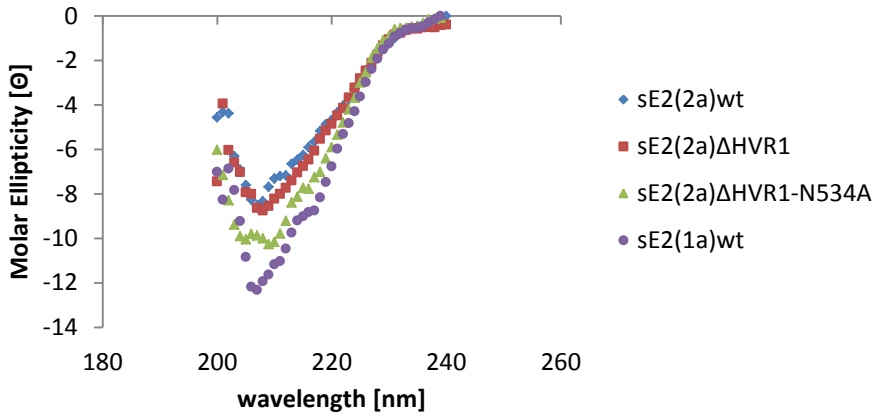

Figure 4.13: CD spectra of sE2 variants
The far-UV spectra of recombinant sE2 variants were obtained with a J815 CD Spectrometer (JASCO) in 1 mm quartz cuvettes (Hellma analytics). The displayed proteins were applied in 20 mM TrisHCl pH 7.4, 50 mM NaCl and were diluted depending on initial measurements.

These spectra were further used for secondary structure prediction using the online secondary structure prediction tool K2D3 (Louis-Jeune, Andrade-Navarro and Perez-Iratxeta, 2012). The thereby predicted secondary structure elements of each protein are listed in Table 4-1.

Table 4-1: Predicted secondary structure elements of sE2 variants by K2D3 prediction tool

SE2 variant	α-helix	β-strand
sE2(1a)wt	16.47 %	25.67 %
sE2(2a)wt	6.02 %	37.05 %
E2(2a)ΔHVR1	8.56 %	34.01 %
sE2(2a)ΔHVR1-N534	11.29 %	29.93 %

The published structures of the E2 core domain have a globular fold comprising mostly beta-strands and random coils (Kong *et al.*, 2013; Khan *et al.*, 2014). Thus, the accuracy of secondary structure prediction by these methods is not too high for the sE2 variants. High accuracy is only obtained when predicting α-helical content in proteins, because these helical structures have a well-defined backbone conformation that produces very similar spectra. The estimation of extended β-strand content, however, is unfortunately far less accurate. Referring to published secondary structure determinations of various E2 or E1E2 variants the predicted secondary structure elements lie in the range of 5 – 13 % α-helices, 30 – 50 % extended β-sheets and 40 – 60 % non-ordered structures (Whidby *et al.*, 2009; Rodríguez-Rodríguez *et al.*, 2009; Krey *et al.*, 2010; Tello *et al.*, 2015; Castelli *et al.*, 2017). Compared to these observations the prediction for the distinct elements of sE2 variants of genotype 2a fits quite well. In case of sE2 of genotype 1a the α-helical content was predicted to be little bit higher, while the β-strand content was a little reduced. However, they still lie in the roughly same range as the published ones. Discrepancies in secondary structure determination are likely due

to the usage of the different constructs expressed with or in absence of E1 and due to the lack of accuracy for secondary structure elements other than α-helices.

4.3.2 Glycosylation analysis of sE2 variants

Since E2 is usually heavily glycosylated, the glycosylation of the sE2 variants was analyzed. Glycans have been shown to be essential for proper folding and functioning of glycoproteins. Indeed, it was already shown that nine out of the 11 glycosylation sites with the E2 protein are strongly conserved (Goffard and Dubuisson, 2003). All of those sites lie within the E2 ectodomain and thus are covered within the recombinant sE2 variants created during this project. Therefore glycosylation analysis was performed exemplary with the two recombinant variants sE2(1a)wt and sE2(2a)ΔHVR1. For this approach deglycosylation analysis was performed by usage of two different endoglycosidases and the glycosylation of the proteins was verified by mass spectrometry.

While PNGase F removes almost all types of *N*-linked glycosylation except when the α(1–3) core is fucosylated, Endo H removes only high mannose and some hybrid types of *N*-linked carbohydrates. The experiments were performed with both native and denatured proteins according to the manufacturers' protocol. With this approach it is possible to analyze the potential of each endoglycosidase to fully deglycosylate the proteins under native conditions, while deglycosylation with denatured protein serves as kind of positive control. Samples were taken at different time points after the start of the experiments. The first samples were taken after the recommended incubation time of 1 h in case of Endo H and 4 h in case of PNGase F, respectively. Additionally incubation was prolonged up to 24 h incubation to analyze if prolonged incubation is necessary for the complete removing of glycans. Last but not least negative controls were used with equal conditions without endoglycosidases that were incubated for 24 h in order to test their stability under these conditions. The deglycosylation experiment was analyzed via SDS-PAGE, depicted in Figure 4.14.

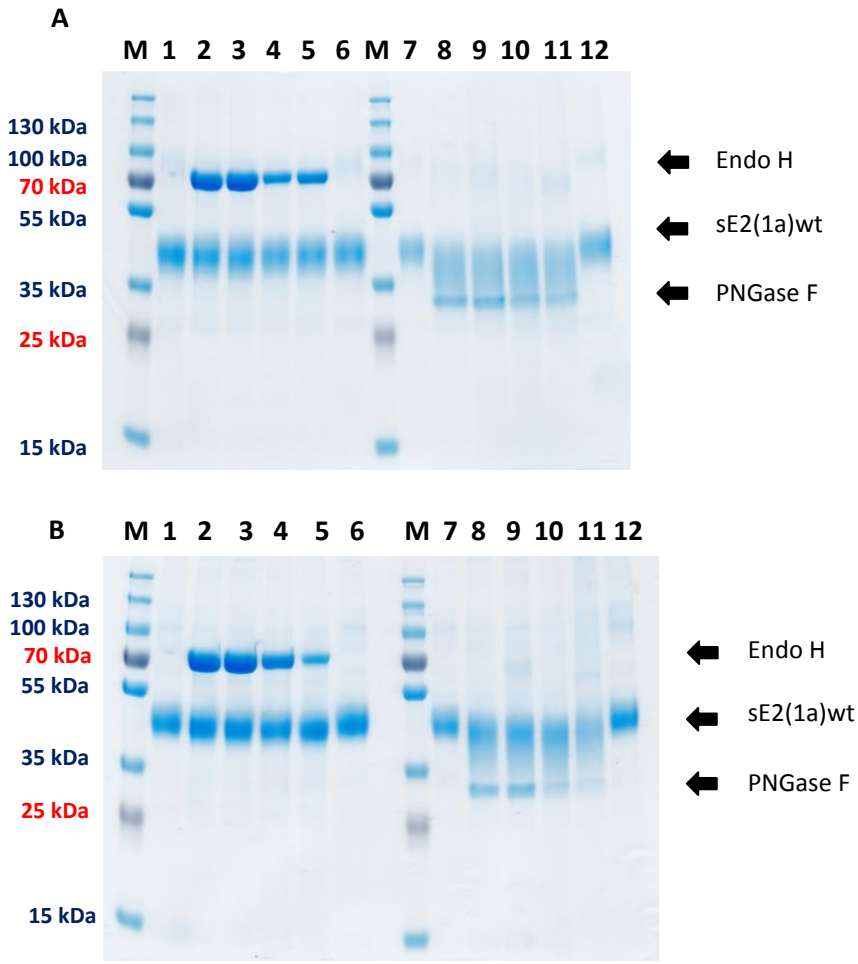

Figure 4.14: Deglycosylation analysis of sE2(1a)wt and sE2(2a)ΔHVR1
Deglycosylation was performed with 4 µg of sE2(1a)wt (A) and sE2(2a)ΔHVR1 (B) per sample. M: PageRuler Prestained Plus, 1: sample prior to deglycosylation, 2 – 5: samples of deglycosylation with EndoH, 2: deglycosylation under native conditions after 1 h incubation, 3: deglycosylation under native conditions after 24 h incubation, 4: deglycosylation of denatured protein after 1 h incubation, 5: deglycosylation of denatured protein after 24 h incubation, 6: negative control, 7: sample prior to deglycosylation, 8 – 11: samples of deglycosylation with PNGaseF, 8: deglycosylation under native conditions after 4 h incubation, 9: deglycosylation under native conditions after 24 h incubation, 10: deglycosylation of denatured protein after 4 h incubation, 11: deglycosylation of denatured protein after 24 h incubation, 12: negative control.

Both analyzed sE2 variants were only marginally affected by the different deglycosylation setups. While sE2(1a)wt seemed to be not deglycosylated at all after treatment with Endo H, the protein bands of Endo H treated sE2(2a)ΔHVR1 display a slight decrease in size. Deglycosylation of both variants with PNGase F, however, results in a much more smeary protein band that is also decreased little in size. All in all, the proteins are not sensitive to be fully deglycosylated neither by Endo H nor PNGase F. Moreover, deglycosylation with PNGase F even increases the heterogeneity by the attached glycans and thus is inappropriate for crystallization setups.

4.3.3 Functional analysis of sE2 variants

In order to analyze their competence as functional antigens the different sE2 variants were used in inhibition assays and in vaccination studies of mice by our cooperation partners at Twincore and HZI.
At first, a dose-dependent inhibition assay was conducted by Tanvi Khera at Twincore with each recombinant sE2 variant for analyzing their potential to inhibit HCV infection, depicted in Figure 4.15. For this assay Huh 7.5 cells are used, that are highly permissive for HCV replication (Blight, McKeating and Rice, 2002). The protein variants were mixed with jc1 reporter virus (genotype 2) prior to 4 h incubation with Huh 7.5 hepatocyte cells. After 4 h additional media was added and the infection was stopped at 72 h. The inhibition data is normalized to the signal corresponding to the control, so that the signal for virus only was set to 100. Inhibition is indicated by low luciferase signals.
Notably, an inhibition effect of the buffer was observed in all analyzed samples. Nevertheless, greater inhibition was detected with the sE2(2a) variants in a dose-dependent manner, whereas no further effect was observed within the negative control H1. Remarkably, the sE2(1a)wt variant displays an inhibitory effect that seems to decrease with higher doses. Inhibition induced by the E2(2b) control protein appeared to have a minor effect compared to the recombinant sE2 variants produced in the scope of this thesis. However, it should be noted that no buffer effect was observed within this control sample, resulting in overall higher signals. For a detailed comparison the experiments would need to be repeated with all protein samples applied in the same buffer. Even so, an obvious inhibitory effect was observed for all tested sE2 variants confirming proper folding and functionality.

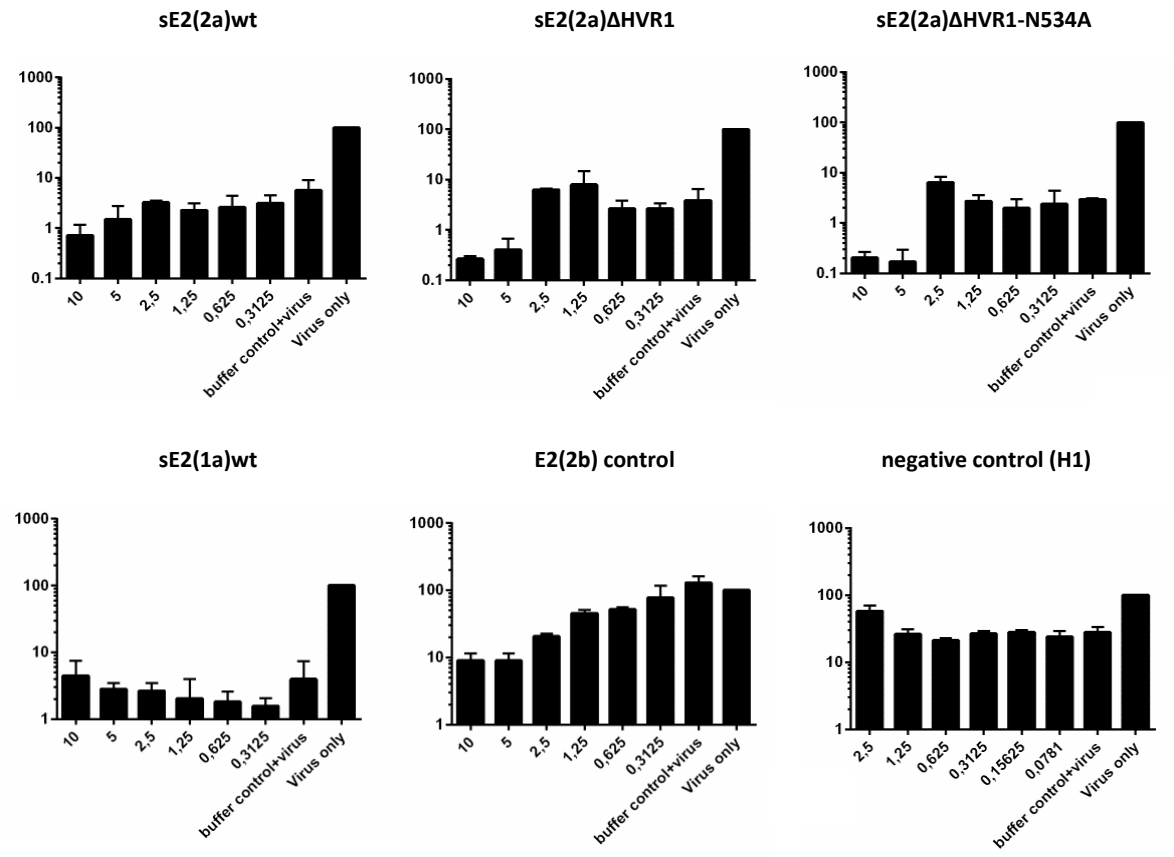

Figure 4.15: HCV inhibition assay

Dose-dependent inhibition of infection by recombinant sE2 variants was analyzed. Huh 7.5 cells were incubated with recombinant sE2 variants in the corresponding recombinant protein concentration and were infected with HCV jc1 reporter virus. An E2 variant of genotype 2b was used as control for comparing the inhibition effect with another recombinant E2 protein. Recombinant hemagglutinin H1 derived from the same expression host as the applied sE2 proteins was used as negative control. Infection was determined by renilla luciferase. The columns represent mean values of technical triplicates in a representative experiment, bars indicate mean deviation. A signal of 100 corresponds to the mean value of the infection in the presence of the control (virus only). Experiments and evaluation was performed by Tanvi Kehra (Twincore).

Besides, the vaccination of five mice per sE2 variant was performed at the department of Vaccinology and Applied Microbiology at the HZI. Primary immunization was followed by two immunization boosts at an interval of 14 days, as depicted in Figure 4.16. 14 days after the last dose the mice were euthanized and their blood was analyzed for the production of wt E2-specific IgG antibodies.

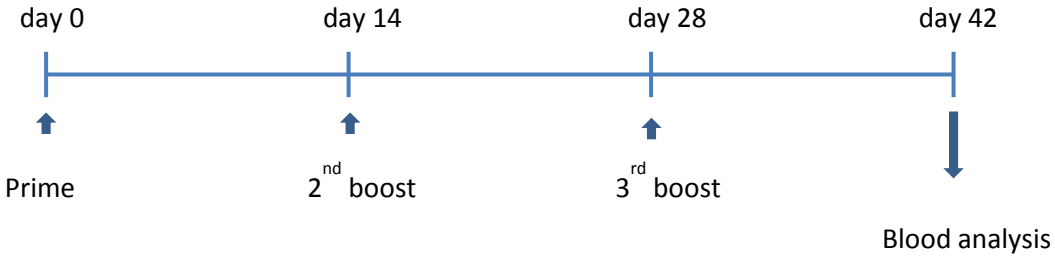

Figure 4.16: sE2 vaccination strategy

Schematic representation of the vaccination strategy performed at the department of Vaccinology and Applied Microbiology at the HZI. Primary immunization on day 0 was followed by two immunization boosts on day 14 and 28. The sera were analyzed 14 days after the third immunization on day 42.

The sera of euthanized mice were analyzed for wt E2-specific IgG antibodies by Kai Schulze and Thomas Ebensen (HZI) via ELISA. The data was kindly provided by Kai Schulze. As depicted in Figure 4.17 vaccination led to the production of E2-specific antibodies for all four tested variants.

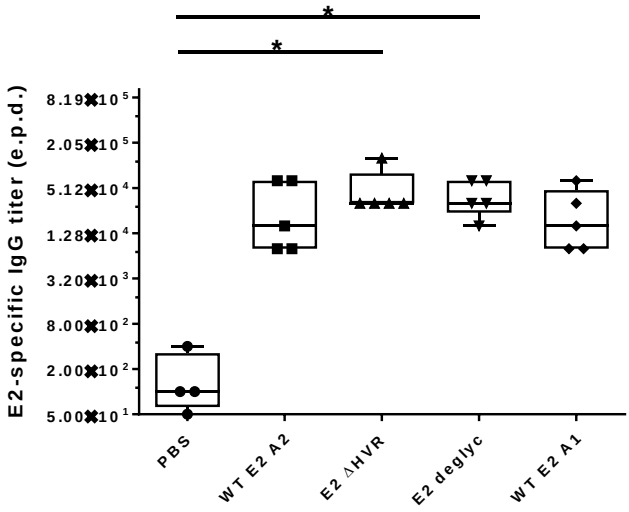

Figure 4.17: ELISA with sera of immunized mice after third immunization boost
The sera of mice immunized with recombinant sE2 variants were analyzed for wt E2-specific IgG antibodies after the third immunization boost on day 42. Sera were diluted by end point dilution (e.p.d.) and measurement was performed after 5 min. of incubation with the substrate. PBS was used as negative control, n = 5 mice per group, * $p < 0.05$.

The sera of vaccinated animals are currently under investigation for assessing the cross-neutralizing activity of those E2-specific antibodies by Tanvi Khera at Twincore. Cross-neutralizing antibodies are needed in order to protect against as many HCV strains as possible.

Overall, a strategy for efficient expression of four different recombinant secreted E2 ectodomain variants was established. First, the most suitable expression constructs and expression system were evaluated. Thereby the TGE in Hi5 insect cells was identified as the most qualified expression system. Subsequently, an efficient downstream processing was established and the whole production process was optimized. This approach led to remarkably increased protein titers of 6 – 11 mg/L for the different sE2 variants. Stepwise performed buffer adjustments were effective for shifting the SEC elution profile from mostly aggregates towards higher monomer and dimer compositions, albeit the major part of the samples remained as higher oligomers. Further attempts for monomer isolation should be performed in the future. Moreover, the purified E2 variants were applied to biochemical analysis and vaccination studies for further analysis of their structure and function. First results clearly indicate proper folding and functionality of biologically active protein variants. The antigenic properties of those recombinant sE2 variants have to be further evaluated as soon as new data is available.

5 Discussion

5.1 Recombinant HA expression

Influenza A infection is a serious threat to human health affecting millions of people every year. The infection process is initiated through binding and fusion of the viral to the host cell membrane via the surface glycoprotein HA that needs to be cleaved by host cell proteases into its active form prior to fusion. In order to get deeper insights into HA cleavage activation structural analysis of the uncleaved, non-modified cleavage loop of HA subtypes with differences in protease specificity was intended. Besides, a protocol for large scale expression and purification of HA of the H1N1 strain A/Puerto Rico/8/34 should be developed for its application in transfollicular vaccination strategies. For recombinant expression of unprocessed HA homotrimers the HA ectodomain was fused to a C-terminal 'foldon' sequence (Figure 3.1) from the bacteriophage T4 fibritin (Tao *et al.*, 1997) that was already used for successful trimerization before (Stevens *et al.*, 2004; Lu, Welsh and Swartz, 2014)

5.1.1 Evaluation of the most suitable expression host for recombinant HA expression

In order to find the most suitable expression host expression was initially tested for HA of different subtypes in the multi host expression system (Meyer *et al.*, 2013). It comprises transient transfection of HEK293-6E in serum-free suspension culture, expression via BEVS and stable CHO production cell lines generated by RMCE. Next to that, TGE in Hi5 insect cells was analyzed for its potential of recombinant expression of unprocessed HA after its successful establishment in our laboratories in the course of this thesis (discussed later).

Recombinant HA of the subtypes H1, H3 and H7 was successfully expressed and purified in Hi5 cells. While H1 and H3 were predominantly purified in its uncleaved form, high amounts of H7 were already cleaved by host proteases during insect cell cultivation and purification. In case of transient transfection of HEK293-6E cells recombinant HA expression was detectable for all three HA subtypes during small scale expression experiments. The expression and subsequent purification of H1 in large scale, however, led to protein that was not very stable and tended to precipitate after purification. Stable HA-expressing glycosylation deficient CHO cell lines were successfully generated and isolated. However, too little HA expression was detectable within the isolated clones so that this approach was not pursued further.

One key criterion for structure elucidation of glycoproteins is a short and uniform glycosylation. In order to analyze the suitability of the recombinant HA glycovariants for crystallization they were subjected to deglycosylation experiments and analysis by mass spectrometry. The glycosylation of H1 derived from Hi5 cells should not hinder crystallization, which indeed was proven in crystallization

setups in section 3.4. The more diverse glycosylation of H1 transiently expressed in HEK293-6E cells on the contrary would probably do (Chang *et al.*, 2007; Davis and Crispin, 2010; Nettleship, 2012). Whereas lepidoptera cell lines are widely used for heterologous protein expression for crystallization since they offer a quite simple glycosylation pattern (Tomiya *et al.*, 2004; Nettleship *et al.*, 2010; Nettleship, 2012). Moreover, the HEK-derived glycosylation could not be removed with endoglycosidases without significant protein degradation. All in all, the results indicated that HA produced in Hi5 cells is much more suitable for structural analysis than HA produced in HEK293-6E cells.

In fact, insect cells already have been reported to be a suitable expression host for recombinant HA expression (Stevens *et al.*, 2004; Wang *et al.*, 2006; X. Li *et al.*, 2015). Besides, they represent two of the most common cell lines for protein crystallization following *E. coli* with 4300 and 1335 entries in the PDB for *S. frugiperda* and *T. ni*, respectively (PDB Data Distribution by Expression Organism, status June 2018). Moreover, the recombinant H1 expressed in Hi5 insect cells in the scope of this thesis was already successfully analyzed for its proteolytic activation by the host serine protease TMPRSS2. This enzymatic in vitro assay clearly indicated a properly folded HA that was susceptible to proteolytic activation by this HA-specific protease (Schinkowski, 2017).

5.1.2 HA production process up-scaling

The first approaches for up-scaling the HA production process concerned the attempt to apply the TIPS method by Wasilko and Lee. This method is suitable for large scale expression, because it is based on the application of cryopreserved BIIC stocks for infection and recombinant protein expression. Thus, it was very promising for process up-scaling as it saves time, is easy to handle and additionally provides long-term stable storage of recombinant virus thereby increasing product reproducibility (Wasilko and Lee, 2006; Wasilko *et al.*, 2009). Despite various reports of its successful implementation (Emmons *et al.*, 2009; Cecchini, Virag and Kotin, 2011; Chen, 2016; Scholz and Suppmann, 2016, 2017), this method was not very convenient in the scope of this project. Even after several adjustments and approaches for increasing the infectivity, the infection of the cells was not comparable to that achieved with extracellularly virus stocks before. According to those non-reproducible problems concerning the infection with BIICs, other efforts for increasing the product titer were carried out.

Since previous results showed that Hi5 insect cells are qualified for recombinant HA expression (see section 3.1), the method of TGE in Hi5 cells was analyzed for its potential for process up-scaling with reproducible product titer. Just like TIPS method, it is very suitable for production in large scales, even when it comes to large bioreactors, as the handling is comparable easy (Shen *et al.*, 2015). Via TGE no problems regarding sterile addition of transfection reagents and DNA occur as it would be the case for external virus stocks on bioreactor scale. With this TGE method in Hi5 cells a constantly high

titer of recombinant HA was achieved. Additionally, compared to BEVS the process was much more reproducible and less elaborate, since the cumbersome preparation of fresh and highly infective virus stocks prior to expression experiments can be avoided by applying this TGE method. Moreover, the non-lytic nature of virus-free expression systems prevents degradation and thus ensures an overall increased product quality (Bleckmann, 2016) which in fact was observed for recombinant HA expression (see section 3.3.2).

5.1.3 Optimization of HA downstream processing

The HA purity was increased by replacing Ni-NTA by HisTALON purification, because the applied matrix exhibit less nonspecific protein binding than the Ni^{2+}–NTA resin (Bornhorst & Falke 2000). For the subtype H7, however, most of the purified protein was already cleaved into its subunits HA1 and HA2 during the purification steps. With this strategy for H1 very pure protein with a five-fold increase of product titer was acquired compared to the two-step purification before. The purified protein was used for further analysis comprising thrombin cleavage and SEC. Cleavage of HA with thrombin was necessary to remove the heterologous trimerization domain consisting of foldon and tags. While SEC was performed in order to isolate the trimeric HA without any contaminants. In order to ensure the separation of trimeric and monomeric HA, a column with a suitable pore size range was used. Buffer adjustments were investigated and it was found that increased trimer isolation was achieved by reducing the ionic strength of the buffer during SEC.

After the establishment of this purification strategy the process was analyzed for its potential for further optimizations. The previous strategy encompasses a HA capture from the supernatant in two steps. The harvested cell culture supernatant needed to be buffer exchanged by diafiltration before it was subjected to HisTALON purification. By the use of HisTrap excel columns the supernatants containing the secreted histidine-tagged proteins could be directly loaded onto the column for affinity purification. The implementation of this material was very effective and thus replaced the more cumbersome and time-consuming previous procedure. With this changed protocol the overall purification process was some days up to more than a week faster, depending on the applied expression volume. Overall, the process was not only faster and less work-intense, but the saved time and the gentle process also improved the product quality. Especially in large scale purifications or when it comes to purification in bioreactor scale this implementation is a great improvement.

Last but not least the purification process was complemented by a final reverse Strep-Tactin purification step that was implemented before or after SEC to ensure the complete removal of tagged contaminants. This approach was very effective by the use of both magnetic beads for small scale and with Strep-Tactin columns for larger volumes. This additional purification step further

increased the purity of HA samples for crystallization experiments and thus should facilitate crystal growth.

5.1.4 Crystallization of recombinant HA of the subtypes H1 and H3

The first crystallization setups with H1 and H3 resulted in several crystals of diverse size and shape. In order to generate better diffraction-quality crystals those initial hits were subjected to crystal optimization by individual customized screens. In case of H1, however, the diverse optimization trials did not increase the diffraction of the obtained crystals. Hence, the best diffracting H1 crystal exhibited quite poor diffraction. Furthermore, structure determination was tremendous hampered by the twinned nature of this crystal. Twinning is unflavored and can lead to problems in X-ray crystallography since a twinned crystal does not produce a simple diffraction pattern (Yeates, 1997). So unfortunately, no structural information of the H1 cleavage loop could be obtained. Crystallization of H3 on the contrary, already resulted in a crystal with quite high resolution in the very first crystallization setup. However, data analysis demonstrated low electron density at the location of the cleavage site, thus indicating an open loop structure due to protease cleavage. During crystal optimization a H3 crystal was obtained which exhibits a very high resolution of 1.45 Å. The resulting dataset reveals a very good defined electron density map enabling detailed insights into the H3 structure. Nevertheless, it was obvious that the obtained structure again belongs to a proteolytic cleaved protein. Thus, a well-defined H3 structure was gained, but still no structural information of the H3 cleavage loop was acquired so far.

The lack of diffraction-quality HA crystals with an intact cleavage loop raises the question if the uncleaved HA may hamper crystallization due to higher flexibility. This hypothesis is supported by the observation that most crystallized HAs either contain a modified cleavage site (Chen *et al.*, 1998) or have been proteolytic cleaved prior to crystallization (Skehel *et al.*, 1984; Ha *et al.*, 2002; Russell *et al.*, 2004; Stevens *et al.*, 2006; Yang, Carney and Stevens, 2010; Ni, Kondrashkina and Wang, 2015; Yang *et al.*, 2015). Indeed, so far there is only one H1 HA0 structure of the strain A/South Carolina/1/18 deposited in the PDB, which harbors an intact cleavage site (PDB ID: 1RD8, Stevens *et al*. 2004). While in case of H3, the only available H3 HA0 crystal structure contains a mutated cleavage site (PDB ID: 1HA0, Chen *et al*. 1998). Furthermore, it was already reported that the flexibility of the cleavage loop of a H2 variant prevented modelling, since no electron density could be observed for the associated HA1 and HA2 residues (Zhu *et al.*, 2013). Moreover, a H17 variant was expressed and purified as HA0 precursor, the solved structure, however, was found to belong to the cleaved variant (Sun *et al.*, 2013). All together these findings further support the hypothesis that uncleaved HA hampers crystal formation. However, it remains to be tested if the flexibility of the HA cleavage loop indeed hinders crystallization.

5.2 Recombinant E2 expression

HCV infections constitute a major global health problem with increasing infection rates within the last years (Centers for Disease Control and Prevention, 2017). However, very little is known about the structural properties of the HCV envelope glycoproteins E1 and E2. Especially a complete picture of the E1E2 heterodimeric complex is still missing. Moreover, the generation of effective vaccines is hampered by various strategies of HCV for evading the host immune system. It is therefore an important task to obtain detailed structural information of the glycoproteins and to produce antigens that stimulate the production of broadly neutralizing antibodies.

5.2.1 Selection of the right expression host and expression constructs

For the recombinant expression of E2 for functional and structural analysis different variants were generated that ought to re-direct antibody responses towards more conserved viral epitopes. Next to two *wt* E2 proteins derived from the genotypes 1a and 2a those variants encompass the E2 protein of genotype 2a without its most variable domain (ΔHVR1) and a variant that combines this deletion with the mutation of a glycosylation site involved in epitope masking (ΔHVR1-N534A). These variants were first used in full-length for co-expression with *wt* E1 together with the last 60 AA of core protein (cE1E2) and for stand-alone expression of the E2 ectodomain up to either AA 661 or 688 (sE2) in the transient HEK293-6E system. Upon this co-expression strategy, however, no satisfying expression was detected, so more emphasis was put on the recombinant expression of the sE2 variants.

Recombinant expression of soluble E2 variants ending at AA position 661 was working upon transient transfection in both HEK293-6E cells and Hi5 insect cells. For this truncated E2 protein successful expression and secretion has already been reported (Michalak *et al.*, 1997; Dubuisson *et al.*, 2000; Rodríguez-Rodríguez *et al.*, 2009; Tello *et al.*, 2010; McCaffrey *et al.*, 2012). sE2 expression in Hi5 insect cells, however, was found to be advantageous compared to its expression in HEK293-6E cells. Moreover, all variants expressed in HEK293-6E cells were highly glycosylated which would probably hinder crystallization, since the N-linked glycans make up approximately half of the mass of the E2 protein (Goffard *et al.*, 2005; Falson *et al.*, 2015). Upon expression via TGE in Hi5 insect cells, no unspecific signals were detected and the proteins did not exhibit bands of higher oligomers. Moreover, the proteins seem to have less heterogeneous glycosylation as observed before in the proteins derived from HEK cells. Hence, Hi5 insect cells emerged to be the expression host of choice and large scale expression was performed in order to establish an appropriate purification strategy.

5.2.2 Development of E2 purification strategy

For the development of a suitable purification strategy for the recombinant sE2 variants first of all purification with HisTrap excel columns was implemented, because it was very efficient and advantageous for HA purification. The protocol was adapted to that used for HA, because the monomeric E2 proteins possess only one His tag compared to the trimeric HA. However, this approach needed to be further optimized in order to get a higher degree of purity. The application of this changed protocol resulted in quite pure protein with significantly less protein loss and thus much higher yields up to 11 mg/L.

For further polishing, the proteins were subsequently subjected to SEC. In the very first SEC the applied protein sample eluted in the void volume of the column, indicating protein aggregation. Stepwise performed buffer adjustments led to a shift of the elution profile from mostly aggregates towards higher monomer and dimer compositions by increasing the ionic strength and minimizing hydrophobic interactions. However, the major part of the protein still elutes as higher oligomers and aggregates. Additional approaches aiming at further improving the buffer composition had no effect so far. Indeed, it is a common observation by diverse research groups that recombinant E2 has a high tendency to build higher oligomers and aggregates (McCaffrey *et al*. 2017; Orlova *et al*. 2015; Flint *et al*. 2000; Dubuisson *et al*. 1997; Krey *et al*. 2010; Whidby *et al*. 2009; Michalak *et al*. 1997) . Actually, a non-productive folding pathway has even been proposed as a physiologically relevant part of the HCV life cycle (Dubuisson, 2000). Taken together, this clearly indicates that it is not a trivial task to solve this common problem of E2 aggregation. Besides, this could be a hint that the best way for solving the aggregation problem, is to focus on E1 and E2 co-expression since heterodimer formation upon co-expression could be preferred to E2 self-association.

5.2.3 Characterization of recombinant sE2 variants

In order to characterize the recombinant sE2 variants non-reducing SDS-PAGE, CD spectroscopy and glycosylation analysis was performed. By the use of non-reducing SDS-PAGE the oligomeric state of the purified sE2 variants was found to be made up of monomers, dimers, trimers and higher oligomers as it was often observed before (Lee *et al.*, 1997; Whidby *et al.*, 2009; Afzal *et al.*, 2014; Ortega-Atienza *et al.*, 2014). Moreover, CD spectroscopy was employed and a secondary structure prediction was performed with the obtained spectra. The major part of the sE2 variants comprises non-ordered structures and β-sheets with a small amount of α-helices, thus indicating a correct fold. The acquired results are in accordance with published secondary structure determinations of different recombinant E2 or E1E2 proteins (Rodríguez-Rodríguez *et al*. 2009; Whidby *et al*. 2009; Krey *et al*. 2010; Tello *et al*. 2015; Castelli *et al*. 2017).

Furthermore the sE2 variants were used to analyze their competence as functional antigens by our cooperation partners at Twincore and HZI. A dose-dependent inhibition assay was performed with each recombinant sE2 variant for analyzing their potential to inhibit HCV infection. Upon this assay an obvious inhibitory effect was observed for all recombinant sE2 variants. Besides, vaccination of humanized mice induced production of E2-specific antibodies in case of all four tested variants. These antibodies are currently under investigation for assessing their cross-neutralizing activity at Twincore. Taken together these first results clearly indicate proper folding and functionality of biologically active E2 variants. Their antigenic properties have to be further evaluated as soon as new data is available.

6 Conclusions and outlook

In this thesis the expression and purification of biological active viral surface proteins of IAV and HCV has been established. The purified proteins were produced for the generation of new antigens for vaccination and for the investigation of their structure and function relations. The newly established TGE method in Hi5 insect cells was demonstrated as a powerful expression system for recombinant expression of viral surface glycoproteins.

In the first part of this thesis, a method was developed for the secretory expression of the full-length ectodomain of IAV HA subtypes H1 and H3 in its uncleaved pre-fusion state. Hi5 insect cells were discovered to be the most suitable expression host for the recombinant production of HA precursors for crystallization studies. Moreover, a protocol was established for HA expression up-scaling that was reliable, economic, easy to handle, comparatively fast and accessible for a scale-up in bioreactor dimensions. Furthermore, the production process and its optimized downstream processing resulted in very pure protein of high-quality. As quality control the HA protein was used in functional assays to ensure that it was properly folded and susceptible to proteolytic activation by a HA-specific protease (Schinkowski, 2017) and to analyze its antigenic potential (Schulze, unpublished work).

However, the major bottleneck within the scope of this project was the successful crystallization of the intact HA cleavage loop. Although it was possible to generate a diverse range of crystals of HA H1, none of them was of good diffraction quality, even after several rounds of crystal optimization. While H3 seems to tend to produce diffraction-quality crystals only after proteolytic cleavage in the crystallization plate, uncleaved H1 hardly causes any diffraction-quality crystal at all. It therefore should be investigated if uncleaved HA may hamper crystallization due to higher flexibility. In order to examine this hypothesis, both H1 and H3 proteins with mutated cleavage sites and proteolytic cleaved proteins could be submitted to crystallization. Besides, co-crystallization experiments with inactivated HA-specific proteases like Tmprss2-D343N (Schinkowski, 2017), that are desired anyway, could result in stabilization of the HA cleavage loop during crystal formation.

In the second part of this thesis, a strategy for recombinant expression of secreted E2 ectodomain variants via TGE in Hi5 insect cells was established. This method was advantageous compared to TGE in HEK293-6E cells in many ways. First of all, the transfection was much more reliable resulting in more uniform transfection efficiencies. Besides, compared to transient expression in HEK cells, no unspecific signals were obtained in western blot analysis. Moreover, the purified proteins had a less heterogeneous glycosylation which is favorable for structural elucidation by crystallization. Last but not least, the TGE in Hi5 cells exhibited a much better expression.

After the evaluation of the best expression constructs and expression system, the development of an appropriate purification strategy was a serious hurdle. The successful adaptation of the HisTrap excel

purification strategy yielded up to 6 - 11 mg recombinant E2 per L expression culture for the different sE2 variants. During further purification by SEC, however, the sE2 variants tend to form aggregates and higher oligomers. Stepwise performed buffer adjustments were effective for shifting the SEC elution profile from mostly aggregates towards higher monomer and dimer compositions. Nevertheless, the major part of the samples remained as higher oligomers and there was no time left for continuing buffer optimization.

Next to further buffer optimization, another strategy to avoid E2 oligomerization and aggregation during the purification process could be an approach of E1 and E2 co-expression. Since heterodimer formation should be preferred to E2 self-association, the co-expression and co-purification could avoid those unwanted oligomers. Co-expression and subsequent E1E2 heterodimer purification would be advantageous for functional and structural analysis anyhow. Just recently a promising co-expression strategy of Fc-tagged E1E2 was reported to form functional E1E2 heterodimers (Logan *et al.*, 2017). Another strategy would be to produce VLPs in insect cells as it is a common approach for vaccination (Metz and Pijlman, 2011; Vicente *et al.*, 2011). For example there are VLP-based vaccines available for influenza (Treanor *et al.*, 2011) and vaccines against hepatitis E (Shrestha *et al.*, 2007; Zhang *et al.*, 2015). Moreover, only recently this approach was published to be very promising for the development of a HCV VLP-based vaccine (Torresi, 2017).

The recombinant sE2 variants were able to inhibit HCV infection in a dose-dependent in vitro inhibition assay and to induce the production of E2-specific antibodies in mice. All in all, these first results indicate proper folding and functionality of biologically active E2 variants. Their antigenic properties, however, have to be further evaluated as soon as new data is available.

7 Bibliography

Abe, Y., Takashita, E., Sugawara, K., Matsuzaki, Y., Muraki, Y. and Hongo, S. (2004) 'Effect of the addition of oligosaccharides on the biological activities and antigenicity of influenza A/H3N2 virus hemagglutinin'. American Society for Microbiology, 78(18). doi: 10.1128/JVI.78.18.9605-9611.2004.

Afonine, P. V., Grosse-Kunstleve, R. W., Echols, N., Headd, J. J., Moriarty, N. W., Mustyakimov, M., Terwilliger, T. C., Urzhumtsev, A., Zwart, P. H. and Adams, P. D. (2012) 'Towards automated crystallographic structure refinement with *phenix.refine*', *Acta Crystallographica Section D Biological Crystallography*, 68(4), pp. 352–367. doi: 10.1107/S0907444912001308.

Afzal, M. S., Alsaleh, K., Farhat, R., Belouzard, S., Danneels, A., ronique Descamps, V., Duverlie, G., Wychowski, C., Zaidi, N. us S. S., Dubuisson, J. and Rouillé, Y. (2014) 'Regulation of core expression during the hepatitis C virus life cycle', *Journal of General Virology*, 96, pp. 311–321. doi: 10.1099/vir.0.070433-0.

Alcami, A. and Koszinowski, U. H. (2000) 'Viral mechanisms of immune evasion', *Immunology Today*. Elsevier Current Trends, 21(9), pp. 447–455. doi: 10.1016/S0167-5699(00)01699-6.

Almo, S. C. and Love, J. D. (2014) 'Better and faster: improvements and optimization for mammalian recombinant protein production', *Current Opinion in Structural Biology*, 26, pp. 39–43. doi: 10.1016/j.sbi.2014.03.006.

Altmann, F., Staudacher, E., Wilson, I. B. H. and März, L. (1999) 'Insect cells as hosts for the expression of recombinant glycoproteins.pdf', *Glycoconjugate Journal*. Boston, MA: Springer US, 16(2), pp. 109–123. doi: 10.1023/A:1026488408951.

Apweiler, R., Hermjakob, H. and Sharon, N. (1999) 'On the frequency of protein glycosylation, as deduced from analysis of the SWISS-PROT database.', *Biochimica et biophysica acta*, 1473(1), pp. 4–8.

Arnau, J., Lauritzen, C., Petersen, G. E. and Pedersen, J. (2006) 'Current strategies for the use of affinity tags and tag removal for the purification of recombinant proteins.', *Protein expression and purification*, 48(1), pp. 1–13. doi: 10.1016/j.pep.2005.12.002.

Backliwal, G., Hildinger, M., Chenuet, S., Wulhfard, S., De Jesus, M. and Wurm, F. M. (2008) 'Rational vector design and multi-pathway modulation of HEK 293E cells yield recombinant antibody titers exceeding 1 g/l by transient transfection under serum-free conditions.', *Nucleic acids research*. Oxford University Press, 36(15), p. e96. doi: 10.1093/nar/gkn423.

Bandaranayake, A. D. and Almo, S. C. (2014) 'Recent advances in mammalian protein production.', *FEBS letters*. NIH Public Access, 588(2), pp. 253–60. doi: 10.1016/j.febslet.2013.11.035.

Baneyx, F. (1999) 'Recombinant protein expression in Escherichia coli.', *Current opinion in biotechnology*, 10(5), pp. 411–21.

Bankwitz, D., Steinmann, E., Bitzegeio, J., Ciesek, S., Friesland, M., Herrmann, E., Zeisel, M. B., Baumert, T. F., Keck, Z., Foung, S. K. H., Pécheur, E.-I. and Pietschmann, T. (2010) 'Hepatitis C virus hypervariable region 1 modulates receptor interactions, conceals the CD81 binding site, and protects conserved neutralizing epitopes.', *Journal of virology*, 84(11), pp. 5751–63. doi: 10.1128/JVI.02200-09.

Bankwitz, D., Vieyres, G., Hueging, K., Bitzegeio, J., Doepke, M., Chhatwal, P., Haid, S., Catanese, M. T., Zeisel, M. B., Nicosia, A., Baumert, T. F., Kaderali, L. and Pietschmann, T. (2014) 'Role of hypervariable region 1 for the interplay of hepatitis C virus with entry factors and lipoproteins.', *Journal of virology*. American Society for Microbiology, 88(21), pp. 12644–55. doi: 10.1128/JVI.01145-14.

Bartenschlager, R., Lohmann, V. and Penin, F. (2013) 'The molecular and structural basis of advanced antiviral therapy for hepatitis C virus infection.', *Nature reviews. Microbiology*. Nature Publishing Group, 11(7), pp. 482–96. doi: 10.1038/nrmicro3046.

Baser, B., Spehr, J., Büssow, K. and van den Heuvel, J. (2015) 'A method for specifically targeting two independent genomic integration sites for co-expression of genes in CHO cells', *Methods*. Elsevier Inc., 95, pp. 3–12. doi: 10.1016/j.ymeth.2015.11.022.

De Beeck, A. O., Montserret, R., Duvet, S., Cocquerel, L., Cacan, R., Barberot, B., Maire, M. Le, Penin, F., Dubuisson, J., Op De Beeck, A., Montserret, R., Duvet, S., Cocquerel, L., Cacan, R., Barberot, B., Le Maire, M., Penin, F. and Dubuisson, J. (2000) 'The transmembrane domains of hepatitis C virus envelope glycoproteins E1 and E2 play a major role in heterodimerization', *Journal of Biological Chemistry*. American Society for Biochemistry and Molecular Biology, 275(40), pp. 31428–31437. doi: 10.1074/jbc.M003003200.

von Bergen, M., Barghorn, S., Biernat, J., Mandelkow, E.-M. and Mandelkow, E. (2005) 'Tau aggregation is driven by a transition from random coil to beta sheet structure', *Biochimica et Biophysica Acta (BBA) - Molecular Basis of Disease*. Elsevier, 1739(2–3), pp. 158–166. doi: 10.1016/J.BBADIS.2004.09.010.

Bertram, S., Glowacka, I., Blazejewska, P., Soilleux, E., Allen, P., Danisch, S., Steffen, I., Choi, S.-Y., Park, Y., Schneider, H., Schughart, K. and Pöhlmann, S. (2010) 'TMPRSS2 and TMPRSS4 facilitate trypsin-independent spread of influenza virus in Caco-2 cells.', *Journal of virology*, 84(19), pp. 10016–25. doi: 10.1128/JVI.00239-10.

Bertram, S., Glowacka, I., Steffen, I., Kühl, A. and Pöhlmann, S. (2010) 'Novel insights into proteolytic cleavage of influenza virus hemagglutinin', *Reviews in Medical Virology*, 20(5), pp. 298–310. doi: 10.1002/rmv.657.

Bertram, S., Heurich, A., Lavender, H., Gierer, S., Danisch, S., Perin, P., Lucas, J. M., Nelson, P. S., Pöhlmann, S. and Soilleux, E. J. (2012) 'Influenza and SARS-coronavirus activating proteases TMPRSS2 and HAT are expressed at multiple sites in human respiratory and gastrointestinal tracts.', *PloS one*, 7(4), p. e35876. doi: 10.1371/journal.pone.0035876.

Bieniossek, C., Richmond, T. J. and Berger, I. (2008) 'MultiBac: multigene baculovirus-based eukaryotic protein complex production.', *Current protocols in protein science / editorial board, John E. Coligan ... [et al.]*. Hoboken, NJ, USA: John Wiley & Sons, Inc., Chapter 5, p. Unit 5.20. doi: 10.1002/0471140864.ps0520s51.

Bleckmann, M. (2016) *IMPROVEMENT OF RECOMBINANT PROTEIN EXPRESSION IN INSECT CELLS*. TU Braunschweig.

Bleckmann, M., Fritz, M. H.-Y. M. H.-Y. Y., Bhuju, S., Jarek, M., Schürig, M., Geffers, R., Benes, V., Besir, H., Van Den Heuvel, J. and Li, Y. Y. (2015) 'Genomic Analysis and Isolation of RNA Polymerase II Dependent Promoters from Spodoptera frugiperda.', *PloS one*, 10(8), p. e0132898. doi: 10.1371/journal.pone.0132898.

Bleckmann, M., Schürig, M., Chen, F.-F., Yen, Z.-Z., Lindemann, N., Meyer, S., Spehr, J. and van den Heuvel, J. (2016) 'Identification of Essential Genetic Baculoviral Elements for Recombinant Protein Expression by Transactivation in Sf21 Insect Cells.', *PloS one*. Public Library of Science, 11(3), p. e0149424. doi: 10.1371/journal.pone.0149424.

Blight, K. J., McKeating, J. A. and Rice, C. M. (2002) 'Highly permissive cell lines for subgenomic and genomic hepatitis C virus RNA replication.', *Journal of virology*, 76(24), pp. 13001–14.

Blissard, G. W. and Rohrmann, G. F. (1990) 'Baculovirus diversity and molecular biology.', *Annual review of entomology*, 35, pp. 127–55. doi: 10.1146/annurev.en.35.010190.001015.

Boivin, S., Kozak, S. and Meijers, R. (2013) 'Optimization of protein purification and characterization using Thermofluor screens', *Protein Expression and Purification*. Elsevier Inc., 91(2), pp. 192–206. doi: 10.1016/j.pep.2013.08.002.

Bommakanti, G., Citron, M. P., Hepler, R. W., Callahan, C., Heidecker, G. J., Najar, T. A., Lu, X., Joyce, J. G., Shiver, J. W., Casimiro, D. R., ter Meulen, J., Liang, X. and Varadarajan, R. (2010) 'Design of an HA2-based Escherichia coli expressed influenza immunogen that protects mice from pathogenic challenge', *Proceedings of the National Academy of Sciences*, 107(31), pp. 13701–13706. doi: 10.1073/pnas.1007465107.

Bornhorst, J. A. and Falke, J. J. (2000) 'Purification of proteins using polyhistidine affinity tags.', *Methods in enzymology*. NIH Public Access, 326, pp. 245–54.

Bosch, F. X. X., Garten, W., Klenk, H.-D. D. and Rott, R. (1981) 'Proteolytic cleavage of influenza virus hemagglutinins: primary structure of the connecting peptide between HA1and HA2determines proteolytic cleavability and pathogenicity of avian influenza viruses', *Virology*. Academic Press, 113(2), pp. 725–735. doi: 10.1016/0042-6822(81)90201-4.

Böttcher-Friebertshäuser, E., Klenk, H.-D. and Garten, W. (2013) 'Activation of influenza viruses by proteases from host cells and bacteria in the human airway epithelium.', *Pathogens and disease*, 69(2), pp. 87–100. doi: 10.1111/2049-632X.12053.

Böttcher-Friebertshäuser, E., Stein, D. A., Klenk, H.-D. and Garten, W. (2011) 'Inhibition of Influenza Virus Infection in Human Airway Cell Cultures by an Antisense Peptide-Conjugated Morpholino Oligomer Targeting the Hemagglutinin-Activating Protease TMPRSS2', *Journal of Virology*, 85(4), pp. 1554–1562. doi: 10.1128/JVI.01294-10.

Böttcher, E., Matrosovich, T., Beyerle, M., Klenk, H.-D., Garten, W. and Matrosovich, M. (2006) 'Proteolytic activation of influenza viruses by serine proteases TMPRSS2 and HAT from human airway epithelium.', *Journal of virology*. American Society for Microbiology, 80(19), pp. 9896–8. doi: 10.1128/JVI.01118-06.

Boussif, O., Lezoualc'h, F., Zanta, M. A., Mergny, M. D., Scherman, D., Demeneix, B. and Behr, J. P. (1995) 'A versatile vector for gene and oligonucleotide transfer into cells in culture and in vivo: polyethylenimine.', *Proceedings of the National Academy of Sciences of the United States of America*, 92(16), pp. 7297–301.

Bradley, D. W., McCaustland, K. A., Cook, E. H., Schable, C. A., Ebert, J. W. and Maynard, J. E. (1985) 'Posttransfusion non-A, non-B hepatitis in chimpanzees. Physicochemical evidence that the tubule-forming agent is a small, enveloped virus.', *Gastroenterology*, 88(3), pp. 773–9.

Bragg, W. L. (1913) 'The diffacrtion of short electromagnetic waves by a crystal', *Proceedings of the Cambridge Philosophical Society* , 17, pp. 43–57.

Brown, K. S., Keogh, M. J., Owsianka, A. M., Adair, R., Patel, A. H., Arnold, J. N., Ball, J. K., Sim, R. B., Tarr, A. W. and Hickling, T. P. (2010) 'Specific interaction of hepatitis C virus glycoproteins with mannan binding lectin inhibits virus entry', *Protein & Cell*, 1(7), pp. 664–674. doi: 10.1007/s13238-010-0088-9.

Brown, R. J. P., Juttla, V. S., Tarr, A. W., Finnis, R., Irving, W. L., Hemsley, S., Flower, D. R., Borrow, P. and Ball, J. K. (2005) 'Evolutionary dynamics of hepatitis C virus envelope genes during chronic infection', *Journal of General Virology*. Microbiology Society, 86(7), pp. 1931–1942. doi: 10.1099/vir.0.80957-0.

Brown, R. J. P., Tarr, A. W., McClure, C. P., Juttla, V. S., Tagiuri, N., Irving, W. L. and Ball, J. K. (2007) 'Cross-genotype characterization of genetic diversity and molecular adaptation in hepatitis C virus envelope glycoprotein genes', *Journal of General Virology*. Microbiology Society, 88(2), pp. 458–469. doi: 10.1099/vir.0.82357-0.

Brünger, A. T. (1992) 'Free R value: a novel statistical quantity for assessing the accuracy of crystal structures', *Nature*. Nature Publishing Group, 355(6359), pp. 472–475. doi: 10.1038/355472a0.

Carter, P. J. (2006) 'Potent antibody therapeutics by design.', *Nature reviews. Immunology*, 6(5), pp. 343–57. doi: 10.1038/nri1837.

Castelli, M., Clementi, N., Pfaff, J., Sautto, G. A., Diotti, R. A., Burioni, R., Doranz, B. J., Dal Peraro, M., Clementi, M. and Mancini, N. (2017) 'A Biologically-validated HCV E1E2 Heterodimer Structural Model', *Scientific Reports*. Nature Publishing Group, 7(1), p. 214. doi: 10.1038/s41598-017-00320-7.

Cecchini, S., Virag, T. and Kotin, R. M. (2011) 'Reproducible high yields of recombinant adeno-associated virus produced using invertebrate cells in 0.02- to 200-liter cultures.', *Human gene therapy*, 22(8), pp. 1021–30. doi: 10.1089/hum.2010.250.

Centers for Disease Control and Prevention (2017) *New Hepatitis C Infections Nearly Tripled over Five Years*. Available at: https://www.cdc.gov/nchhstp/newsroom/2017/Hepatitis-Surveillance-Press-Release.html (Accessed: 5 April 2018).

Chaipan, C., Kobasa, D., Bertram, S., Glowacka, I., Steffen, I., Tsegaye, T. S., Takeda, M., Bugge, T. H., Kim, S., Park, Y., Marzi, A. and Pöhlmann, S. (2009) 'Proteolytic activation of the 1918 influenza virus hemagglutinin.', *Journal of virology*, 83(7), pp. 3200–11. doi: 10.1128/JVI.02205-08.

Chang, V. T., Crispin, M., Aricescu, A. R., Harvey, D. J., Nettleship, J. E., Fennelly, J. A., Yu, C., Boles, K. S., Evans, E. J., Stuart, D. I., Dwek, R. A., Jones, E. Y., Owens, R. J. and Davis, S. J. (2007) 'Glycoprotein Structural Genomics: Solving the Glycosylation Problem', *Structure*. Elsevier Ltd, 15(3), pp. 267–273. doi: 10.1016/j.str.2007.01.011.

Chayen, N. E. (2004) 'Turning protein crystallisation from an art into a science', *Current Opinion in Structural Biology*. Elsevier Current Trends, 14(5), pp. 577–583. doi: 10.1016/J.SBI.2004.08.002.

Chen, J., Lee, K. H. K. . H., Steinhauer, D. . a D. A., Stevens, D. . D. J., Skehel, J. J. . J. and Wiley, D. C. C. D. C. (1998) 'Structure of the hemagglutinin precursor cleavage site, a determinant of influenza pathogenicity and the origin of the labile conformation.', *Cell*, 95(3), pp. 409–417. doi: 10.1016/S0092-8674(00)81771-7.

Chen, S. (2016) 'Alternative Strategies for Expressing Multicomponent Protein Complexes in Insect Cells', in *Methods in molecular biology (Clifton, N.J.)*, pp. 317–326. doi: 10.1007/978-1-4939-3043-2_15.

Chen, W., Sun, S. and Li, Z. (2012) 'Two glycosylation sites in H5N1 influenza virus hemagglutinin that affect binding preference by computer-based analysis.', *PloS one*, 7(6), p. e38794. doi: 10.1371/journal.pone.0038794.

Cheng, Z., Zhou, J., To, K. K.-W., Chu, H., Li, C., Wang, D., Yang, D., Zheng, S., Hao, K., Bossé, Y., Obeidat, M., Brandsma, C.-A., Song, Y.-Q., Chen, Y., Zheng, B.-J., Li, L. and Yuen, K.-Y. (2015) 'Identification of *TMPRSS2* as a Susceptibility Gene for Severe 2009 Pandemic A(H1N1) Influenza and A(H7N9) Influenza', *Journal of Infectious Diseases*. Oxford University Press, 212(8), pp. 1214–1221. doi: 10.1093/infdis/jiv246.

Cherry, J. L., Lipman, D. J., Nikolskaya, A. and Wolf, Y. I. (2009) 'Evolutionary Dynamics of N-Glycosylation Sites of Influenza Virus Hemagglutinin', *PLoS Currents*. Public Library of Science, 1, p. RRN1001. doi: 10.1371/currents.RRN1001.

Chevaliez, S. and Pawlotsky, J.-M. (2006) *HCV Genome and Life Cycle*, *Hepatitis C Viruses: Genomes and Molecular Biology*. Horizon Bioscience. doi: pmid: 21250393.

Choo, Q. L., Richman, K. H., Han, J. H., Berger, K., Lee, C., Dong, C., Gallegos, C., Coit, D., Medina-Selby, R., Barr, P. J. and al., et (1991) 'Genetic organization and diversity of the hepatitis C virus.', *Proceedings of the National Academy of Sciences of the United States of America*. National Academy of Sciences, 88(6), pp. 2451–5.

Cocquerel, L., Meunier, J. C., Pillez, A., Wychowski, C. and Dubuisson, J. (1998) 'A retention signal necessary and sufficient for endoplasmic reticulum localization maps to the transmembrane domain of hepatitis C virus glycoprotein E2.', *Journal of virology*, 72(3), pp. 2183–91.

Cohen, M. (2015) 'Notable Aspects of Glycan-Protein Interactions.', *Biomolecules*. Multidisciplinary Digital Publishing Institute (MDPI), 5(3), pp. 2056–72. doi: 10.3390/biom5032056.

Cohen, S. N., Chang, A. C., Boyer, H. W. and Helling, R. B. (1973) 'Construction of biologically functional bacterial plasmids in vitro.', *Proceedings of the National Academy of Sciences of the United States of America*, 70(11), pp. 3240–4.

Collin, E. A., Sheng, Z., Lang, Y., Ma, W., Hause, B. M. and Li, F. (2015) 'Cocirculation of Two Distinct Genetic and Antigenic Lineages of Proposed Influenza D Virus in Cattle', *Journal of Virology*. Edited by A. García-Sastre, 89(2), pp. 1036–1042. doi: 10.1128/JVI.02718-14.

Cox, M. M. J., Patriarca, P. A. and Treanor, J. (2008) 'FluBlok, a recombinant hemagglutinin influenza vaccine.', *Influenza and other respiratory viruses*. Wiley-Blackwell, 2(6), pp. 211–9. doi: 10.1111/j.1750-2659.2008.00053.x.

Van Craenenbroeck, K., Vanhoenacker, P. and Haegeman, G. (2000) 'Episomal vectors for gene expression in mammalian cells', *European Journal of Biochemistry*. Blackwell Science Ltd, 267(18), pp. 5665–5678. doi: 10.1046/j.1432-1327.2000.01645.x.

Cross, K. J., Langley, W. A., Russell, R. J., Skehel, J. J. and Steinhauer, D. A. (2009) 'Composition and functions of the influenza fusion peptide.', *Protein and peptide letters*, 16(7), pp. 766–78.

D'Arcy, A., Bergfors, T., Cowan-Jacob, S. W. and Marsh, M. (2014) 'Microseed matrix screening for optimization in protein crystallization: what have we learned?', *Acta crystallographica. Section F, Structural biology communications*. International Union of Crystallography, 70(Pt 9), pp. 1117–26. doi: 10.1107/S2053230X14015507.

Davis, S. J. and Crispin, M. (2010) 'Solutions to the Glycosylation Problem for Low- and High-Throughput Structural Glycoproteomics', in *Functional and Structural Proteomics of Glycoproteins*. Dordrecht: Springer Netherlands, pp. 127–158. doi: 10.1007/978-90-481-9355-4_6.

Deng, L., Ma, L., Virata-Theimer, M. L., Zhong, L., Yan, H., Zhao, Z., Struble, E., Feinstone, S., Alter, H. and Zhang, P. (2014) 'Discrete conformations of epitope II on the hepatitis C virus E2 protein for antibody-mediated neutralization and nonneutralization.', *Proceedings of the National Academy of Sciences of the United States of America*. National Academy of Sciences, 111(29), pp. 10690–5. doi: 10.1073/pnas.1411317111.

Deng, L., Zhong, L., Struble, E., Duan, H., Ma, L., Harman, C., Yan, H., Virata-Theimer, M. L., Zhao, Z., Feinstone, S., Alter, H. and Zhang, P. (2013) 'Structural evidence for a bifurcated mode of action in the antibody-mediated neutralization of hepatitis C virus.', *Proceedings of the National Academy of Sciences of the United States of America*. National Academy of Sciences, 110(18), pp. 7418–22. doi: 10.1073/pnas.1305306110.

Dreux, M., Pietschmann, T., Granier, C., Voisset, C., Ricard-Blum, S., Mangeot, P.-E., Keck, Z., Foung, S., Vu-Dac, N., Dubuisson, J., Bartenschlager, R., Lavillette, D. and Cosset, F.-L. (2006) 'High Density Lipoprotein Inhibits Hepatitis C Virus-neutralizing Antibodies by Stimulating Cell Entry via Activation of the Scavenger Receptor BI', *Journal of Biological Chemistry*, 281(27), pp. 18285–18295. doi: 10.1074/jbc.M602706200.

Drummer, H. E. (2014) 'Challenges to the development of vaccines to hepatitis C virus that elicit neutralizing antibodies', 5(JULY), p. 329. doi: 10.3389/fmicb.2014.00329.

Drummer, H. E. and Poumbourios, P. (2004) 'Hepatitis C virus glycoprotein E2 contains a membrane-proximal heptad repeat sequence that is essential for E1E2 glycoprotein heterodimerization and viral entry', *Journal of Biological Chemistry*, 279(29), pp. 30066–30072. doi: 10.1074/jbc.M405098200.

Dubuisson, J. (2000) 'Folding, Assembly and Subcellular Localization of Hepatitis C Virus Glycoproteins', in. Springer, Berlin, Heidelberg, pp. 135–148. doi: 10.1007/978-3-642-59605-6_7.

Dubuisson, J., Choukhi, A., Meunier, J. C., Michalak, J. P., Wychowski, C., Rice, C. M. and Ung, S. (1997) 'Characterization of truncated forms of hepatitis C virus glycoproteins.', *Journal of General Virology*, 78(9), pp. 2299–2306. doi: 10.1099/0022-1317-78-9-2299.

Dubuisson, J., Cocquerel, L., Fournillier, A., Meunier, J. C., Cahour, A., Choukhi, A. and Wychowski, C. (1999) 'Analysis of the glycosylation sites of hepatitis C virus (HCV) glycoprotein E1 and the influence of E1 glycans on the formation of the HCV glycoprotein complex.', *Journal of General Virology*, 80(4), pp. 887–896. doi: 10.1099/0022-1317-80-4-887.

Dubuisson, J., Duvet, S., Meunier, J.-C., Op, A., Beeck, D., Cacan, R., Wychowski, C. and Cocquerel, L. (2000) 'Glycosylation of the Hepatitis C Virus Envelope Protein E1 Is Dependent on the Presence of a Downstream Sequence on the Viral Polyprotein*'. doi: 10.1074/jbc.M004326200.

Dubuisson, J., Hsu, H. H., Cheung, R. C., Greenberg, H. B., Russell, D. G. and Rice, C. M. (1994) 'Formation and intracellular localization of hepatitis C virus envelope glycoprotein complexes expressed by recombinant vaccinia and Sindbis viruses.', *Journal of virology*, 68(10), pp. 6147–60.

Dubuisson, J. and Rice, C. M. (1996) 'Hepatitis C virus glycoprotein folding: disulfide bond formation and association with calnexin.', *Journal of virology*. American Society for Microbiology, 70(2), pp. 778–86.

Durocher, Y., Perret, S. and Kamen, A. (2002) 'High-level and high-throughput recombinant protein production by transient transfection of suspension-growing human 293-EBNA1 cells.', *Nucleic acids research*, 30(2), p. E9.

Duvet, S., Cocquerel, L., Pillez, A., Cacan, R., Verbert, A., Moradpour, D., Wychowski, C. and Dubuisson, J. (1998) 'Hepatitis C virus glycoprotein complex localization in the endoplasmic reticulum involves a determinant for retention and not retrieval.', *The Journal of biological chemistry*. American Society for Biochemistry and Molecular Biology, 273(48), pp. 32088–95. doi: 10.1074/JBC.273.48.32088.

Edros, R. Z., McDonnell, S. and Al-Rubeai, M. (2013) 'Using Molecular Markers to Characterize Productivity in Chinese Hamster Ovary Cell Lines', *PLoS ONE*. Edited by H. Wanjin. Public Library of Science, 8(10), p. e75935. doi: 10.1371/journal.pone.0075935.

Egli, M. (2016) 'Diffraction Techniques in Structural Biology.', *Current protocols in nucleic acid chemistry*. NIH Public Access, 65, p. 7.13.1-7.13.41. doi: 10.1002/cpnc.4.

Elbein, A. D., Solf, R., Dorling, P. R. and Vosbeck, K. (1981) 'Swainsonine: an inhibitor of glycoprotein processing.', *Proceedings of the National Academy of Sciences of the United States of America*, 78(12), pp. 7393–7.

Elbein, A. D., Tropea, J. E., Mitchell, M. and Kaushal, G. P. (1990) 'Kifunensine, a potent inhibitor of the glycoprotein processing mannosidase I.', *The Journal of biological chemistry*, 265(26), pp. 15599–605.

Emmons, T. L., Mathis, K. J., Shuck, M. E., Reitz, B. A., Curran, D. F., Walker, M. C., Leone, J. W., Day, J. E., Bienkowski, M. J., Fischer, H. D. and Tomasselli, A. G. (2009) 'Purification and characterization of recombinant human soluble guanylate cyclase produced from baculovirus-infected insect cells', *Protein Expression and Purification*, 65(2), pp. 133–139. doi: 10.1016/j.pep.2009.01.001.

Emsley, P., Lohkamp, B., Scott, W. G. and Cowtan, K. (2010) 'Features and development of *Coot*', *Acta Crystallographica Section D Biological Crystallography*, 66(4), pp. 486–501. doi: 10.1107/S0907444910007493.

Ericsson, U. B., Hallberg, B. M., DeTitta, G. T., Dekker, N. and Nordlund, P. (2006) 'Thermofluor-based high-throughput stability optimization of proteins for structural studies', *Analytical Biochemistry*, 357(2), pp. 289–298. doi: 10.1016/j.ab.2006.07.027.

European Association for Study of Liver (2014) 'EASL Clinical Practice Guidelines: Management of hepatitis C virus infection', *Journal of Hepatology*, 60(2), pp. 392–420. doi: 10.1016/j.jhep.2013.11.003.

Falson, P., Bartosch, B., Alsaleh, K., Tews, B. A., Loquet, A., Ciczora, Y., Riva, L., Montigny, C., Montpellier, C., Duverlie, G., Pécheur, E.-I., le Maire, M., Cosset, F.-L., Dubuisson, J. and Penin, F. (2015) 'Hepatitis C Virus Envelope Glycoprotein E1 Forms Trimers at the Surface of the Virion.', *Journal of virology*. Edited by M. S. Diamond. American Society for Microbiology, 89(20), pp. 10333–46. doi: 10.1128/JVI.00991-15.

Federal Ministry of Education and Research (2018) *Pooling research to tackle common diseases - BMBF*. Available at: https://www.bmbf.de/en/pooling-research-to-tackle-common-diseases-2592.html (Accessed: 11 April 2018).

Flint, M., Dubuisson, J., Maidens, C., Harrop, R., Guile, G. R., Borrow, P. and McKeating, J. A. (2000) 'Functional characterization of intracellular and secreted forms of a truncated hepatitis C virus E2 glycoprotein.', *Journal of virology*. American Society for Microbiology, 74(2), pp. 702–9. doi: 10.1128/JVI.74.2.702-709.2000.

Foni, E., Chiapponi, C., Baioni, L., Zanni, I., Merenda, M., Rosignoli, C., Kyriakis, C. S., Luini, M. V., Mandola, M. L., Bolzoni, L., Nigrelli, A. D. and Faccini, S. (2017) 'Influenza D in Italy: towards a better understanding of an emerging viral infection in swine', *Scientific Reports*. Nature Publishing Group, 7(1), p. 11660. doi: 10.1038/s41598-017-12012-3.

Freedman, H., Logan, M. R., Hockman, D., Koehler Leman, J., Law, J. L. M. and Houghton, M. (2017) 'Computational Prediction of the Heterodimeric and Higher-Order Structure of gpE1/gpE2 Envelope Glycoproteins Encoded by Hepatitis C Virus', *Journal of Virology*. Edited by J.-H. J. Ou, 91(8), pp. e02309-16. doi: 10.1128/JVI.02309-16.

Freedman, H., Logan, M. R., Law, J. L. M. and Houghton, M. (2016) 'Structure and Function of the Hepatitis C Virus Envelope Glycoproteins E1 and E2: Antiviral and Vaccine Targets', *ACS Infectious Diseases*. American Chemical Society, 2(11), pp. 749–762. doi: 10.1021/acsinfecdis.6b00110.

Freeze, H. H. and Kranz, C. (2010) 'Endoglycosidase and glycoamidase release of N-linked glycans.', *Current protocols in molecular biology*. NIH Public Access, Chapter 17, p. Unit 17.13A. doi: 10.1002/0471142727.mb1713as89.

Frenzel, A., Hust, M. and Schirrmann, T. (2013) 'Expression of recombinant antibodies.', *Frontiers in immunology*. Frontiers Media SA, 4, p. 217. doi: 10.3389/fimmu.2013.00217.

Gallagher, P. J., Henneberry, J. M., Sambrook, J. F. and Gething, M. J. (1992) 'Glycosylation requirements for intracellular transport and function of the hemagglutinin of influenza virus.', *Journal of virology*. American Society for Microbiology (ASM), 66(12), pp. 7136–45.

Gao, R., Cao, B., Hu, Y., Feng, Z., Wang, D., Hu, W., Chen, J., Jie, Z., Qiu, H., Xu, K., Xu, X., Lu, H., Zhu, W., Gao, Z., Xiang, N., Shen, Y., He, Z., Gu, Y., Zhang, Z., Yang, Y., Zhao, X., Zhou, L., Li, X., Zou, S., Zhang, Y., Li, X., Yang, L., Guo, J., Dong, J., Li, Q., Dong, L., Zhu, Y., Bai, T., Wang, S., Hao, P., Yang, W., Zhang, Y., Han, J., Yu, H., Li, D., Gao, G. F., Wu, G., Wang, Y., Yuan, Z. and Shu, Y. (2013) 'Human Infection with a Novel Avian-Origin Influenza A (H7N9) Virus', *New England Journal of Medicine*, 368(20), pp. 1888–1897. doi: 10.1056/NEJMoa1304459.

Garab, G. and van Amerongen, H. (2009) 'Linear dichroism and circular dichroism in photosynthesis research.', *Photosynthesis research*. Springer, 101(2–3), pp. 135–46. doi: 10.1007/s11120-009-9424-4.

Garten, W. and Klenk, H. D. (1999) 'Understanding influenza virus pathogenicity.', *Trends in microbiology*, 7(3), pp. 99–100.

Geijtenbeek, T. B. H. and Gringhuis, S. I. (2009) 'Signalling through C-type lectin receptors: shaping immune responses', *Nature Reviews Immunology*, 9(7), pp. 465–479. doi: 10.1038/nri2569.

Geiss, G. K., Salvatore, M., Tumpey, T. M., Carter, V. S., Wang, X., Basler, C. F., Taubenberger, J. K., Bumgarner, R. E., Palese, P., Katze, M. G. and García-Sastre, A. (2002) 'Cellular transcriptional profiling in influenza A virus-infected lung epithelial cells: the role of the nonstructural NS1 protein in the evasion of the host innate defense and its potential contribution to pandemic influenza.', *Proceedings of the National Academy of Sciences of the United States of America*. National Academy of Sciences, 99(16), pp. 10736–41. doi: 10.1073/pnas.112338099.

Ghany, M. G., Nelson, D. R., Strader, D. B., Thomas, D. L., Seeff, L. B. and American Association for Study of Liver Diseases (2011) 'An update on treatment of genotype 1 chronic hepatitis C virus infection: 2011 practice guideline by the American Association for the Study of Liver Diseases', *Hepatology*, 54(4), pp. 1433–1444. doi: 10.1002/hep.24641.

Goffard, A., Callens, N., Bartosch, B., Wychowski, C., Cosset, F.-L., Montpellier, C. and Dubuisson, J. (2005) 'Role of N-Linked Glycans in the Functions of Hepatitis C Virus Envelope Glycoproteins', *Journal of Virology*. American Society for Microbiology, 79(13), pp. 8400–8409. doi: 10.1128/JVI.79.13.8400-8409.2005.

Goffard, A. and Dubuisson, J. (2003) 'Glycosylation of hepatitis C virus envelope proteins', *Biochimie*, 85(3–4), pp. 295–301. doi: 10.1016/S0300-9084(03)00004-X.

Gogela, N. A., Lin, M. V, Wisocky, J. L. and Chung, R. T. (2015) 'Enhancing our understanding of current therapies for hepatitis C virus (HCV).', *Current HIV/AIDS reports*. NIH Public Access, 12(1), pp. 68–78. doi: 10.1007/s11904-014-0243-7.

Gorrec, F. (2016) 'Protein crystallization screens developed at the MRC Laboratory of Molecular Biology.', *Drug discovery today*. Elsevier, 21(5), pp. 819–25. doi: 10.1016/j.drudis.2016.03.008.

Gotoh, B., Ogasawara, T., Toyoda, T., Inocencio, N. M., Hamaguchi, M. and Nagai, Y. (1990) 'An endoprotease homologous to the blood clotting factor X as a determinant of viral tropism in chick embryo.', *The EMBO journal*. European Molecular Biology Organization, 9(12), pp. 4189–95.

Grace, T. D. C. (1962) 'Establishment of Four Strains of Cells from Insect Tissues Grown in vitro', *Nature*. Nature Publishing Group, 195(4843), pp. 788–789. doi: 10.1038/195788a0.

Granados, R. R., Derksen, A. C. and Dwyer, K. G. (1986) 'Replication of the Trichoplusia ni granulosis and nuclear polyhedrosis viruses in cell cultures.', *Virology*, 152(2), pp. 472–6.

Gravitz, L. (2011) 'Introduction: A smouldering public-health crisis', *Nature*, 474(7350), pp. S2–S4. doi: 10.1038/474S2a.

Gray, D. and Subramanian, S. (2001) 'Choice of cellular protein expression system.', *Current protocols in protein science / editorial board, John E. Coligan ... [et al.]*, Chapter 5, p. Unit5.16. doi: 10.1002/0471140864.ps0516s20.

Greenfield, N. and Fasman, G. D. (1969) 'Computed circular dichroism spectra for the evaluation of protein conformation.', *Biochemistry*, 8(10), pp. 4108–16.

Greenfield, N. J. (2006) 'Using circular dichroism spectra to estimate protein secondary structure.', *Nature protocols*. NIH Public Access, 1(6), pp. 2876–90. doi: 10.1038/nprot.2006.202.

Guarino, L. A. and Summers, M. D. (1987) 'Nucleotide Sequence and Temporal Expression of a Baculovirus Regulatory Gene Nucleotide Sequence and Temporal Expression of a Baculovirus Regulatory Gene', 61(7).

Ha, Y., Stevens, D. J., Skehel, J. J. and Wiley, D. C. (2002) 'H5 avian and H9 swine influenza virus haemagglutinin structures: possible origin of influenza subtypes.', *The EMBO journal*. EMBO Press, 21(5), pp. 865–75. doi: 10.1093/emboj/21.5.865.

von Hahn, T., Yoon, J. C., Alter, H., Rice, C. M., Rehermann, B., Balfe, P. and McKeating, J. a. (2007) 'Hepatitis C Virus Continuously Escapes From Neutralizing Antibody and T-Cell Responses During Chronic Infection In Vivo', *Gastroenterology*, 132(2), pp. 667–678. doi: 10.1053/j.gastro.2006.12.008.

Haid, S., Novodomská, A., Gentzsch, J., Grethe, C., Geuenich, S., Bankwitz, D., Chhatwal, P., Jannack, B., Hennebelle, T., Bailleul, F., Keppler, O. T., Poenisch, M., Bartenschlager, R., Hernandez, C., Lemasson, M., Rosenberg, A. R., Wong–Staal, F., Davioud–Charvet, E., Pietschmann, T., Wong-Staal, F., Davioud-Charvet, E. and Pietschmann, T. (2012) 'A plant-derived flavonoid inhibits entry of all HCV genotypes into human hepatocytes.', *Gastroenterology*, 143(1), p. 213–22.e5. doi: 10.1053/j.gastro.2012.03.036.

Hamilton, B. S., Gludish, D. W. J. and Whittaker, G. R. (2012) 'Cleavage activation of the human-adapted influenza virus subtypes by matriptase reveals both subtype and strain specificities.', *Journal of virology*. American Society for Microbiology (ASM), 86(19), pp. 10579–86. doi: 10.1128/JVI.00306-12.

Hatesuer, B., Bertram, S., Mehnert, N., Bahgat, M. M., Nelson, P. S., Pöhlman, S. and Schughart, K. (2013) 'Tmprss2 is essential for influenza H1N1 virus pathogenesis in mice.', *PLoS pathogens*, 9(12), p. e1003774. doi: 10.1371/journal.ppat.1003774.

Hause, B. M., Ducatez, M., Collin, E. A., Ran, Z., Liu, R., Sheng, Z., Armien, A., Kaplan, B., Chakravarty, S., Hoppe, A. D., Webby, R. J., Simonson, R. R. and Li, F. (2013) 'Isolation of a novel swine influenza virus from Oklahoma in 2011 which is distantly related to human influenza C viruses.', *PLoS pathogens*. Public Library of Science, 9(2), p. e1003176. doi: 10.1371/journal.ppat.1003176.

Hay, A. J., Gregory, V., Douglas, A. R. and Lin, Y. P. (2001) 'The evolution of human influenza viruses.', *Philosophical transactions of the Royal Society of London. Series B, Biological sciences*. The Royal Society, 356(1416), pp. 1861–70. doi: 10.1098/rstb.2001.0999.

Hay, A. J., Wolstenholme, A. J., Skehel, J. J. and Smith, M. H. (1985) 'The molecular basis of the specific anti-influenza action of amantadine.', *The EMBO journal*. European Molecular Biology Organization, 4(11), pp. 3021–4.

Helle, F., Goffard, A., Morel, V., Duverlie, G., McKeating, J., Keck, Z.-Y., Foung, S., Penin, F., Dubuisson, J. and Voisset, C. (2007) 'The Neutralizing Activity of Anti-Hepatitis C Virus Antibodies Is Modulated by Specific Glycans on the E2 Envelope Protein', *Journal of Virology*, 81(15), pp. 8101–8111. doi: 10.1128/JVI.00127-07.

Helle, F., Vieyres, G., Elkrief, L., Popescu, C.-I., Wychowski, C., Descamps, V., Castelain, S., Roingeard, P., Duverlie, G. and Dubuisson, J. (2010) 'Role of N-Linked Glycans in the Functions of Hepatitis C Virus Envelope Proteins Incorporated into Infectious Virions', *Journal of Virology*, 84(22), pp. 11905–11915. doi: 10.1128/JVI.01548-10.

Hitchman, R. B., Possee, R. D. and King, L. A. (2012) 'High-throughput baculovirus expression in insect cells', *Methods in Molecular Biology (Clifton, N.J.)*, 824, pp. 609–627. doi: 10.1007/978-1-61779-433-9_33.

Hoeijmakers, J. H., Odijk, H. and Westerveld, A. (1987) 'Differences between rodent and human cell lines in the amount of integrated DNA after transfection.', *Experimental cell research*, 169(1), pp. 111–9.

Holmberg, S. D., Spradling, P. R., Moorman, A. C. and Denniston, M. M. (2013) 'Hepatitis C in the United States', *New England Journal of Medicine*, 368(20), pp. 1859–1861. doi: 10.1056/NEJMp1302973.

Holzwarth, G. and Doty, P. (1965) 'The ultraviolet circular dichroism of polypeptides.', *Journal of the American Chemical Society*, 87, pp. 218–28.

Horimoto, T. and Kawaoka, Y. (2005) 'Influenza: lessons from past pandemics, warnings from current incidents', *Nature Reviews Microbiology*, 3(8), pp. 591–600. doi: 10.1038/nrmicro1208.

Houghton, M. and Abrignani, S. (2005) 'Prospects for a vaccine against the hepatitis C virus', *Nature*, 436(7053), pp. 961–966. doi: 10.1038/nature04081.

Hussain, M., Galvin, H. D., Haw, T. Y., Nutsford, A. N. and Husain, M. (2017) 'Drug resistance in influenza A virus: the epidemiology and management.', *Infection and drug resistance*. Dove Press, 10, pp. 121–134. doi: 10.2147/IDR.S105473.

Igarashi, M., Ito, K., Yoshida, R., Tomabechi, D., Kida, H. and Takada, A. (2010) 'Predicting the Antigenic Structure of the Pandemic (H1N1) 2009 Influenza Virus Hemagglutinin', *PLoS ONE*. Edited by R. Belshaw. Public Library of Science, 5(1), p. e8553. doi: 10.1371/journal.pone.0008553.

Ingham, K. C. (1990) 'Precipitation of proteins with polyethylene glycol', *Methods in Enzymology*. Academic Press, 182, pp. 301–306. doi: 10.1016/0076-6879(90)82025-W.

Isin, B., Doruker, P. and Bahar, I. (2002) 'Functional Motions of Influenza Virus Hemagglutinin: A Structure-Based Analytical Approach', *Biophysical Journal*, 82(2), pp. 569–581. doi: 10.1016/S0006-3495(02)75422-2.

Jäger, V., Büssow, K., Wagner, A., Weber, S., Hust, M., Frenzel, A. and Schirrmann, T. (2013) 'High level transient production of recombinant antibodies and antibody fusion proteins in HEK293 cells.', *BMC biotechnology*, 13(1), p. 52. doi: 10.1186/1472-6750-13-52.

Jäger, V., Groenewold, J., Krüger, D., Schwarz, D. and Vollmer, V. (2015) 'High-titer expression of recombinant antibodies by transiently transfected HEK 293-6E cell cultures', *BMC Proceedings*. BioMed Central Ltd, 9(Suppl 9), pp. 4–6. doi: 10.1186/1753-6561-9-S9-P40.

Jarvis, D. L. (2009) *Baculovirus-insect cell expression systems.* 1st edn, *Methods in enzymology*. 1st edn. Elsevier Inc. doi: 10.1016/S0076-6879(09)63014-7.

Johnson, W. C. (1990) 'Protein secondary structure and circular dichroism: a practical guide.', *Proteins*, 7(3), pp. 205–14. doi: 10.1002/prot.340070302.

Kadam, R. U. and Wilson, I. A. (2017) 'Structural basis of influenza virus fusion inhibition by the antiviral drug Arbidol.', *Proceedings of the National Academy of Sciences of the United States of America*. National Academy of Sciences, 114(2), pp. 206–214. doi: 10.1073/pnas.1617020114.

Karste, K., Bleckmann, M. and van den Heuvel, J. (2017) 'Not Limited to E. coli: Versatile Expression Vectors for Mammalian Protein Expression', in. Humana Press, New York, NY, pp. 313–324. doi: 10.1007/978-1-4939-6887-9_20.

Kaufman, R. J., Wasley, L. C., Spiliotes, A. J., Gossels, S. D., Latt, S. A., Larsen, G. R. and Kay, R. M. (1985) 'Coamplification and coexpression of human tissue-type plasminogen activator and murine dihydrofolate reductase sequences in Chinese hamster ovary cells.', *Molecular and cellular biology*, 5(7), pp. 1750–9.

Kawaoka, Y. and Webster, R. G. (1989) 'Interplay between carbohydrate in the stalk and the length of the connecting peptide determines the cleavability of influenza virus hemagglutinin.', *Journal of virology*, 63(8), pp. 3296–300.

Keck, Z., Girard-Blanc, C., Wang, W., Lau, P., Zuiani, A., Rey, F. A., Krey, T., Diamond, M. S. and Foung, S. K. H. (2016) 'Antibody Response to Hypervariable Region 1 Interferes with Broadly Neutralizing Antibodies to Hepatitis C Virus'. Edited by J.-H. J. Ou. American Society for Microbiology, 90(6). doi: 10.1128/JVI.02458-15.

Kelly, M. L., Cook, J. A., Brown-Augsburger, P., Heinz, B. A., Smith, M. C. and Pinto, L. H. (2003) 'Demonstrating the intrinsic ion channel activity of virally encoded proteins.', *FEBS letters*, 552(1), pp. 61–7.

Khan, A. G., Miller, M. T. and Marcotrigiano, J. (2015) 'HCV glycoprotein structures: what to expect from the unexpected', *Current Opinion in Virology*, 12, pp. 53–58. doi: 10.1016/j.coviro.2015.02.004.

Khan, A. G., Whidby, J., Miller, M. T., Scarborough, H., Zatorski, A. V, Cygan, A., Price, A. A., Yost, S. A., Bohannon, C. D., Jacob, J., Grakoui, A. and Marcotrigiano, J. (2014) 'Structure of the core ectodomain of the hepatitis C virus envelope glycoprotein 2.', *Nature*. Nature Publishing Group, a division of Macmillan Publishers Limited. All Rights Reserved., advance on. doi: 10.1038/nature13117.

Khatchikian, D., Orlich, M. and Rott, R. (1989) 'Increased viral pathogenicity after insertion of a 28S ribosomal RNA sequence into the haemagglutinin gene of an influenza virus', *Nature*, 340(6229), pp. 156–157. doi: 10.1038/340156a0.

Kido, H., Yokogoshi, Y., Sakai, K., Tashiro, M., Kishino, Y., Fukutomi, A. and Katunuma, N. (1992) 'Isolation and characterization of a novel trypsin-like protease found in rat bronchiolar epithelial Clara cells. A possible activator of the viral fusion glycoprotein.', *The Journal of biological chemistry*, 267(19), pp. 13573–9.

Kielian, M. (2006) 'Class II virus membrane fusion proteins', *Virology*. Academic Press, 344(1), pp. 38–47. doi: 10.1016/J.VIROL.2005.09.036.

Kielian, M. and Rey, F. A. (2006) 'Virus membrane-fusion proteins: more than one way to make a hairpin', *Nature Reviews Microbiology*. Nature Publishing Group, 4(1), pp. 67–76. doi: 10.1038/nrmicro1326.

Kiseljak, D., Rajendra, Y., Manoli, S. S., Baldi, L., Hacker, D. L. and Wurm, F. M. (2011) 'The use of filler DNA for improved transfection and reduced DNA needs in transient gene expression with CHO and HEK cells.', *BMC proceedings*. BioMed Central, 5 Suppl 8(Suppl 8), p. P33. doi: 10.1186/1753-6561-5-S8-P33.

Klenk, H.-D., Wagner, R., Heuer, D. and Wolff, T. (2002) 'Importance of hemagglutinin glycosylation for the biological functions of influenza virus.', *Virus research*, 82(1–2), pp. 73–5.

Klenk, H. D. and Garten, W. (1994) 'Host cell proteases controlling virus pathogenicity.', *Trends in microbiology*, 2(2), pp. 39–43.

Klenk, H. D. and Rott, R. (1973) 'Formation of influenza virus proteins.', *Journal of virology*, 11(6), pp. 823–31.

Klenk, H. D., Rott, R., Orlich, M. and Blödorn, J. (1975) 'Activation of influenza A viruses by trypsin treatment.', *Virology*, 68(2), pp. 426–39.

Komurian-Pradel, F., Rajoharison, A., Berland, J.-L., Khouri, V., Perret, M., van Roosmalen, M., Pol, S., Negro, F. and Paranhos-Baccala, G. (2004) 'Antigenic relevance of F protein in chronic hepatitis C virus infection', *Hepatology*, 40(4), pp. 900–909. doi: 10.1002/hep.20406.

Kong, L., Giang, E., Nieusma, T., Kadam, R. U., Cogburn, K. E., Hua, Y., Dai, X., Stanfield, R. L., Burton, D. R., Ward, A. B., Wilson, I. A. and Law, M. (2013) 'Hepatitis C Virus E2 Envelope Glycoprotein Core Structure', *Science*, 342(6162), pp. 1090–1094. doi: 10.1126/science.1243876.

Kong, L., Giang, E., Nieusma, T., Robbins, J. B., Deller, M. C., Stanfield, R. L., Wilson, I. A. and Law, M. (2012) 'Structure of hepatitis C virus envelope glycoprotein E2 antigenic site 412 to 423 in complex with antibody AP33.', *Journal of virology*. American Society for Microbiology, 86(23), pp. 13085–8. doi: 10.1128/JVI.01939-12.

Kong, L., Giang, E., Robbins, J. B., Stanfield, R. L., Burton, D. R., Wilson, I. A. and Law, M. (2012) 'Structural basis of hepatitis C virus neutralization by broadly neutralizing antibody HCV1.', *Proceedings of the National Academy of Sciences of the United States of America*. National Academy of Sciences, 109(24), pp. 9499–504. doi: 10.1073/pnas.1202924109.

Kong, L., Jackson, K. N., Wilson, I. A. and Law, M. (2015) 'Capitalizing on knowledge of hepatitis C virus neutralizing epitopes for rational vaccine design', *Current Opinion in Virology*. Elsevier B.V., 11, pp. 148–157. doi: 10.1016/j.coviro.2015.04.001.

Kong, L., Lee, D. E., Kadam, R. U., Liu, T., Giang, E., Nieusma, T., Garces, F., Tzarum, N., Woods, V. L., Ward, A. B., Li, S., Wilson, I. A. and Law, M. (2016) 'Structural flexibility at a major conserved antibody target on hepatitis C virus E2 antigen.', *Proceedings of the National Academy of Sciences of the United States of America*. National Academy of Sciences, 113(45), pp. 12768–12773. doi: 10.1073/pnas.1609780113.

Kontermann, R. E. (2010) 'Alternative antibody formats.', *Current opinion in molecular therapeutics*, 12(2), pp. 176–83.

Kool, M., Voncken, J. W., van Lier, F. L., Tramper, J. and Vlak, J. M. (1991) 'Detection and analysis of Autographa californica nuclear polyhedrosis virus mutants with defective interfering properties.', *Virology*, 183(2), pp. 739–46.

Krämer, A., Kretzschmar, M. and Krickeberg, K. (2010) *Modern infectious disease epidemiology : concepts, methods, mathematical models, and public health*. Springer.

Krell, P. J. (1996) 'Passage effect of virus infection in insect cells', *Cytotechnology*, 20(1–3), pp. 125–137. doi: 10.1007/BF00350393.

Krey, T., d'Alayer, J., Kikuti, C. M., Saulnier, A., Damier-Piolle, L., Petitpas, I., Johansson, D. X., Tawar, R. G., Baron, B., Robert, B., England, P., Persson, M. A. A. A., Martin, A. and Rey, F. A. (2010) 'The disulfide bonds in glycoprotein E2 of hepatitis C virus reveal the tertiary organization of the molecule', *PLoS Pathogens*. Edited by C. M. Rice. Public Library of Science, 6(2), p. e1000762. doi: 10.1371/journal.ppat.1000762.

Krey, T., Meola, A., Keck, Z., Damier-Piolle, L., Foung, S. K. H. and Rey, F. A. (2013) 'Structural Basis of HCV Neutralization by Human Monoclonal Antibodies Resistant to Viral Neutralization Escape', *PLoS Pathogens*. Edited by M. S. Diamond. Public Library of Science, 9(5), p. e1003364. doi: 10.1371/journal.ppat.1003364.

Król, E., Rychłowska, M. and Szewczyk, B. (2014) 'Antivirals--current trends in fighting influenza.', *Acta biochimica Polonica*, 61(3), pp. 495–504.

Kühn, N. (2015) 'Studies on the host response to influenza A virus infections in mouse knock-out mutants'.

Kühn, N., Bergmann, S., Kösterke, N., Lambertz, R. L. O., Keppner, A., van den Brand, J. M. A., Pöhlmann, S., Weiß, S., Hummler, E., Hatesuer, B. and Schughart, K. (2016) 'The Proteolytic Activation of (H3N2) Influenza A Virus Hemagglutinin Is Facilitated by Different Type II Transmembrane Serine Proteases.', *Journal of virology*. American Society for Microbiology, 90(9), pp. 4298–307. doi: 10.1128/JVI.02693-15.

Kumar, M. S., Ramachandran, A., Hasnain, S. E. and Bashyam, M. D. (2009) 'Octamer and heat shock elements regulate transcription from the AcMNPV polyhedrin gene promoter', *Archives of Virology*, 154(3), pp. 445–456. doi: 10.1007/s00705-009-0324-x.

Kunert, R. and Reinhart, D. (2016) 'Advances in recombinant antibody manufacturing.', *Applied microbiology and biotechnology*. Springer, 100(8), pp. 3451–61. doi: 10.1007/s00253-016-7388-9.

Kuzio, J., Rohel, D. Z., Curry, C. J., Krebs, A., Carstens, E. B. and Faulkner, P. (1984) 'Nucleotide sequence of the p10 polypeptide gene of Autographa californica nuclear polyhedrosis virus.', *Virology*, 139(2), pp. 414–8.

Laemmli, K. U. (1970) 'Cleavage of Structural Proteins during the Assembly of the Head of Bacteriophage T4', *Nature*. Nature Publishing Group, 227(5259), pp. 680–685. doi: 10.1038/227680a0.

Laporte, M. and Naesens, L. (2017) 'Airway proteases: an emerging drug target for influenza and other respiratory virus infections', *Current Opinion in Virology*. Elsevier, 24, pp. 16–24. doi: 10.1016/J.COVIRO.2017.03.018.

Lavie, M., Goffard, A. and Dubuisson, J. (2006) *HCV Glycoproteins: Assembly of a Functional E1–E2 Heterodimer*, *Hepatitis C Viruses: Genomes and Molecular Biology*. Horizon Bioscience.

Lazarowitz, S. G., Compans, R. W. and Choppin, P. W. (1973) 'Proteolytic cleavage of the hemagglutinin polypeptide of influenza virus. Function of the uncleaved polypeptide HA.', *Virology*, 52(1), pp. 199–212.

Lee, K. J., Suh, Y. A., Cho, Y. G., Cho, Y. S., Ha, G. W., Chung, K. H., Hwang, J. H., Yun, Y. D., Lee, D. S., Kim, C. M. and Sung, Y. C. (1997) 'Hepatitis C virus E2 protein purified from mammalian cells is frequently recognized by E2-specific antibodies in patient sera.', *The Journal of biological chemistry*. American Society for Biochemistry and Molecular Biology, 272(48), pp. 30040–6. doi: 10.1074/JBC.272.48.30040.

Li, W. (2014) *Structural Analysis of Bacterial and Viral Infections and a Cysteine Proteinase Legumain*.

Li, X., van Oers, M. M., Vlak, J. M. and Braakman, I. (2015) 'Folding of influenza virus hemagglutinin in insect cells is fast and efficient', *Journal of Biotechnology*, 203, pp. 77–83. doi: 10.1016/j.jbiotec.2015.03.018.

Li, Y., Pierce, B. G., Wang, Q., Keck, Z.-Y. Y., Fuerst, T. R., Foung, S. K. H. and Mariuzza, R. A. (2015) 'Structural basis for penetration of the glycan shield of hepatitis C virus E2 glycoprotein by a broadly neutralizing human antibody', *Journal of Biological Chemistry*. American Society for Biochemistry and Molecular Biology, 290(16), pp. 10117–10125. doi: 10.1074/jbc.M115.643528.

van Lier, F. L., van der Meijs, W. C., Grobben, N. G., Olie, R. A., Vlak, J. M. and Tramper, J. (1992) 'Continuous beta-galactosidase production with a recombinant baculovirus insect-cell system in bioreactors.', *Journal of biotechnology*, 22(3), pp. 291–8.

Lindenbach, B. D. and Rice, C. M. (2013) 'The ins and outs of hepatitis C virus entry and assembly', *Nature Reviews Microbiology*. Nature Research, 11(10), pp. 688–700. doi: 10.1038/nrmicro3098.

Liu, Y. and Eisenberg, D. (2002) '3D domain swapping: as domains continue to swap.', *Protein science : a publication of the Protein Society*. Wiley-Blackwell, 11(6), pp. 1285–99. doi: 10.1110/ps.0201402.

Logan, M., Law, J., Wong, J. A. J.-X., Hockman, D., Landi, A., Chen, C., Crawford, K., Kundu, J., Baldwin, L., Johnson, J., Dahiya, A., LaChance, G., Marcotrigiano, J., Law, M., Foung, S., Tyrrell, L. and Houghton, M. (2017) 'Native Folding of a Recombinant gpE1/gpE2 Heterodimer Vaccine Antigen from a Precursor Protein Fused with Fc IgG', *Journal of Virology*, 91(1), pp. e01552-16. doi: 10.1128/JVI.01552-16.

Lorber, B., Fischer, F., Bailly, M., Roy, H. and Kern, D. (2012) 'Protein analysis by dynamic light scattering: Methods and techniques for students', *Biochemistry and Molecular Biology Education*. Wiley Subscription Services, Inc., A Wiley Company, 40(6), pp. 372–382. doi: 10.1002/bmb.20644.

Louis-Jeune, C., Andrade-Navarro, M. A. and Perez-Iratxeta, C. (2012) 'Prediction of protein secondary structure from circular dichroism using theoretically derived spectra', *Proteins: Structure, Function and Bioinformatics*. Wiley Subscription Services, Inc., A Wiley Company, 80(2), pp. 374–381. doi: 10.1002/prot.23188.

Lu, X., Shi, Y. Y., Gao, F., Xiao, H., Wang, M., Qi, J. and Gao, G. F. (2012) 'Insights into avian influenza virus pathogenicity: the hemagglutinin precursor HA0 of subtype H16 has an alpha-helix structure in its cleavage site with inefficient HA1/HA2 cleavage.', *Journal of virology*. American Society for Microbiology, 86(23), pp. 12861–70. doi: 10.1128/JVI.01606-12.

Lu, Y., Welsh, J. P. and Swartz, J. R. (2014) 'Production and stabilization of the trimeric influenza hemagglutinin stem domain for potentially broadly protective influenza vaccines.', *Proceedings of the National Academy of Sciences of the United States of America*. National Academy of Sciences, 111(1), pp. 125–30. doi: 10.1073/pnas.1308701110.

Malhotra, A. (2009) 'Chapter 16 Tagging for Protein Expression', in *Methods in enzymology*, pp. 239–258. doi: 10.1016/S0076-6879(09)63016-0.

McCaffrey, K., Boo, I., Owczarek, C. M., Hardy, M. P., Perugini, M. A., Fabri, L., Scotney, P., Poumbourios, P. and Drummer, H. E. (2017) 'An Optimized Hepatitis C Virus E2 Glycoprotein Core Adopts a Functional Homodimer That Efficiently Blocks Virus Entry.', *Journal of virology*. American Society for Microbiology, 91(5), pp. e01668-16. doi: 10.1128/JVI.01668-16.

McCaffrey, K., Boo, I., Tewierek, K., Edmunds, M. L., Poumbourios, P. and Drummer, H. E. (2012) 'Role of conserved cysteine residues in hepatitis C virus glycoprotein e2 folding and function.', *Journal of virology*. American Society for Microbiology, 86(7), pp. 3961–74. doi: 10.1128/JVI.05396-11.

McPherson, A. (1976) 'Crystallization of proteins from polyethylene glycol.', *The Journal of biological chemistry*, 251(20), pp. 6300–3.

McPherson, A., Malkin, A. J. and Kuznetsov, Y. G. (2000) 'Atomic Force Microscopy in the Study of Macromolecular Crystal Growth', *Annual Review of Biophysics and Biomolecular Structure*, 29(1), pp. 361–410. doi: 10.1146/annurev.biophys.29.1.361.

McPherson, A., Malkin, A. and Kuznetsov, Y. (1995) 'The science of macromolecular crystallization', *Structure*. Cell Press, 3(8), pp. 759–768. doi: 10.1016/S0969-2126(01)00211-8.

Meertens, L., Bertaux, C. and Dragic, T. (2006) 'Hepatitis C virus entry requires a critical postinternalization step and delivery to early endosomes via clathrin-coated vesicles.', *Journal of virology*. American Society for Microbiology (ASM), 80(23), pp. 11571–8. doi: 10.1128/JVI.01717-06.

Meola, A., Tarr, A. W., England, P., Meredith, L. W., McClure, C. P., Foung, S. K. H., McKeating, J. A., Ball, J. K., Rey, F. A. and Krey, T. (2015) 'Structural flexibility of a conserved antigenic region in hepatitis C virus glycoprotein E2 recognized by broadly neutralizing antibodies.', *Journal of virology*. American Society for Microbiology, 89(4), pp. 2170–81. doi: 10.1128/JVI.02190-14.

Metz, S. W. and Pijlman, G. P. (2011) 'Arbovirus vaccines; opportunities for the baculovirus-insect cell expression system', *Journal of Invertebrate Pathology*. Academic Press, 107, pp. S16–S30.

Meunier-Durmort, C., Grimal, H., Sachs, L., Demeneix, B. and Forest, C. (1997) 'Adenovirus enhancement of polyethylenimine-mediated transfer of regulated genes in differentiated cells', *Gene Therapy*, 4(8), pp. 808–814. doi: 10.1038/sj.gt.3300450.

Meunier, J.-C., Engle, R. E., Faulk, K., Zhao, M., Bartosch, B., Alter, H., Emerson, S. U., Cosset, F.-L., Purcell, R. H. and Bukh, J. (2005) 'Evidence for cross-genotype neutralization of hepatitis C virus pseudo-particles and enhancement of infectivity by apolipoprotein C1', *Proceedings of the National Academy of Sciences*, 102(12), pp. 4560–4565. doi: 10.1073/pnas.0501275102.

Meyer, S. (2012) *Development of an Integrated Expression Platform for Protein Production in Eukaryotic Hosts*.

Meyer, S., Lorenz, C., Baser, B., Wördehoff, M., Jäger, V. and van den Heuvel, J. (2013) 'Multi-host expression system for recombinant production of challenging proteins.', *PloS one*, 8(7), p. e68674. doi: 10.1371/journal.pone.0068674.

Michalak, J. P., Wychowski, C., Choukhi, A., Meunier, J. C., Ung, S., Rice, C. M. and Dubuisson, J. (1997) 'Characterization of truncated forms of hepatitis C virus glycoproteins.', *Journal of General Virology*, 78(9), pp. 2299–2306. doi: 10.1099/0022-1317-78-9-2299.

Milián, E. and Kamen, A. A. (2015) 'Current and Emerging Cell Culture Manufacturing Technologies for Influenza Vaccines', *BioMed Research International*. Hindawi, 2015, pp. 1–11. doi: 10.1155/2015/504831.

Munk, K., Pritzer, E., Kretzschmar, E., Gutte, B., Garten, W. and Klenk, H. D. (1992) 'Carbohydrate masking of an antigenic epitope of influenza virus haemagglutinin independent of oligosaccharide size.', *Glycobiology*, 2(3), pp. 233–40.

Nayak, D. P., Balogun, R. A., Yamada, H., Zhou, Z. H. and Barman, S. (2009) 'Influenza virus morphogenesis and budding', *Virus Research*, 143(2), pp. 147–161. doi: 10.1016/j.virusres.2009.05.010.

Nayak, D. P., Hui, E. K.-W. and Barman, S. (2004) 'Assembly and budding of influenza virus', *Virus Research*, 106(2), pp. 147–165. doi: 10.1016/j.virusres.2004.08.012.

Nelson, M. I. and Holmes, E. C. (2007) 'The evolution of epidemic influenza', *Nature Reviews Genetics*. Nature Publishing Group, 8(3), pp. 196–205. doi: 10.1038/nrg2053.

Nettleship, J. E., Assenberg, R., Diprose, J. M., Rahman-Huq, N. and Owens, R. J. (2010) 'Recent advances in the production of proteins in insect and mammalian cells for structural biology.', *Journal of Structural Biology*. Elsevier Inc., 172(1), pp. 55–65. doi: 10.1016/j.jsb.2010.02.006.

Nettleship, J. J. E. (2012) 'Structural Biology of Glycoproteins', *Biochemistry, Genetics and Molecular Biology*, pp. 41–62. doi: 10.5772/48154.

Neumann, G., Noda, T. and Kawaoka, Y. (2009) 'Emergence and pandemic potential of swine-origin H1N1 influenza virus', *Nature*. Nature Publishing Group, 459(7249), pp. 931–939. doi: 10.1038/nature08157.

Newman, J. (2004) 'Novel buffer systems for macromolecular crystallization', *Acta Crystallographica Section D Biological Crystallography*, 60(3), pp. 610–612. doi: 10.1107/S0907444903029640.

Neyshabouri, S. Y.-, Aghasadeghi, M. R., Najafabadi, A. J., Bouzari, S., Arashkia, A., Sadat, S. M., Siadat, S. D., Sadigh, Z. and Hekmat, S. (2012) 'Expression of recombinant Hepatitis C virus (HCV) Core , E1 and E2 proteins by the baculovirus expression vector system', 6(19), pp. 4152–4157. doi: 10.5897/AJMR11.1494.

Ni, F., Kondrashkina, E. and Wang, Q. (2015) 'Structural and Functional Studies of Influenza Virus A/H6 Hemagglutinin', *PLOS ONE*. Edited by T. Takimoto. Public Library of Science, 10(7), p. e0134576. doi: 10.1371/journal.pone.0134576.

Niesen, F. H., Berglund, H. and Vedadi, M. (2007) 'The use of differential scanning fluorimetry to detect ligand interactions that promote protein stability', *Nature Protocols*, 2(9), pp. 2212–2221. doi: 10.1038/nprot.2007.321.

Nobusawa, E. and Sato, K. (2006) 'Comparison of the Mutation Rates of Human Influenza A and B Viruses', *Journal of Virology*, 80(7), pp. 3675–3678. doi: 10.1128/JVI.80.7.3675-3678.2006.

van Oers, M. M., Vlak, J. M., Voorma, H. O. and Thomas, a a (1999) 'Role of the 3' untranslated region of baculovirus p10 mRNA in high-level expression of foreign genes.', *The Journal of general virology*, 80 (Pt 8), pp. 2253–62.

Ogay, I. D., Lihoradova, O. A., Azimova, S. S., Abdukarimov, A. A., Slack, J. M. and Lynn, D. E. (2006) 'Transfection of insect cell lines using polyethylenimine.', *Cytotechnology*. Springer, 51(2), pp. 89–98. doi: 10.1007/s10616-006-9022-7.

Ohuchi, M., Ohuchi, R., Feldmann, A. and Klenk, H. D. (1997) 'Regulation of receptor binding affinity of influenza virus hemagglutinin by its carbohydrate moiety.', *Journal of virology*. American Society for Microbiology (ASM), 71(11), pp. 8377–84.

Ohuchi, M., Orlich, M., Ohuchi, R., Simpson, B. E., Garten, W., Klenk, H. D. and Rott, R. (1989) 'Mutations at the cleavage site of the hemagglutinin after the pathogenicity of influenza virus A/chick/Penn/83 (H5N2).', *Virology*, 168(2), pp. 274–80.

Ohuchi, R., Ohuchi, M., Garten, W. and Klenk, H. D. (1991) 'Human influenza virus hemagglutinin with high sensitivity to proteolytic activation.', *Journal of virology*, 65(7), pp. 3530–7.

El Omari, K., Iourin, O., Kadlec, J., Sutton, G., Harlos, K., Grimes, J. M. and Stuart, D. I. (2014) 'Unexpected structure for the N-terminal domain of hepatitis C virus envelope glycoprotein E1.', *Nature Communications*. Nature Publishing Group, 5, p. 4874. doi: 10.1038/ncomms5874.

Orlova, O. V, Drutsa, V. L., Spirin, P. V, Prasolov, V. S., Rubtsov, P. M., Kochetkov, S. N. and Beljelarskaya, S. N. (2015) 'The role of HCV e2 protein glycosylation in functioning of virus envelope proteins in insect and Mammalian cells.', *Acta naturae*, 7(1), pp. 87–97.

Ortega-Atienza, S., Lombana, L., Gómez-Gutiérrez, J., Yélamos, B., Peterson, D. L. and Gavilanes, F. (2014) 'Production and Characterization of the Ectodomain of E2 Envelope Glycoprotein of Hepatitis C Virus Folded in the Presence of Full-length E1 glycoprotein', *Protein Expression and Purification*, 104, pp. 20–25. doi: 10.1016/j.pep.2014.09.009.

Owsianka, A. M., Timms, J. M., Tarr, A. W., Brown, R. J. P., Hickling, T. P., Szwejk, A., Bienkowska-Szewczyk, K., Thomson, B. J., Patel, A. H. and Ball, J. K. (2006) 'Identification of conserved residues in the E2 envelope glycoprotein of the hepatitis C virus that are critical for CD81 binding.', *Journal of virology*. American Society for Microbiology, 80(17), pp. 8695–704. doi: 10.1128/JVI.00271-06.

Pantua, H., Diao, J., Ultsch, M., Hazen, M., Mathieu, M., McCutcheon, K., Takeda, K., Date, S., Cheung, T. K., Phung, Q., Hass, P., Arnott, D., Hongo, J. A., Matthews, D. J., Brown, A., Patel, A. H., Kelley, R. F., Eigenbrot, C. and Kapadia, S. B. (2013) 'Glycan shifting on hepatitis C virus (HCV) E2 glycoprotein is a mechanism for escape from broadly neutralizing antibodies', *Journal of Molecular Biology*. Elsevier Ltd, 425(11), pp. 1899–1914. doi: 10.1016/j.jmb.2013.02.025.

Pawlotsky, J.-M., Feld, J. J., Zeuzem, S. and Hoofnagle, J. H. (2015) 'From non-A, non-B hepatitis to hepatitis C virus cure', *Journal of Hepatology*. Elsevier, 62(1), pp. S87–S99. doi: 10.1016/J.JHEP.2015.02.006.

PDB Data Distribution by Expression Organism (2018) *PDB Data Distribution by Expression Organism*. Available at: https://www.rcsb.org/stats/distribution_expression-organism-gene (Accessed: 5 June 2018).

Perdue, M. L., García, M., Senne, D. and Fraire, M. (1997) 'Virulence-associated sequence duplication at the hemagglutinin cleavage site of avian influenza viruses', *Virus Research*. Elsevier, 49(2), pp. 173–186. doi: 10.1016/S0168-1702(97)01468-8.

Pfaender, S., Walter, S., Grabski, E., Todt, D., Bruening, J., Romero-Brey, I., Gather, T., Brown, R. J. P., Hahn, K., Puff, C., Pfankuche, V. M., Hansmann, F., Postel, A., Becher, P., Thiel, V., Kalinke, U., Wagner, B., Bartenschlager, R., Baumgärtner, W., Feige, K., Pietschmann, T., Cavalleri, J. M. V. and Steinmann, E. (2017) 'Immune protection against reinfection with nonprimate hepacivirus', *Proceedings of the National Academy of Sciences*, 114(12), pp. E2430–E2439. doi: 10.1073/pnas.1619380114.

Pietschmann, T. (2017) 'Clinically Approved Ion Channel Inhibitors Close Gates for Hepatitis C Virus and Open Doors for Drug Repurposing in Infectious Viral Diseases.', *Journal of virology*. American Society for Microbiology, 91(2), pp. e01914-16. doi: 10.1128/JVI.01914-16.

Pijlman, G. P. (2003) 'Spontaneous excision of BAC vector sequences from bacmid-derived baculovirus expression vectors upon passage in insect cells', *Journal of General Virology*, 84(10), pp. 2669–2678. doi: 10.1099/vir.0.19438-0.

Pijlman, G. P., van Schinjndel, J. E. and Vlak, J. M. (2003) 'Spontaneous excision of BAC vector sequences from bacmid-derived baculovirus expression vectors upon passage in insect cells', *Journal of General Virology*, 84(10), pp. 2669–2678. doi: 10.1099/vir.0.19438-0.

Pinto, L. H. and Lamb, R. A. (2007) 'Controlling influenza virus replication by inhibiting its proton channel', *Mol. BioSyst.* The Royal Society of Chemistry, 3(1), pp. 18–23. doi: 10.1039/B611613M.

Polyak, S. J., Klein, K. C., Shoji, I., Miyamura, T. and Lingappa, J. R. (2006) 'Assemble and Interact : Pleiotropic Functions of the HCV Core Protein', *Hepatitis C Viruses: Genome and Molecular Biology*, pp. 89–119.

Possee, R. D., Hitchman, R. B., Richards, K. S., Mann, S. G., Siaterli, E., Nixon, C. P., Irving, H., Assenberg, R., Alderton, D., Owens, R. J. and King, L. A. (2008) 'Generation of baculovirus vectors for the high-throughput production of proteins in insect cells', *Biotechnology and Bioengineering*. Wiley Subscription Services, Inc., A Wiley Company, 101(6), pp. 1115–1122. doi: 10.1002/bit.22002.

Potter, J. A., Owsianka, A. M., Jeffery, N., Matthews, D. J., Keck, Z.-Y., Lau, P., Foung, S. K. H., Taylor, G. L. and Patel, A. H. (2012) 'Toward a hepatitis C virus vaccine: the structural basis of hepatitis C virus neutralization by AP33, a broadly neutralizing antibody.', *Journal of virology*. American Society for Microbiology, 86(23), pp. 12923–32. doi: 10.1128/JVI.02052-12.

Puck, T. T., Cieciura, S. J. and Robinson, A. (1958) 'Genetics of somatic mammalian cells. III. Long-term cultivation of euploid cells from human and animal subjects.', *The Journal of experimental medicine*. The Rockefeller University Press, 108(6), pp. 945–56.

Radner, S., Celie, P. H. N. N., Fuchs, K., Sieghart, W., Sixma, T. K., Stornaiuolo, M., Celie, P. H. N. N., Radner, S. and Sieghart, W. (2012) 'Transient transfection coupled to baculovirus infection for rapid protein expression screening in insect cells.', *Journal of structural biology*. Elsevier Inc., 179(1), pp. 46–55. doi: 10.1016/j.jsb.2012.04.013.

Raman, R., Tharakaraman, K., Sasisekharan, V. and Sasisekharan, R. (2016) 'Glycan-protein interactions in viral pathogenesis.', *Current opinion in structural biology*. NIH Public Access, 40, pp. 153–162. doi: 10.1016/j.sbi.2016.10.003.

Reeves, P. J., Callewaert, N., Contreras, R. and Khorana, H. G. (2002) 'Structure and function in rhodopsin: High-level expression of rhodopsin with restricted and homogeneous N-glycosylation by a tetracycline-inducible N-acetylglucosaminyltransferase I-negative HEK293S stable mammalian cell line', *Proceedings of the National Academy of Sciences*, 99(21), pp. 13419–13424. doi: 10.1073/pnas.212519299.

Reid, A. H., Fanning, T. G., Hultin, J. V, Taubenberger, J. K., Coombs, P. J., Russell, R. J., Gamblin, S. J. and Skehel, J. J. (1999) 'Origin and evolution of the 1918 "Spanish" influenza virus hemagglutinin gene.', *Proceedings of the National Academy of Sciences of the United States of America*. National Academy of Sciences, 96(4), pp. 1651–6. doi: 10.1073/pnas.96.4.1651.

Rhodes, G. (2006a) 'Chapter 2 – An Overview of Protein Crystallography', in *Crystallography Made Crystal Clear*, pp. 7–30. doi: 10.1016/B978-012587073-3/50004-0.

Rhodes, G. (2006b) 'Chapter 4 – Collecting Diffraction Data', in *Crystallography Made Crystal Clear*, pp. 49–89. doi: 10.1016/B978-012587073-3/50006-4.

Rhodes, G. (2006c) 'Chapter 5 – From Diffraction Data to Electron Density', in *Crystallography Made Crystal Clear*, pp. 91–107. doi: 10.1016/B978-012587073-3/50007-6.

Ringenbach, L., Bohbot, A., Tiberghien, P., Oberling, F. and Feugeas, O. (1998) 'Polyethylenimine-mediated transfection of human monocytes with the IFN-gamma gene: an approach for cancer adoptive immunotherapy.', *Gene therapy*, 5(11), pp. 1508–16. doi: 10.1038/sj.gt.3300756.

Roberts, P. C., Garten, W. and Klenk, H. D. (1993) 'Role of conserved glycosylation sites in maturation and transport of influenza A virus hemagglutinin.', *Journal of virology*, 67(6), pp. 3048–60.

Rodríguez-Rodríguez, M., Tello, D., Yélamos, B., Gómez-Gutiérrez, J., Pacheco, B., Ortega, S., Serrano, A. G., Peterson, D. L. and Gavilanes, F. (2009) 'Structural properties of the ectodomain of hepatitis C virus E2 envelope protein', *Virus Research*, 139(1), pp. 91–99. doi: 10.1016/j.virusres.2008.10.013.

Rosano, G. L. and Ceccarelli, E. A. (2014) 'Recombinant protein expression in Escherichia coli: advances and challenges.', *Frontiers in microbiology*. Frontiers Media SA, 5, p. 172. doi: 10.3389/fmicb.2014.00172.

Rothwangl, K. B., Manicassamy, B., Uprichard, S. L. and Rong, L. (2008) 'Dissecting the role of putative CD81 binding regions of E2 in mediating HCV entry: putative CD81 binding region 1 is not involved in CD81 binding.', *Virology journal*. BioMed Central, 5, p. 46. doi: 10.1186/1743-422X-5-46.

Rouillé, Y., Helle, F., Delgrange, D., Roingeard, P., Voisset, C., Blanchard, E., Belouzard, S., McKeating, J., Patel, A. H., Maertens, G., Wakita, T., Wychowski, C. and Dubuisson, J. (2006) 'Subcellular Localization of Hepatitis C Virus Structural Proteins in a Cell Culture System That Efficiently Replicates the Virus', *Journal of Virology*. American Society for Microbiology, 80(6), pp. 2832–2841. doi: 10.1128/JVI.80.6.2832-2841.2006.

Russell, R. . J., Gamblin, S. . J., Haire, L. . F., Stevens, D. . J., Xiao, B., Ha, Y. and Skehel, J. . J. (2004) 'H1 and H7 influenza haemagglutinin structures extend a structural classification of haemagglutinin subtypes.', *Virology*. Academic Press, 325(2), pp. 287–96. doi: 10.1016/j.virol.2004.04.040.

Russell, R. J., Kerry, P. S., Stevens, D. J., Steinhauer, D. A., Martin, S. R., Gamblin, S. J. and Skehel, J. J. (2008) 'Structure of influenza hemagglutinin in complex with an inhibitor of membrane fusion', *Proceedings of the National Academy of Sciences*. National Academy of Sciences, 105(46), pp. 17736–17741. doi: 10.1073/pnas.88.24.11525.

Russell, W. C., Graham, F. L., Smiley, J. and Nairn, R. (1977) 'Characteristics of a Human Cell Line Transformed by DNA from Human Adenovirus Type 5', *Journal of General Virology*, 36(1), pp. 59–72. doi: 10.1099/0022-1317-36-1-59.

Sabahi, A., Uprichard, S. L., Wimley, W. C., Dash, S. and Garry, R. F. (2014) 'Unexpected structural features of the hepatitis C virus envelope protein 2 ectodomain.', *Journal of virology*. American Society for Microbiology (ASM), 88(18), pp. 10280–8. doi: 10.1128/JVI.00874-14.

Sakai, K., Ami, Y., Nakajima, N., Nakajima, K., Kitazawa, M., Anraku, M., Takayama, I., Sangsriratanakul, N., Komura, M., Sato, Y., Asanuma, H., Takashita, E., Komase, K., Takehara, K., Tashiro, M., Hasegawa, H., Odagiri, T. and Takeda, M. (2016) 'TMPRSS2 Independency for Haemagglutinin Cleavage In Vivo Differentiates Influenza B Virus from Influenza A Virus', *Scientific Reports*. Nature Publishing Group, 6(1), p. 29430. doi: 10.1038/srep29430.

Sakai, K., Ami, Y., Tahara, M., Kubota, T., Anraku, M., Abe, M., Nakajima, N., Sekizuka, T., Shirato, K., Suzaki, Y., Ainai, A., Nakatsu, Y., Kanou, K., Nakamura, K., Suzuki, T., Komase, K., Nobusawa, E., Maenaka, K., Kuroda, M., Hasegawa, H., Kawaoka, Y., Tashiro, M. and Takeda, M. (2014) 'The host protease TMPRSS2 plays a major role in in vivo replication of emerging H7N9 and seasonal influenza viruses.', *Journal of virology*. American Society for Microbiology, 88(10), pp. 5608–16. doi: 10.1128/JVI.03677-13.

Sakai, K., Sekizuka, T., Ami, Y., Nakajima, N., Kitazawa, M., Sato, Y., Nakajima, K., Anraku, M., Kubota, T., Komase, K., Takehara, K., Hasegawa, H., Odagiri, T., Tashiro, M., Kuroda, M. and Takeda, M. (2015) 'A mutant H3N2 influenza virus uses an alternative activation mechanism in TMPRSS2 knockout mice by loss of an oligosaccharide in the hemagglutinin stalk region.', *Journal of virology*. American Society for Microbiology, 89(9), pp. 5154–8. doi: 10.1128/JVI.00124-15.

Sawoo, O., Dublineau, A., Batéjat, C., Zhou, P., Manuguerra, J.-C. and Leclercq, I. (2014) 'Cleavage of Hemagglutinin-Bearing Lentiviral Pseudotypes and Their Use in the Study of Influenza Virus Persistence', *PLoS ONE*. Edited by R. Tripp. Public Library of Science, 9(8), p. e106192. doi: 10.1371/journal.pone.0106192.

Schinkowski, C. I.-S. (2017) *Establishing site - specific recombination mediated cassette exchange in Pichia pastoris and development of an optimized process for the production of mouse Tmprss2*.

Scholz, J. and Suppmann, S. (2016) 'A re-usable wave bioreactor for protein production in insect cells', *MethodsX*, 3, pp. 497–501. doi: 10.1016/j.mex.2016.08.001.

Scholz, J. and Suppmann, S. (2017) 'A new single-step protocol for rapid baculovirus-driven protein production in insect cells', *BMC Biotechnology*. BioMed Central, 17(1), p. 83. doi: 10.1186/s12896-017-0400-3.

Shen, X., Hacker, D. L., Baldi, L. and Wurm, F. M. (2014) 'Virus-free transient protein production in Sf9 cells'. Elsevier, 171, pp. 61–70.

Shen, X., Pitol, A. K., Bachmann, V., Hacker, D. L., Baldi, L. and Wurm, F. M. (2015) 'A simple plasmid-based transient gene expression method using High Five cells', *Journal of Biotechnology*. Elsevier, 216, pp. 67–75. doi: 10.1016/J.JBIOTEC.2015.10.007.

Shimizu, Y. K., Hijikata, M., Iwamoto, A., Alter, H. J., Purcell, R. H. and Yoshikura, H. (1994) 'Neutralizing antibodies against hepatitis C virus and the emergence of neutralization escape mutant viruses.', *Journal of virology*. American Society for Microbiology (ASM), 68(3), pp. 1494–500.

Shope, R. E. (1936) 'IMMUNIZATION EXPERIMENTS WITH SWINE INFLUENZA VIRUS.', *The Journal of experimental medicine*. The Rockefeller University Press, 64(1), pp. 47–61.

Shrestha, M. P., Scott, R. M., Joshi, D. M., Mammen, M. P., Thapa, G. B., Thapa, N., Myint, K. S. A., Fourneau, M., Kuschner, R. A., Shrestha, S. K., David, M. P., Seriwatana, J., Vaughn, D. W., Safary, A., Endy, T. P. and Innis, B. L. (2007) 'Safety and Efficacy of a Recombinant Hepatitis E Vaccine', *New England Journal of Medicine*. Massachusetts Medical Society , 356(9), pp. 895–903. doi: 10.1056/NEJMoa061847.

Simmonds, P. (2004) 'Genetic diversity and evolution of hepatitis C virus - 15 years on', *Journal of General Virology*, 85(11), pp. 3173–3188. doi: 10.1099/vir.0.80401-0.

Skehel, J. J., Stevens, D. J., Daniels, R. S., Douglas, A. R., Knossow, M., Wilson, I. A., Wiley, D. C., Walker, P. A., Liu, J., Skehel, J. J., Gamblin, S. J., Hay, A. J., Daniels, R. S. and McCauley, J. W. (1984) 'A carbohydrate side chain on hemagglutinins of Hong Kong influenza viruses inhibits recognition by a monoclonal antibody.', *Proceedings of the National Academy of Sciences of the United States of America*. National Academy of Sciences, 81(6), pp. 1779–83. doi: 10.1073/pnas.81.6.1779.

Smith, D. B., Bukh, J., Kuiken, C., Muerhoff, A. S., Rice, C. M., Stapleton, J. T. and Simmonds, P. (2014) 'Expanded classification of hepatitis C virus into 7 genotypes and 67 subtypes: updated criteria and genotype assignment web resource.', *Hepatology (Baltimore, Md.)*. Wiley-Blackwell, 59(1), pp. 318–27. doi: 10.1002/hep.26744.

Smith, D. B., Bukh, J., Kuiken, C., Muerhoff, A. S., Rice, C. M., Stapleton, J. T. and Simmonds, P. (2017) *International Committee on Taxonomy of Viruses (ICTV)*. Available at: https://talk.ictvonline.org/ictv_wikis/flaviviridae/w/sg_flavi/56/hcv-classification (Accessed: 14 November 2017).

Sommer, M. T. (2016) *Herstellung von Expressionsvektoren und Analyse der rekombinanten Expression verschiedener Varianten des Hepatitis C Oberflächenproteins E2*. Technische Universität Braunschweig.

Song, H., Qi, J., Xiao, H., Bi, Y., Zhang, W., Xu, Y., Wang, F., Shi, Y. and Gao, G. F. (2017) 'Avian-to-Human Receptor-Binding Adaptation by Influenza A Virus Hemagglutinin H4', *Cell Reports*. Cell Press, 20(5), pp. 1201–1214. doi: 10.1016/J.CELREP.2017.07.028.

South Dakota State University (2016) 'New virus gets official name, influenza D', *ScienceDaily*.

Sriram, S., Palhan, V. B. and Gopinathan, K. P. (1997) 'Heterologous promoter recognition leading to high-level expression of cloned foreign genes in Bombyx mori cell lines and larvae.', *Gene*, 190(1), pp. 181–9.

Stanley, P. (1989) 'Chinese hamster ovary cell mutants with multiple glycosylation defects for production of glycoproteins with minimal carbohydrate heterogeneity.', *Molecular and cellular biology*, 9(2), pp. 377–383. doi: 10.1128/MCB.9.2.377.Updated.

Steinhauer, D. A. (1999) 'MINIREVIEW Role of Hemagglutinin Cleavage for the Pathogenicity of Influenza Virus', 20, pp. 1–20.

Stevens, J., Blixt, O., Tumpey, T. M., Taubenberger, J. K., Paulson, J. C. and Wilson, I. A. (2006) 'Structure and receptor specificity of the hemagglutinin from an H5N1 influenza virus.', *Science (New York, N.Y.)*. American Association for the Advancement of Science, 312(5772), pp. 404–10. doi: 10.1126/science.1124513.

Stevens, J., Corper, A. L., Basler, C. F., Taubenberger, J. K., Palese, P. and Wilson, I. A. (2004) 'Structure of the uncleaved human H1 hemagglutinin from the extinct 1918 influenza virus.', *Science (New York, N.Y.)*. American Association for the Advancement of Science, 303(5665), pp. 1866–70. doi: 10.1126/science.1093373.

Stieneke-Gröber, A., Vey, M., Angliker, H., Shaw, E., Thomas, G., Roberts, C., Klenk, H. D. and Garten, W. (1992) 'Influenza virus hemagglutinin with multibasic cleavage site is activated by furin, a subtilisin-like endoprotease.', *The EMBO journal*. European Molecular Biology Organization, 11(7), pp. 2407–14.

Stolt-Bergner, P., Benda, C., Bergbrede, T., Besir, H., Celie, P. H. N., Chang, C., Drechsel, D., Fischer, A., Geerlof, A., Giabbai, B., van den Heuvel, J., Huber, G., Knecht, W., Lehner, A., Lemaitre, R., Nordén, K., Pardee, G., Racke, I., Remans, K., Sander, A., Scholz, J., Stadnik, M., Storici, P., Weinbruch, D., Zaror, I., Lua, L. H. L. and Suppmann, S. (2018) 'Baculovirus-driven protein expression in insect cells: A benchmarking study', *Journal of Structural Biology*, (March). doi: 10.1016/j.jsb.2018.03.004.

Summers, M. D. (2006) 'Milestones leading to the genetic engineering of baculoviruses as expression vector systems and viral pesticides.', *Advances in virus research*, 68, pp. 3–73. doi: 10.1016/S0065-3527(06)68001-9.

Summers, M. D., Station, T. A. E. and Smith, G. E. (1987) *A Manual of Methods for Baculovirus Vectors and Insect Cell Culture Procedures*.

Sun, X., Shi, Y., Lu, X., He, J., Gao, F., Yan, J., Qi, J. and Gao, G. F. (2013) 'Bat-Derived Influenza Hemagglutinin H17 Does Not Bind Canonical Avian or Human Receptors and Most Likely Uses a Unique Entry Mechanism', *Cell Reports*. Cell Press, 3(3), pp. 769–778. doi: 10.1016/J.CELREP.2013.01.025.

Suzuki, R., Suzuki, T., Ishii, K., Matsuura, Y. and Miyamura, T. (1999) 'Processing and functions of Hepatitis C virus proteins.', *Intervirology*, 42(2–3), pp. 145–152. doi: 24973.

Tao, Y., Strelkov, S. V, Mesyanzhinov, V. V and Rossmann, M. G. (1997) 'Structure of bacteriophage T4 fibritin: a segmented coiled coil and the role of the C-terminal domain.', *Structure (London, England : 1993)*, 5(6), pp. 789–98.

Tarnow, C., Engels, G., Arendt, A., Schwalm, F., Sediri, H., Preuss, A., Nelson, P. S., Garten, W., Klenk, H.-D., Gabriel, G. and Böttcher-Friebertshäuser, E. (2014) 'TMPRSS2 is a host factor that is essential for pneumotropism and pathogenicity of H7N9 influenza A virus in mice.', *Journal of virology*. American Society for Microbiology, 88(9), pp. 4744–51. doi: 10.1128/JVI.03799-13.

Tate, M. D., Job, E. R., Deng, Y.-M., Gunalan, V., Maurer-Stroh, S. and Reading, P. C. (2014) 'Playing hide and seek: how glycosylation of the influenza virus hemagglutinin can modulate the immune response to infection.', *Viruses*. Multidisciplinary Digital Publishing Institute (MDPI), 6(3), pp. 1294–316. doi: 10.3390/v6031294.

Taubenberger, J. K. and Kash, J. C. (2010) 'Influenza virus evolution, host adaptation, and pandemic formation.', *Cell host & microbe*. NIH Public Access, 7(6), pp. 440–51. doi: 10.1016/j.chom.2010.05.009.

Taubenberger, J. K. and Morens, D. M. (2008) 'The pathology of influenza virus infections.', *Annual review of pathology*. NIH Public Access, 3, pp. 499–522. doi: 10.1146/annurev.pathmechdis.3.121806.154316.

Taubenberger, J. K. and Morens, D. M. (2009) 'Pandemic influenza--including a risk assessment of H5N1.', *Revue scientifique et technique (International Office of Epizootics)*, 28(1), pp. 187–202.

Tello, D., Rodríguez-Rodríguez, M., Yélamos, B., Gómez-Gutiérrez, J., Ortega, S., Pacheco, B., Peterson, D. L. and Gavilanes, F. (2010) 'Expression and structural properties of a chimeric protein based on the ectodomains of E1 and E2 hepatitis C virus envelope glycoproteins', *Protein Expression and Purification*, 71(2), pp. 123–131. doi: 10.1016/j.pep.2010.02.012.

Tello, D., Rodríguez-Rodríguez, M., Yélamos, B., Gómez-Gutiérrez, J., Peterson, D. L. and Gavilanes, F. (2015) 'High-yield production of a chimeric glycoprotein based on permuted E1 and E2 HCV envelope ectodomains', *Journal of Virological Methods*, 213, pp. 38–44. doi: 10.1016/j.jviromet.2014.11.020.

Terwilliger, T. C., Grosse-Kunstleve, R. W., Afonine, P. V, Moriarty, N. W., Zwart, P. H., Hung, L. W., Read, R. J. and Adams, P. D. (2008) 'Iterative model building, structure refinement and density modification with the PHENIX AutoBuild wizard.', *Acta crystallographica. Section D, Biological crystallography*. International Union of Crystallography, 64(Pt 1), pp. 61–9. doi: 10.1107/S090744490705024X.

Theilmann, D. A. and Stewart, S. (1991) 'Identification and characterization of the IE-1 gene of Orgyia pseudotsugata multicapsid nuclear polyhedrosis virus.', *Virology*, 180(2), pp. 492–508.

Theilmann, D. A. and Stewart, S. (1992) 'Molecular analysis of the trans-activating IE-2 gene of Orgyia pseudotsugata multicapsid nuclear polyhedrosis virus', *Virology*, 187(1), pp. 84–96.

Thomssen, R., Bonk, S., Propfe, C., Heermann, K. H., Köchel, H. G. and Uy, A. (1992) 'Association of hepatitis C virus in human sera with beta-lipoprotein.', *Medical microbiology and immunology*, 181(5), pp. 293–300.

Thomssen, R., Bonk, S. and Thiele, A. (1993) 'Density heterogeneities of hepatitis C virus in human sera due to the binding of beta-lipoproteins and immunoglobulins.', *Medical microbiology and immunology*, 182(6), pp. 329–34.

Tomiya, N., Narang, S., Lee, Y. C. and Betenbaugh, M. J. (2004) 'Comparing N-glycan processing in mammalian cell lines to native and engineered lepidopteran insect cell lines.', *Glycoconjugate journal*, 21(6), pp. 343–60. doi: 10.1023/B:GLYC.0000046275.28315.87.

Tong, S., Zhu, X., Li, Y., Shi, M., Zhang, J., Bourgeois, M., Yang, H., Chen, X., Recuenco, S., Gomez, J., Chen, L.-M., Johnson, A., Tao, Y., Dreyfus, C., Yu, W., McBride, R., Carney, P. J., Gilbert, A. T., Chang, J., Guo, Z., Davis, C. T., Paulson, J. C., Stevens, J., Rupprecht, C. E., Holmes, E. C., Wilson, I. A. and Donis, R. O. (2013) 'New World Bats Harbor Diverse Influenza A Viruses', *PLoS Pathogens*. Edited by K. Subbarao. Public Library of Science, 9(10), p. e1003657. doi: 10.1371/journal.ppat.1003657.

Torresi, J. (2017) 'The Rationale for a Preventative HCV Virus-Like Particle (VLP) Vaccine.', *Frontiers in microbiology*. Frontiers Media SA, 8, p. 2163. doi: 10.3389/fmicb.2017.02163.

Treanor, J. J., Sahly, H. El, King, J., Graham, I., Izikson, R., Kohberger, R., Patriarca, P. and Cox, M. (2011) 'Protective efficacy of a trivalent recombinant hemagglutinin protein vaccine (FluBlok®) against influenza in healthy adults: A randomized, placebo-controlled trial', *Vaccine*, 29(44), pp. 7733–7739. doi: 10.1016/j.vaccine.2011.07.128.

Trowitzsch, S., Bieniossek, C., Nie, Y., Garzoni, F. and Berger, I. (2010) 'New baculovirus expression tools for recombinant protein complex production.', *Journal of structural biology*, 172(1), pp. 45–54. doi: 10.1016/j.jsb.2010.02.010.

Vasiliauskaite, I., Owsianka, A., England, P., Khan, A. G., Cole, S., Bankwitz, D., Foung, S. K. H., Pietschmann, T., Marcotrigiano, J., Rey, F. A., Patel, A. H. and Krey, T. (2017) 'Conformational Flexibility in the Immunoglobulin-Like Domain of the Hepatitis C Virus Glycoprotein E2.', *mBio*. American Society for Microbiology, 8(3), pp. e00382-17. doi: 10.1128/mBio.00382-17.

Vaughn, J. L., Goodwin, R. H., Tompkins, G. J. and McCawley, P. (1977) 'The establishment of two cell lines from the insectspodoptera frugiperda (lepidoptera; noctuidae)', *In Vitro*, 13(4), pp. 213–217. doi: 10.1007/BF02615077.

Vicente, T., Roldão, A., Peixoto, C., Carrondo, M. J. T. and Alves, P. M. (2011) 'Large-scale production and purification of VLP-based vaccines', *Journal of Invertebrate Pathology*, 107, pp. S42–S48. doi: 10.1016/j.jip.2011.05.004.

Vieyres, G., Dubuisson, J. and Pietschmann, T. (2014) 'Incorporation of hepatitis C virus E1 and E2 glycoproteins: The keystones on a peculiar virion', *Viruses*. Multidisciplinary Digital Publishing Institute, 6(3), pp. 1149–1187. doi: 10.3390/v6031149.

Vigerust, D. J. and Shepherd, V. L. (2007) 'Virus glycosylation: role in virulence and immune interactions', *Trends in Microbiology*, 15(5), pp. 211–218. doi: 10.1016/j.tim.2007.03.003.

Voisset, C., Op de Beeck, A., Horellou, P., Dreux, M., Gustot, T., Duverlie, G., Cosset, F.-L., Vu-Dac, N. and Dubuisson, J. (2006) 'High-density lipoproteins reduce the neutralizing effect of hepatitis C virus (HCV)-infected patient antibodies by promoting HCV entry', *Journal of General Virology*, 87(9), pp. 2577–2581. doi: 10.1099/vir.0.81932-0.

Voronina, E. V, Seregin, Y. A., Litvinova, N. A., Shvets, V. I. and Shukurov, R. R. (2016) 'Design of a stable cell line producing a recombinant monoclonal anti-TNFα antibody based on a CHO cell line.', *SpringerPlus*. Springer, 5(1), p. 1584. doi: 10.1186/s40064-016-3213-2.

de Vries, R. P., de Vries, E., Bosch, B. J., de Groot, R. J., Rottier, P. J. M. and de Haan, C. A. M. (2010) 'The influenza A virus hemagglutinin glycosylation state affects receptor-binding specificity.', *Virology*, 403(1), pp. 17–25. doi: 10.1016/j.virol.2010.03.047.

Walski, T., De Schutter, K., Van Damme, E. J. M. and Smagghe, G. (2017) 'Diversity and functions of protein glycosylation in insects', *Insect Biochemistry and Molecular Biology*. Elsevier Ltd, 83(February), pp. 21–34. doi: 10.1016/j.ibmb.2017.02.005.

Wang, K., Holtz, K. M., Anderson, K., Chubet, R., Mahmoud, W. and Cox, M. M. J. J. (2006) 'Expression and purification of an influenza hemagglutinin--one step closer to a recombinant protein-based influenza vaccine.', *Vaccine*. Elsevier, 24(12), pp. 2176–85. doi: 10.1016/j.vaccine.2005.11.005.

Wang, Y., Wang, J., Wu, S. and Zhu, H. (2017) 'The unexpected structures of hepatitis C virus envelope proteins', *Experimental and Therapeutic Medicine*, 14(3), pp. 1859–1865. doi: 10.3892/etm.2017.4745.

Wasilko, D. J. and Lee, S. E. (2006) 'TIPS: Titerless Infected-Cells Preservation and Scale-Up', pp. 29–32.

Wasilko, D. J., Lee, S. E., Stutzman-Engwall, K. J., Reitz, B. A., Emmons, T. L., Mathis, K. J., Bienkowski, M. J., Tomasselli, A. G. and Fischer, H. D. (2009) 'The titerless infected-cells preservation and scale-up (TIPS) method for large-scale production of NO-sensitive human soluble guanylate cyclase (sGC) from insect cells infected with recombinant baculovirus.', *Protein expression and purification*, 65(2), pp. 122–32. doi: 10.1016/j.pep.2009.01.002.

Webster, R. G. and Rott, R. (1987) 'Influenza virus A pathogenicity: the pivotal role of haemagglutinin', *Cell*, 50, pp. 665 – 666.

Wei, X., Decker, J. M., Wang, S., Hui, H., Kappes, J. C., Wu, X., Salazar-Gonzalez, J. F., Salazar, M. G., Kilby, J. M., Saag, M. S., Komarova, N. L., Nowak, M. A., Hahn, B. H., Kwong, P. D. and Shaw, G. M. (2003) 'Antibody neutralization and escape by HIV-1', *Nature*. Nature Publishing Group, 422(6929), pp. 307–312. doi: 10.1038/nature01470.

Weiner, A. J., Christopherson, C., Hall, J. E., Bonino, F., Saracco, G., Brunetto, M. R., Crawford, K., Marion, C. D., Crawford, K. A., Venkatakrishna, S., Miyamura, T., McHutchinson, J., Cuypers, T. and Houghton, M. (1991) 'Sequence variation in hepatitis C viral isolates', *Journal of Hepatology*. Elsevier, 13, pp. S6–S14. doi: 10.1016/0168-8278(91)90015-4.

Weis, W. I., Brünger, A. T., Skehel, J. J. and Wiley, D. C. (1990) 'Refinement of the influenza virus hemagglutinin by simulated annealing', *Journal of Molecular Biology*. Academic Press, 212(4), pp. 737–761. doi: 10.1016/0022-2836(90)90234-D.

Whidby, J., Mateu, G., Scarborough, H., Demeler, B., Grakoui, A. and Marcotrigiano, J. (2009) 'Blocking hepatitis C virus infection with recombinant form of envelope protein 2 ectodomain.', *Journal of virology*. American Society for Microbiology (ASM), 83(21), pp. 11078–89. doi: 10.1128/JVI.00800-09.

Whidby, J., Mateu, G., Scarborough, H., Demeler, B., Grakoui, A. and Marcotrigiano, J. (2009) 'Blocking Hepatitis C Virus Infection with Recombinant Form of Envelope Protein 2 Ectodomain', *Journal of Virology*, 83(21), pp. 11078–11089. doi: 10.1128/JVI.00800-09.

Wickham, T. J. and Nemerow, G. R. (1993) 'Optimization of growth methods and recombinant protein production in BTI-Tn-5B1-4 insect cells using the baculovirus expression system.', *Biotechnology progress*, 9(1), pp. 25–30. doi: 10.1021/bp00019a004.

Wilde, M., Klausberger, M., Palmberger, D., Ernst, W. and Grabherr, R. (2014) 'Tnao38, high five and Sf9—evaluation of host–virus interactions in three different insect cell lines: baculovirus production and recombinant protein expression', *Biotechnology Letters*. Springer Netherlands, 36(4), pp. 743–749. doi: 10.1007/s10529-013-1429-6.

Wiley, D. C. and Skehel, J. J. (1987) 'THE STRUCTURE AND FUNCTION OF TIIE HEMAGGLUTININ MEMBRANE GLYCOPROTEIN OF INFL1JENZA VIRUS', *Biochem*, 56, pp. 365–94. doi: 10.1146/annurev.bi.56.070187.002053.

Williams, G. V, Rohel, D. Z., Kuzio, J. and Faulkner, P. (1989) 'A cytopathological investigation of Autographa californica nuclear polyhedrosis virus p10 gene function using insertion/deletion mutants.', *The Journal of general virology*, 70 (Pt 1), pp. 187–202.

Worch, R. (2014) 'Structural biology of the influenza virus fusion peptide.', *Acta biochimica Polonica*, 61(3), pp. 421–6.

World Health Organization (2016) *WHO | Influenza (Seasonal)*. World Health Organization.

World Health Organization (2017) 'GLOBAL HEPATITIS REPORT, 2017', *Who*. World Health Organization.

World Health Organization (2018) 'WHO | Influenza (Seasonal) Fact sheet', *WHO*. World Health Organization.

Wright, P., Neumann, G. and Kawaoka, Y. (2007) *Orthomyxoviruses*. 5th ed. Edited by D. Knipe, P. Howley, D. Griffin, R. Lamb, M. Martin, B. Roizman, and S. Straus. Philadelphia, PA: Williams & Wilkins.

Wu, Y. Y., Wu, Y. Y., Tefsen, B., Shi, Y. and Gao, G. F. (2014) 'Bat-derived influenza-like viruses H17N10 and H18N11', *Trends in Microbiology*. Elsevier Current Trends, 22(4), pp. 183–191. doi: 10.1016/J.TIM.2014.01.010.

Wulhfard, S., Baldi, L., Hacker, D. L. and Wurm, F. (2010) 'Valproic acid enhances recombinant mRNA and protein levels in transiently transfected Chinese hamster ovary cells', *Journal of Biotechnology*, 148(2–3), pp. 128–132. doi: 10.1016/j.jbiotec.2010.05.003.

Xu, Z., Choi, J., Yen, T. S., Lu, W., Strohecker, A., Govindarajan, S., Chien, D., Selby, M. J. and Ou, J. (2001) 'Synthesis of a novel hepatitis C virus protein by ribosomal frameshift', *The EMBO Journal*, 20(14), pp. 3840–3848. doi: 10.1093/emboj/20.14.3840.

Yang, H., Carney, P. J., Chang, J. C., Guo, Z., Villanueva, J. M. and Stevens, J. (2015) 'Structure and receptor binding preferences of recombinant human A(H3N2) virus hemagglutinins.', *Virology*. Academic Press, 477, pp. 18–31. doi: 10.1016/j.virol.2014.12.024.

Yang, H., Carney, P. J., Chang, J. C., Villanueva, J. M. and Stevens, J. (2015) 'Structure and receptor binding preferences of recombinant hemagglutinins from avian and human H6 and H10 influenza A virus subtypes.', *Journal of virology*. American Society for Microbiology, 89(8), pp. 4612–23. doi: 10.1128/JVI.03456-14.

Yang, H., Carney, P. and Stevens, J. (2010) 'Structure and Receptor binding properties of a pandemic H1N1 virus hemagglutinin.', *PLoS currents*, 2, p. RRN1152. doi: 10.1371/currents.RRN1152.

Yang, L. P. H. (2013) 'Recombinant Trivalent Influenza Vaccine (Flublok®): A Review of Its Use in the Prevention of Seasonal Influenza in Adults', *Drugs*, 73(12), pp. 1357–1366. doi: 10.1007/s40265-013-0103-6.

Yeates, T. O. (1997) 'Detecting and overcoming crystal twinning', *Methods in Enzymology*. Academic Press, 276, pp. 344–358. doi: 10.1016/S0076-6879(97)76068-3.

Zambon, M. C. (1999) 'Epidemiology and pathogenesis of influenza.', *The Journal of antimicrobial chemotherapy*, 44 Suppl B, pp. 3–9.

Zhang, J., Zhang, X.-F., Huang, S.-J., Wu, T., Hu, Y.-M., Wang, Z.-Z., Wang, H., Jiang, H.-M., Wang, Y.-J., Yan, Q., Guo, M., Liu, X.-H., Li, J.-X., Yang, C.-L., Tang, Q., Jiang, R.-J., Pan, H.-R., Li, Y.-M., Shih, J. W.-K., Ng, M.-H., Zhu, F.-C. and Xia, N.-S. (2015) 'Long-Term Efficacy of a Hepatitis E Vaccine', *New England Journal of Medicine*. Massachusetts Medical Society, 372(10), pp. 914–922. doi: 10.1056/NEJMoa1406011.

Zhang, M., Gaschen, B., Blay, W., Foley, B., Haigwood, N., Kuiken, C. and Korber, B. (2004) 'Tracking global patterns of N-linked glycosylation site variation in highly variable viral glycoproteins: HIV, SIV, and HCV envelopes and influenza hemagglutinin', *Glycobiology*, 14(12), pp. 1229–1246. doi: 10.1093/glycob/cwh106.

Zhu, X., Yu, W., McBride, R., Li, Y., Chen, L.-M., Donis, R. O., Tong, S., Paulson, J. C. and Wilson, I. A. (2013) 'Hemagglutinin homologue from H17N10 bat influenza virus exhibits divergent receptor-binding and pH-dependent fusion activities.', *Proceedings of the National Academy of Sciences of the United States of America*. National Academy of Sciences, 110(4), pp. 1458–63. doi: 10.1073/pnas.1218509110.

Zibert, A., Schreier, E. and Roggendorf, M. (1995) 'Antibodies in Human Sera Specific to Hypervariable Region 1 of Hepatitis C Virus Can Block Viral Attachment', *Virology*, 208(2), pp. 653–661. doi: 10.1006/viro.1995.1196.

Zulauf, M. and D'Arcy, A. (1992) 'Light scattering of proteins as a criterion for crystallization', *Journal of Crystal Growth*. North-Holland, 122(1–4), pp. 102–106. doi: 10.1016/0022-0248(92)90232-8.

8 Appendix

Appendix I

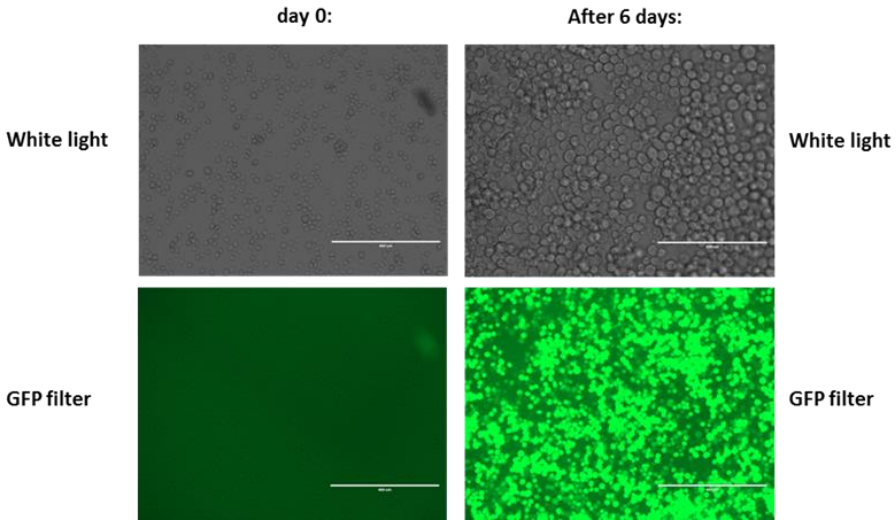

Figure 8.1: Fluorescence microscopy of Sf21 cells transfected with recombinant bacmid DNA derived from pFlpBtM-II-H1
Pictures were taken prior transfection (day 0) and 6 days post transfetion with evos microscope under white light and with GFP filter (470 nm excitation, 525 nm emission). Cells transfected with EMBacY reveal fluorescence in the green filter due to the encoded YFP.

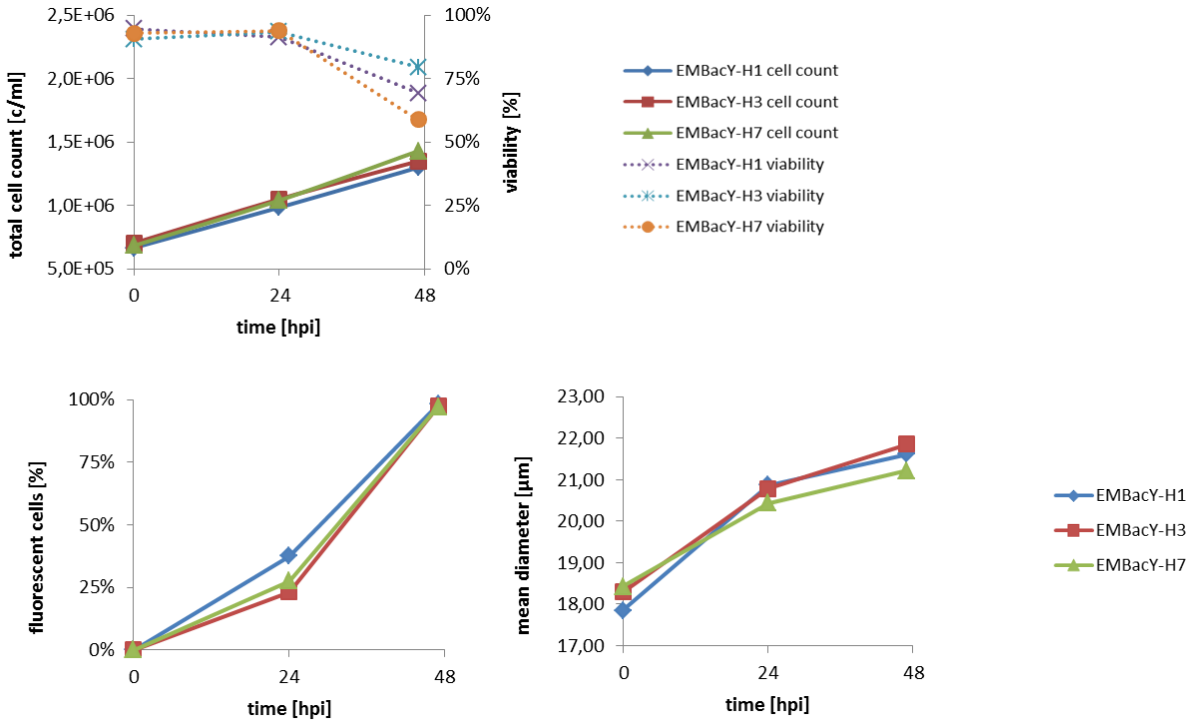

Figure 8.2: Growth kinetics, cell diameter and fluorescence of Sf21 cells infected with recombinant baculovirus
The graphical data depicts the daily assessed growth and infection parameters. The cells were counted manually with a Neubauer hemocytometer. The vitality was assessed by trypan blue staining. The YFP expression of EmBacY was monitored by flow cytometry in the GFP channel (488 nm excitation). The mean cell diameter was analyzed with CASY counter. Significant increase in cell diameter of approximately 20 % and an amount of fluorescent cells (YFP fluorescence) of almost 100 % 48 hpi indicate a successful infection.

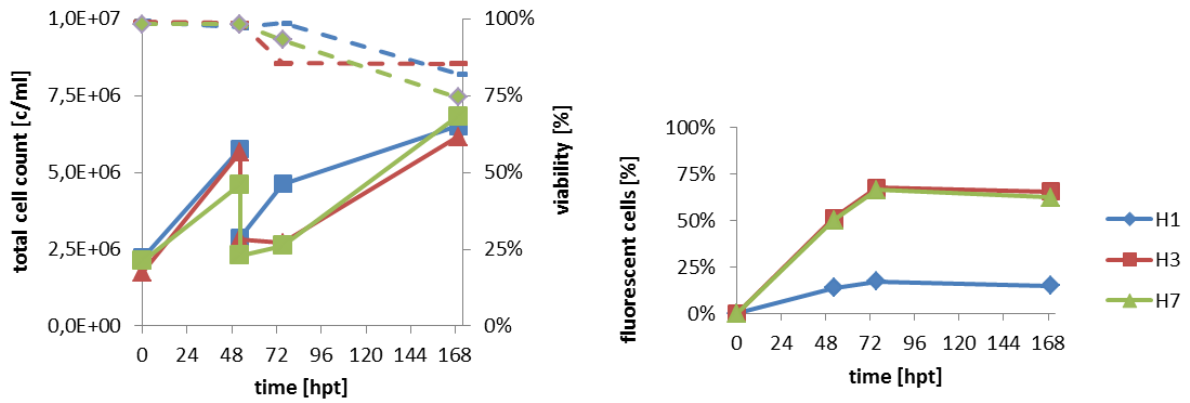

Figure 8.3: Growth kinetics and transfection efficiency

The graphical data depicts the daily assessed growth and transfection efficiency upon transient transfection in HEK293-6E cells. The cells were counted manually with a Neubauer hemocytometer. The vitality was assessed by trypan blue staining. The GFP expression of pTTo/GFP was monitored by flow cytometry in the GFP channel (488 nm excitation).

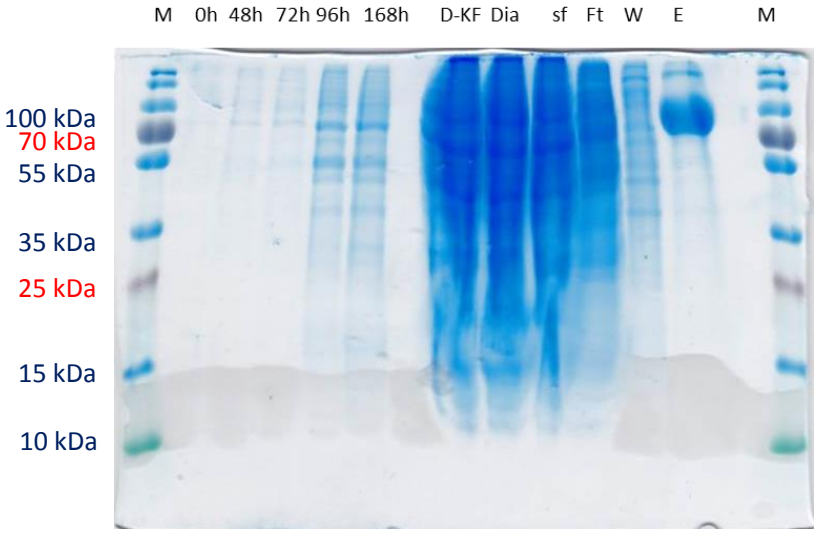

Figure 8.4: SDS-PAGE of H1 HEK-purification

The H1 protein was expressed in HEK392-6E cells after transient transfection. SDS-PAGE shows samples during cultivation as well as the elution fractions of the purification with Profinia and was stained with InstantBlue. M = P PageRuler™ Plus Protein Ladder, 0h/48h/72h/96h/168h = samples of the supernatant during cultivation at indicated time points, D-KF: Flowtrough Krosflow, Dia: sample after dialysis, sf: sample after sterile filtration, Ft = flow through, W = wash, E = eluate.

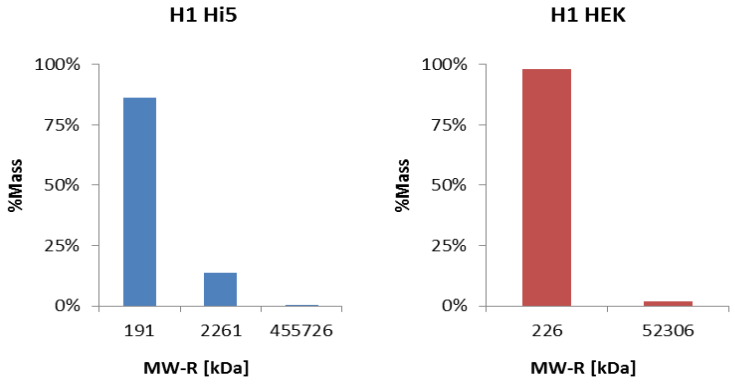

Figure 8.5: Dynamic light scattering analysis of Hi5 and HEK 293-6E derived H1

Dynamic light scattering (DLS) was performed with non-cleaved H1 expressed in Hi5 and HEK cells in order to confirm trimeric expression and to further investigate each size.

Appendix II

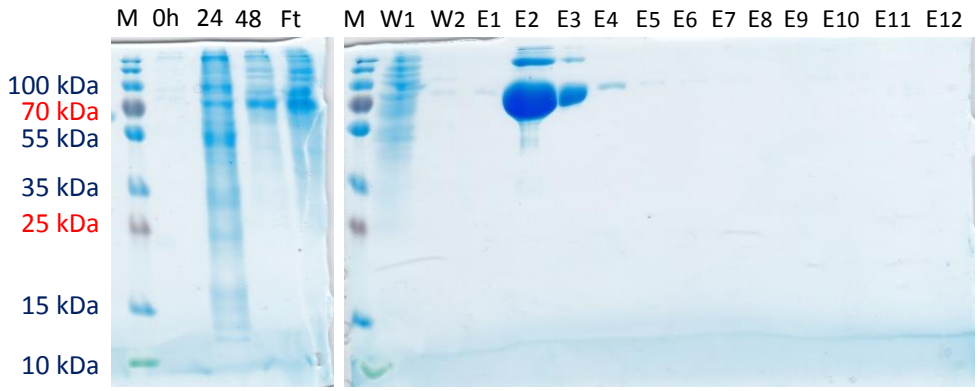

Figure 8.6: SDS-PAGE of the expression and purification of H1 with HisTALON

The H1 protein was expressed in Hi5 insect cells via BEVS using an EMBacY-pFlpBtM-II-H1 virus. SDS-PAGE shows samples during cultivation as well as the elution fractions of the purification with His TALON and was stained with InstantBlue. M = P PageRuler™ Plus Protein Ladder, 0h/24/48 = samples of the supernatant during cultivation at indicated time points (0h/24h/48h after infection), Ft = flow through, W1 = wash fraction 1, W2 = wash fraction 2, E1 – E12 = elution fractions 1 – 12.

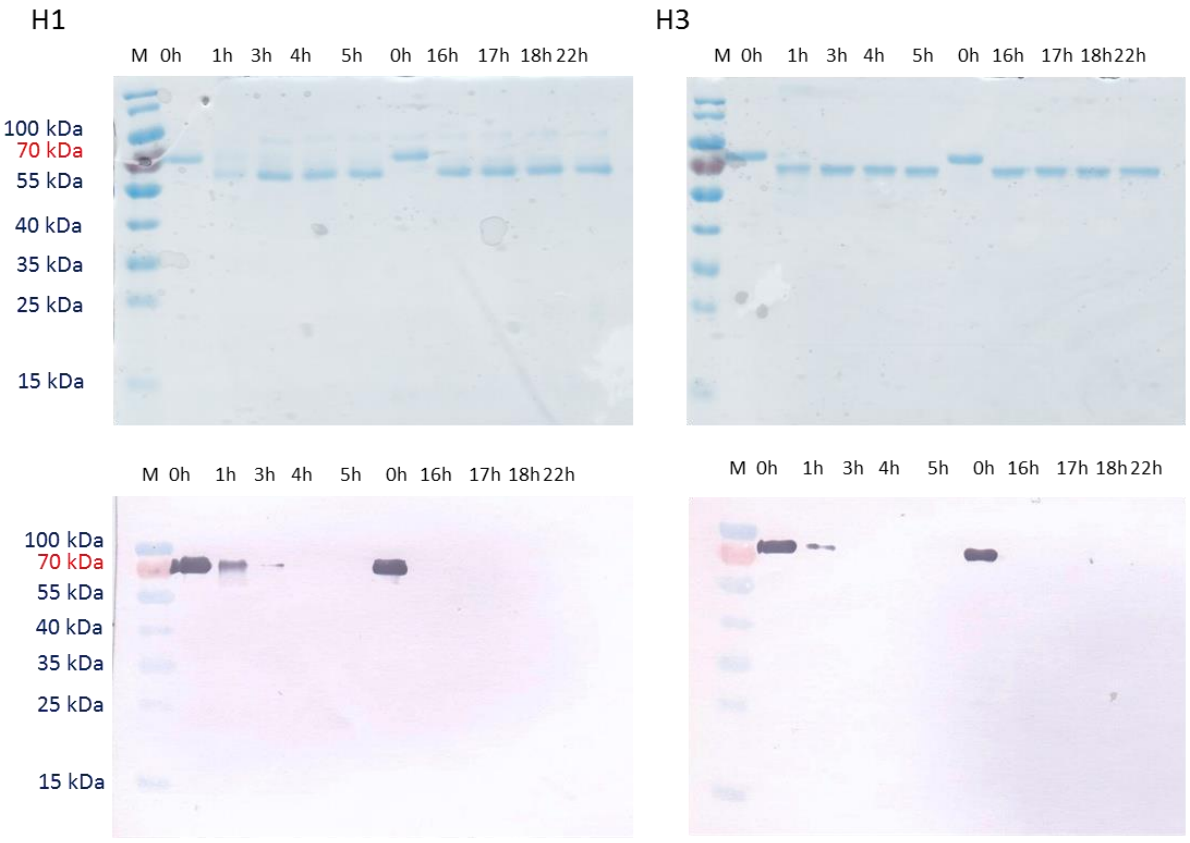

Figure 8.7: Thrombin cleavage analysis with H1 and H3

H1 and H3 protein samples were incubated with 2.5 U/mg thrombin and incubated at RT. At different time points cleavage was stopped by addition of loading buffer and incubation for 5 min. at 95 °C. Successful cleavage was observed through a reduction in size of about 10 kDa. For further verifying complete cleavage western blot analysis was performed in order to detect even small amounts of uncleaved HA. Western blot was performed using a primary mouse α-His mAb and a secondary goat AP-conjugated α-mouse pAb. Colorimetric AP staining of the western blot was done with NBT and BCIP. The SDS gel was stained with InstantBlue. M: PageRuler Prestained, 0h – 22h indicate the time point of each sample.

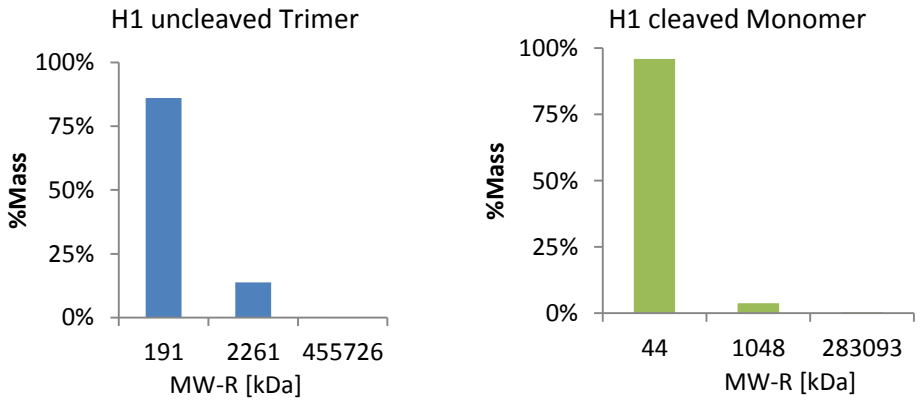

Figure 8.8: Dynamic light scattering analysis of uncleaved trimeric and cleaved monomeric H1
Dynamic light scattering (DLS) experiments were performed to determine the molecular weight of uncleaved H1 (left hand site) and H1 that was thought to have dissociated into monomeric conformation (right hand site).

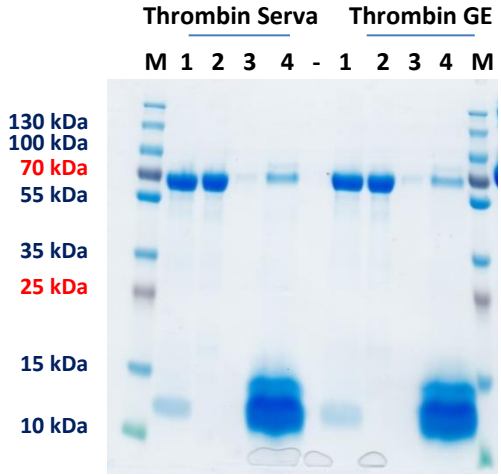

Figure 8.9: Small scale H3-purification with mgnetic strep beads
For removing tagged contaminants small scale purification of H3 was performed with magnetic beads (MagStrep "type3" XT beads, iba) according to the manufacturers' protocol. H3 cleaved with Thrombin from SERVA or GE Healthcare (indicated above the gel) was incubated with 5 µl beads/ mg protein and eluted after 3 washing steps under denaturing conditions by addition of SDS gel loading buffer and boiling. M = P PageRuler™ Plus Protein Ladder, 1 = sample after thrombin cleavage, 2 = supernatant containing purified protein, 3 = wash fraction, 4 = elution fraction.

Appendix III

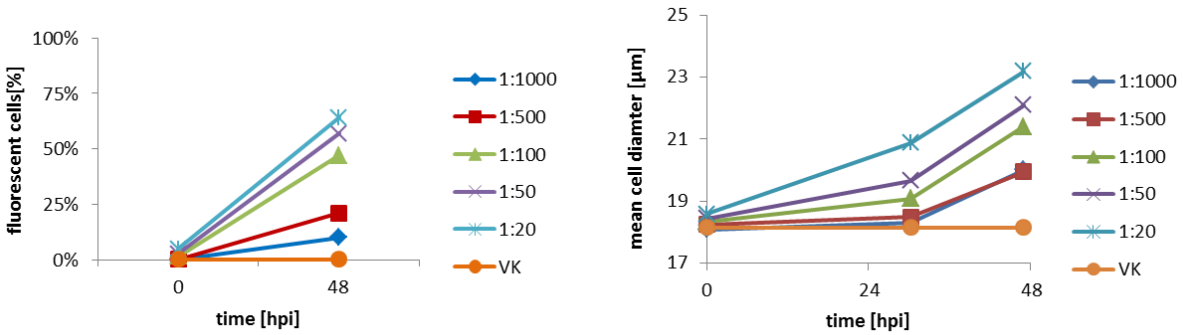

Figure 8.10: Infection kinetics of BIIC dilution test

The graphical data depicts the daily assessed infection parameters after infection with different BIIC dilutions (1:1000 – 1:20). The YFP expression of EmBacY was monitored by flow cytometry in the GFP channel (488 nm excitation). The mean cell diameter was analyzed with CASY counter. Significant increase in cell diameter and fluorescent cells (YFP fluorescence) indicate successful infection. A culture without infection was used as control (VK).

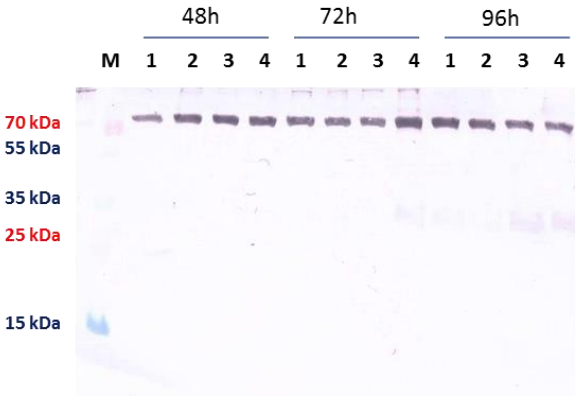

Figure 8.11: Western blot analysis of H1 expression in Hi5 and Hi5 + Sf21 cells upon BIIC infection

Different setups for the recombinant H1 expression using BIICs were tested for their potential in large scale. H1 was expressed via BEVS using an EMBacY-pFlpBtM-II-H1 virus stored in BIICs. Either Hi5 cells (1 + 3) or a combination of 90 % Hi5 and 10 % Sf21 cells (2 + 4) was used. Besides different BIIC stocks were applied (BIIC 719: 1 + 2, BIIC 716: 3 + 4) in order to test their infectivity. The Western blot was performed with primary anti-His mAb together with a secondary goat-anti-mouse AP-conjugated pAb. Colorimetric AP staining was done with NBT and BCIP. The samples of crude supernatant of the different setups are presented at different time points after infection as indicated above. M = P PageRuler™ Plus Protein Ladder, 1: Hi5 + BIIC 719, 2: Hi5 + Sf21 + BIIC 719, 3: Hi5 + BIIC 716, 4: Hi5 + Sf21 + BIIC 716.

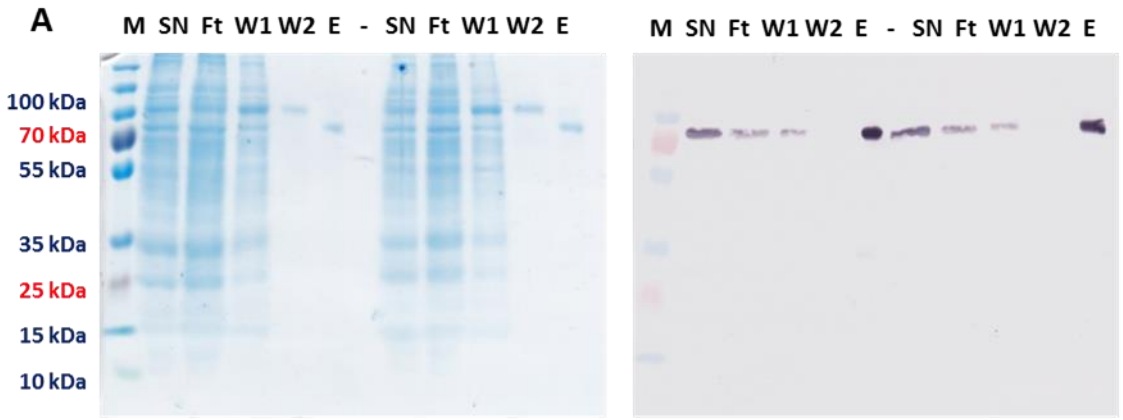

Figure 8.12: SDS-PAGE and Western Blot analysis of H1 expression and purification with VA in Hi5 and Hi5 and Sf21 cells
Suspension cultures of Hi5 cells (left hand site) and of Hi5 and Sf21 cells (right hand site) were infected with external virus stock (VA) and were purified with Profinia IMAC system after harvesting at 96 hpi. M = P PageRuler™ Plus Protein Ladder, SN = cell culture supernatant, Ft = flow through, W1 = wash fraction 1, W2 = wash fraction 2, E = eluate.

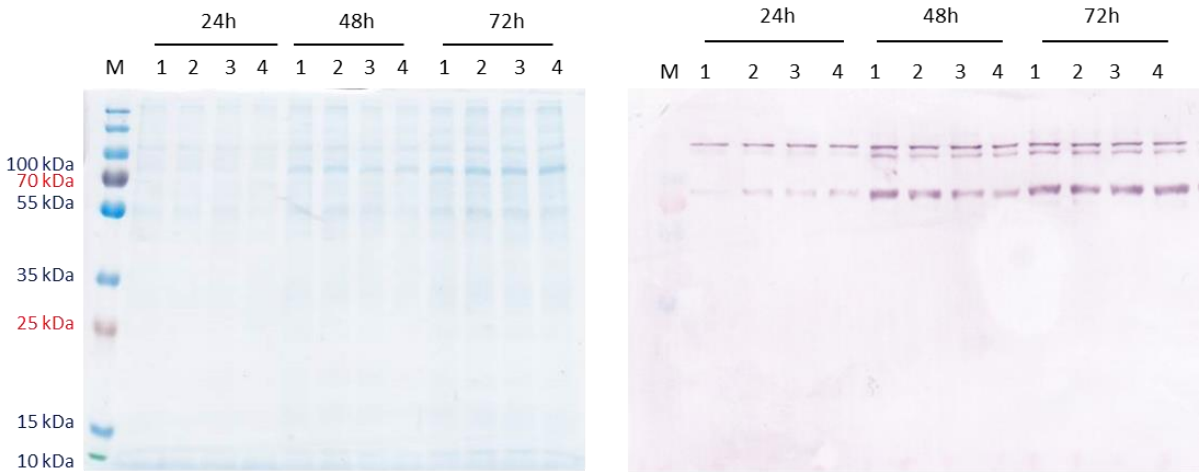

Figure 8.13: SDS-PAGE and Western Blot analysis of H1 expression via TGE
Recombinant H1 Expression via TGE was detected in crude culture supernatants by SDS-PAGE and western blot analyses. Samples were taken at 24 hpt, 48 hpt and 72 hpt (as indicated) and anaylzed for recombinant expression using a primary mouse α-His mAb and a secondary goat AP-conjugated α-mouse pAb. Colorimetric AP staining of the western blot was done with NBT and BCIP. The SDS gel was stained with InstantBlue. M: PageRuler Prestained, all samples were taken at 96 hpi. 1-4 correspond to numbering of culture flasks.

Appendix IV

Table 8-1: Buffer conditions of first H1 crystallization hits

H1 Crystal	Buffer compositions
Fig. 3.17 A	20% (v/v) 2-Methyl-2,4-pentanediol + 0.1 M TRIS pH 8.5
Fig. 3.17 B	0.2 M Trimethylamine N-oxide + 0.1 M TRIS pH 8.5
Fig. 3.17 C	20% (w/v) Polyethylene glycol (PEG) 3350 + 0.15 M di-Sodium DL-malate
Fig. 3.17 D	25% (v/v) PEG monomethyl ether (MME) 550 + 0.1 M HEPES pH 7.5

Table 8-2: Buffer conditions of first H3 crystallization hits

H3 Crystal	Buffer compositions
Fig. 3.18 A	30% (w/v) PEG MME 2000 + 0.1 M Potassium thiocyanate
Fig. 3.18 B	30% (w/v) PEG MME 2000 + 0.1 M Potassium bromide
Fig. 3.18 C	20% (w/v) PEG MME 2000 + 0.2 M Trimethylamine N-oxide
Fig. 3.18 D	20% (w/v) PEG 3350 + 0.24 M di-Sodium malonate

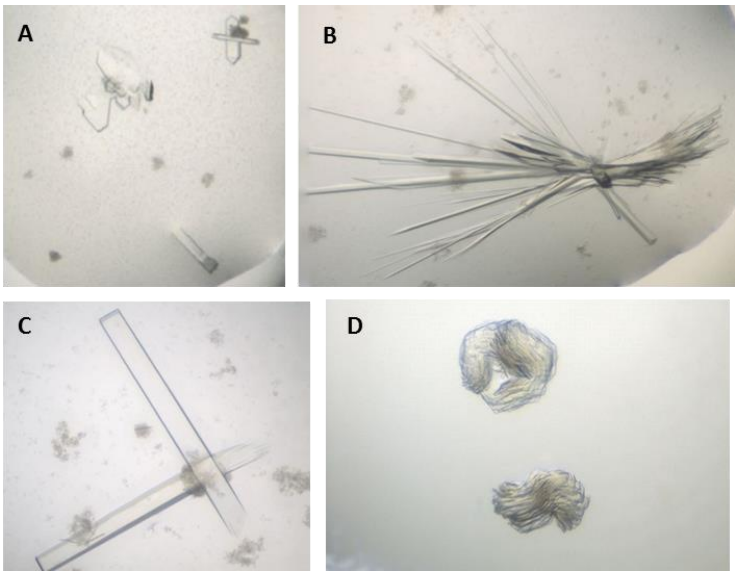

Figure 8.14: H1 crystals in optimization screen RI and commercial JCSG+ screen
First hits of H1 crystals obtained from TGE in Hi5 cells. The harvested cell culture supernatant was directly subjected to HisTrap excel purification, followed by thrombin cleavage and SEC with a S200 Increase 10/300 GL column. The isolated trimer was concentrated to 10 mg/mL before crystallization was carried out at 19 °C with 1:1 protein to reservoir volume by using commercial available JCSG+ and self-prepared RI screen. First crystals in RI were observed as late as 33 days after crystallization setup due to a defect of the imager system. The buffer conditions in which the depicted crystals were grown are listed in Table 8-3.

Table 8-3: Buffer conditions of H1 crystals grown in first optimization trail

H1 Crystal	Buffer compositions
Fig. 8.14 A	0.2 M di-Sodium malonate + 27.8% (w/v)PEG 3350 + 0.133M Magnesium sulfate + 0.1 M BIS-TRIS pH 7.022
Fig. 8.14 B	0.1 M di-Sodium malonate + 23.3% (w/v) PEG 3350 + 0.1 M HEPES pH 7.889
Fig. 8.14 C	0.15 M di-Sodium malonate + 25.6% (w/v) PEG 3350 + 0.1 M TRIS-BASE pH 7.667
Fig. 8.14 D	0.2 M Lithium sulfate + 40% (w/v) PEG 400 + 0.1 M TRIS pH 8.5

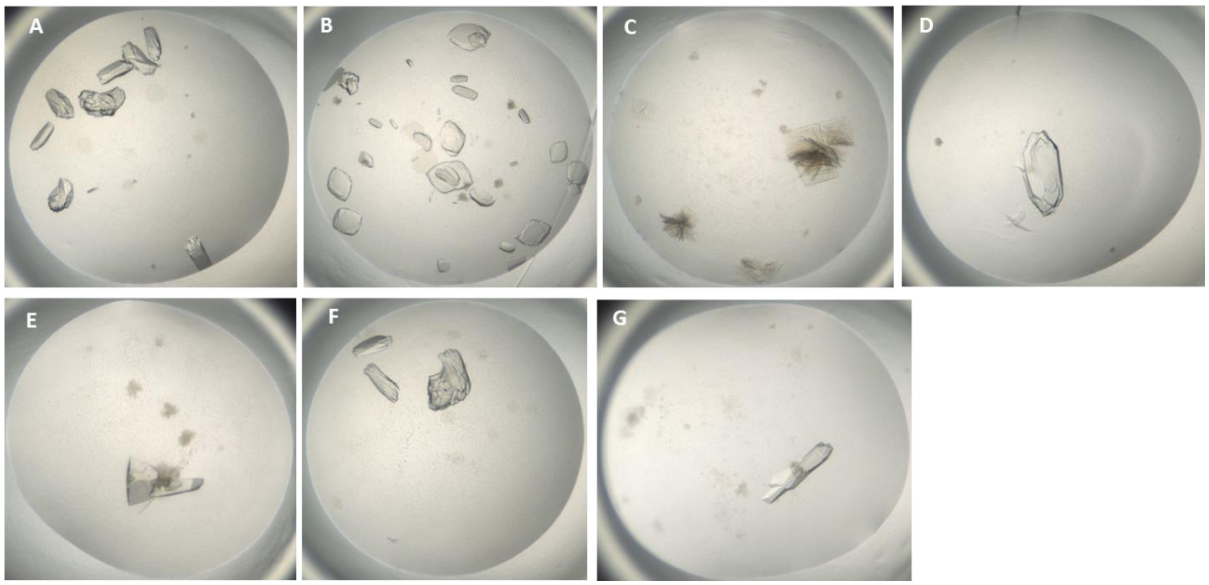

Figure 8.15: H1 crystals of second optimization trail grown in commercial PEG Suite I screen
H1 crystals obtained from baculoviral expression in Hi5 cells upon second optimization trail. The harvested cell culture supernatant was directly subjected to HisTrap excel purification, followed by thrombin cleavage and SEC with a S200 Increase 10/300 GL column. The isolated trimer was concentrated to 10 mg/mL before crystallization was carried out at 19 °C with 1:1 protein to reservoir volume by using commercial available PEGs screen. First crystals were observed 82 days after crystallization start. The buffer conditions in which the depicted crystals were grown are listed in Table 8-4.

Table 8-4: Buffer compositions of H1 crystals grown in PEGs screen during second optimization trail

H1 Crystal	Buffer compositions
Fig. 8.15 A	0.2 M Lithium chloride + 20% (w/v) PEG 3350
Fig. 8.15 B	0.2 M Sodium chloride + 20% (w/v) PEG 3350
Fig. 8.15 C	0.2 M Potassium chloride + 20% (w/v) PEG 3350
Fig. 8.15 D	0.2 M Lithium nitrate + 20% (w/v) PEG 3350
Fig. 8.15 E	0.2 M Potassium formate + 20% (w/v) PEG 3350
Fig. 8.15 F	0.2 M Potassium acetate + 20% (w/v) PEG 3350
Fig. 8.15 G	0.2 M K/Na tartrate + 20% (w/v) PEG 3350

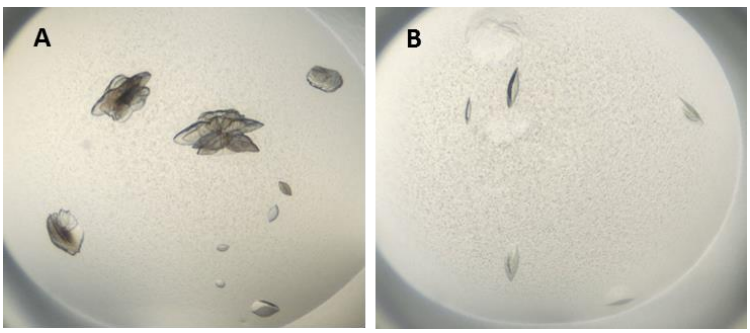

Figure 8.16: H1 crystals of second optimization trial in random screen RII
Hits of H1 obtained from baculoviral expression in Hi5 cells in screen RII. The harvested cell culture supernatant was directly subjected to HisTrap excel purification, followed by thrombin cleavage and SEC with a S200 Increase 10/300 GL column. The isolated trimer was concentrated to 10 mg/mL before crystallization was carried out at 19 °C with 1:1 protein to reservoir volume by using commercial available JCSG+ and self-prepared RI screen. First crystals in RII were observed 3 days after crystallization setup, the following grew on day 18 or 82. The buffer conditions in which the depicted crystals were grown are listed in Table 8-5.

Table 8-5: Buffer compositions of H1 crystals grown in RII during second optimization trail

H1 Crystal	Buffer composition
Fig. 8.16 A	0.17 M Magnesium sulfate + 45 % v/v PEG 300
Fig. 8.16 B	0.1 M TRIS-BASE + 50 % v/v PEG 300

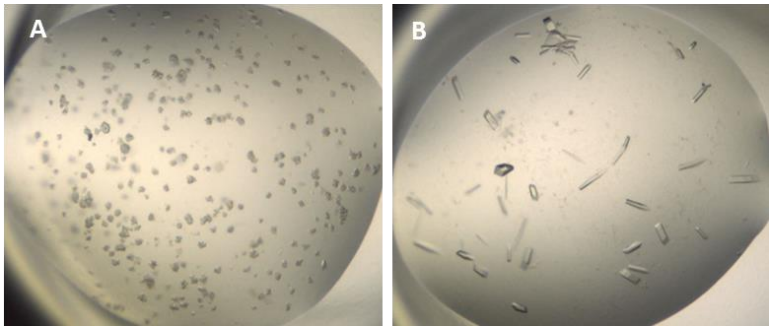

Figure 8.17: H1 crystals of third optimization trial
Hits obtained in the crystallization setup with H1 derived from both baculoviral expression and TGE in Hi5 insect cells. The cell culture supernatant was directly subjected to HisTrap excel purification, followed by thrombin cleavage and SEC with a S200 Increase 10/300 GL column for trimer isolation. Additional Strep-Tactin purification was performed before the samples were concentrated to 10 mg/mL and crystallization was carried out at 19 °C with 1:1 protein to reservoir volume. In this setup the commercial available PEG Suite I and self-prepared screens RI and H1-Grid were used. First crystals of H1 obtained from baculoviral expression were observed on day 12 in PEG Suite I, whereas no crystals obtained in the other applied screens. The buffer conditions of depicted crystals are listed in Table 8-6.

Table 8-6: Buffer compositions of H1 crystals grown in the last optimization trail

H1 Crystal	Buffer compositions
Fig. 8.17 A	0.2 M Sodium chloride + PEG 3350 (20 % w/v)
Fig. 8.17 B	0.2 M Magnesium formate + PEG 3350 (20 % w/v)

Table 8-7: Buffer compositions of H3 crystals grown in optimization trail

H3 crystal	Buffer composition
Fig. 3.18 A	0.35 M di-Sodium malonate + 16.7 % w/v PEG 3350 + 0.1 M HEPES pH 7.733 + 6.33 % w/v PEG 200
Fig. 3.18 B	0.1 M di-Sodium malonate + 14.4 % w/v PEG 3350 + 0.272 M Lithium sulfate + 0.1 M TRIS-BASE pH 7.667 + 15 % w/v PEG 200
Fig. 3.18 C	0.16 M Calcium acetate + 14.4 % w/v PEG 8000 + 20 % v/v Glycerol + 0.08 M Sodium cacodylate pH 6.5
Fig. 3.18 D	30 % w/v PEG MME 2000 + 0.1 M Potassium thiocyanate
Fig. 3.18 E	0.2 M Ammonium sulfate + 25.6 % w/v PEG 3350 + 16.7 % v/v Glycerol + 0.272 M Lithium acetate + 0.1 M TRIS-BASE pH 7
Fig. 3.18 F	0.1 M di-Sodium malonate + 23.3 % w/v PEG 3350 + 0.1 M HEPES pH 7.889
Fig. 3.18 G	20 % w/v PEG 8000 + 0.1 M CHES pH 9.5

Table 8-8: Data collection of H3 crystal

X-ray Data-Processing Statistics		
Space group:	$H3_2$	
Cell constants a; b; c (Å)	102.39 102.39 272.99	
Cell angles α; β; γ (°)	90.0 90.0 120.0	
Resolution range (Å)	84.333 - 1.446	
Highest resolution shell (Å)	1.471 - 1.446	
	overall	Highest resolution shell
Reflections, unique	98474	4841
R_{merge} (%)	8.1	6.4
R_{pim} (%)	8.3	1.5
Completeness overall (%)	8.5	100
Multiplicity	8.6	19.8
I/σ(I)	26.4	2.3
CC1/2 (%)	8.9	100

Table 8-9: Refinement statistics of H3 crystal

Refinement Statistics	
R_{work} (%)	17.7
R_{free} (%)	19.0
Non hydrogen atoms	5172
Non hydrogen protein atoms	4350
Ligands/ions/others	158
Solvent molecules	664
R.m.s. deviations from ideal values	
Bond lengths (Å)	0.0093
Bond angles (º)	1.052
Average B values (Å2)	
All atoms	30.531
Protein main chain atoms	25.699
Protein all atoms	30.676
Ligands/ions/others	65.620
Solvent	36.069
Φ, Ψ angle distribution for residues	
In most favoured regions (%)	95.3
In additional allowed regions (%)	4.5
In disallowed regions (%)	0.2

Appendix V

Table 8-10: Thermofluor test conditions

	1	2	3	4	5	6	7	8	9	10	11	12
A	50 mM NaAcetate - pH 4.0	50 mM NaAcetate - pH 4.5	50 mM NaCitrate - pH 5.0	50 mM NaCitrate - pH 5.5	50 mM MES - pH 6.0	50 mM Bis-Tris - pH 6.0	50 mM MES - pH 6.5	50 mM Bis-Tris - pH 6.5	50 mM Bis-Tris - pH 7.0	50 mM Tris-HCl - pH 7.0	50 mM MOPS - pH 7.0	50 mM HEPES - pH 7.0
B	50 mM NaAcetate 100 mM NaCl pH 4.0	50 mM NaAcetate 100 mM NaCl pH 4.5	50 mM NaCitrate 100 mM NaCl pH 5.0	50 mM NaCitrate 100 mM NaCl pH 5.5	50 mM MES 100 mM NaCl pH 6.0	50 mM Bis-Tris 100 mM NaCl pH 6.0	50 mM MES 100 mM NaCl pH 6.5	50 mM Bis-Tris 100 mM NaCl pH 6.5	50 mM Bis-Tris 100 mM NaCl pH 7.0	50 mM Tris-HCl 100 mM NaCl pH 7.0	50 mM MOPS 100 mM NaCl pH 7.0	50 mM HEPES 100 mM NaCl pH 7.0
C	50 mM NaAcetate 200 mM NaCl pH 4.0	50 mM NaAcetate 200 mM NaCl pH 4.5	50 mM NaCitrate 200 mM NaCl pH 5.0	50 mM NaCitrate 200 mM NaCl pH 5.5	50 mM MES 200 mM NaCl pH 6.0	50 mM Bis-Tris 200 mM NaCl pH 6.0	50 mM MES 200 mM NaCl pH 6.5	50 mM Bis-Tris 200 mM NaCl pH 6.5	50 mM Bis-Tris 200 mM NaCl pH 7.0	50 mM Tris-HCl 200 mM NaCl pH 7.0	50 mM MOPS 200 mM NaCl pH 7.0	50 mM HEPES 200 mM NaCl pH 7.0
D	50 mM NaAcetate 500 mM NaCl pH 4.0	50 mM NaAcetate 500 mM NaCl pH 4.5	50 mM NaCitrate 500 mM NaCl pH 5.0	50 mM NaCitrate 500 mM NaCl pH 5.5	50 mM MES 500 mM NaCl pH 6.0	50 mM Bis-Tris 500 mM NaCl pH 6.0	50 mM MES 500 mM NaCl pH 6.5	50 mM Bis-Tris 500 mM NaCl pH 6.5	50 mM Bis-Tris 500 mM NaCl pH 7.0	50 mM Tris-HCl 500 mM NaCl pH 7.0	50 mM MOPS 500 mM NaCl pH 7.0	50 mM HEPES 500 mM NaCl pH 7.0
E	50 mM Tris-HCl - pH 7.5	50 mM MOPS - pH 7.5	50 mM HEPES - pH 7.5	50 mM Tris-HCl - pH 8.0	50 mM HEPES - pH 8.0	50 mM BICINE - pH 8.0	50 mM Tris-HCl - pH 8.5	50 mM BICINE - pH 8.5	50 mM CHES - pH 9.0	50 mM CHES - pH 9.5	50 mM CAPS - pH 10.0	50 mM CAPS - pH 10.5
F	50 mM Tris-HCl 100 mM NaCl pH 7.5	50 mM MOPS 100 mM NaCl pH 7.5	50 mM HEPES 100 mM NaCl pH 7.5	50 mM Tris-HCl 100 mM NaCl pH 8.0	50 mM HEPES 100 mM NaCl pH 8.0	50 mM BICINE 100 mM NaCl pH 8.0	50 mM Tris-HCl 100 mM NaCl pH 8.5	50 mM BICINE 100 mM NaCl pH 8.5	50 mM CHES 100 mM NaCl pH 9.0	50 mM CHES 100 mM NaCl pH 9.5	50 mM CAPS 100 mM NaCl pH 10.0	50 mM CAPS 100 mM NaCl pH 10.5
G	50 mM Tris-HCl 200 mM NaCl pH 7.5	50 mM MOPS 200 mM NaCl pH 7.5	50 mM HEPES 200 mM NaCl pH 7.5	50 mM Tris-HCl 200 mM NaCl pH 8.0	50 mM HEPES 200 mM NaCl pH 8.0	50 mM BICINE 200 mM NaCl pH 8.0	50 mM Tris-HCl 200 mM NaCl pH 8.5	50 mM BICINE 200 mM NaCl pH 8.5	50 mM CHES 200 mM NaCl pH 9.0	50 mM CHES 200 mM NaCl pH 9.5	50 mM CAPS 200 mM NaCl pH 10.0	50 mM CAPS 200 mM NaCl pH 10.5
H	50 mM Tris-HCl 500 mM NaCl pH 7.5	50 mM MOPS 500 mM NaCl pH 7.5	50 mM HEPES 500 mM NaCl pH 7.5	50 mM Tris-HCl 500 mM NaCl pH 8.0	50 mM HEPES 500 mM NaCl pH 8.0	50 mM BICINE 500 mM NaCl pH 8.0	50 mM Tris-HCl 500 mM NaCl pH 8.5	50 mM BICINE 500 mM NaCl pH 8.5	50 mM CHES 500 mM NaCl pH 9.0	50 mM CHES 500 mM NaCl pH 9.5	50 mM CAPS 500 mM NaCl pH 10.0	50 mM CAPS 500 mM NaCl pH 10.5

9 Danksagung

Zunächst möchte ich Prof. Dr. Wulf Blankenfeldt meinen herzlichen Dank für die Betreuung meiner Doktorarbeit als Mentor sowie für die Unterstützung während der Thesis Committees aussprechen. Außerdem bedanke ich mich bei Prof. Dr. Stefan Dübel und Prof. Dr. Michael Hust für die Übernahme des Korreferats und des Prüfungsvorsitzes.

Darüber hinaus gilt meinem Betreuer Dr. Joop van den Heuvel besonderer Dank für die Möglichkeit in seiner Arbeitsgruppe in diesem interessanten und vielseitigen Themengebiet zu promovieren. Zudem ermöglichte er mir die Teilnahme an diversen internationalen Konferenzen und Kursen, die sowohl fachlich als auch persönlich eine enorme Bereicherung waren.

Ganz besonders möchte ich mich an dieser Stelle auch bei Prof. Dr. Thomas Pietschmann für die Zusammenarbeit und die fortwährende Unterstützung während der gesamten Dauer der Doktorarbeit bedanken.

Außerdem möchte ich mich ganz herzlich bei all meinen Kollegen, insbesondere bei meinen Mitdoktoranden, für die gemeinsame Zeit bedanken. Mit Christian Schinkowski habe ich mir nicht nur jahrelang ein Büro geteilt, auch thematisch war es eine sehr enge und gewinnbringende Zusammenarbeit. Katharina Karste danke ich besonders für die gemeinsam besuchten Fortbildungsveranstaltungen, die Zeit auf dem Retreat sowie für ihre Unterstützung vor allem in persönlichen Belangen. Maren Bleckmann danke ich dafür, dass wir immer ein super Team im Bereich der Insektenkultivierung und darüber hinaus waren. Gemeinsam haben wir sogar ein tolles Paper geschrieben, was ohne ihre Beharrlichkeit wahrscheinlich nie zur Veröffentlichung gekommen wäre. Bahar Baser danke ich insbesondere in meiner Anfangszeit für die tolle kollegiale Zusammenarbeit. Nina Schwemmlein, Monika Popp und Florian Witzgall danke ich für ihre Unterstützung im Labor und bei Fragen zur Strukturbiologie oder zur Doktorarbeit. Außerdem danke ich ihnen für die schöne Zeit auch außerhalb der Arbeit, vor allem am Ende, da es ohne sie wahrscheinlich ganz schön langweilig gewesen wäre.

Mein herzlichster Dank gilt zudem Dr. Peer Lukat, ohne dessen Hilfe ich in den strukturbiologischen Fragen nicht so weit gekommen wäre. Sowohl im Labor, bei der Vermessung der Kristalle, als auch bei der Auswertung der Daten war er mir eine riesengroße Hilfe. Zudem danke ich Dr. Ruth Lambertz und Dr. Jörn Krauße für die Zusammenarbeit und die Unterstützung im Influenza Projekt. Ruth und Peer danke ich zudem für's Korrekturlesen. Für die Unterstützung in immunologischen Belangen und der unheimlich freundlichen Art des Kontakts danke ich Dr. Kai Schulze. Es war immer eine Freude mit ihm zusammenzuarbeiten und ich würde mich freuen wenn es auch in Zukunft noch Gelegenheit

dazu gibt. Außerdem danke ich Tanvi Khera für die Zusammenarbeit im HCV Projekt und für ihre Unterstützung durch funktionelle Analysen der E2 Proteine.

Weiterhin danke ich all meinen ehemaligen Studenten, Auszubildenden und Praktikanten für die gemeinsame Zeit. Besonders danke ich hierbei Mirjam Sommer und Gesa Martens für ihre exzellente Unterstützung und die schöne Zeit. Gerne hätte ich länger mit euch zusammengearbeitet und wünsche euch alles Gute für eure Zukunft.

Darüber hinaus bedanke ich mich bei Anke Samuels, Nadine Konisch und Daniela Gebauer für ihre Unterstützung im Labor sowie für ein stets nettes Arbeitsumfeld. Anke danke ich zudem besonders dafür, dass sie mir in schweren Zeiten stets eine Stütze und immer für mich da war. Obendrein danke ich ihr für ihren sportlichen Antrieb, ohne den ich wohl kaum die sportlichen Erfolge der letzten Jahre erzielt hätte sowie für zahlreiche Rotkappen Treffen.

Neben all meinen Kollegen und Kooperationspartnern möchte ich auch meinen Freunden und meiner Familie für die Unterstützung während der Promotion und den Gelegenheiten diese ab und zu auch mal zu vergessen und wieder Kraft zu tanken danken. Besonderer Dank gilt hierbei meinem Vater, der mir durch seine Unterstützung im Studium überhaupt erst ermöglicht hat diesen Weg einzuschlagen und dem ich daher unheimlich dankbar bin. Auch bei meiner Zwillingsschwester Doro möchte ich ausdrücklich für all ihre Unterstützung danken und dafür dass sie wesentlich daran beteiligt war, dass es mich überhaupt nach Braunschweig verschlagen hat. Zu guter Letzt danke ich meinem Schatz Christian, der mich während der Promotion immer wieder aufgebaut hat, wenn im am Boden war und der für mich einfach das größte Glück überhaupt bedeutet.

Schnabel, Schnabel!